④

AD

AD-A193 197

USER'S MANUAL FOR C-HEMP, A TWO-DIMENSIONAL WAVE PROPAGATION CODE VOLUME I: DESCRIPTION AND DERIVATIONS OF THE CODE

SRI INTERNATIONAL
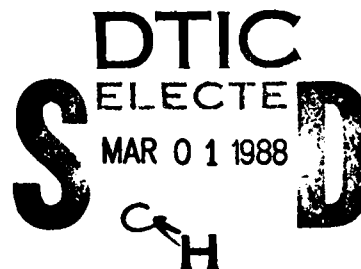333 RAVENSWOOD AVENUE
MENLO PARK, CA 94025

DTIC
S ELECTE D
MAR 0 1 1988
C H

OCTOBER 1987

US ARMY BALLISTIC RESEARCH LABORATORY
ABERDEEN PROVING GROUND, MARYLAND

88 2 29 122

DESTRUCTION NOTICE

REPORT DOCUMENTATION PAGE

Form Approved
OMB No 0704-0188
Exp Date Jun 30 1986

1a REPORT SECURITY CLASSIFICATION	1b RESTRICTIVE MARKINGS
Unclassified	

2a SECURITY CLASSIFICATION AUTHORITY	3. DISTRIBUTION/AVAILABILITY OF REPORT
2b DECLASSIFICATION/DOWNGRADING SCHEDULE	

4 PERFORMING ORGANIZATION REPORT NUMBER(S)	5. MONITORING ORGANIZATION REPORT NUMBER(S)
PYU 6423	

6a NAME OF PERFORMING ORGANIZATION	6b OFFICE SYMBOL (If applicable)	7a. NAME OF MONITORING ORGANIZATION
SRI International		Ballistic Research Laboratory ATTN: SLCBR-TB

6c ADDRESS (City, State, and ZIP Code)	7b. ADDRESS (City, State, and ZIP Code)
333 Ravenswood Avenue Menlo Park, CA 94025	Aberdeen Proving Ground, MD 21005-5066

8a. NAME OF FUNDING/SPONSORING ORGANIZATION	8b OFFICE SYMBOL (If applicable)	9 PROCUREMENT INSTRUMENT IDENTIFICATION NUMBER
		DAAK11-83-R-0105

8c ADDRESS (City, State, and ZIP Code)	10 SOURCE OF FUNDING NUMBERS			
	PROGRAM ELEMENT NO	PROJECT NO	TASK NO	WORK UNIT ACCESSION NO

11 TITLE (Include Security Classification)
USER'S MANUAL FOR C-HEMP, A TWO-DIMENSIONAL WAVE PROPAGATION CODE
Volume I: Description and Derivations of the Code

12 PERSONAL AUTHOR(S)
L. Seaman, T. Cooper, and D. Erlich

13a TYPE OF REPORT	13b TIME COVERED	14 DATE OF REPORT (Year, Month, Day)	15 PAGE COUNT
Contract Report	FROM Sep 83 TO Oct 85		

16 SUPPLEMENTARY NOTATION

17	COSATI CODES		18 SUBJECT TERMS (Continue on reverse if necessary and identify by block number)
FIELD	GROUP	SUB-GROUP	Two-dimensional wave propagation code, Armor Penetration, Explosive Detonation, Computational Model, Micromechanical Model, Shear Banding, Brittle Fracture, Ductile Fracture
11	06		
19	04		

19 ABSTRACT (Continue on reverse if necessary and identify by block number)

C-HEMP is a two-dimensional finite-difference computer program for treating stress waves propagation, in either planar or axisymmetric flow, caused by impacts or explosive detonation. It was designed, implemented, and tested at SRI International under a three-year contract for the U.S. Army Ballistic Research Laboratory to develop a computational model for armor penetration.

The manual for the C-HEMP stress wave propagation code consists of two volumes. This first volume contains the descriptions and derivations of the code.

20 DISTRIBUTION/AVAILABILITY OF ABSTRACT	21. ABSTRACT SECURITY CLASSIFICATION
☒ UNCLASSIFIED/UNLIMITED ☐ SAME AS RPT ☐ DTIC USERS	Unclassified

22a NAME OF RESPONSIBLE INDIVIDUAL	22b TELEPHONE (Include Area Code)	22c OFFICE SYMBOL
Michael Scheidler	301-278-6836	SLCBR-TB-W

DD FORM 1473, 84 MAR

83 APR edition may be used until exhausted
All other editions are obsolete

SECURITY CLASSIFICATION OF THIS PAGE

UNCLASSIFIED

PREFACE

The manual for the C-HEMP stress wave propagation code consists of two volumes. The first volume contains the descriptions and derivations of the code. The second contains brief descriptions of each subroutine and the listing of the code.

The C-HEMP code was written under the sponsorship of Dr. Gerald Moss of Ballistic Research Laboratory. He, and his coworker Dr Michael Scheidler, have contributed significantly to the development of the code and the manual by exercising the code and reviewing the manual. They have provided SRI with a large list of needed clarifications in the manual to aid the beginning user.

After the completion of the contract to write this manual, an SRI-sponsored project was undertaken to study rotation problems in two dimensions. The internal report that resulted from this effort is included as Appendix D because of its relevance to the C-HEMP code.

Several other researchers at SRI have contributed to the manual and code effort. Jim Kempf has used the code and has written the auxiliary programs for plotting the C-HEMP output. Bonita Lew helped with making C-HEMP calculations and in expanding the layout capabilities. Dr. Donald R. Curran has provided overall guidance and aided in policy decisions.

Accession For	
NTIS GRA&I	☑
DTIC TAB	☐
Unannounced	☐
Justification	

By_____
Distribution/
Availability Codes

Dist	Avail and/or Special

A-1

iii

CONTENTS

v

FIGURES

I INTRODUCTION

C-HEMP is a two-dimensional finite-difference computer program for treating stress wave propagation, in either planar or axisymmetric flow, caused by impacts or explosive detonations. It was designed, implemented, and tested at SRI International under a three-year contract for the U. S. Army Ballistic Research Laboratory to develop a computational model for armor penetration [Refs. 1-5].

A. Background

C-HEMP (the "C" is short for "Composite") is a synthesis of several two-dimensional finite-difference codes, including HEMP [Ref. 6], TOODY [Refs. 7-8], STEALTH [Ref. 9], TROTT [Ref. 10], and SWE2D [Ref. 11]. Various features of C-HEMP were adapted from each of these other codes (e.g., the input from HEMP, the rezoner from STEALTH, the slide lines from TOODY and SWE2D, the storage and model provisions from TROTT). These features were then augmented and combined with new features to form a computer code that could handle many of the complex wave propagation and failure problems associated with armor penetration. The versatility of C-HEMP makes it suitable for a wide variety of other wave propagation problems, including those involving unusual geometries, multiple impacts, and large shear deformations.

Like most other finite-difference codes, C-HEMP uses the Lagrangian form of the equations of motions, so that the coordinates move with the materials, and uses artificial viscosity to spread wave fronts over several cells. Its special features include finite-element node numbering, free-field input, advanced slide-line logic, and an automatic rezoner. Several complex material models are included, in addition to the standard Mie-Gruneisen equation of state, and the code is designed so that new models can be readily inserted.

1

It should be noted that C-HEMP is not a polished program product, but rather a research tool actively undergoing refinement and extension to make it applicable to an increasingly wider class of problems. Nevertheless, we have made extensive tests of the code and are confident that the core of the code is working as intended. The user should exercise discretion in interpreting the results of calculations made with C-HEMP (or any other code of this type), if only because particular applications may extend into physical behavior not anticipated by the authors. Special caution is called for in the use of complex material models.

B. Review of Other Wave Propagation Codes

A review was made of many codes that have been used for penetration calculations. The review was limited to general-purpose wave propagation codes written for large-deformation problems in solids treated by complex material models. Here only some of the special advantages or features of these codes are described.

The Eulerian codes HELP [Ref. 12] and HULL [Ref. 13] are able to treat large distortion problems, although this advantage leads to difficulties in treating sharply defined boundaries and slide lines. Also there tends to be smearing of cell properties such as the fracture quantities.

The Lagrangian finite element code EPIC [Ref. 14] has both two- and three-dimensional versions and thus is particularly suited to oblique impacts. The triangular cells resist large distortions, but falsify the stresses computed from pressure-sensitive stress-strain relations. A simple, frictionless slide-line treatment is available in the code.

STEALTH [Ref. 9] is also Lagrangian and has two- and three-dimensional versions. It features automatic rezoning and slide-line capabilities.

The Lagrangian code TOODY [Ref. 7] has been used in many penetration calculations. It has a discrete rezoner: wave propagation

2

calculations are halted, the entire mesh is reconfigured, and then the calculation continues. The slide line treatment is particularly accurate. The cells on each side of the slide line are accounted for in detail so that, if no slip occurs, the presence of the line should be undetected. Stick or frictionless conditions and Coulomb friction properties are provided on the slide line. The slide line is tied to the usual row-and-column scheme. The number of variables per cell can be readily increased, but all cells are assigned the same number of variables.

WAVEL [Ref. 15] is a Lagrangian code with advanced slide line and continuous or automatic rezoning. It has been developed for penetration problems and extended to a quasi-three-dimensional form for oblique impacts.

HEMP [Ref. 6] is the forerunner of many two- and three-dimensional, finite-difference Lagrangian codes used in penetration calculations. It has a discrete rezoner, as TOODY has, and a slide line capability that is tied to the row-and-column cell numbering. A recent version is HEMPDS [Ref. 16], which has a double slide line (intersecting slide line) capability, but no rezoner. The double slide provision required a major restructuring of HEMP, so it is not a minor addition nor an element that can be readily transferred to another code. The HEMP code has many versions, each with different capabilities. The version available at AMMRC has an input provision termed a NAMELIST READ statement. This provision permits all numerical quantities to be identified by name and all data to occur in a free-field format (no fixed positions on an input line). This greatly simplified input provision speeds the laying out of new problems and minimizes errors.

DYNA2D [Ref. 17] is a large finite-element code that has been used for simulating self-forging fragments and penetrations. It has a capability for a slide line that can extend both horizontally and vertically at the same time. Elements of higher order than the constant strain elements in HEMP are available for use on elastic or other small-distortion problems. There is also a DYNA3D [Ref. 18] for three-

3

dimensional problems. Both codes are equipped with preprocessors for laying out the finite-difference mesh and postprocessors for examining and plotting the results.

The small two-dimensional Lagrangian code TROTT [Ref. 10], which we have used in many of our applications, has the advantage of simplicity in adding new material models with large numbers of variables. The new model is added by the insertion of one or two call statements. Extra variables for the cells treated by special material models are available, and the number of extra variables is designated in the input. The number of variables per cell varies from cell to cell so that relatively inactive cells can have a minimum number of variables, while cells in the region of fracturing, for example, can have 50 or 100 extra variables. TROTT also has automatic rezoning, like that in WAVEL and STEALTH. A simple frictionless slide line treatment is available.

The review of available codes indicated to us that there are many good candidates. Although no one code has all the desired features, all the desired features are available. Therefore, a synthesis from existing codes seemed desirable.

C. Features for a General Code for Penetration

The basic problem considered is the penetration of a long-rod missile into one or a series of armor plates. The target may be defeated by formation of a plug, excessive plastic flow allowing perforation, rear-surface spall, or a combination of these effects. The rod may be defeated by excessive plastic flow, shear banding and fracture near the tip, or by fracture along its length. The initial problem we are considering is two-dimensional: either a normal impact of an axisymmetric missile onto a plate or an oblique impact of a slab onto a slab. Eventually, simulations of oblique impacts of symmetric missiles (a three-dimensional problem) will be investigated.

Our attempts and those of others to simulate the penetration encounter have led us to outline several basic requirements for a computer program for the simulation:

4

- Slide Lines
- Rezoning
- Material model for fracture damage.

The slide lines permit materials to slip past each other or to impact and separate. The penetrator nose and sides must be able to slide along the upper surface of the target and on the sides of the crater as it forms. In addition, the target may be severed to form a plug: the interface between the plug and the remainder of the target requires a slide line if the relative motion is significant. The length and direction of the severing line is determined during the penetration, so the slide lines must be able to unzip gradually and to wander through the finite difference or finite element grid.

The combination of these slide line features introduces requirements not yet available in any of the present codes. The provision of a wandering slide line may have been attempted in some codes, but is not a standard feature. The capability for allowing one object to interact (slide on) several other objects is available in a rudimentary way in HEMPDS, and is present in a smeared manner in Eulerian codes such as HELP.

The large distortions experienced by both penetrator and target during a simulation indicate a capability to rezone or reconfigure the computational grid at intervals during the calculation. We have used automatic rezoning in which each node is permitted to move to an optimum location every five time steps. This rezoning provision is still not adequate for some of the more severe distortions that occur around the lip of a crater and in the adjacent projectile material. Some additional rezoning features which may aid in representing the material in such cases are: free Lagrange reconnections, deletion of nodes, addition of nodes, and removal of distorted material. The free Lagrange method is used only with pairs of triangular cells which form a quadrilateral with nodes A, B, C, D: if the common side BD between the triangles becomes excessively elongated, the triangles can be reformed by disconnecting

5

nodes B and D, and connecting A and C. The free Lagrange procedure permits large shear flows and assists in maintaining compact cells for an accurate calculation. Deletion of material is an extreme measure, but has been done regularly in codes for penetration. It has the disadvantage of losing both mass and momentum conservation. It may be justified when the distorted material is a small fraction of the entire material of interest, and that material is not governing the main processes of interest.

The material property model is essential for determining the ballistic limit and for predicting the fragment spray at the end of the event. Because such a model requires many variables, the penetration code must be configured to permit large data arrays for cells in which the material is undergoing damage.

Besides these basic requirements, there are a number of nominal requirements that make a computer program readily usable:

- Input in a free-field format, like the AMMRC version of HEMP
- Finite element numbering, as in EPIC
- Usable on available computers
- Documentation.
- Extensive provisions for plotting and examining the results.

The convenience of a simple input form is important because it may greatly reduce the time required to lay out a new problem and it makes the problem definition more apparent to other users.

The finite element numbering method allows the cells to be configured in a more general way than in rows and columns. This numbering is convenient for discretizing nonrectangular or multiply connected bodies. It seems essential for providing slide lines that extend in both x and y directions, as along the nose of a projectile and then along the side. The computational logic of a self-directed slide line seems more straight-forward with finite element numbering because new nodes can be readily added and the relationship between these nodes and the cells can be easily updated.

6

D. Scope of this Manual

This manual is intended as both an introduction for a new user to
C-HEMP and as a complete reference for an experienced user. Chapter II
derives the logic for many of the basic computational features of C-
HEMP, including the solution procedure for the wave propagation equa-
tions, the finite-element numbering scheme, the time-step control and
stability conditions, the rezoner, and the slide line routines.

Chapter III is an introduction to constitutive models for
materials. First some of the standard models for pressure and deviator
stress are introduced. Then more complex models for composites, explo-
sives, and porous materials are outlined. A series of micromechanical
fracture models are introduced: these are especially important for
penetration and other large distortion calculations.

Chapter IV describes in detail the input parameters and format
required for C-HEMP, while Chapter V describes the various printed and
plotted output obtained during a calculation. Chapter VI presents five
sample problems that have been run on C-HEMP, with emphasis on the input
format and the layout logic. A new user to C-HEMP should begin with
chapter IV to gain familiarity with the order of specifying input
parameters and the input format, and then continue with Chapter VI to
see examples of input specifications.

Following the main text are five appendices. Appendix A contains a
brief description of the program flow and a list of all the subroutines
and COMMON blocks in C-HEMP. Appendix B describes the procedure for
inserting new equation-of-state subroutines into C-HEMP. Appendix C is
a glossary of all the input and output parameters, and other key
variables in the code. Appendix D describes the cell rotation
provisions and the last Appendix gives the storage locations for cell
and coordinate variables in the main array.

II PROPAGATION CALCULATIONS

A. Introduction

The motion and stresses throughout the material are determined as a function of time in the code. The solution is obtained by solving the mass, momentum, and energy conservation relations together with constitutive relations for the material. This section presents the conservation relations and their solution by finite difference procedures. The layout of the finite difference mesh (division of the material into cells) is treated in Section IV and the constitutive relations are left to Section III. Included in the current section are the determination of the strain and material rotation from the boundary motions of the cells. The artificial viscous stress, which eliminates shock discontinuities, is described. The stability requirements and time step control are outlined. Both rezoning procedures and the slide line treatment are in this section.

B. Solution Procedure for Wave Propagation

The wave propagation calculations in C-HEMP are based on the solution of the Lagrangian equations governing motion of a continuous medium. The solution technique is called the method of artificial viscosity because of the introduction of viscous forces to permit a continuous-flow computation in regions of high stress gradients. Such regions are interpreted as locations of shock fronts, although no discontinuities occur in the computed flow field. With this artificial viscosity method, the equations of continuous flow can be used everywhere and no special equations are required at shock fronts. C-HEMP uses the leapfrog method of von Neumann and Richtmyer [Ref. 19] to integrate the flow equations. This method provides second-order precision in time and space without the use of second differences.

9

In the following paragraphs we first introduce the Lagrangian set of partial differential equations governing one-dimensional planar flow. These are then changed to integral and numerical form, and those requiring it are extended to multidimensional form. Then the solution procedure is outlined.

The Lagrangian partial differential equations to be solved for one-dimensional planar flow are

$$\left(\frac{\partial X}{\partial t}\right)_h = U \qquad \text{(velocity)} \qquad (1)$$

$$\left(\frac{\partial U}{\partial t}\right)_h = -\frac{1}{\rho_o}\left(\frac{\partial T}{\partial h}\right)_t \qquad \text{(momentum)} \qquad (2)$$

$$\left(\frac{\partial E}{\partial t}\right)_h = -T\left(\frac{\partial V}{\partial t}\right)_h \qquad \text{(energy)} \qquad (3)$$

$$\left(\frac{\partial X}{\partial h}\right)_t = \frac{\rho_o}{\rho} \qquad \text{(mass)} \qquad (4)$$

$$T = P + \sigma' + Q = f(E, \rho, \ldots) \qquad \text{(constitutive relations)} \qquad (5)$$

where X = Eulerian or current position

t = time

h = Lagrangian or initial position

U = particle velocity

ρ, ρ_o = current and original density

T, σ' = total mechanical stress and deviator stress in the direction of propagation

V = 1/ρ, specific volume

P, Q = pressure and artificial viscous stress

E = internal energy.

These equations relate velocity to coordinate motion; provide for conservation of momentum, energy, and mass; and give the stress-strain or constitutive relations.

10

In the leapfrog scheme of von Neumann and Richtmyer [Ref. 19], the five fundamental equations are not solved simultaneously, but in a prescribed order. This order is suggested in the diagram in Figure 1. First there are the cell calculations at the time t^n and mid-node positions $j - 1/2$ and $j + 1/2$:

$$\rho^n, \epsilon^n, E^n, \sigma^n, T^n.$$

These are followed by the node point calculations:

$$U_j^{n+1/2} \qquad , \qquad X_j^{n+1}$$

These steps are undertaken for each cell and node. Then the time is incremented and the process is repeated. In C-HEMP, these calculations are performed in two separate loops: one over all cells and one over all nodes.

Now each of these five equations is examined, extended to two or three dimensions, and put into numerical form. The velocity relation, Eq. (1), is expanded to a vector form

$$\left(\frac{\partial X_i}{\partial t}\right)_h = U_i \tag{6}$$

where i runs over the three coordinate directions and h refers to all three directions. In numerical form the integral of Eq. (6) is simply

$$X_{ij}^{n+1} = X_{ij}^n + U_{ij}^{n+1/2} \Delta t^{n+1/2} \tag{7}$$

Here n and $n+1$ refer to times t^n and t^{n+1} and j refers to the node number. Velocity U and time increment Δt are labeled to indicate that they are centered midway between t^n and t^{n+1}.

The momentum equation (2) takes the following three-dimensional form:

11
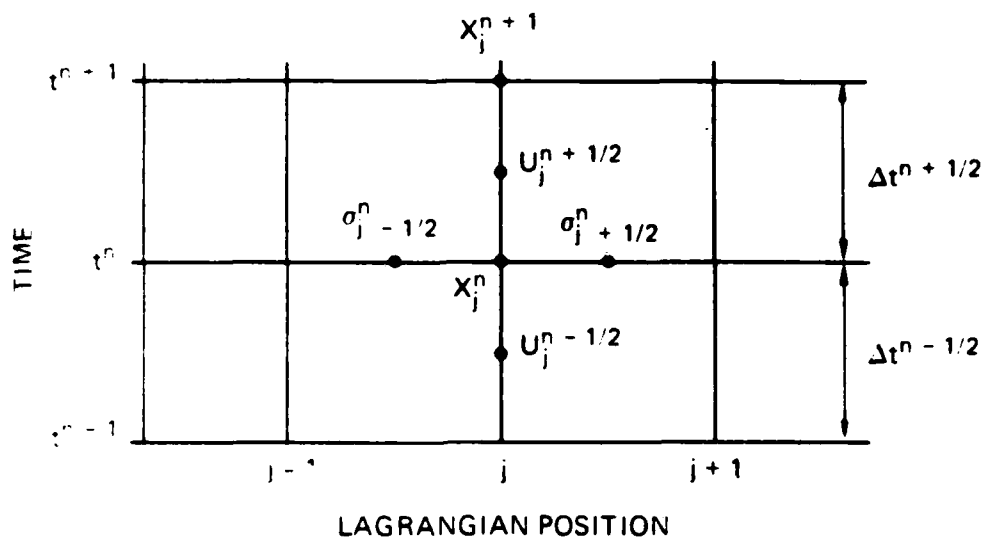
FIGURE 1 GRID FOR LEAPFROG CALCULATIONS SHOWING INCREMENTS
IN SPACE AND TIME
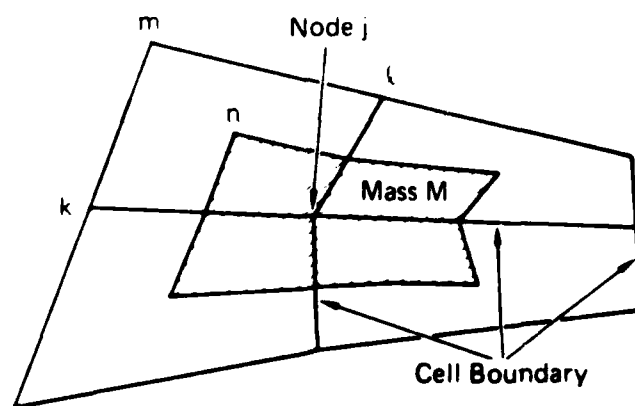
FIGURE 2 CONFIGURATION OF FOUR CELLS SURROUNDING
NODE j AND ITS ASSOCIATED MASS M

12

$$\left(\frac{\partial U_i}{\partial t}\right)_h = -\frac{1}{\rho_o}\left(\frac{\partial T_{ix}}{\partial h_x} + \frac{\partial T_{iy}}{\partial h_y} + \frac{\partial T_{iz}}{\partial h_z}\right) \tag{8}$$

Here i again takes the values x, y, and z, and h_x, h_y, h_z are Lagrangian coordinates. The leapfrog method makes a centering of this equation possible. The acceleration $\partial U/\partial t$ is represented by

$$\frac{\partial U}{\partial t} \approx \frac{U_j^{n+1/2} - U_j^{n-1/2}}{\Delta t^n}$$

which is centered at (j,n). Similarly, the gradient $\partial T/\partial h$ is approximated by

$$\frac{1}{\rho_o}\frac{\partial T}{\partial h} \approx \frac{T_{j+1/2}^n - T_{j-1/2}^n}{1/2\left(M_{j+1/2} + M_{j-1/2}\right)}$$

where $M_{j+1/2}$ is the mass of the cell between nodes j and j+1. This gradient is also centered at the point (j,n); therefore, we can expect the results of the leapfrog treatment of Equation 8 to be numerically stable and accurate.

Several strategies, such as those in HEMP, TOODY, and STEALTH, are available in the literature for putting Equation (8) into suitable numerical form. Instead of using any of these, we return to a simple integral form of (8):

$$\left(\frac{\partial U_i}{\partial t}\right)_h = \frac{\Sigma F_i}{M} \tag{9}$$

which is clearly F = Ma. The mass M is the sum of the partial masses of the cells surrounding the node j as indicated in Figure 2. (Equations for M are derived in subsection C.) The partial masses are defined in different ways for the planar and axisymmetric geometries. For the planar case, the partial mass is taken as one-fourth of the mass of the whole cell. The geometry of the partial mass is only partly defined: its coordinates are the node j in Figure 1, midpoints along the sides jk and jl, and a central point n which is not defined. To determine the

13

forces acting on this partial mass it is not necessary to prescribe the actual location of the point n, so no location is specified. For the axisymmetric geometry, the partial mass is fully defined. The coordinates are node j, the midpoints along jk and jl, and the central node which is the average of the coordinates at j, k, l, and m. (For very badly distorted cells, this location of the node n may tend to augment the distortion.) With the given node positions for the axisymmetric case, a detailed calculation of the mass of the ring-shaped partial cell is made.

To provide for exact momentum conservation, the masses associated with each node are calculated only on the first cycle, and remain constant thereafter, except under rezoning. To examine how the constancy of the masses affects the momentum conservation, let us consider the two major steps. First the nodal forces are applied to the nodal masses. Because the forces are applied equally to both sides of every surface they act upon, there is an exact momentum balance.

In the next step the nodes move. If we then recomputed the new cell center and assigned areas and masses to the surrounding nodes, the nodal masses would change. However, if the mass associated with each node is not constant, then some mass is transferred from one node to another. But the nodal velocities are not altered in this transfer operation; hence, some amount of mass has changed its velocity. Therefore, momentum is not conserved during the motion. To avoid this loss of momentum, we need to hold the masses around each node constant.

When we choose to hold the masses around each node constant, we must either determine the exact location of the boundaries of this mass, or approximate the boundaries and hence the forces that act on these areas. We are approximating the boundaries and thus approximating the velocity calculation. Because we use the same forces along the boundaries in both directions, the momentum balance is exact. These momentum balance considerations are of importance for the axisymmetric case only, because the planar masses always retain just one-fourth of the adjacent cell masses.

14

The summation over F in Equation 9 is constructed from the i-th components of the products of the stresses in each cell times the area (of the mass M) on which they act. These i-th components of the forces can be written as a stress times a projected area ΔA

$$F_i = T_{ik}\Delta A_k \qquad (10)$$

Equations for the area ΔA are derived in subsection C. Hence we have effectively found a discretization for the derivatives in Equation (8)

$$-\frac{1}{\rho_o}\frac{\partial T_{ik}}{\partial h_k} \rightarrow \frac{T_{ik}\Delta A_k}{M} \qquad (11)$$

Hence in the indicial notation of Equation (7), Equation (8) becomes

$$U_{ij}^{n+1/2} = U_{ij}^{n-1/2} + \frac{\Delta t^n}{M_j}\sum_{\ell,k} T_{ik\ell}\Delta A_{\ell k} \qquad (12)$$

Here the subscript ℓ refers to the four cells (in two dimensions) surrounding the j-th node. In planar two-dimensional flow, the sum will contain eight terms for each direction i. The time increment Δt^n is

$$\Delta t^n = t^{n+1/2} - t^{n-1/2} = \frac{\Delta t^{n+1/2} + \Delta t^{n-1/2}}{2} \qquad (13)$$

Although (12) is obtained from a finite element viewpoint, it agrees exactly with the results of finite-difference derivations for planar two-dimensional flow. Differences arise only in axisymmetric flow.

The energy equation (3) is rewritten in tensor form as

$$\frac{\partial E}{\partial t} = V \sum_{i,k} \bar{T}_{ik}^n \frac{\partial \epsilon_{ik}}{\partial t} \qquad (14)$$

where ϵ_{ik} is the strain tensor. For each cell this expression takes the numerical form

$$E^n = E^{n-1} + \bar{V}^n \sum_{i,k} \bar{T}_{ik}^n \Delta\epsilon_{ik}^{n-1/2} \qquad (15)$$

15

Here the barred quantities are averages

$$\bar{V}^n = \frac{V^n + V^{n-1}}{2} \text{ and } \bar{T}^n = \frac{T^n + T^{n-1}}{2}$$

The sum in Eq. (15) runs over four terms in two dimensions.

The expression for the conservation of mass (4) takes the simple form

$$\rho^n = \rho_o \frac{\Delta V_o}{V^n} = \frac{M}{V^n} \tag{16}$$

where V^n is the cell volume at time t^n.

The constitutive relation (5) is expanded to

$$T_{ik} = P + \sigma'_{ik} + Q \tag{17}$$

where P and Q remain scalar pressures.

C. Numerical Calculations of Area, Volume, and Momentum

For several of the numerical integrations presented in the preceding section, it is necessary to evaluate the areas and volumes of the appropriate finite difference cells. These quantities are derived in this subsection. Then the momentum equation is exhibited in the form used in the code.

Two types of quadrilateral cells are defined for the wave propagation calculation. Both are shown in Figure 3, which contains a grid of coordinate points. Cell A is a standard cell surrounded by four coordinate points. This is the cell for which the strains and stresses, which are homogeneous throughout each cell, are computed. The momentum computation determines the velocity of the coordinate points. For these calculations cell B, containing the mass around a coordinate point, is used. The calculations are broken into four portions corresponding to the parts lying in each of the surrounding stress cells. One typical portion is shown in Figure 4 with the nomenclature and sign conventions

16

Coordinate Points

Cell For Stress
Computations

A

Cell For Momentum
Computations

B
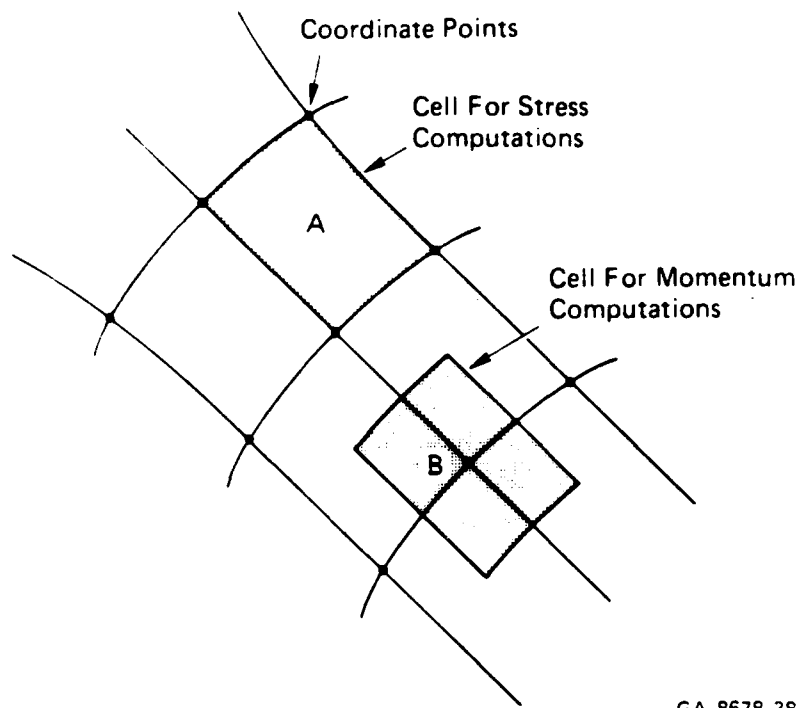
GA-8678-38

FIGURE 3   TYPES OF CELLS FOR STRESS AND MOMENTUM COMPUTATIONS

17

(a) Cell in the x–y Plane

(b) Axisymmetric Cell Cross Section

(c) Planar Cell Cross Section
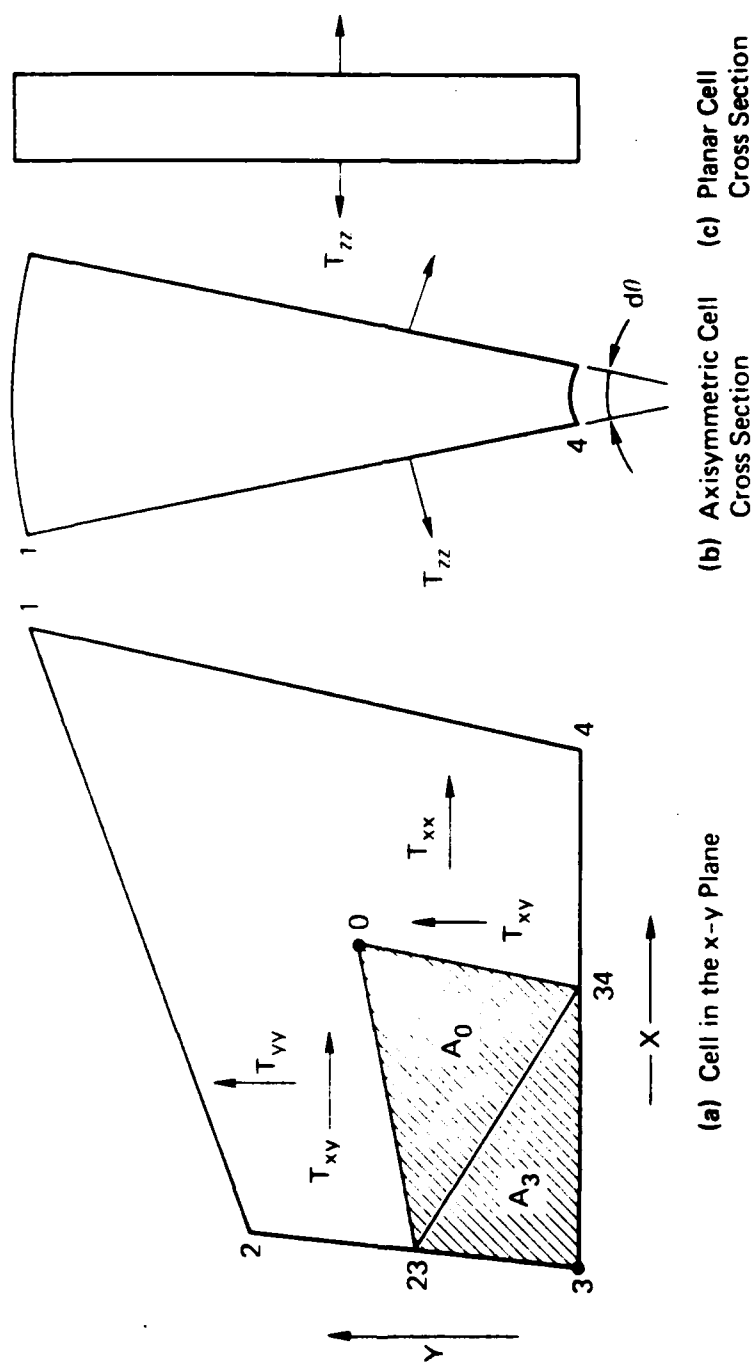
GA-8678-39A

FIGURE 4 STRESS AND COORDINATE NOMENCLATURE FOR AXISYMMETRIC AND PLANAR CELLS

that are used in the derivation of momentum conservation or velocity change at point 3. (Stress is positive in tension.) Note that the standard axisymmetric shell is a ring or doughnut, whereas the planar cell is quadrilateral with indefinite thickness in the Z direction.

The configuration of the shaded element in Figure 4 is defined in such a way that the x and y coordinates of the point 0 are averages of the coordinates at the four corners of the stress cell. End views are shown in Figure 4 as a reminder of the three-dimensional character of the elements. For an axisymmetric cell, the areas of the shaded element on which stresses act in the x and y directions are:

$$A_{xx} = \frac{d\theta}{4} \left(y_2 - y_4 \right) \left(\frac{y_2 + y_4}{2} + y_3 \right) \tag{18}$$

$$A_{yy} = \frac{d\theta}{2} \left[\left(\frac{y_2 + y_3}{2} + y_0 \right) \left(x_0 - \frac{x_2 + x_3}{2} \right) - \left(\frac{y_3 + y_4}{2} + y_0 \right) \left(x_0 - \frac{x_3 + x_4}{2} \right) \right] \tag{19}$$

For planar cells the areas in the x and y directions are:

$$A_{xx} = 1/2 \left(y_2 - y_4 \right) \tag{20}$$

$$A_{yy} = 1/2 \left(x_4 - x_2 \right) \tag{21}$$

For the axisymmetric case, the area in the x-y plane on which the stress acts is broken into two portions A_0 and A_3 as shown in Figure 4. These portions and the total are:

$$A_0 = 1/8 \left[\left(2x_0 - x_3 \right) \left(y_2 - y_4 \right) + x_2 \left(y_3 + y_4 - 2y_0 \right) \right.$$
$$\left. + x_4 \left(2y_0 - y_2 - y_3 \right) \right] \tag{22}$$

19

$$A_3 = 1/8 \left[x_4(y_2 - y_3) + x_3(y_4 - y_2) + x_2(y_3 - y_4) \right] \tag{23}$$

$$A_{xy} = A_0 + A_3 \tag{24}$$

Equations (22) and (23) are derived by simplifying the usual general relations for the area A of a triangle with nodes i, j and k:

$$2A = x_i (y_j - y_k) + x_j (y_h - y_i) + x_h (y_i - y_j)$$

The sign of the area is positive if the nodes are listed in counter-clockwise order.

The forces in the x and y directions applied to the small mass represented by the shaded area in Figure 4 are determined by multiplying the stresses shown in Figure 4 times the areas in Eqs. (18) - (21) and (24). The expressions for the forces are:

$$F_x = T_{xy} A_{yy} + T_{xx} A_{xx} \tag{26}$$

and

$$F_y = T_{yy} A_{yy} + T_{xy} A_{xx} - T_{zz} A_{xy} d\theta \qquad \text{(axisymmetric)}$$

$$= T_{yy} A_{yy} + T_{xy} A_{xx} \qquad \text{(planar)} \tag{27}$$

For the axisymmetric case, each force term contains the angle $d\theta$, which is taken as 2π. When force is divided by mass to obtain the velocity change, $d\theta$ is removed. The sign convention for the area computations is such that the product of stress and area is positive in the increasing x and y directions. Because each cell is written with point 3 as the one for which velocity is to be determined, the preceding forces and areas are valid for all quadrilateral cells around the point.

20

The mass of the small element is determined by multiplying the average density, ρ, of the cell shown in Figure 4 times the volume of the element. The axisymmetric cell mass is obtained from Pappus' Rule:

$$M = \rho \frac{2\pi}{3} \left[A_0 \left(y_0 + y_3 + \frac{y_2 + y_4}{2} \right) + A_3 \left(\frac{y_2 + y_4}{2} + 2y_3 \right) \right] \qquad (28)$$

For the planar cells the mass is simply

$$M = \rho A_{xy} \qquad (29)$$

Newton's second law (Eq. 9) is applied to obtain the change in velocity at the coordinate point 3, considering force and mass contributions from four quadrilateral elements around the point. (The index i runs over these elements.)

$$\Delta U = U_{n+1/2} - U_{n-1/2} = \frac{\left(\sum\limits_{i=1}^{4} F_{xi} \right) \Delta t_n}{\sum\limits_{i=1}^{4} M_i} \qquad (30)$$

where ΔU is the change in velocity in the x direction over the time increment Δt_n. A similar relation is used for ΔV. The spatial and temporal relationships between the cell variables are shown in Figure 1.

D. Strain and Rotation Calculations

The strain computations in the two-dimensional wave propagation program are based on the assumption that the strains are uniform throughout each quadrilateral cell of type A shown in Figure 3. The required strains are true strain increments. The strain computations are constructed to meet the following compatibility requirements:

$$\Delta \epsilon_x + \Delta \epsilon_y = \frac{\Delta A}{A} \qquad (31)$$

21

$$\Delta \varepsilon_x + \Delta \varepsilon_y + \Delta \varepsilon_z = \frac{\Delta V}{V} \qquad (32)$$

where

$\Delta \varepsilon_x$, $\Delta \varepsilon_y$, $\Delta \varepsilon_z$ = changes in the strain that occur during a time increment

$\quad\quad \Delta A$ = change in the cell area A in the x-y plane

$\quad\quad \Delta V$ = change in the volume V of the cell.

To ensure that compatibility of strains is enforced, we assume a velocity field (which is unique), rather than a strain field. Strains that are uniform throughout a cell are produced by the following linearly varying velocity field.

$$u = u_0 + u_x x + u_y y \qquad (33)$$

$$v = v_0 + v_x x + v_y y \qquad (34)$$

where u, v = particle velocity in the x, y directions, respectively. The strain rates corresponding to these velocities are:

$$\dot{\varepsilon}_x = \frac{\partial u}{\partial x} = u_x \qquad (35)$$

$$\dot{\varepsilon}_y = \frac{\partial v}{\partial y} = v_y \qquad (36)$$

$$\varepsilon_{xy} = 1/2 \left(\frac{\partial v}{\partial x} + \frac{\partial u}{\partial y} \right) = 1/2 \left(v_x + u_y \right) \qquad (37)$$

$$\dot{\omega}_{xy} = 1/2 \left(\frac{\partial v}{\partial x} - \frac{\partial u}{\partial y} \right) = 1/2 \left(v_x - u_y \right) \qquad (38)$$

22

where

$$\dot{\varepsilon}_{xy} = \text{tensor shear strain rate}$$

$$\dot{\omega}_{xy} = \text{rotation rate in the xy plane, positive counterclockwise.}$$

The velocity fields of Equations (33) and (34) can be determined for any triangle if the velocities at the coordinate points are known. Consider for example the triangle in Figure 5 with coordinates 1, 2, and 3 and velocities in the x direction of u_1, u_2, and u_3. The velocity field parameters u_0, u_x, and u_y can then be determined from the following three equations:

$$u_1 = u_0 + u_x x_1 + u_y y_1$$

$$u_2 = u_0 + u_x x_2 + u_y y_2 \tag{39}$$

$$u_3 = u_0 + u_x x_3 + u_y y_3$$

where the $x_i y_i$ are coordinates of the ith point at a common time. Solution of Equations (39) gives the following results for u_x and u_y:

$$u_x = \frac{(u_1 - u_2)(y_1 - y_3) - (u_1 - u_3)(y_1 - y_2)}{2A} \tag{40}$$

$$u_y = \frac{(u_1 - u_2)(x_1 - x_3) - (u_1 - u_3)(x_1 - x_2)}{2A} \tag{41}$$

23
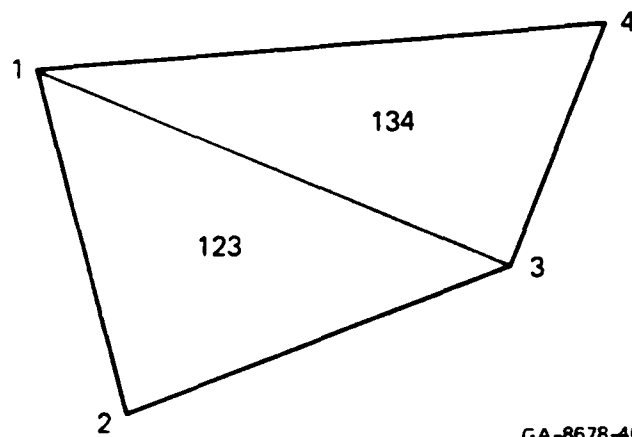
GA-8678-40

FIGURE 5   QUADRILATERAL ELEMENT PRODUCED FROM TWO TRIANGLES

where A, the area of the triangle 123 shown in Figure 5, is

$$2A = (x_1 - x_2)(y_1 - y_3) - (x_1 - x_3)(y_1 - y_2) \tag{42}$$

$$= x_1(y_2 - y_3) + x_2(y_3 - y_1) + x_3(y_1 - y_2)$$

Similarly the strain in the y direction can be determined.

$$v_x = \frac{(v_1 - v_2)(y_1 - y_3) - (v_1 - v_3)(y_1 - y_2)}{2A} \tag{43}$$

$$v_y = -\frac{(v_1 - v_2)(x_1 - x_3) - (v_1 - v_3)(x_1 - x_2)}{2A} \tag{44}$$

The next step is to specify x_i, y_i in Equations (40) through (44) in such a way that Equation (31) is satisfied. This calculation is performed in two steps: first, the requirements are satisfied for each of the two triangles shown in Figure 5 and then the computation is made for the whole quadrilateral. To meet the requirement for triangle 123, the area A of Equation (42) is taken as the average of the areas at the beginning and end of the time increment, that is,

$$A = 1/2(A^0 + A^1) \tag{45}$$

A compatible form for the strain rate in the x direction is given by

$$\dot{\varepsilon}_x = \frac{A^0 u_x^0 + A^1 u_x^1}{A^0 + A^1} \tag{46}$$

25

where values with a superscript 0 are computed with initial values of x and y, and values with a superscript 1 are evaluated with final values of x and y. These final values of coordinates are

$$x_i^1 = x_i^0 + u_i \Delta t$$

$$y_i^1 = y_i^0 + v_i \Delta t \qquad (47)$$

Next we test the compatibility in Equation (31) by substituting A from Equation (45) (replacing the coordinates in A^1 with their values from Equation 47), the strains from Equation (46), and a comparable relation for ε_y, and letting $\Delta A = A^1 - A^0$. Then Equation (31) is satisfied exactly, indicating that the expression for strain in Equation (46) meets the first compatibility requirement.

For use in the computer program, Equation (46) takes the form

$$\dot{\varepsilon}_x = \frac{u_{12} y_{13}^m - u_{13} y_{12}^m}{A^0 + A^1} \qquad (48)$$

and

$$\dot{\varepsilon}_y = \frac{v_{13} x_{12}^m - v_{12} x_{13}^m}{A^0 + A^1} \qquad (49)$$

for a triangle with nodes 1, 2, 3, and where the doubly subscripted velocities and coordinates have the following meaning

$$u_{ij} = u_i - u_j \qquad (50)$$

$$x_{ij}^m = x_i - x_j + 1/2 \left(u_i - u_j \right) \Delta t \qquad (51)$$

26

The above result is extended to the full quadrilateral by using the following definition of the strain rate

$$\dot{\varepsilon}_x = \frac{A_1^0 u_{1x}^0 + A_1^1 u_{1x}^1 + A_2^0 u_{2x}^0 + A_2^1 u_{2x}^1}{A_1^0 + A_1^1 + A_2^0 + A_2^1} \tag{52}$$

where subscript 1 refers to the triangle 123 and subscript 2 to triangle 134 in Figure 5. For satisfying Eq. (31) the area A is taken as one-half the denominator in Eq. (39), that is, the average of the areas at the beginning and end of the time increment.

For use in the computer program, Eq. (52) is recast into the following form with the aid of Eqs. (40) - (44), (50) and (51):

$$\dot{\varepsilon}_x = \frac{u_{13} y_{24}^m - u_{24} y_{13}^m}{A^0 + A^1} \tag{53}$$

Similarly

$$\dot{\varepsilon}_y = \frac{v_{24} x_{13}^m - v_{13} x_{24}^m}{A^0 + A^1} \tag{54}$$

$$\dot{\varepsilon}_{xy} = \frac{u_{24} x_{13}^m - u_{13} x_{24}^m + v_{13} y_{24}^m - v_{24} y_{13}^m}{2(A^0 + A^1)} \tag{55}$$

$$\dot{\omega}_{xy} = \frac{u_{13} x_{24}^m - u_{24} x_{13}^m + v_{13} y_{24}^m - v_{24} y_{13}^m}{2(A^0 + A^1)} \tag{56}$$

The requirement given by Eq. (32) is met somewhat more readily in the computer program. The values of $\dot{\varepsilon}_x$ and $\dot{\varepsilon}_y$ are first determined from

27

Eqs. (53) and (54), and the specific volume change is determined from calculations of the volume before and after a time step. The volume change is from a density calculation, which is in turn based on the mass conservation relations. The mass of an axisymmetric cell is computed from

$$M_s = \int_0^{2\pi} \frac{d\theta}{3} \sum_i A_i \sum_j y_{ij} = \frac{2\pi}{3} \sum_i A_i \sum_j y_{ij} \tag{57}$$

where A_i is the area of the ith triangle in the xy plane and y_{ij} are the radial positions of the vertices. For the planar cells, the mass is simply

$$M = \rho A_{xy} \tag{58}$$

Then during strain calculations, the density is determined by

$$\rho = \frac{M}{A_{xy}} \tag{59}$$

for example, using Eq. (58). The relative volume change required in Eq. (32) is then

$$\frac{\Delta V}{V} = \frac{2(\rho_1 - \rho_2)}{\rho_1 + \rho_2} \tag{60}$$

where ρ_1 and ρ_2 are densities before and after the current time increment. With $\dot{\epsilon}_x$, $\dot{\epsilon}_y$, and $\Delta V/V$ known, $\dot{\epsilon}_z$ is obtained from Eq. (32), and the volume constraint is satisfied exactly.

The rotation quantities, $\dot{\omega}_{xy}$ in Eqs. 38 and 56, represent the average of the instantaneous rotation rates of lines in the x and y directions. These quantities are used in the code to compute several rotation factors:

- Average rotation of the cell material, θ

- Transformation of the stress tensor to account for the material motion during each time interval.

- Rotation of specific material planes occurring in the fracture models BFRACT and SHEAR and in the composite model REBAR.

These rotation calculations are derived in Appendix D.

F. Energy Computation in the Code

The internal energy is computed from the conservation of energy equation at two points in the program. First, an estimate of the energy is made just preceding the stress calculation; then a refined value is obtained following the stress calculation. This approximation procedure is required because energy depends on stresses, yet the stresses depend on the energy. However, for general constitutive relations, stress and energy cannot be readily computed simultaneously. For the usual calculation in which energy varies slowly, this energy approximation gives satisfactory accuracy.

The estimate of energy at the time t^n is made by approximating the strain energy that is generated during the time step. In C-HEMP the first internal energy calculation immediately follows the determination of density and strain, but the only stresses available are T_{ij}^{n-1}, those from the previous time t^{n-1}. The first estimate then is

$$
E_{est} = E^{n-1/2} + \frac{V}{2} \left(T_{xx}^{n-1} \, \Delta\varepsilon_{xx}^{n-1/2} + T_{yy}^{n-1/2} \, \Delta\varepsilon_{yy}^{n-1/2} + 2T_{xy}^{n-1} \, \Delta\varepsilon_{xy}^{n-1/2} \right) \quad (61)
$$

where E^n, $E^{n-1/2}$ = internal energies at the times t^n and $t^{n-1/2}$, V = specific volume, T_{ij}^{n-1}, $\Delta\varepsilon_{ij}^{n-1/2}$ = stress and strain increment tensor elements. Equation 61 is the form for the planar problem. The sign convention in Eq. 61 reflects the fact that both stresses and strains are positive in tension.

29

Following the stress computation, the energy computation is repeated, but the calculation is made at time $t^{n+1/2}$, and modified to ensure exact energy conservation. We require that the external energy increments - external work on the boundaries and chemical energy additions for explosives - equal the changes in kinetic and internal energies. The external energy increment is

$$\Delta E^n_{TOT} = 1/2 \sum_{bound.} \left(U^{n+1/2}_i + U^{n-1/2}_{io} \right) F^n_i \Delta t^n + \Delta E^n_{add} \qquad (62)$$

where T^n_i are tractions on the ith nodes along the boundary. The kinetic energy change is simply

$$\Delta E^n_{kin} = 1/2 \sum_i m_i \left[\left(U^{n+1/2}_i \right)^2 - \left(U^{n-1/2}_i \right)^2 \right]$$

$$= 1/2 \sum_i m_i \left(U^{n+1/2}_i - U^{n-1/2}_i \right) \left(U^{n+1/2}_i + U^{n-1/2}_i \right)$$

$$= 1/2 \sum_i F^n_i \Delta t \left(U^{n+1/2}_i + U^{n-1/2}_i \right)$$

$$= 1/2 \left[\sum_{bound} F^n_i \Delta t \left(U^{n+1/2}_i + U^{n-1/2}_i \right) \right.$$

$$\left. + \sum_{internal} F^n_i \Delta t \left(U^{n+1/2}_i + U^{n-1/2}_i \right) \right] \qquad (63)$$

Now we form the energy balance.

$$\Delta E^n_{TOT} = \Delta E^n_{kin} + \Delta E^n_{int'l} \qquad (64)$$

and write the internal energy change as

$$\Delta E^n_{int'l} = \Delta E^n_{TOT} - \Delta E^n_{kin}$$

$$= \Delta E^n_{add} - 1/2 \sum_{internal} F^n_i \, \Delta t_n \left(U^{n+1/2}_i + U^{n-1/2}_i \right) \qquad (65)$$

Here we note that the sum over the boundary nodes in Eq. 63 is just the external work term in Eq. 62, so these terms cancel in Eq. 65. The internal energy that is stored in the main arrays for the jth cell is computed as

$$E^{n+1/2}_j = E^{n-1/2}_j + \Delta E^n_{j,add} - 1/2 \sum_{jth \ cell} F^n_i \, \Delta t^n \left(U^{n+1/2}_i + U^{n-1/2}_i \right) \qquad (66)$$

The estimated energy E^e_{est} is computed in CYCLE before the stress calculations. $\Delta E^n_{j,add}$ is derived during the stress calculations. CFORCE calculates the cell forces F^n_i within each cell in preparation for the nodal motions in CYCLE. Then, following the motion calculations in CYCLE, $E^{n+1/2}_j$ is computed.

F. Artificial Viscous Stress

An artificial viscous stress is required in finite-difference wave propagation calculations to smooth out shock waves so that the entire flow field can be treated by the conservation equations of continuous flow. In multidimensional calculations, a triangular artificial viscous stress is also required to combat certain types of cell distortion. Here we describe first the standard artificial viscosity and its implementation in the code.

The artificial viscous stress (Q) is added to the thermodynamic equilibrium stress (σ) from the constitutive relations to produce the nonequilibrium mechanical stress (T). The mechanical stress is therefore the total stress acting between masses and is the appropriate stress for the momentum calculations exhibited earlier. The artificial viscous stress represents real stresses occurring in the nonequilibrium states of a shock front, but the basis for computing Q is artificial

31

because it depends on the computational cell size and on viscosity coefficients that are not derived from physical processes.

In C-HEMP the usual linear and quadratic forms of artificial viscosity are provided. Both are related to the rate of compression of the material and are zero while the material is extending. For one-dimensional calculations the linear and quadratic stresses are:

$$Q_L = C_L C_s \, \Delta X \, \frac{\partial \rho}{\partial t} \tag{67}$$

$$Q_Q = C_Q^2 \, \rho \, \left(\frac{\Delta X}{\rho} \frac{\partial \rho}{\partial t}\right)^2 \tag{68}$$

for $\partial \rho / \partial t > 0$. In these equations C_L and C_Q are coefficients of the linear and quadratic artificial viscosities, and C_s is the local sound speed. If $\partial \rho / \partial t$ is negative, then Q_L and Q_Q are zero. It is common to replace one derivative $\partial \rho / \partial t$ in the quadratic expression with an equivalent expression from the Eulerian form of mass conservation in one dimension:

$$\frac{1}{\rho} \frac{\partial \rho}{\partial t} = - \frac{\partial U}{\partial X} \tag{69}$$

Then the combined expression for Q, obtained by summing Eqs. 67 and 68, and accounting for Eq. 69, is

$$Q = \Delta X \, \frac{\partial \rho}{\partial t} \left[C_L C_s + C_Q^2 \, |\Delta U| \right] \quad \frac{\partial \rho}{\partial t} > 0 \tag{70}$$

and we have approximated $\partial U / \partial X$ as $\Delta U / \Delta X$.

For two-dimensional problems we use $\sqrt{A_{xy}}$ in place of ΔX, the cell dimension, and recast Eqs. 67 and 68 in difference form:

$$Q_L = C_L C_s \, \sqrt{A_{xy}} \, \frac{\Delta \rho}{\Delta t} \tag{71}$$

32

$$Q_Q = C_Q^2 \frac{A_{xy}}{\rho} \left(\frac{\Delta\rho}{\Delta t}\right)^2 \qquad\qquad (72)$$

for $\Delta\rho > 0$.   The artificial stress Q is the sum of the linear and quadratic contributions from Eqs. 71 and 72.

The nominal values of the artificial viscosity coefficients are $C_L = 0.15$, and $C_Q^2 = 4.0$. These values are appropriate for most problems. If sharper definition of shock fronts is required, C_L could be reduced to as low as 0.05. For more rapid smoothing of wave fronts for quasi-static problems, C_L could be increased up to 0.5.

The triangular artificial viscous stress is used to minimize a type of cell distortion termed hour-glassing (shown in Figure 6). Hour-glassing is a parasitic behavior that is not corrected by the normal momentum, strain, and constitutive relations previously outlined. The motion shown in Figure 6 gives rise to zero values of $\Delta\varepsilon_{xx}$, $\Delta\varepsilon_{yy}$, and $\Delta\varepsilon_{xy}$. Hence, no stresses caused by these strains arise to correct the hour-glassing motion. Also, any of the usual cell-centered stresses acting on the coordinates would be applied equally to all four coordinates and could not simultaneously pull inward on points 1 and 2, and push out on 3 and 4 to correct the behavior.

The hour-glassing motion in quadrilateral cells represents two additional degrees of freedom that arise because of the averaging process used in calculating the strains (Section II-D). A triangular cell does not exhibit hour-glassing because the three coordinate points have just six degrees of freedom that can be represented by two rigid body translations, one rotation (ω_{xy}) and three strains. The quadrilateral cell has eight degrees of freedom, but only the same six motions and strains as for the triangular cell are accounted for in the equations that provide the resistance to the motions. The triangular artificial viscosity provides resistance to the hour-glassing motion that arises because of the extra degrees of freedom.

The anti-hour-glassing forces are computed to be proportional to the hour-glassing velocities, and directed in the opposite sense. The

33
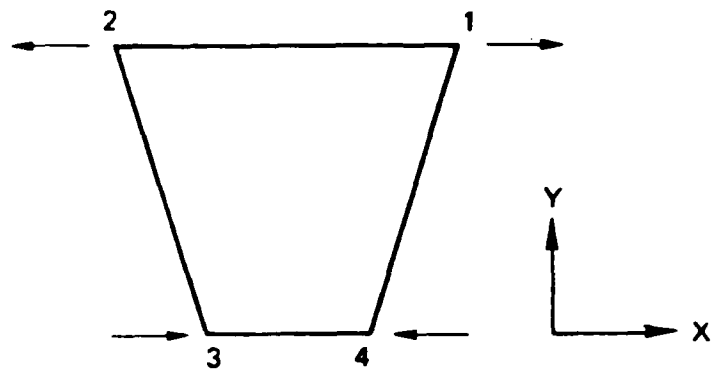
(a) A Quadrilateral with Coordinate Velocities
that Lead to Hour-Glassing
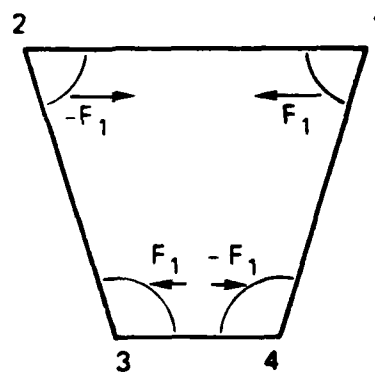
(b) Orientation of Hour-Glassing Forces
for the X-direction

MA-6802-18A

FIGURE 6 APPEARANCE OF A QUADRILATERAL UNDERGOING
HOUR-GLASS DISTORTION, PLUS THE RESTORING
FORCES PROVIDED BY THE CODE

34

general form of these restoring forces was given by Steven Hancock [Ref. 20]. The hour-glassing velocities U_H and V_H are given by the X and Y velocities of the four nodes as follows:

$$U_H = U_1 - U_2 + U_3 - U_4 \tag{73}$$

$$V_H = V_1 - V_2 + V_3 - V_4 \tag{74}$$

Then the hourglassing forces are

$$F_{HX} = \frac{T_H \, Z \, \overline{\Delta X}^2 U_H}{4(\overline{\Delta X}^2 + \overline{\Delta Y}^2)\Delta t} \tag{75}$$

and a similar expression for F_{HY}. T_H is a dimensionless coefficient, Z is the node mass, $\overline{\Delta X}$ and $\overline{\Delta Y}$ are representative cell dimensions, and Δt is the time step. The forces applied on the four nodes are

$$F_{H1x} = F_{HX}$$

$$F_{H2x} = - F_{HX}$$

$$F_{H3x} = F_{HX}$$

$$F_{H4x} = - F_{HX}$$

as indicated in Figure 6b. With this pattern of forces, there is force equilibrium and no change of momentum. These forces are simply added to the other nodal forces caused by the strains or boundary conditions.

The coefficient T_H should be a small fraction to appropriately correct hour-glassing. Hancock [Ref. 20] recommends using a T_H value of 0.05. With this value, there are small restoring forces on each cycle to eliminate the hour-glassing motion. An initialized hour-glass

velocity pattern would be eliminated in about 30 time steps. This small coefficient will minimize hour-glassing but not overly impede this motion (which occurs naturally in regions of high shear strains and high shear strain gradients) when it is required by the conditions of the problem. The factor T_H is TSR(M) in the code.

G. Time Step Control and Stability Conditions

The time step used in the integration of the wave propagation equations is determined within the code based on stability conditions. Two time step calculations are made, and the minimum of the two provides the time increment actually used. Here we present first the time step based on the Courant condition and later the one based on the stability considerations for the artificial viscosity.

The Courant condition requires that the computational time step not exceed the time for stress waves to cross a cell. Thus the time step is

$$\Delta t < \frac{\Delta X}{C} \tag{76}$$

where ΔX is the cell dimension and C is the sound speed. This condition is required for stability of wave propagation calculations in which an explicit solution method is used, as in HEMP.

The time step control procedure is derived below, including

- Expansion of the Courant stability condition to allow treatment of general, time-dependent stress-strain relations and the artificial viscous stress.

- Addition of a convective term, which is especially important in regions of large distortion and wherever particle velocity is comparable to sound speed.

- Extension of the Courant condition and convective correction from the usual one-dimensional form to a two-dimensional form.

- An alternate stability condition based on growth of disturbances by the artificial viscosity.

36

Courant Stability Condition. For one-dimensional hydrodynamic calculations, a fairly full investigation of the Courant condition has been undertaken by Richtmyer and Morton[21] and by Herrmann et al.[22] However, a further development is required for a situation in which more general, time-dependent, stress-strain relations are included in one- or two-dimensional calculations.

Here a new concept for stability is developed based on the hypothesis that all forms of stability depend simply on an effective sound speed. The addition of artificial viscosity or other types of viscosity tend to require shorter time steps in the calculations because they increase the effective sound speed. This effective sound speed is related to an effective modulus for the material as follows:

$$M_e = \frac{\Delta P + 2Q}{-\frac{\Delta V}{V}} + \frac{2/3 \, \Delta \sigma_i'}{\varepsilon_i - \frac{\Delta V}{3V}} \tag{77}$$

where

ΔP = the change in pressure at a given cell during the current time increment

Q = the artificial viscous stress

$\frac{\Delta V}{V}$ = the relative change in volume

$\Delta \sigma_i'$ = the change in deviator stress

ε_i = the strain in the ith direction.

The factor 2 with Q is used because the Q is computed at $\Delta t/2$, providing twice the stiffness that would occur if M_Q were averaged over the time interval.

37

First a calculation is made for the one-dimensional problem to compare the results from the hypothesis above with that of the more usual approach followed by Herrmann, et al [Ref. 22]. Referring back to Eqs. 67 and 68 for Q, we can define a modulus as in Eq. 74; that is,

$$M_Q = \frac{2Q}{-\Delta V/V} = \frac{2Q}{\Delta\rho/\rho} = 2\left[C_L C_s \sqrt{A_{xy}}\, \rho/\Delta t + C_Q^2\, A_{xy}\, \Delta\rho/(\Delta t)^2\right] \tag{78}$$

Then the effective sound speed that will govern stability of the calculations is from Eqs. (77) and (78)

$$\bar{c}^2 = \frac{M_e}{\rho} = \frac{\Delta\rho}{-\rho\,\frac{\Delta V}{V}} + \frac{2Q}{-\rho\,\frac{\Delta V}{V}} + \frac{2/3\,\Delta\sigma_i'}{\rho\left(\epsilon_i - \frac{\Delta V}{3V}\right)} \tag{79a}$$

$$= \frac{K}{\rho} + \frac{M_Q}{\rho} + \frac{4/3\,\mu}{\rho} \tag{79b}$$

$$= c^2 + 2\left(C_Q^2\,|\Delta U| + C_L c\right)\frac{\Delta X}{\Delta t} \tag{79c}$$

where

    K = bulk modulus

    μ = shear modulus

    C = the usual sound speed based on these moduli.

Now let us examine whether Eq. 79 will determine a stable time step by comparing this result with those of Herrmann, et al [Ref. 22]. For stable calculations, the Courant-Friedrichs-Lewy condition (Eq. 76) is used to determine the time increment permitted. The sound speed C used in Eq. 76 is taken here as the effective sound speed from Eq. 79. Insertion of Eq. (79) into relation (76) gives

$$\Delta t^2 \leq \frac{\Delta X^2}{C^2} = \frac{\Delta X^2}{C^2 + (c_Q^2 |\Delta U| + c_L C) \frac{\Delta X}{\Delta t}} \tag{80}$$

When this quadratic is solved for the maximum time increment, the criterion is found to be

$$\Delta t \leq \frac{\Delta X}{C} \left[- \left(c_Q^2 \left| \frac{\Delta U}{C} \right| + c_L \right) + \sqrt{\left(c_Q^2 \left| \frac{\Delta U}{C} \right| + c_L \right)^2 + 1} \right] \tag{81}$$

This expression is identical to that found on page 73 of Reference 22. Hence the new concept does appear to give the correct stability criterion for one-dimensional flow.

For multidimensional problems, the last term in Eq. (79a) is taken as the maximum of the values in the three principal directions. An alternate, and simpler, course is to use the last term from Eq. (79b), with μ equal to the largest shear modulus. Then the effective sound speed is

$$C^{-2} = \frac{\Delta P + 2Q}{- \rho \frac{\Delta V}{V}} + \frac{4\mu_{max}}{3\rho} \tag{82}$$

This criterion is sufficiently general for stress relaxation and other time-dependent stress-strain relations.

Particle Velocity (Convective) Effective in One Dimension. In the time step algorithm used here, we introduce a convective term to account for the fact that ΔX changes size during the time step. In small-disortion problems, this correction is unnecessarily meticulous, but it is vital in preventing the cell tangling that occurs in large-distortion problems. Cell tangling occurs when any node of a quadrilateral moves through an opposite side. Such motion can have no physical meaning in a

continuum, so the physical relevance of the calculation ceases at that time.

The convection calculation begins with the Courant condition (Eq. 76). Here ΔX is rewritten as the average cell dimension during the time step. That is,

$$\Delta t = \frac{\Delta X}{C} = \frac{X_2^{n+1} + X_2^n - X_1^{n+1} - X_1^n}{2C} \tag{83}$$

The cell extends from X_1 to X_2. The superscripts n and n+1 refer to time increments such that $t^{n+1} - t^n = \Delta t$. The locations at the n+1 time are replaced by using the velocity relation:

$$X^{n+1} = X^n + U^{n+1/2} \Delta t \tag{84}$$

where $U^{n+1/2}$ is the particle velocity at $t^n + \Delta t/2$. Then Eq. (83) becomes

$$\Delta t = \frac{X_2^n - X_1^n + 1/2 \left(U_2^{n+1/2} - U_1^{n+1/2} \right) \Delta t}{C}$$

Combining the Δt terms, we obtain

$$\Delta t = \frac{X_2^n + X_1^n}{C\left(1 - \frac{U_2^{n+1/2} - U_1^{n+1/2}}{2C} \right)} \tag{85}$$

In the denominator this expression for Δt contains the convective correction $\Delta U/C$, which characterizes the cell compression during the time interval.

Crossing Time and Convective Effect in Two Dimensions. A two-dimensional geometry is examined here to determine the effective cell dimension ΔX for Eqs. (76) or (85) and the convective correction $\Delta U/C$. For a quadrilateral cell, the minimum distances for waves to travel are from a node to an opposite side. The eight possible minimum paths for a general quadrilateral are shown in Figure 7. Some perpendiculars from the nodes to the sides, such as a and b, lie outside the cell; in this case the minimum path is the side 1-2. If the interior angle at a node such as 1 is greater than 90°, then perpendiculars from adjacent nodes (2 and 4) to sides intersecting at 1 will lie outside the cell (perpendiculars b and h). The paths are therefore computed by calculating the interior angle for each node and then the two paths pertaining to that node. After the paths are determined, the relative velocity along each path is found. Then the time step is computed from Eq. (85).

The computation of the minimum crossing distance ΔX and the convective correction $\Delta U/C$ requires calculation of the following quantities:

- The lengths of the sides of the quadrilateral.

- The angles between the sides of the quadrilateral at each joint.

- The relative velocity in the direction of a side.

- The perpendicular distance from a node to a line.

- The relative velocity along the perpendicular distance between a node and a line.

The derivations, which are not included here, are all readily performed by treating the quadrilateral sides and other lines as vectors and using dot or cross products.

Time Step Criterion Based on Artificial Viscosity. The second stability criterion is based on maintaining a time step that does not cause growth of the particle velocity. Let a change in velocity associated with Q be $\Delta U'$. Then the momentum equation gives the following:

41
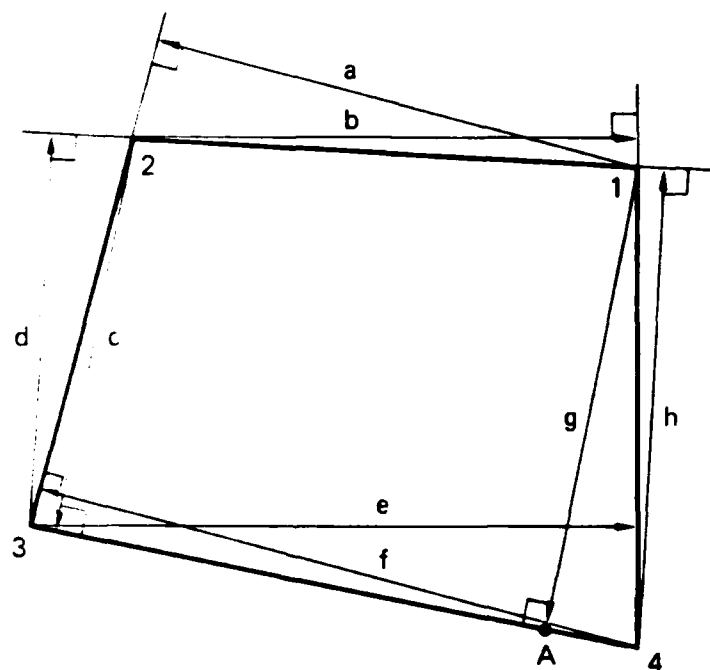
MA-7893-135

FIGURE 7   MINIMUM WAVE PATHS FOR A QUADRILATERAL CELL

42

$$\Delta U' = \frac{2Q\Delta t}{m} \tag{86}$$

And Q is computed as usual from the following relation to velocities:

$$Q = C_L C_s \Delta X \frac{\partial \rho}{\partial t} + C_Q^2 \rho \left(\frac{\Delta X}{\rho} \frac{\partial \rho}{\partial t}\right) \tag{87}$$

Replace $\partial \rho / \partial t$ as follows:

$$\frac{1}{\rho} \frac{\partial \rho}{\partial t} = - \frac{\partial U}{\partial X} \tag{88}$$

Then the expression for Q becomes:

$$Q = C_L C_s \rho \, |\Delta U| + C_Q^2 \rho \, (\Delta U)^2 \tag{89}$$

Now consider a small change in velocity to $\Delta U + \varepsilon$. Then Q will be

$$Q_\varepsilon = \rho \left[C_L C_s \, (|\Delta U| + \varepsilon) + C_Q^2 (\Delta U + \varepsilon)^2 \right] \tag{90}$$

Now presume that the change in velocity is dependent only on the force Q. Then compute the alteration in ΔU associated with Q_ε.

$$\Delta U' = \frac{2\Delta t \rho}{m} \left[C_L C_s \, (|\Delta U| + \varepsilon) + C_Q^2 (\Delta U + \varepsilon)^2 \right] \tag{91}$$

$$= \frac{2\Delta t \rho}{m} \, |\Delta U| \, (C_L C_s + C_Q^2 \, |\Delta U|)$$

$$+ \frac{2\Delta t \rho}{m} \left[C_Q^2 \, |\Delta U| + C_L C_s \, \varepsilon + 2 C_Q^2 \, |\Delta U| \, \varepsilon + C_Q^2 \varepsilon^2 \right]$$

43

$$= \Delta U' + \varepsilon'$$

If we neglect terms in ε^2, then ε' is

$$\varepsilon' = \frac{2\Delta t \varepsilon}{\Delta X} \left(C_L C_s + 2C_Q^2 \ |\Delta U| \right) \tag{92}$$

For stability, we require that ε' be less than ε.   That is,

$$\Delta t = \frac{\Delta X}{2C_L C_s + 4C_Q^2 \ |\Delta U|} \tag{93}$$

This equation for Δt is used as an alternate stability criterion to that in Eq. 85.

H.   Rezoning of the Mesh Configuration

One frequently encounters problems with large mesh distortions in Lagrangian finite difference calculations. In the penetrator problem shown in Figure 8, the cells in the target immediately below the penetrator get progressively thinner in the direction of impact because they expand laterally. These cell distortions cause two problems in the code calculation:

(1)   The minimum crossing time for the cell leads to a small stable computational time step.

(2)   Non-square cells give an inaccurate description of the material behavior.

One remedy to the cell distortion is to rearrange or rezone the mesh as shown in Figure 9. The computational mesh has been moved so that it describes the material better. We note that the new cell B now contains some of the material that before the rearrangement was contained in cells A, B, E, and F. A second means of minimizing the

44
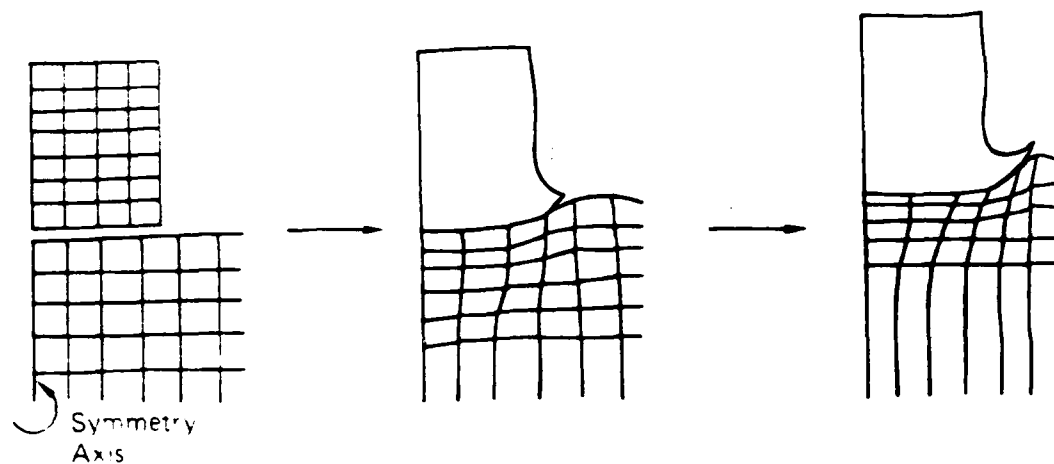
JA-6423-5A

FIGURE 8   A SHORT ROD PENETRATOR IMPACTING A SURFACE

The cells in the target become progressively distorted.

(a)

(b)
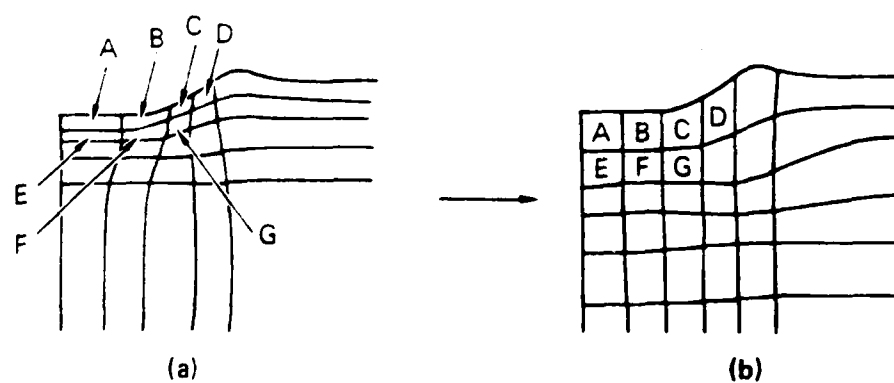
JA-6423-6A

FIGURE 9   CELL CONFIGURATION BEFORE (a) AND AFTER (b)
REZONING

distortion is to restrict the relative motion of some nodes. Both methds are used in C-HEMP. The second method is outlined briefly at the end of this subsection.

Rezoning or rearrangement of the mesh in Lagrangian codes may be either discrete or continuous. For a discrete rezoner, the wave propagation calculation is halted at a predetermined time or when some rezoning criterion has been reached. Then the old mesh is overlaid with a completely new one. The rezoning is handled by a separate computer program. This rezoning program writes a restart file based on the new mesh and the wave propagation simulation is restarted from that file.

In penetration calculations, the mesh distortion may progress very fast and discrete rezoning like that mentioned above can grow intolerably time consuming. We have therefore developed an automatic rezoner that rearranges the mesh as a part of the wave propagation calculation and does not require user intervention during the computation. An automatic rezoner has to limit its rezoning considerations to local conditions to give a tractable problem. It therefore usually gives less improvement than overlaying the old mesh with a completely new one. It makes small changes in some of the coordinate locations at regular intervals, rather than moving all coordinate locations at a few discrete times during a wave propagation problem. From our review of rezoners used with STEALTH, TOODY, and HEMP, the continuous rezoner was selected as being more reliable, requiring less programmer intervention in running a problem, and being easier to write. (The disadvantage of the continuous rezoner is that it tends to smear properties more than a discrete rezoner does.)

The basic principle of the rezoning algorithm is illustrated in Figure 10. We have a node 1 with eight neighbors, nb1-8. Several of the cells around the node have a small time step that can be enlarged by relocating the node to a more central position like the configuration to the right. The rezoner examines the cell configuration around node 1 and tests to see whether a shift of the node position will improve the time step. If so, the node is shifted. Then the properties of the new

46

(a) Old Configuration

(b) New Configuration

(c) Enlargement of New Quadrilateral A' Showing
How it Includes Areas from all Four Original
Quadrilaterals
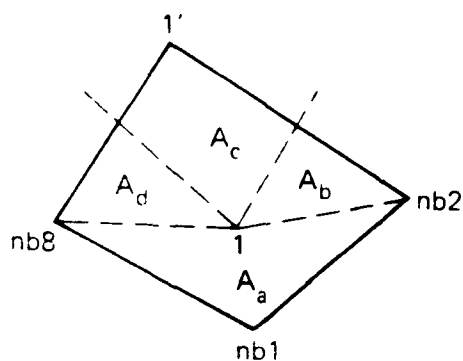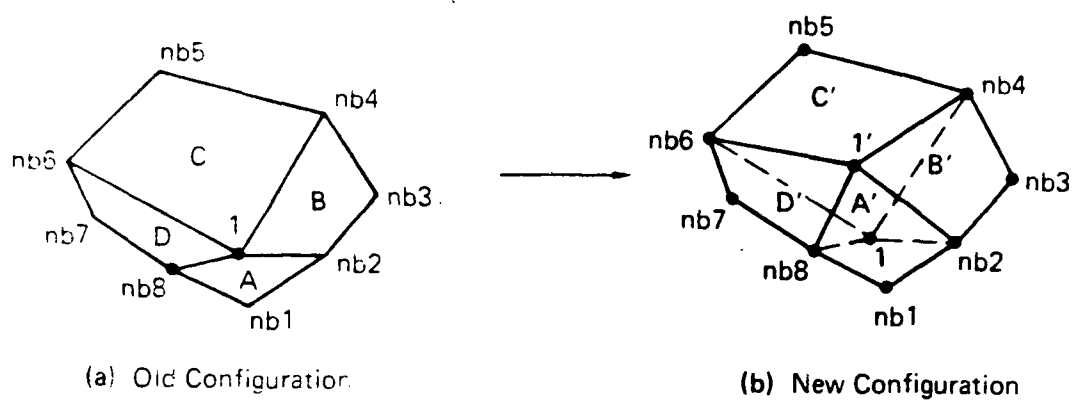
JA-6423-7B

FIGURE 10   NOTATION FOR FOUR CELLS AND EIGHT NEIGHBORING
NODES SURROUNDING NODE 1

47

cells are computed from the properties of the old cells. Described
below are the sequence for testing each nodal position, tests for
examining the cell configuration, the procedure for allocating stresses
and other properties to the newly configured cells, and the system for
computing velocities so that momentum is conserved.

The sequence for scanning the nodes for possible rezoning occurs
over four standard computational cycles. Following the first cycle, all
odd-numbered nodes are scanned. After the second cycle, even-numbered
nodes are scanned. After the third and fourth cycles, odd- and even-
numbered nodes, respectively, are scanned starting with the last node
and proceeding toward the first. The frequency of this four-cycle scan
of all the nodes is controlled by an input parameter NFREQ.

When each interior node (such as node 1 in Figure 10) is scanned, a
new nodal position 1' is computed at the centroid of the polygon formed
by the eight neighbors nb1-nb8. (An algorithm that computes the posi-
tion of 1' from the mean rather than the centroid gives a considerably
worse result in certain difficult cases.) If the time step of the new
configuration is smaller than for the old one, we will iteratively try
positions nearer to the old node position a certain number of times. If
it is not possible to find a position with a better time step, no
operation is done and the node is left as it is. The test for an
increase in the natural time step is essential to avoid situations in
which the move toward the centroid would actually produce a smaller time
step. For example, if the neighbor polygon is half-moon shaped, the
centroid may actually lie outside the polygon; then moving the node to
the centroid would produce cell inversions. This algorithm for calcu-
lating the new node position has been implemented in the program and
tested to verify that it does improve the mesh configuration. This
simple iterative procedure was used because we could not derive an
analytical expression for the optimum position in a mesh of arbitrary
shape.

For a boundary node, we relocate the node to the mean of the
positions of its two neighbors along the boundary. That is, if nb4 in

48

Figure 10 were the boundary node to be rezoned, the node would be moved along a line parallel to nb3-nb5 and passing through nb4. This motion conserves the area on each side of the boundary. As for interior nodes, the node motion is tested to ensure that it produces an increase in the time step.

Having determined the new nodal position, we go on to calculate the new cell and node data. We take the view that we move the logical mesh, but the physical material stays in the same place. This means that a new cell will represent the properties of portions of several old cells, generally. We solve this problem by letting the old cells that are covered by the new cell contribute to the new cell properties in a mass-weighted fashion.

The area of the cell A' in Figure 10c is composed of the partial areas A_a, A_b, A_c, A_d, where A_a is the intersection of new cell A' and old cell A and so on. The volume corresponding to the partial area A_a is V_{aa}, A_b is V_{ab}, and so on. In plane symmetry $V_{aa} = A_a$; in cylindrical symmetry V_{aa} is the volume of a toroid with cross-sectional area A_a. The new mass M_a' of cell A' is

$$M_a' = D_a V_{aa} + D_b V_{ab} + D_c V_{ac} + D_d V_{ad} \tag{94}$$

where D_a is the density of the old cell A. The other cell variables are computed by mass weighting. For instance, the new pressure of cell A' is

$$P_a' = (M_{aa} P_a + M_{ab} P_b + M_{ac} P_c + M_{ad} P_d)/M_a' \tag{95}$$

where $M_{aa} = D_a V_{aa}$, $M_{ab} = D_b V_{ab}$, P_a is the pressure of old cell A, P_b is the pressure of old cell B, and so on. Doing this for each of the new cells A', B', C', D', we obtain the properties of the new cells. We note that the internal energy is conserved exactly by this treatment.

49

The node quantities we need to calculate are the node mass and velocity. The node mass is calculated the same way it was calculated when the mesh was originally generated: each cell contributes a fraction of its mass to each of the four nodes that define it. The velocities of the eight neighbors are simply left as they are and the new velocity of the center node is calculated from momentum conservation. This procedure usually does not conserve the kinetic energy. To partially account for this energy change, the kinetic energy change (usually a loss) is computed and added in a mass-weighted way to the internal energy of the cells A', B', C', D'.

Relocating a boundary node poses some special geometric problems. However, we use the same basic method of mass weighting and calculating the new node velocity from momentum conservation as for interior nodes.

The motion-restricting procedure for minimizing cell distortion is illustrated in Figure 11. Node 3 has almost collapsed onto side 1-4. To prevent further cell distortion or even penetration of the side, the motion of node 3 is restricted. In the controlled condition, node 3 cannot move closer to side 1-4 than the control line which is parallel to the side. Hence the motion of node 3 tends to follow the motions of nodes 1 and 4. For this collapsed cell, the distance between node 3 and side 1-4 is not used in the time step calculation. This collapsed-cell feature certainly introduces a non-physical rigidity into the material motions. But when these collapsed cells appear far from the region of main interest, they have little effect on the computed results. This provision does allow the calculation to continue with a reasonable time step, instead of halting because of excessive cell distortion.

I. Slide Line Treatment

A slide line is provided to permit relative shearing and relative normal motion between two objects or between two parts of an object. As an example of the use of a slide, Figure 12 shows two materials in contact undergoing a relative shearing motion. After some deformation with no slip along the interface as in Figure 12(b), there are severe

Control Line

4   3   1   2
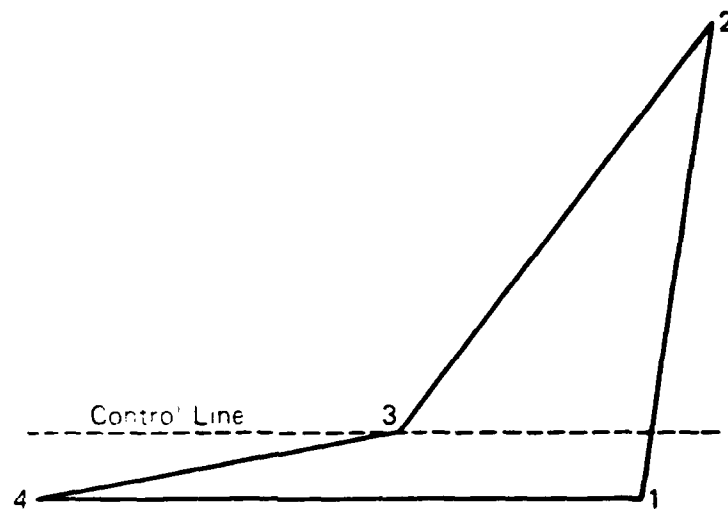
JA-314532-150

FIGURE 11   QUADRILATERAL IN WHICH ONE NODE HAS ALMOST
COLLAPSED ONTO AN OPPOSITE SIDE

51
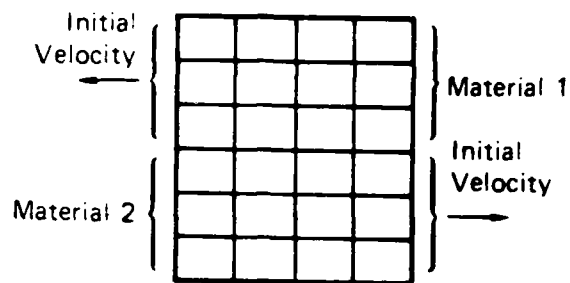
(a) Initial Configuration
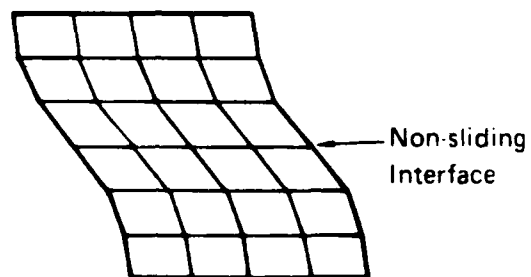
(b) Deformation with no Slide Line
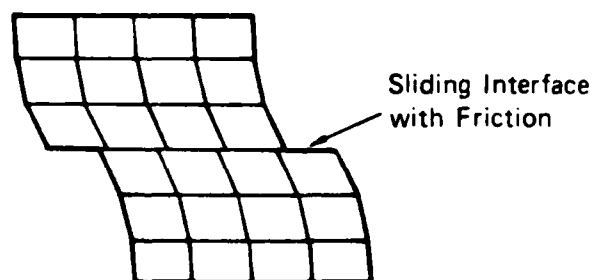
(c) Deformation with a Slide Line that has a
Frictional Coefficient

JA-6423-1A

FIGURE 12   TWO TREATMENTS OF AN INTERFACE BETWEEN TWO
MATERIALS UNDERGOING RELATIVE SHEAR DISTORTION

52

distortions of both materials near the interface. Figure 12(c) shows the deformation at some later time when there is a slide line with friction between the two materials. Inclusion of the slide line permits a more physically accurate treatment of the motion in this case.

Relative normal motion across a slide line is illustrated by the impact problem in Figure 13. The round object is not initially in contact with the flat surface, but as the simulation proceeds a contact line develops between them. The configuration of the objects makes it impossible to describe the materials with one single mesh. Sliding as well as normal motion may be permitted along the slide line.

The present slide line treatment allows the interaction of one master and one slave line of nodes. There is no provision for the simultaneous interaction of three objects, and thus, three lines of nodes. Also, the slide line is predesignated by the user: it cannot be allowed to develop gradually (to unzip). We believe that the present slide line development readily allows for the inclusion of these advanced sliding features.

The slide line method permits shearing resistance to the sliding, based on Coulomb friction and viscous drag. The Coulomb model provides a shearing resistance of the form:

$$\tau = C_0 + \sigma_n \, Tan(\phi) \tag{96}$$

where C_0 is the cohesion, σ_n is the normal stress, and ϕ is the internal friction angle. The viscous drag force is computed only when there is relative slip occurring between the two sides of the slide line. This viscous shear stress is

$$\tau = \eta \Delta U \tag{97}$$

where η is the coefficient of viscosity and ΔU is the relative velocity.

53
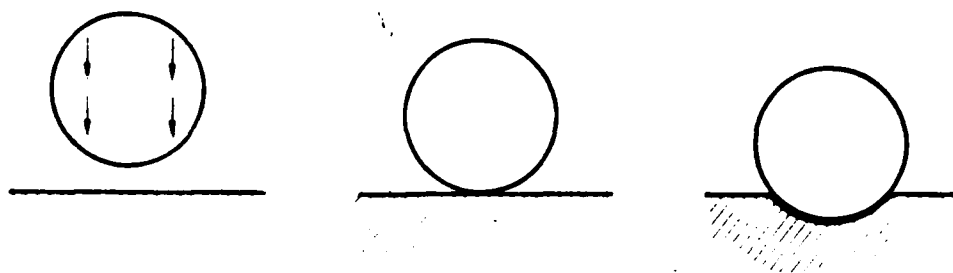
(a) A Sphere Impacting a Plane Surface
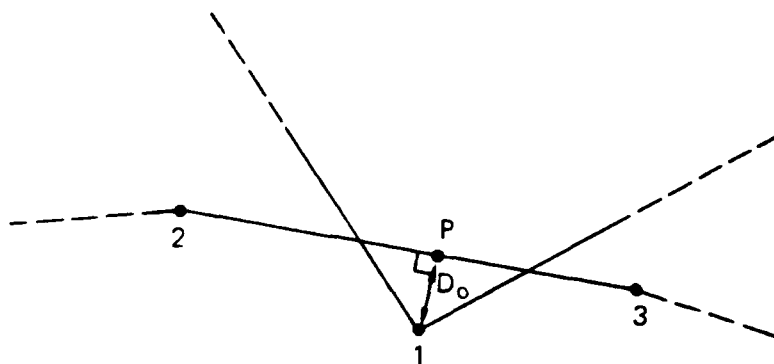
(b) Configuration of Nodes when Penetration is Detected
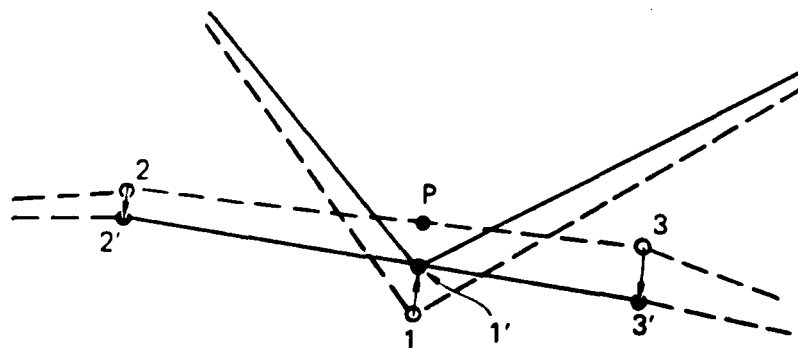
(c) Configuration of Nodes after Penetration is Removed

JA-6423-3B

FIGURE 13   SLIDE LINE INTERACTION FOR A CASE OF PENETRATION

54

The Method. The equations described here allow opening and closing of the slide line, sliding with viscous drag or friction, or sliding with free slip.

The basic idea behind the slide line algorithms is that the slide line nodes are first treated as if they were free surface nodes. Then we check whether the two sides of the slide line overlap, and if that is the case we displace the nodes so that the overlap disappears. This method does not require any special algorithms for void opening, making it easy to handle opening and closing of the slide line.

The first operation is to search for overlaps. We systematically examine for each node whether it is behind a line segment of the other side of the slide line, like in Figure 14. This is done for both sides of the slide line.

Having found that node 1 is behind the line segment defined by nodes 2 and 3 in Figure 14, we have to calculate the slide line inter-action between the three nodes. For this calculation, we restrict our attention to the penetration of node 1 through the line 2-3, and dis-regard that nodes 2 and 3 may have penetrated into material 1, or that our corrections to remove the penetration at 1 will cause penetrations elsewhere. We will here assume that this interaction between node 1 and line-23 can be separated into one component normal to the slide line that cancels the overlap and another component parallel to the slide line that involves the frictional or viscous forces. We will further assume that the normal direction is perpendicular to the line 2-3. We make these assumptions because they are simple and straightforward and are physically reasonable. In a more rigorous slide line model, the overlap could be cancelled, taking into account how the nodes are moving, possibly also the interface conditions, maybe even the constitu-tive models for the materials that border the slide line, but we feel that such a calculation is too complicated to be practical. The assump-tions above give us a manageable problem. We will first treat the displacements normal to the slide line and then go on to calculate the

55

changes in the motion parallel to the slide caused by any frictional or viscous interface model.

With these assumptions, node 1 will be moved to a point 1' on the line 2'-3' when the overlap is cancelled. P is the projection of 1 down on the line 2-3. Having assumed that all three nodes displace normal to the line 2-3 we need three equations to calculate the displacements. These are:

(1) Cancellation of the overlap

(2) Conservation of linear momentum

(3) Conservation of angular momentum.

If D_1 is the displacement of 1 to point 1' and D_p the displacement of P to 1', then the condition that the overlap D_o between points 1 and P should cancel gives us

$$D_1 - D_p = D_o \qquad (98)$$

where the minus sign is used because D_1 and D_p are in opposite directions.

Geometric requirements allow us to relate the displacement at P to the displacements D_2 and D_3 at points 2 and 3.

$$D_p = (1 - X_p) D_2 + X_p D_3 \qquad (99)$$

where X_p is the length of the line 2-P relative to the line 2-3. Combining Eqs. (98) and (99) to eliminate D_p, we obtain

$$D_1 - (1 - X_p) D_2 - X_p D_3 = D_o \qquad (100)$$

The forces, F_i, on the nodes that cause the displacements have to fulfill linear momentum conservation:

$$F_1 + F_2 + F_3 = 0 \qquad (101)$$

56

The third equation represents the conservation of angular momentum around node 2:

$$X_p F_1 + F_3 = 0 \qquad (102)$$

This gives us

$$F_3 = - X_p F_1 \qquad . \qquad (103)$$

Eliminating F_3 by combining (101) and (102) gives us

$$F_2 = - (1 - X_p) F_1 \qquad . \qquad (104)$$

A displacement D_i corresponds to a velocity change $V_i = D_i/\Delta t$, where Δt is the time step. A change V_i in velocity requires a force

$$F_i = M_i V_i/\Delta t = M_i D_i/(\Delta t)^2 \qquad (105)$$

where M_i is the node mass. Combining Eqs. (105) with (103) and (104), we write expressions for the displacements in terms of F_1.

$$D_1 = F_1 (\Delta t)^2/M_1 \qquad (106a)$$

$$D_2 = F_2 (\Delta t)^2/M_2 = - (1 - X_p) F_1 (\Delta t)^2/M_2 \qquad (106b)$$

$$D_3 = F_3 (\Delta t)^2/M_3 = - X_p F_1 (\Delta t)^2/M_3 \qquad (106c)$$

Inserting relations (106) into (100) gives an equation for F_1:

$$F_1 (\Delta t)^2/M_1 + (1 - X_p)^2 F_1 (\Delta t)^2/M_2 + X_p^2 F_1 (\Delta t)^2/M_3 = D_o \qquad (107)$$

or

$$F_1 = D_o/(\Delta t)^2/[1/M_1 + (1 - X_p)^2/M_2 + X_p^2/M_3] \qquad (108)$$

With the additional relations (103) and (104) for F_2 and F_3, we have complete specifications--for the changes in velocity and position of the three nodes--that cancel the overlap.

The displacements parallel to the slide line may be controlled by viscous or frictional forces or may be allowed to slip freely. If the user has specified free slip, the parallel motion calculations are complete at this point. For frictional resistance to sliding the frictional force is computed:

$$F_f = C_o L_s + F_n \ Tan(\phi) \qquad (109)$$

where C_o is a user-specified cohesion, L_s is the distance between nodes 2 and 3, F_n = MAX $(F_1, 0)$ is the normal force, and $Tan(\phi)$ is a user-specified coefficient of friction. We calculate the velocity difference parallel to the boundary, i.e., parallel to the line 2-3:

$$V_d = (1 - X_p) \ V_{p2} + X_p \ V_{p3} - V_{p1} \qquad (110)$$

where V_{pi} are the velocities parallel to the boundary. We calculate the forces it takes to cancel out V_d:

$$F_{d1} = V_d/D_t/[1/M_1 + (1 - X_p)^2/M_2 + X_p^2/M_3] \qquad (111)$$

$$F_{d2} = - (1 - X_p) \ F_{d1} \qquad (112)$$

58

$$F_{d3} = - X_p F_{d1} \qquad (113)$$

These relations can be derived analogously to relations (108), (103), and (104). If the frictional resistance F_f is greater than $\text{abs}|F_{d1}|$, the friction is strong enough to cancel the velocity difference and equations (111-113) stand as they are. If the friction force is less than $\text{abs}|F_{d1}|$ and the user has not specified a viscous model,

$$F_{d1} = F_f \, \text{sign} \, (V_d) \qquad (114)$$

and F_{d2} and F_{d3} are calculated from Eqs. (112) and (113). If the user has specified a viscous model, we calculate a viscous force:

$$F_v = A_v \, L_s \, |V_d| \qquad (115)$$

where A_v is a user-specified coefficient of viscosity. Similarly to the friction force above, we investigate whether $\text{abs}|F_{d1}|$ is greater or less than F_v. These friction and viscous forces are then added vectorially to the normal forces in (108), (103), and (112).

Because we correct the overlap immediately when we have found it as we search through the nodes, there is an order dependence in the algorithm. Therefore, we alternatingly search one side of the slide line first on one time step and the other side first on the next time step. We also search in one direction along the slide line on one time step and in the other direction on the next time step. To minimize the searching time for each node on the slide line, we store the number of the nearest node on the other side of the slide line at each time step. On the next time step, we start the search from that node proceeding in both directions along the slide line.

59

After the slide line calculations, the new node velocities and positions are calculated. This means the positions and velocities above were trial values using only the cell forces. The slide line forces are stored among the node data and then used in the final node calculation. For instance, for node 1 the X velocity and position are calculated as:

$$U_{xn} = U_{xo} + \left(F_{xc} + F_{xb} \right) \Delta t / M \qquad (116)$$

$$X_n = X_o + U_{xn} \Delta t \qquad (117)$$

where U_{xn} is the new velocity, U_{xo} is the old velocity, F_{xc} is the sum of the cell forces around node 1, F_{xb} is the sum of the slide line and other boundary forces on node 1, Δt is time step, and M is the node mass.

We note that the slide line calculations above are constructed such that the final positions do not give any overlap along the slide line in the ideal case. Because of interference between the various slide line calculations, this might not work our perfectly. Node number 1, for instance, may be involved in further slide line interactions that modify the force calculations we have already made. To obtain a perfect cancellation of the overlaps, one would have to solve all the slide line interactions simultaneously. Our experience has indicated that the present sequential algorithms are satisfactory in practical computation.

J. Finite-Element Numbering of Nodes and Cells

The storage of node, cell, and material information is handled in a manner which is unusual for finite-difference wave propagation codes. These unique features are briefly outlined here and provided in more detail in Appendix E.

All cell and node information is stored in a large one-dimensional array called COM1. Each cell has at least 18 storage locations assigned to it for storing mass, density, area, stresses, and indicators. Additional storage locations are provided in the same group by requesting

60

them in the input lines. For each node 24 storage locations are provided for node location, velocity, and indicators. A list of these quantities and their positions in the COM1 array are given in Tables E.1 and E.2 in Appendix E. The starting locations for cell and node storage are present in the LC and LN arrays. For example, information for the ith cell begins at location LC(i) in the COM1 array.

Similarly, all the material data available in the main arrays is in the COM2 array. This array contains the moduli, yield strength, density, material name, fracture quantities, and indicators for the model to be used. A list of these quantities and their positions in the COM2 array are given in Table 1. The starting location in the COM2 array for data for the mth material is LE(m), where LE is the locator array. The ESC array is equivalent to the constitutive property portion of the COM2 array, as shown. Usually these properties are passed to material models by providing the ESC array.

Table 1

VARIABLES IN COM2 ARRAY FOR EACH MATERIAL

Number	Location in COM1	Location in ESC	Name	Description
1	COM2(L)	–	WCMP(L)	Indicator for composite model
2	COM2(L+1)	–	WFR(L)	Indicator for fracture model
3	COM2(L+2)	–	WPOR(L)	Indicator for porous model
4	COM2(L+3)	–	WDS(L)	Indicator for deviator stress model
5	COM2(L+4)	–	WPR(L)	Indicator for pressure model
6	COM2(L+5)	–	WVAR(L)	Number of extra cell variables needed
7	COM2(L+6)	–	WTRI(L)	Indicator for triangular cells, unused
8	COM2(L+7)	–	WYAM(L)	Indicator for thermal strength, unused
9	COM2(L+8)	–	WEQS(L)	Number of ESC parameters allotted to material L
10	COM2(L+9)	ESC(L)	ESC(L)	Array for equation of state variables
10	COM2(L+9)	ESC(L)	RHO(L)	Initial density, g/cm^3
11	COM2(L+10)	ESC(L+1)	EQSTC(L)	Bulk modulus at zero pressure, dyn/cm^2
12	COM2(L+11)	ESC(L+2)	EQSTD(L)	2nd term in series for bulk modulus, dyn/cm^2
13	COM2(L+12)	ESC(L+3)	EQSTS(L)	3rd term in series for bulk modulus, dyn/cm^2
14	COM2(L+13)	ESC(L+4)	MU(L)	Shear modulus, dyn/cm^2
15	COM2(L+14)	ESC(L+5)	YAD(L)	Work hardening modulus, dyn/cm^2

Table 1 (Concluded)

16	COM2(L+15)	ESC(L+6)	RHOS(L)	Initial solid density, g/cm^3
17	COM2(L+16)	ESC(L+7)	AMAT(L)	Name for the material
18	COM2(L+17)	ESC(L+8)	EQSTG(L)	Grueneisen ratio
19	COM2(L+18)	ESC(L+9)		Coulomb friction coefficient
21	COM2(L+20)	ESC(L+11)	YC(L)	Initial yield strength, dyn/cm^2
22	COM2(L+21)	ESC(L+12)	EQSTE(L)	Sublimation energy, erg/g
23	COM2(L+22)	ESC(L+13)	EQSTH(L)	Grueneisen ratio for expanded states
24	COM2(L+23)	ESC(L+14)	EQSTN(L)	Exponent in equation for expanded states, EQSTC/(EQSTG * EQSTE * RHOS)
25	COM2(L+24)	ESC(L+15)	EMELT(L)	Melt energy, erg/g
26	COM2(L+25)	ESC(L+16)	EQSTA(L)	Coefficient of the 2nd term in the series for the Grueneisen ratio
27	COM2(L+26)	ESC(L+17)	EQSTV(L)	Exponent for determining the Grueneisen ratio in expanded state
28	COM2(L+27)	ESC(L+18)	SP(L)	Sound speed, cm/s
29	COM2(L+28)	ESC(L+19)	G2(L)	2MU(L), dyn/cm^2
30	COM2(L+29)	ESC(L+20)	PMIN(L)	Tensile pressure limit, dyn/cm^2
31	COM2(L+30)	ESC(L+21)	TSR(L)	Material parameters for hour glassing viscosity
36	COM2(L+35)	ESC(L+26)	BFR(L)	Array containing fracture parameters

Note: L = LE(m) for the m-th material. The LE array provides the starting location for material data in the COM2 array.

63

A finite-element numbering procedure is used for the nodes and cells to allow for flexible relationships between the cells and nodes.

With finite-element numbering, each cell and node is numbered independently of its position in the grid. This contrasts with the i, j-numbering common to most finite difference codes in which a fixed numbering relationship exists between each node or cell and its neighbors. This finite-element numbering allows a somewhat more flexible layout of cells in problems with complex shapes. It is essential for problems in which new cells or nodes are created as by wandering slide lines or by general rezoning (grid reconfiguration). The disadvantage is that the nodes around each cell and cells around each node must be individually designated because there is no automatic node-cell relationship as in the i,j-numbering system. Here we describe the indicator arrays required to show these relationships and then exhibit some cell layouts that are possible with the finite-element numbering.

At present the finite-element numbering procedure has been developed only for the case of quadrilateral cells. It is expected that triangular cells will be added later.

Adjacency Arrays. During layout, the nodes and cells are numbered in the order in which they are constructed. A partial node and cell numbering for a quadrilateral is shown in Figure 14. During layout three special arrays are constructed to provide the needed adjacency relationships. The WNOD array of four integers designates the nodes surrounding each cell. For cell 10 in Figure 14, the WNOD array is 12, 13, 8, and 7. The nodes are provided in counterclockwise order.

The neighboring nodes for each node and the cells around each node must be available to the rezoner; this information is stored in the WNDND and WCELL arrays. As an example, consider node 7 in Figure 14. The neighboring nodes are WNDND = 2, 6, 12, and 8. WCELL stores the cell-variable location coordinate (LC value) for the cells 1, 9, 10, and 2. These sets of cell and node numbers are both in counter-clockwise order. Also the nodes given by WNDND(i) and WNDND(i+1) are on either side of the cell indicated by WCELL(i).

64
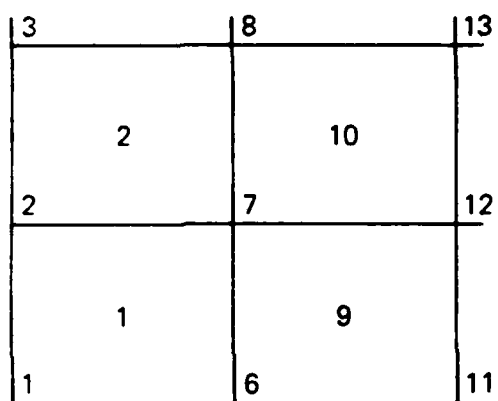
MA-7893-126

FIGURE 14   A PORTION OF A GRID SHOWING
INDEPENDENT NUMBERING
OF NODES AND CELLS

65

Both WCELL and WNDND have five storage locations. The extra space beyond the four normally required provides for some special layouts in which five cells may surround a node. The counter for WCELL is the quantity SCELL: the negative of the number of cells around the node. Hence, for an internal cell, SCELL is usually equal to −4. External nodes require fewer WCELL values. For example, for node 6 in Figure 14, the WCELL array is LC(9), LC(1), 0, 0, 0, where LC(i) means the location coordinate of the ith cell. For this same node the WNDND array is 11, 7, 1, 0, and 0.

In BLOCK these two arrays are filled with cell and node numbers in ascending order. Then ORDER is called by GENR to rearrange the elements of each array to produce the special relationships referred to above.

Grids Using Finite-Element Numbering. The finite-element numbering provides some added flexibility in laying out the grid or in changing it during a calculation. Here we describe three situations--a problem where a varying grid size is required, a computation with a nonrectangular object, and a calculation with a moving slide line.

Often it is of interest to provide small cells in one region of a problem and large cells elsewhere. For accuracy, the cells should vary gradually from small to large and should remain nearly square. In general, these requirements cannot be met with an i,j-numbering procedure without introducing slide-line discontinuities in the grid. Even then the slide line is restricted to one direction (i or j, not both) so the cell size can be varied in only one direction. Figure 15 shows four cell configurations that permit gradual changes in cell sizes in one or two directions in a finite-element number scheme. Because of the irregular adjacency relations, these schemes cannot be used with i,j-numbering procedures. They all show regions in which the cell size varies 10% to 50%. This variation may be too rapid for wave propagation problems, but it is satisfactory for intermediate rate problems such as projectile penetrations. The patterns in Figures 15c and 15d are constructed using BLCAS3, a subroutine used in cell layout.

66
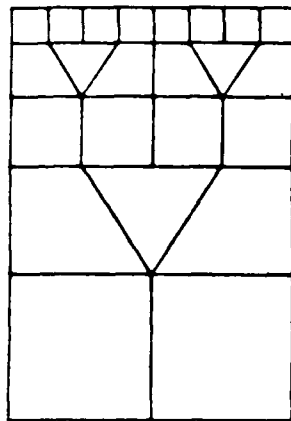
(a) A One-Directional
    Cell Size Variation
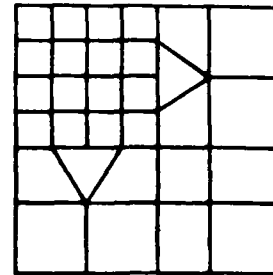
(b) One Possible Two-Directional
    Cell Size Variation Derived
    From the One-Directional
    Variation
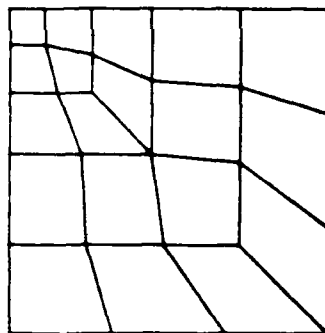
(c) Pattern for a 25% Cell Size
    Increase Per Cell in Two
    Directions
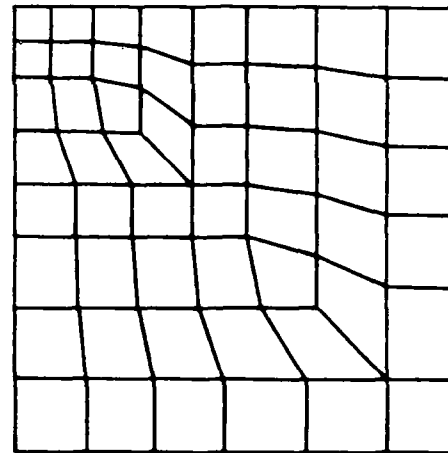
(d) Pattern for a 10% Cell Size
    Increase Per Cell in Two
    Directions

MA-7893-127

FIGURE 15   CELL SIZE VARIATION PATTERNS THAT MAY BE USED
            WITH A FINITE-ELEMENT NUMBERING TECHNIQUE

67

Odd-shaped objects such as projectiles and spheres are difficult to construct with nearly square cells with an i,j-numbering technique. Figure 16 shows a sphere (modeling a human head) with a finite-element numbering technique. Note that all cells are approximately equal in area and have aspect ratios near one. Figure 17 shows a sample of the layout obtained with the BLCIRC subroutine called by BLOCK. A solid cylinder of explosive was contained within a series of steel cylinders. This figure shows that nearly uniform sized cells can be obtained automatically for circles and arches. Node locations of successive arches can be made to match or not as desired.

A third feature of codes that shows the need for finite-element numbering is the slide line, especially a slide line that could propagate during a calculation along an irregular and unpredetermined direction. Such a general slide line is illustrated in Figure 18 (but is not yet available in C-HEMP). As the slide line would move through the grid, we presume that it might move to any adjacent node along its general direction of travel. In some moves it would merely separate cells. Then one node such as A would be divided into two nodes to permit separate motions of the adjacent cells. However, if the slide line divided a quadrilateral (as along BC) into two triangles, additional nodes would be required at B, C, D, and E. The nodes at D and E are needed to turn the new triangles back into quadrilaterals. Following the construction of a new node, the WNOD, WCELL, and WNDND arrays of adjacent nodes and cells would be revised to account for the new node and new cell (if any). The new node (or cell) is merely added to the node (or cell) list and provided with the usual properties. None of these steps is trivial, but they can be accomplished without modifying the basic computational algorithm; the only changes are those required at the point in the code where the new cell or node is created.

68

Applied Pressure
with Cosine
Spatial
Distribution

Skull

Brain

Cerebrospinal
Fluid

GA-314582-16B
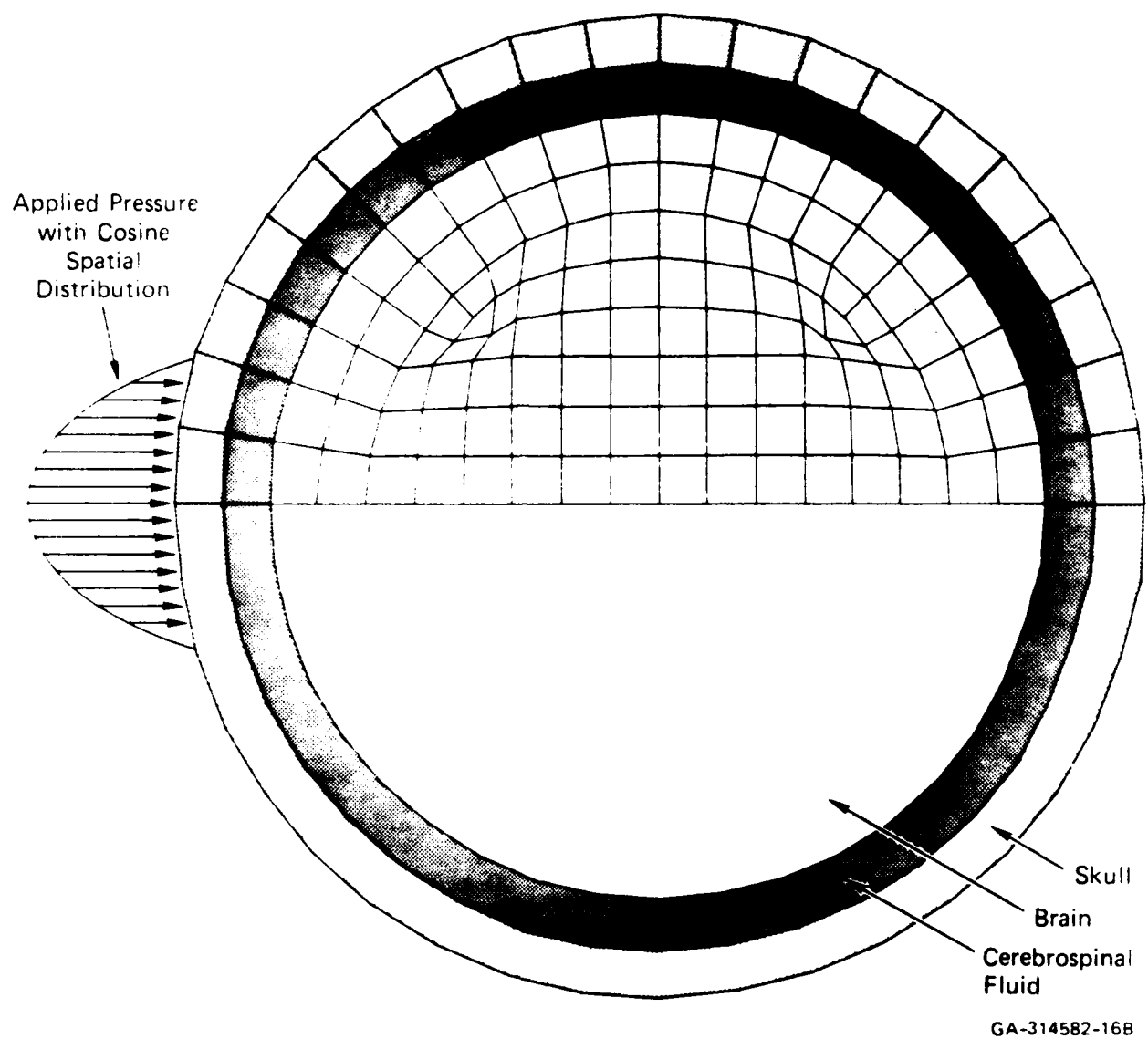
FIGURE 16   GEOMETRY OF HUMAN HEAD FOR STUDY OF IMPACT AND CONCUSSION
SHOWING FINITE-ELEMENT LAYOUT FOR CIRCULAR OBJECT
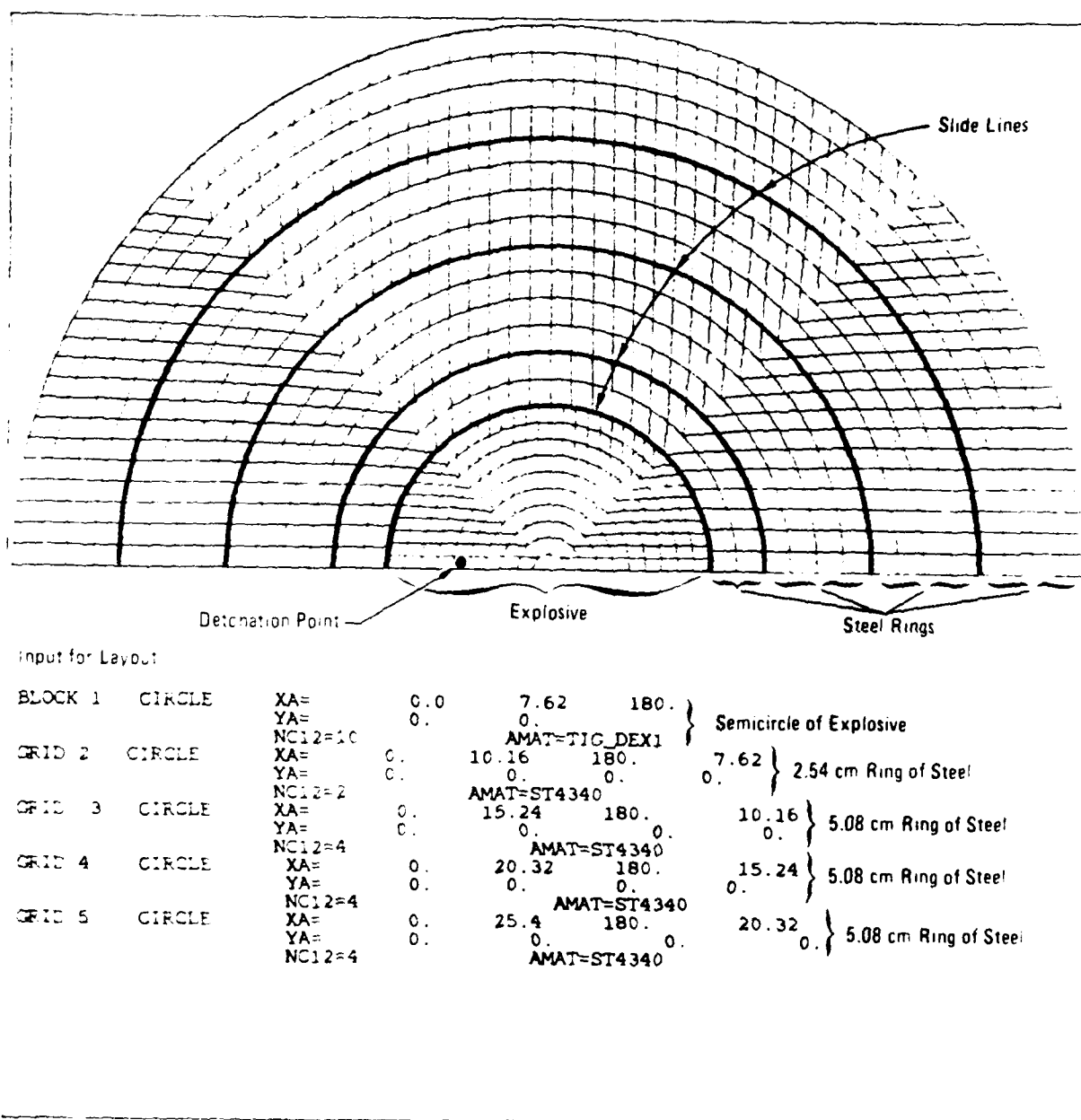
FIGURE 17 SAMPLE LAYOUT OF A SEMICIRCLE COMPOSED OF FIVE MATERIALS
WITH SLIDE LINE DISCONTINUITIES BETWEEN MATERIALS

Computed by BLCIRC

70
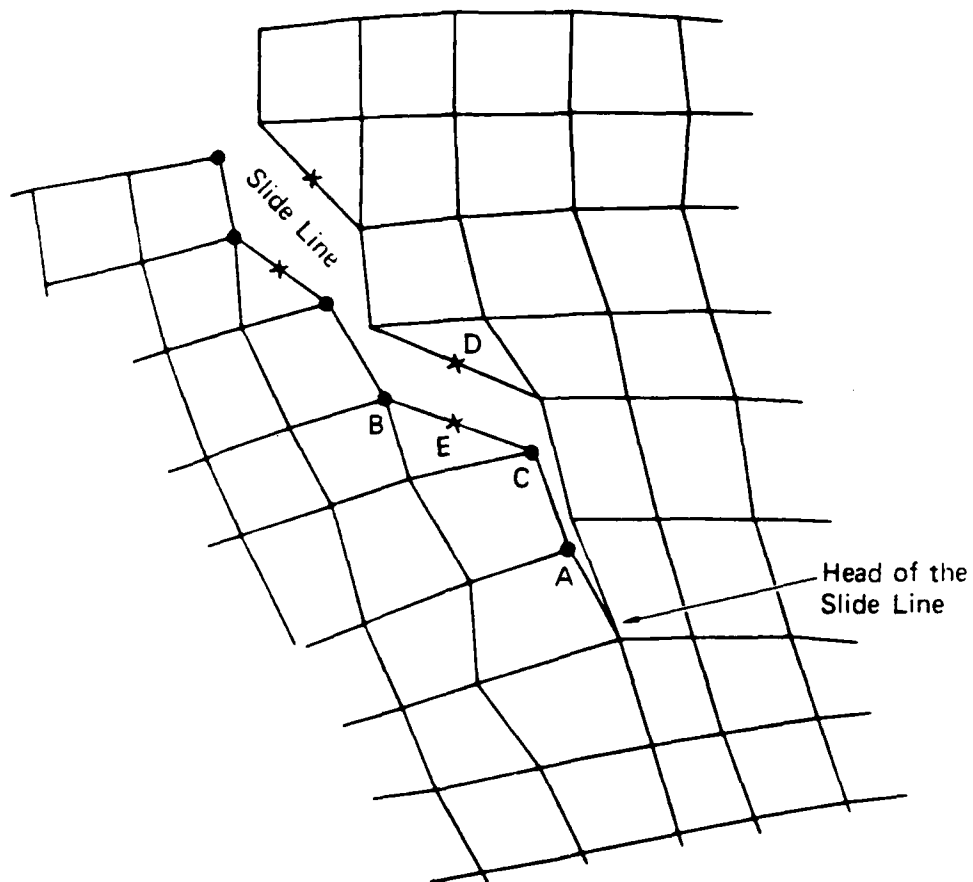
● Nodes added to permit separation of cells at nodes

x Nodes added to maintain quadrilateral cells

MA-7893-128

FIGURE 18   POSSIBLE CONFIGURATION OF CELLS AND NODES ALONG A WANDERING
SLIDE LINE REPRESENTING A GROWING CRACK OR SHEAR BAND

71

III STRESS COMPUTATIONS

A. Introduction

The constitutive relations provide the stress as a function of density, strains, internal energy, and other quantities. This section describes the common constitutive relations and outlines the constitutive models available in C-HEMP. Models for pressure only, for deviator stress, and for total stress are given.

In the standard constitutive relations, the stress tensor is separated into a pressure and a stress deviator tensor. The pressure is the average stress

$$P = 1/3 \sum_{i} \sigma_{ii} \tag{118}$$

and the stress deviator elements are

$$\sigma'_{ij} = \sigma_{ij} - P\delta_{ij} \tag{119}$$

where σ_{ij} are stress tensor elements and δ_{ij} is the Kronecker delta. The standard pressure and deviator models are presented in the following sections. Later sections describe more complex models available in C-HEMP. Procedures for adding more models are given in Appendix B.

B. Mie-Grueneisen Pressure Model

The pressure is computed from a simplified form of an equation of state, the locus of all possible thermodynamic equilibrium states for a substance. Each state is a set of values of the following thermodynamic quantities: stress tensor, specific volume, entropy, specific internal energy and temperature. In the simplified equation of state used in most wave propagation codes, the only variables considered are pressure

73

(the deviator components of stress are treated separately), specific
volume (V) or density ($\rho = 1/V$), and internal energy (E). The equation
of state is then

$$P = P(E, V) \tag{120}$$

which defines a surface or locus of points in energy-pressure-volume
space.

An equation of state represents equilibrium states. As a material
undergoes gradual change, such as heating or compression, the successive
states describe a path on the equation-of-state surface. If the
material is compressed by passing through a steady-state shock front,
the initial and final states lie on the P-V-E surface. These initial
and final states are connected by a straight line, the Rayleigh line,
which does not lie on the surface, but above the P-V-E surface. The
states of transition within a shock front are not states of thermo-
dynamic equilibrium. A complete equation of state describes the
material behavior in solid, liquid, and gaseous phases. The standard
pressure model present here in the subroutine CYCLE gives a physically
reasonable treatment of the solid behavior only.

First, we examine the paths taken on the equation-of-state surface
by material under shock loading. Shock experiments lead to the
determination of a Hugoniot or Rankine-Hugoniot equation of state that
is represented by one curve on the equation-of-state surface. This line
is the locus of final states that can be obtained by a steady-state
shock transition from a given initial state. The pressure-volume path
taken by the material during the shock and a subsequent unloading is
shown in Figure 19. The shock path follows a Rayleigh line to a point
on the equation-of-state surface. Pressures on the Rayleigh line can be
considered to be decomposed into an equilibrium pressure represented by
a point on the equation-of-state surface plus a nonequilibrium pressure
component. In code calculations the equilibrium pressure is computed
from the equation of state, and the nonequilibrium component is computed

74
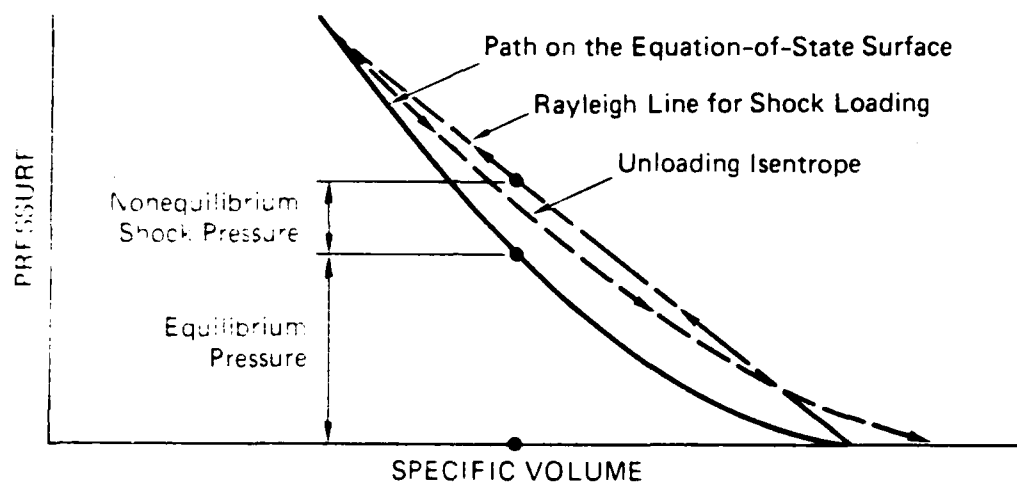
FIGURE 19   PRESSURE PATHS FOR SHOCK LOADING AND UNLOADING
OF A MATERIAL

as the artificial viscous stress. Figure 20 shows the Rayleigh line and unloading isentrope on the equation-of-state surface with a Hugoniot curve. During the shock loading the internal energy increases, as indicated in this figure. Less internal energy is used in the elastic recovery on unloading down the isentrope; hence the unloading does not coincide with loading, and the final, unloaded state is warmer than the initial state and at a larger specific volume (for materials that expand during heating).

Several other lines of interest are shown in Figure 20. The adiabatic compression path is followed by a rapid but nonshock loading in which no heat conduction occurs. The unloading isentrope is a similar, equilibrium process without heat conduction. The zero pressure line is the locus of points obtained by simply heating the material without external mechanical confinement. Heating increases the internal energy, and thermal expansion occurs. For small increases in internal energy, the zero pressure curve describes the usual expression for volumetric thermal expansion

$$V = V_o \ (1 + \alpha \Delta \theta) \tag{121}$$

where V_o = the initial specific volume

α = the volumetric thermal expansion coefficient

$\Delta \theta$ = the change in temperature.

The spall path is shown only to indicate the direction taken in tension. Spall, or fracture, is a rate-dependent process that generally depends on the stress tensor (not simply the pressure) and on the internal energy.

Having outlined some properties of the equation of state, we now introduce the analytical forms used in the standard pressure model. The equation which is generally used to describe compression is the Mie-Gruneisen equation:

76

Hugoniot

Adiabatic
Compression

Vapor

Specific
Internal
Energy

Rayleigh
Line

Liquid

Pressure

Specific
Volume

Constant Initial Volume

Zero Pressure Line

Unloading Isentrope

Spall Criterion

Path to Spalling
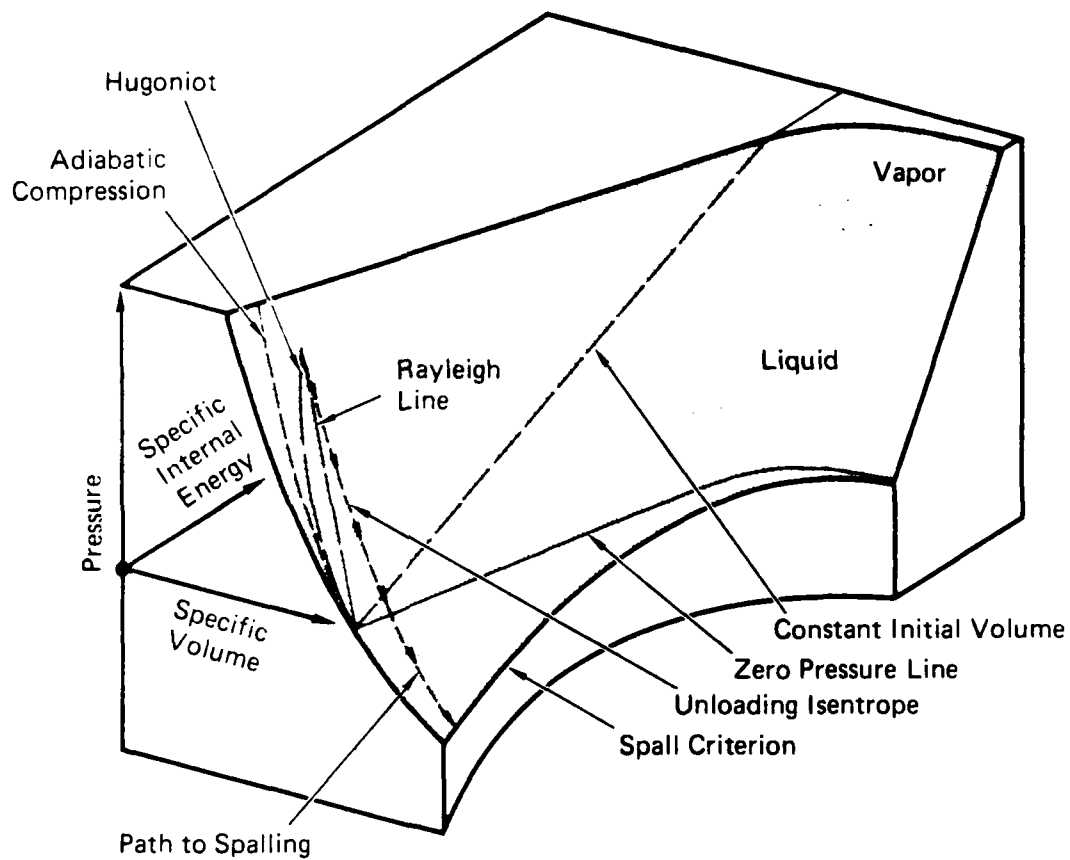
GA-6586-23B

FIGURE 20   ENERGY-PRESSURE-VOLUME (E-P-V) SURFACE FOR A SOLID
             MATERIAL

$$P - P_H = \frac{\Gamma(V)}{V} \left(E - E_H \right) \tag{122}$$

where

P_H and E_H = a point on some reference curve at the same specific volume V

Γ = the Gruneisen ratio.

Equation (122) was derived by assuming that Γ is a function of V only. Equation (122) provides a means for extending the information of a known P-V relation (such as the Hugoniot) to other values of internal energy. Because the Hugoniot is the P-V relation that is most likely to be known, the computations are constructed so that the Hugoniot is the reference curve used. The Hugoniot P-V equation is presumed to be in the form

$$P_H = C\mu + D\mu^2 + S\mu^3 \tag{123}$$

where

$$\mu = \frac{\rho}{\rho_o} - 1 = \frac{V_o}{V} - 1$$

C = zero-pressure bulk modulus

D, S = coefficients with the units of moduli.

The internal energy along the Hugoniot is

$$E_H = \frac{P_H}{2} \left(V_o - V_H \right) \tag{124}$$

Equation (124) assumes that the initial internal energy is zero and that the Hugoniot is concave upward throughout. In general, the latter assumption excludes consideration of changes of state. Although these relations are strictly true only for the stress Hugoniot, not the pressure Hugoniot, little inaccuracy is introduced by this approximation for stress states well above yielding. With the aid of Eq. (123) and (124), the Mie-Gruneisen equation takes the following form in the program

$$P = \left(C\mu + D\mu^2 + S\mu^3 \right)\left(1 - \frac{\Gamma\mu}{2} \right) + \Gamma\rho E \qquad (125)$$

When material is held at a particular volume and heated (internal energy is added), it goes through states that are straight lines on the equation-of-state surface. this indicates that, for constant volume V_1, the analytical equations for the surface have the form

$$E = A\left(V_1 \right) \cdot P \qquad (126)$$

where $A(V_1)$ = a function of V_1 only. The equation-of-state surface is constructed simply by translating the Hugoniot curve parallel to itself to higher energy states.

Many of the equation-of-state parameters are available in standard handbooks. For example, C is the isentropic bulk modulus at low pressures. According to Rice, McQueen, and Walsh, [Ref. 23] D in Eq. (123) may be estimated from $D = \Gamma_o C$. The sublimation energy, E_s, is the difference between the internal energy of the fully expanded vapor at a temperature of absolute zero. This quantity is referred to as ΔH_{fo}^o in the JANAF tables [Ref. 24] for the gas state.

The Gruneisen ratio Γ may be estimated from thermal expansion data, using the relation

$$\Gamma = \frac{C\alpha}{\rho_{so} C_p} \qquad (127)$$

where

α = the volumetric thermal expansion coefficient

C_p = the specific heat at constant pressure.

79

The results from Eq. (127) should be relied on only if all quantities pertain to the same density, pressure, and temperature. For many materials, Γ lies between 1.0 and 2.0; if internal energy is not important in the problem, an estimate can be made in this range.

C. Elastic-Plastic Deviator Stress Model

The deviator stress is the part of the stress tensor that arises because of the resistance of the material to shearing deformation. In C-HEMP the standard model for deviator stresses accounts for elastic response, plastic flow, work hardening, and Coulomb friction.

1. Elastic Relations. The elastic relations between stress and strain are cast in the following form

$$\sigma'_{ij} = 2G\left(\varepsilon^E_{ij} - \frac{\delta_{ij}}{3} \sum_{\ell} \varepsilon^E_{\ell\ell}\right) \tag{128}$$

$$P = C \sum \varepsilon_{ii} \tag{129}$$

Here, σ'_{ij} and ε^E_{ij} are the deviatoric stress and elastic strain in the ij direction, G is the shear modulus, δ_{ij} is the Kronecker delta, P is pressure, and C is the bulk modulus. For the elastic case, $\varepsilon_{ij} = \varepsilon^E_{ij}$, all the strain is elastic. But Eqs. (128) and (129) are also applicable to the plastic case where the strain increments are separated into elastic and plastic components.

$$d\varepsilon_{ij} = d\varepsilon^E_{ij} + d\varepsilon^P_{ij} \tag{130}$$

where $d\varepsilon_{ij}$ is the total strain increment and $d\varepsilon^P_{ij}$ is the plastic strain increment. For convenience, the terms in the parentheses of Eq. (128) can be named a deviator strain defined as follows:

80

$$\varepsilon'^{E}_{ij} = \varepsilon^{E}_{ij} - \frac{\delta_{ij}}{3} \sum_{\ell} \varepsilon^{E}_{\ell\ell} \tag{131}$$

Then Eq. (128) becomes

$$\sigma'_{ij} = 2G \varepsilon'^{E}_{ij} \tag{132}$$

2. Plastic Relations. The Reuss plasticity relations or "incremental plasticity with an associated flow rule" are considered here first. Modifications to treat Coulomb friction are described later. Yield occurs when the effective stress reaches the yield strength. The effective stress is

$$\bar{\sigma} = \sqrt{3/2 \left(\sigma'_{ij} \sigma'_{ij} \right)} \tag{133}$$

where the repeated subscripts indicate summation. The yield criterion is

$$\bar{\sigma} = Y \tag{134}$$

where Y is the current yield strength. The Reuss flow rule indicates that the deviator stress in any direction is proportional to the plastic strain in that direction:

$$d\varepsilon^{p}_{ij} = \sigma'_{ij} \, d\lambda \tag{135}$$

where $d\lambda$ is a proportionality constant. Now we define a scalar plastic strain quantity as follows:

$$d\bar{\varepsilon}^{p} = \sqrt{2/3 \, d\varepsilon^{p}_{ij} \, d\varepsilon^{p}_{ij}} \tag{136}$$

81

As before, the repeated subscripts indicate summation. Now we square Eq. (135) and make use of the definitions of $\bar{\sigma}$ and $d\bar{\varepsilon}^P$. Then

$$d\bar{\varepsilon}^P = 2/3 \ \bar{\sigma} \ d\lambda \tag{137}$$

Combining this definition with Eq. (135), we find that

$$d\varepsilon_{ij}^P = \sigma'_{ij} \ \frac{3d\bar{\varepsilon}^P}{2\bar{\sigma}} \tag{138}$$

To obtain a solution for an increment of strain, we compute first the stress that would occur if the strain were entirely elastic, that is,

$$\sigma'^N_{ij} = 2G \left(\varepsilon'^E_{ijo} + \Delta\varepsilon'_{ij} \right) = 2G \left(\varepsilon'^E_{ij} + \Delta\varepsilon_{ij}^P \right) \tag{139}$$

where

ε'^E_{ijo} = the elastic deviator up to the current strain step

$\Delta\varepsilon'_{ij}$ = the total deviator strain increment

ε'^E_{ij} = the elastic deviator strain after the current increment

$\Delta\varepsilon_{ij}^P$ = the plastic strain increment.

The second equality in Eq. (139) is obtained by using Eq. (130) to decompose $\Delta\varepsilon'$ and by adding $\varepsilon'^E_{ijo} + \Delta\varepsilon'^E_{ij}$ to obtain ε'^E_{ij}. Quantities ε'^E_{ij} and $\Delta\varepsilon_{ij}^P$ can both be replaced by stress quantities through the use of Eq. (132) and Eq. (138). Then,

$$\sigma'^N_{ij} = \sigma'_{ij} \left(1 + 3Gd\bar{\varepsilon}^P/\bar{\sigma} \right) \tag{140}$$

If both sides of Eq. (140) are squared and a quantity $\bar{\sigma}^N$ is introduced in analogy to the definition of $\bar{\sigma}$, then we obtain

$$\bar{\sigma}^N = \bar{\sigma} \left(1 + 3Gd\bar{\varepsilon}^P/\bar{\sigma} \right) \tag{141}$$

82

Here, $\bar{\sigma} = Y$.

Combining Eqs. (140) and (141) yields a solution for σ'_{ij}

$$\sigma'_{ij} = \sigma'^{N}_{ij} \frac{\bar{\sigma}}{\bar{\sigma}^{N}} \qquad (142)$$

Then, the elastic strain can be obtained from Eq. (142) and the effective plastic strain from Eq. (141)

$$d\bar{\epsilon}^{P} = \frac{\bar{\sigma}^{N} - \bar{\sigma}}{3G} \qquad (143)$$

and finally, each component of plastic strain is found from Eq. (135).

The preceding process is especially appropriate for perfect plasticity where Y is constant. The equations are appropriate for steps from one plastic state to another or from an elastic state to a plastic state.

3. <u>Coulomb Friction</u>. When Coulomb friction is introduced, the preceding equations for Mises plasticity are modified slightly. The fundamental relation provides a shear yield stress τ_c, which is a function of a cohesion c, normal stress σ_N, and the angle of internal friction ϕ.

$$\tau_c = c + \sigma_N \tan \phi \qquad (144)$$

Following Terzaghi, [Ref. 42] this expression is transformed to

$$\sigma_1 = 2c \sqrt{N_\phi} + \sigma_3 N_\phi \qquad (145)$$

where $N_\phi = \tan^2 (45° + \phi/2)$; and σ_1 and σ_3 are the most and least compressive principal stresses. In the derivation we consider that yielding has no effect on volume change (a Coulomb-without-dilation

83

model). Instead of using Eq. (145), which is not symmetric because the intermediate principal stress is absent, we introduce the expression of Drucker and Prager[43]

$$\sqrt{J_2'} = k + 3\alpha P \tag{146}$$

where J_2' is the second invariant of the stress deviator tensor, and k and α are constants. Replacing J_2' by the effective stress $\bar{\sigma} = \sqrt{3J_2'}$, we can obtain the following form for Eq. (146)

$$\bar{\sigma} = \frac{3c\sqrt{N_\phi} + 3/2 \left(N_\phi - 1 \right) P}{1 + N_\phi/2} \tag{147}$$

The constants k and α have been replaced by c and N_ϕ by equating Eqs. (145) and (146) for the case $\sigma_2 = \sigma_3$. The individual deviator stresses are then obtained from Eq. (142).

Equation 147 is now rewritten as simply

$$\bar{\sigma} = Y_o + E_\phi P \left(\bar{\sigma} > 0 \right) \tag{148}$$

where Y_o is the zero-pressure yield strength and E_ϕ is a Coulomb-friction coefficient. For the program, it is expected that the user will calculate the required Y_o and E_ϕ values from the cohesion c and internal friction angle ϕ.

$$Y_o = \frac{3c\sqrt{N_\phi}}{1 + N_\phi/2} \tag{149}$$

$$E_\phi = \frac{3(N_\phi - 1)}{2 + N_\phi} \tag{150}$$

The factor E_ϕ appears as ESC(10) in the program.

4. <u>Work Hardening</u>. A linear work hardening is assumed in the following form:

$$Y = Y_o + Y_D \bar{\epsilon}^P \tag{151}$$

where Y_D is a work-hardening coefficient with the units of dyn/cm^2. A more flexible treatment of Mises-type work-hardening is available in the EPP model.

5. <u>Nonlinear Work-Hardening Model EPP</u>. A general two-dimensional model for elastic-plastic, work-hardening behavior is contained in the subroutine EPP. The model is isotropic, based on von Mises plasticity with the Reuss incremental flow law. The work-hardening yield strength is a function of the scalar plastic strain $\bar{\epsilon}^P$.

Three forms are provided for the yield function. In the first two the yield curve is provided by the user as a series of Y, $\bar{\epsilon}^P$ points. In the first type, a linear interpolation between the points in logarithmic space is used to compute yield Y, for any plastic strain, $\bar{\epsilon}^P$, for the second and later intervals in the Y, $\bar{\epsilon}^P$ series. Hence the form of the function in the ith interval is

$$Y = Y_i + A_i \left(\bar{\epsilon}^P \right)^{n_i} \tag{152}$$

The parameters A_i and n_i are computed within the subroutine from the series of Y, $\bar{\epsilon}^P$ points. The interpolation in the first interval is linear in nonlogarithmic space.

The second type of yield function is similar to the first except that linear interpolation is used between all points in the yield series.

The third yield function provided is a quotient form developed by Norris [Ref. 25].

$$Y = \frac{C_1 + C_2\bar{\epsilon}^P + C_3(\bar{\epsilon}^P)^2 + C_4(\bar{\epsilon}^P)^3}{1 + C_5\bar{\epsilon}^P + C_6(\bar{\epsilon}^P)^2} \qquad (153)$$

The C_j constants are read by EPP into the array used for the yield values associated with the first two types.

D. Special Models for Compressed States

In addition to the Mie-Grueneisen model presented in the previous section for pressure, several special models have been developed. Here we present some sample models for the treatment of explosives, porous materials, and for composites.

1. _Explosives_. Treatments for explosives include a constant volume detonation, a running detonation, and more complex initiation processes. With explosives we must consider both the equation of state for the explosion products and also the transformation from an unreacted state to the detonated state. In C-HEMP we provide only two equations of state for the products and a simple detonation process based on the Chapman-Jouguet (C-J) theory. The calculations are conducted in the EXPLODE subroutine.

The equation of state for the explosion products may be given either by a polytropic gas relation or by a tabular equation of state. A polytropic gas is characterized by the following equation for pressure P as a function of density ρ along an isentrope:

$$P = C \rho^\gamma \qquad (154)$$

where γ is the polytropic gas exponent and C is a constant. For general states not necessarily on an isentrope, the pressure is given by

$$P = (\gamma - 1) \rho E \qquad (155)$$

Hence, γ governs both the variation of pressure as a function of energy, and also the shape of the isentrope in the $P - \rho$ plane.

For the polytropic gas relation for the explosive products, it is necessary to provide the chemical energy Q and the polytropic gas exponent γ. From these the subroutine computes the internal energy, specific volume, and pressure at the Chapman-Jouguet point.

$$E_{cj} = \frac{2Q\gamma}{\gamma + 1} \tag{156}$$

$$V_{cj} = \frac{\gamma}{\rho(\gamma + 1)} \tag{157}$$

$$P_{cj} = 2Q\rho(\gamma - 1) \tag{158}$$

where ρ is the initial explosive density. The detonation velocity, or shock velocity to the C-J point is

$$D = \sqrt{2Q \ (\gamma + 1)(\gamma - 1)} \tag{159}$$

The detonation velocity governs the rate at which the detonation front is propagated through the explosive. During a detonation, the explosive energy Q is deposited in each computational cell. The pressure is computed from Eq. 154, using Eq. 158 to specify the constant C.

The tabular equation of state in EOSTAB may be used to specify the isentrope of the explosion products. Then the isentrope is given by a series of pressure-density points. Pressure values for a given density are determined by interpolating logarithmically between the tabular points. The condition of tangency between the Rayleigh line through the C-J point and the explosion products isentrope provides a means of computing the E_{cj}, P_{cj}, and V_{cj} values as well as the detonation velocity. EOSTAB uses the tangency condition to obtain Q and γ. Then EXPLODE uses the standard relations to obtain the C-J state parameters.

Pressure points that are not on the Hugoniot or the release adiabat passing through the C-J point are computed using a variant of Eq. 155:

87

$$P = P_H + (\gamma - 1)\, \rho \left(E - E_H \right) \tag{160}$$

where P_H and E_H are values on the release adiabat through the C-J point. EOSTAB provides P_H and E_H from the tabular data. Then EXPLODE evaluates P.

A running detonation is simulated by a programmed burn in which each cell is detonated at a time determined during an initialization calculation. The region of detonation can be specified as a point or a line through the explosive.

In the detonation front only a fraction λ of the chemical energy Q has been transformed to internal energy. This fraction is computed as the larger of the amounts determined by the program burn time and the cell density:

$$\lambda = \max\left[\frac{(t - t_b)D}{\Delta Z} \quad , \quad \frac{\rho - \rho_o}{\rho\left(1 - V_{cj}\,\rho_o\right)} \right] \tag{161}$$

where t is time, t_b is the detonation time of the cell, ΔZ is the cell dimension over which the detonation front is spread, ρ_o is the original density, and ρ is the current density. This value of λ is used to increment the internal energy:

$$E_1 = E_o + Q \Delta \lambda \tag{162}$$

where E_1 and E_o are the energies at the end and beginning of the time step, and $\Delta \lambda$ is the change during the time step. This energy E_1 is used to compute the pressure according to Eq. 155.

2. <u>Porous Materials</u>. Several models for porous materials have been developed for representing porous metals, ceramics, plastics, and geologic materials. Prominent among these are Herrmann's P-α model [Ref. 26, 27], Seaman's POREQST and PEST models [Ref. 28, 29], Carroll and Holts' model [Ref. 30, 31] and Butcher's p-α - τ model [Ref. 32].

Each of these models contains a description of an equilibrium pressure-volume loading path, an unloading path, and a means for representing consolidation. In the POREQST model available in C-HEMP, there are also provisions for melting and vaporization of the porous solid material. POREQST, P-α, and Carroll and Holt's model are rate-independent, whereas the others are rate-dependent. In these models we are considering only the pressure component of the stress tensor: the deviator stress is either neglected entirely, or must be treated separately. Later, under CAP models, we outline briefly a model type in which the pressure and deviatoric components of the stress tensor are treated simultaneously.

The general character of the mechanical response of these models to loading and unloading is illustrated in Figure 21. The short-dashed line is the equilibrium loading path specified in all the models. Compaction along this line from the "initial state" produces a gradually decreasing specific volume and increasing pressure until the consolidation point on the long-dashed curve. This curve is the solid pressure-volume relationship. The solid curve with arrows in the figures shows the result of a partial loading to 120 kbar, unloading, and reloading above 500 kbar. The loading follows a rate-dependent process, so the P-V path lies above the equilibrium (short-dashed) line. Unloading follows an essentially elastic line downward into tension. During the tensile phase, the state point strikes a tensile limit and expands at nearly constant stress (probably not an accurate representation of real material behavior). Recompression along the Q path again produces a rate-dependent P-V path which lies above the equilibrium curve. Consolidation occurs at about 400 kbar. Subsequent loading or unloading would follow the solid constitutive relations.

For many applications it is necessary to provide a complete thermodynamic relation for the porous material. Such a relation describes how the material responds to heating and cooling, to melting, and even to vaporization. In POREQST these features are provided by several surfaces defined in energy-pressure-volume space. For example, in Fig. 22 are a compaction surface YBGFCH, a fracture surface DFHE, and an
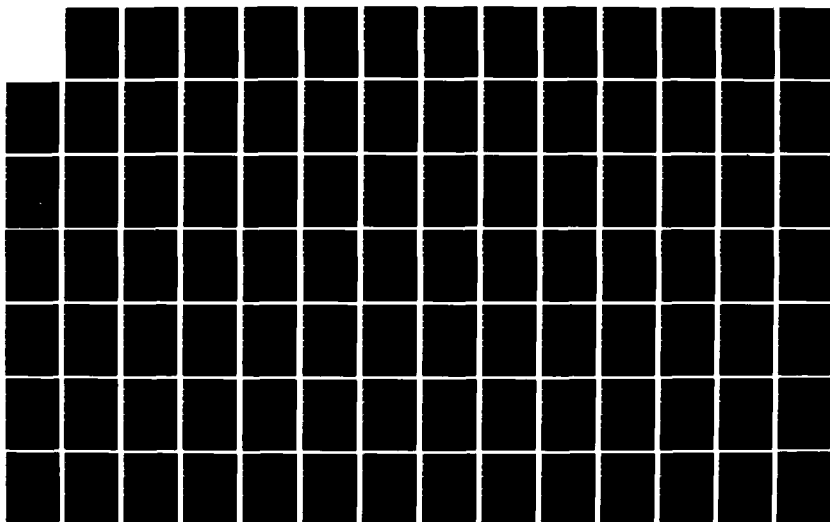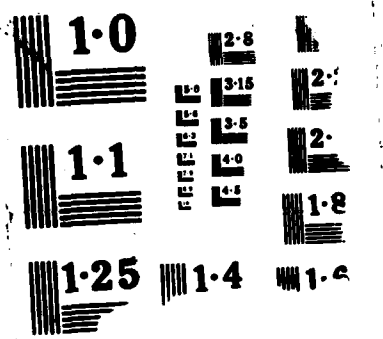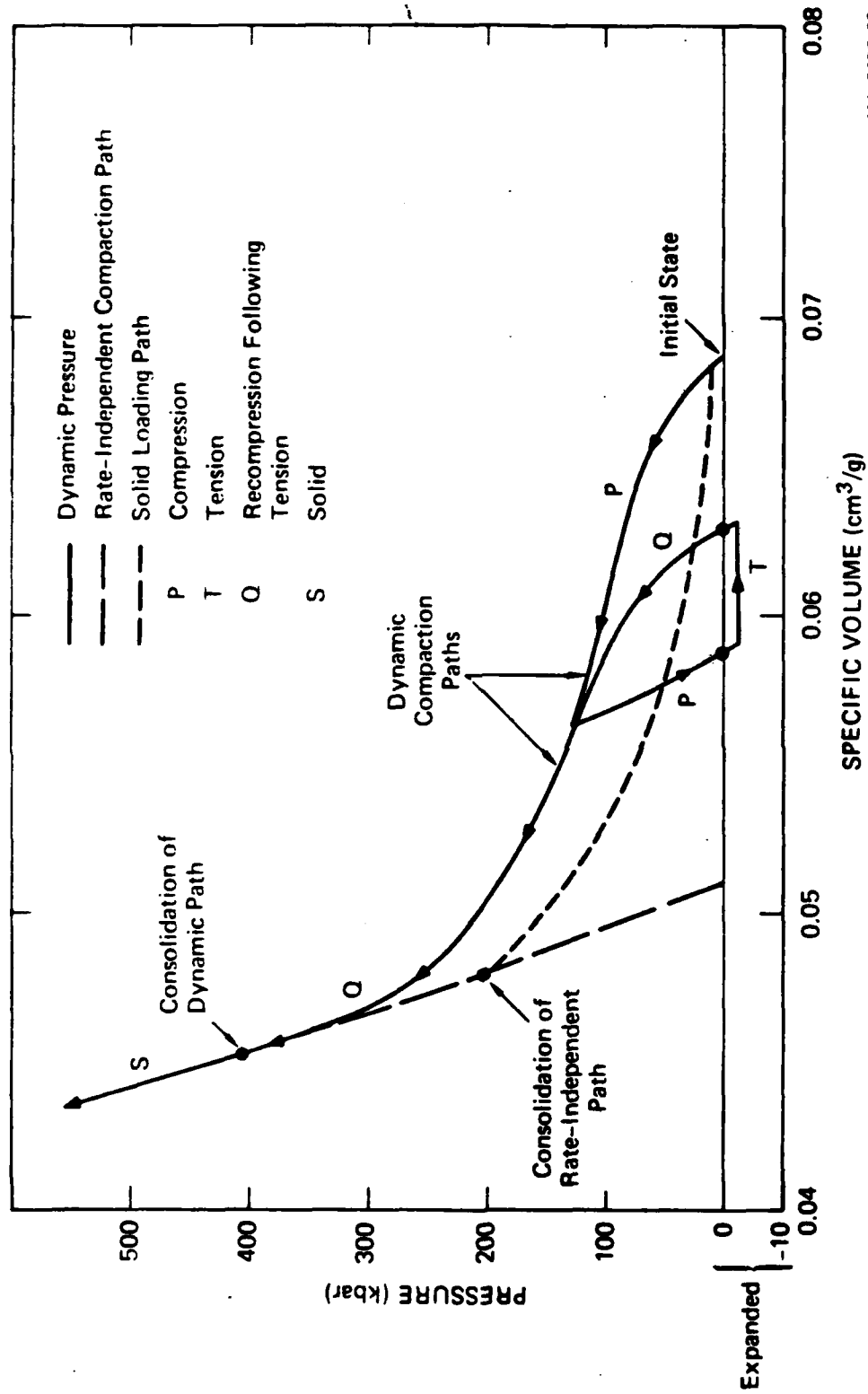
89

FIGURE 21 PRESSURE-VOLUME PATH COMPUTED IN PEST FOR LOADING WITH PORHOLT MODEL, ELASTIC UNLOADING, CARROLL–HOLT MODEL IN TENSION, AND RECOMPRESSION WITH PORHOLT MODEL TO CONSOLIDATION

Data are for porous tungsten.

90
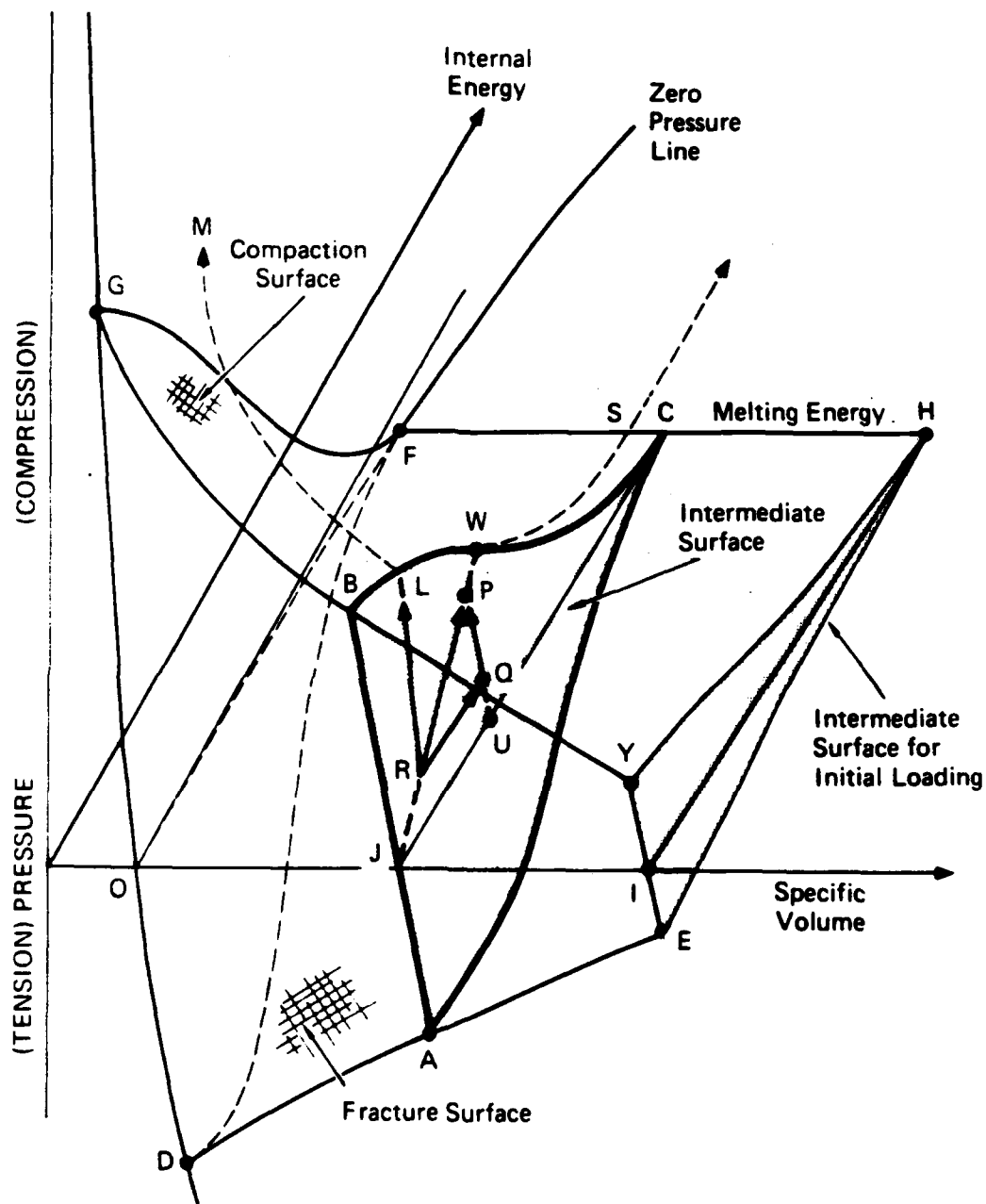
FIGURE 22 CONSTITUTIVE RELATIONS OF A POROUS MATERIAL, EMPHASIZING THE
INTERMEDIATE SURFACE FOR REVERSIBLE LOADING AND HEATING

MA-2407-24

91

intermediate surface ABC, as well as a solid equation-of-state surface defined by the compaction curves GF and DF. The intermediate surface describes elastic behavior of the material during loading, unloading, heating, and cooling.

The foregoing is intended to provide a qualitative description of the behavior of porous materials under fairly general mechanical and thermal loading. Quantitative details of the behavior depend on the particular model being considered and also on the material type.

3. Use of the POREQST Model. The rate-independent compaction curve of Seaman and Linde[28] was constructed to be convenient for fitting experimental data. The compaction curve is divided into a series of parabolic segments as shown in Figure 23. The segments are specified by a series of densities: ρ_1, ρ_2, ... ρ_{n+1}, where n is the number of segments. Up to six segments are permitted. Within each segment, the curve is defined by the pressures at each end of the segment (P$_1$ and P$_2$ for the third segment of Figure 23) and by the variation ΔP. As shown in Figure 23, ΔP is measured midway between the specific volumes at each end of the segment and is the vertical distance from the straight line to the parabola. With this definition, the value of ΔP is negative in the third segment shown. These quantities—densities and pressures—are readily determined from a measured or estimated P-V curve: these are the input data for the model.

For the wave propagation calculations, the input data that define the measured compaction curve are transformed to coefficients of a quadratic series in specific volume. In terms of the input variables the parabolic form is

$$P = P_1 + \left(P_2 - P_1\right) \frac{V - V_i}{V_{i+1} - V_i} - 4 \Delta P \frac{\left(V - V_i\right)\left(V - V_{i+1}\right)}{\left(V_{i+1} - V_i\right)^2} \qquad (163)$$

where V_i and V_{i+1} are specific volumes at either end of the ith segment and correspond to ρ_i and ρ_{i+1}. By gathering terms in V and V^2, we can rewrite Eq. (163) as

92

Pressure-Volume
Relation of Solid

Joint Between Compaction
Curve and Solid Relation

ΔP

PRESSURE

P_2

3

2

P_1

Segment 1

$1/\rho_{P5}$ $1/\rho_{P3}$ $1/\rho_{P2}$ $1/\rho_0 = 1/\rho_{P1}$

SPECIFIC VOLUME
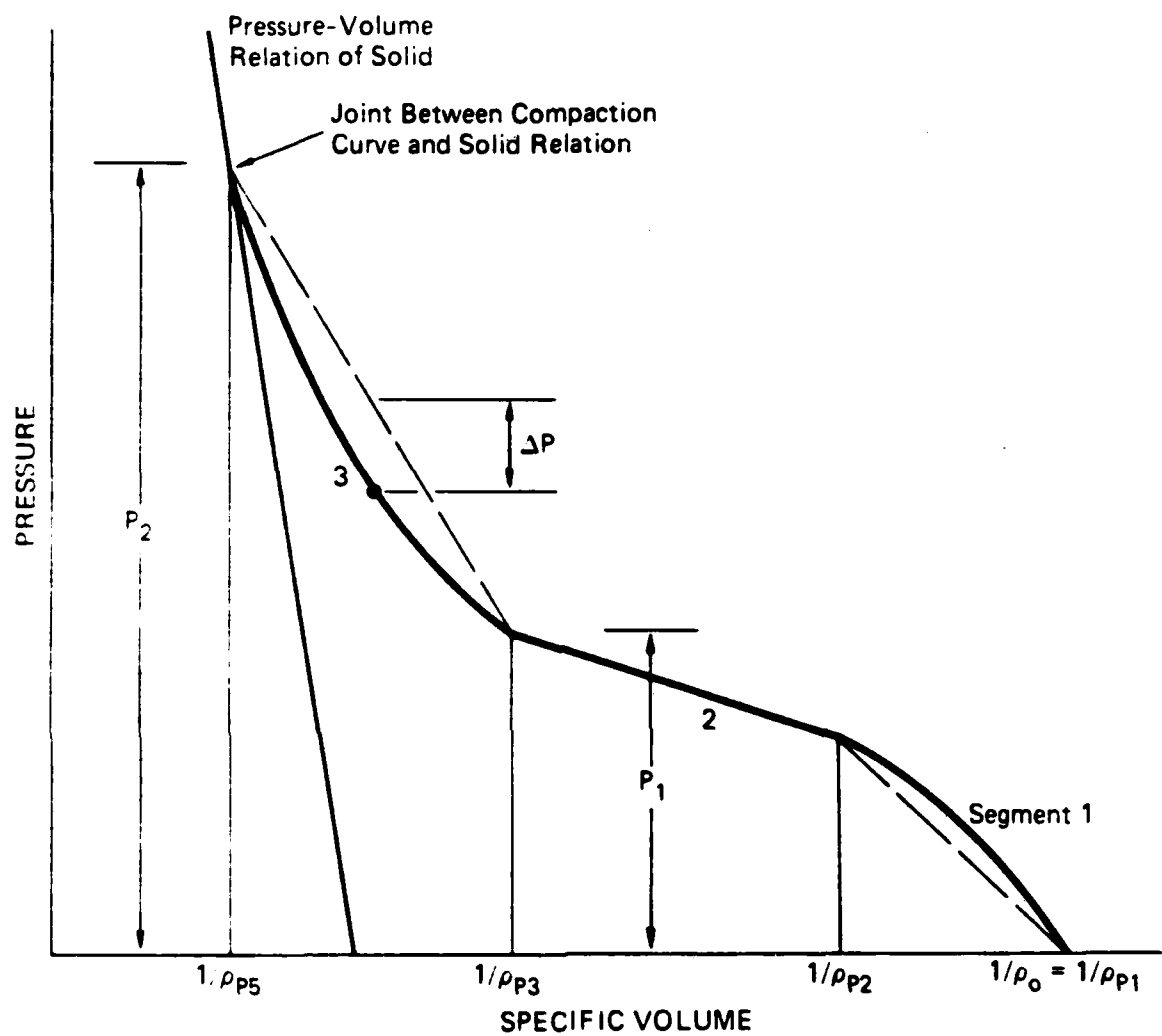
MA-2407-11

FIGURE 23   COMPACTION CURVE OF POREQST MODEL DIVIDED INTO THREE
PARABOLIC SEGMENTS

93

$$P = P_{ai} + P_{bi} V + P_{ci} V^2 \qquad (164)$$

where $P_{ai} = P_1 + \dfrac{\rho_{i+1}}{\rho_{i+1} - \rho_i} \left[P_2 - P_1 - \dfrac{4 \, \Delta P \, \rho_1}{\rho_{i+1} - \rho_i} \right]$

$$P_{bi} = \frac{-\rho_{i+1} \cdot \rho_i}{\rho_{i+1} - \rho_i} \left[P_2 - P_1 - 4 \, \Delta P \, \frac{(\rho_i + \rho_{i+1})}{\rho_{i+1} - \rho_i} \right]$$

$$P_{ci} = - \frac{4 \, \Delta P \, \rho_{i+1}^2 \cdot \rho_i^2}{(\rho_{i+1} - \rho_i)^2}$$

The quantities P_{ai}, P_{bi}, and P_{ci} are computed in the code and stored for use during wave propagation computations.

With only three points to define each segment, the slopes of the data may be poorly represented. The slopes of the parabolic segments can be determined from Eq. (164).

$$\left. \frac{dP}{dV} \right|_{V=V_i} = \frac{P_2 - P_1 + 4 \, \Delta P}{V_{i+1} - V_1}$$

$$\left. \frac{dP}{dV} \right|_{V=\bar{V}} = \frac{P_2 - P_1}{V_{i+1} - V_1} \qquad (165)$$

$$\left. \frac{dP}{dV} \right|_{V=V_{i+1}} = \frac{P_2 - P_1 - 4 \, \Delta P}{V_{i+1} - V_1}$$

where $\bar{V} = \left(V_{i+1} + V_i \right)/2$. These equations should be used to verify that slopes of the data are being fairly modeled by the parabolas. If necessary the slope representation can be improved by using more segments or by repositioning the segment boundaries.

94

The following text outlines briefly the method for fitting the POREQST model. The fitting operation begins with accumulation of the data available on the material. Required data include the bulk and shear moduli and the initial density of the solid material; the pressure-volume loading curve for the porous material; a deviator stress process, including a yield strength, for both porous and solid materials; a Grueneisen ratio; and an initial density for the porous material.

A sample of the data for a soil is shown in Figure 24. The fitting process will be undertaken here by examining this file line by line. The first line provides the name and the initial density of the solid material RHOS.

    AMAT = "WES YUMA"   RHOS = 2.650

The material considered is a soil from Yuma, Arizona with an initial density of 112 pcf. The solid density of 2.65 was selected as that for quartz. The EQST parameters are those for quartz

    EQSTC = 8.659E+11   EQSTS = 8.659E+11   EQSTG = 0.62
    EQSTE = 8.800E+11

The yield data for the solid may include a yield strength (not used) and the shear modulus.

    YIELD = 1.000E+06 MU = 2.000E+11

The initial density of the porous material is read by MATERIAL.

    RHO = 1.810E+00

```
AMAT =   "WES YUMA"    RHOS = 2.65
EQSTG = 8.659E+11      EQSTD =`-8.659E+11      EQSTS = 8.659E+11
EQSTE = 8.800E+10      EQSTG = 0.62            MU = 2.000E+11
RnO   = 1.81
POREQST              FIXED FORMAT
AK =         2.000E+11 MUP =      2.000E+10 YO =        1.000E+06
NREG =          5
RHOP =       1.810E 00 1.976E 00 2.136E 00 2.277E 00 2.423E 00 2.930E 00
COSQ =       1.000E 01 1.000E 01 1.000E 01 1.000E 01 1.000E 01 1.000E 01
C1   =       3.000E-01 5.000E-01 3.000E-01 3.000E-01 3.000E-01 3.000E-01
P1   =       1.000E 07
1 P2 =       1.500E+08 DELP =      1.200E+07
2 P2 =       4.000E+08 DELP =     -4.400E+07
3 P2 =       1.400E+09 DELP =     -1.500E+08
4 P2 =       8.000E+09 DELP =     -1.000E+08
5 P2 =       9.000E+10 DELP =      0.
```

FIGURE 24 SAMPLE INPUT FILE FOR A POROUS MATERIAL

The next line indicates that the POREQST model is used and that it will be read with a fixed format.

POREQST FIXED FORMAT

The data reading by POREQST begins with the moduli. Choose AK and MUP (initial bulk and shear moduli) from the initial loading of the porous material. YO is the initial yield strength of the porous material. AK should exceed the slope of the initial part of the PV loading curve for the porous material.

AK = 2.000E+11   MUP = 2.000E+10   YO = 1.000E+06

The number of density regions into which the PV curve is separated is called NREG. Six regions are permitted.

NREG = 5

The densities corresponding to the boundaries of each density interval are listed in order. The first RHOP value need not coincide with RHO.

RHOP = 1.810E+00   1.96E+00   2.136E+00   2.277E+00   2.423E+00   2.930E+00

The artificial viscosities are listed for each interval. The normal values for COSQ and C1 are 4 and 0.05, but larger values are often required for porous materials. The coefficients can be selected to provide an essentially straight Rayleigh line (plot of R versus V) and to give a minor amount of oscillations.

COSQ = 1.000E+01   2.000E+01   1.000E+01   1.000E+01   1.000E+01   1.000E+01
C1 = 3.000E-01   5.000E-01   3.000E-01   3.000E-01   3.000E-01   3.000E-01

97

The initial yield point of the PV curve is P1.

P1 = 1.000E+07

The following describe the end points of each of the five regions. The DELP values are the central offsets from a straight line in the PV plane in each interval. DELP should not exceed 0.25(P2 - P1) in any interval or the curve in that interval will have a portion with a negative slope.

1 P2 = 1.500E+08 DELP = 1.200E+07
2 P2 = 4.000E+08 DELP = -4.400E+07
3 P2 = 1.400E+09 DELP = -1.500E+08
4 P2 = 8.000E+09 DELP = -1.000E+08
5 P2 = 9.000E+10 DELP = 0.000E+00

A second sample of the data for POREQST is in the input for the last example problem in Section VI.

4. CAP Models. In the preceeding porous models, the pressure is considered alone. In CAP models the shear and compaction behaviors are treated by introducing two yield curves into a plasticity model. One yield curve represents shear failure, and the other represents compaction. CAP models have often been used to represent the stress-strain behavior of geologic materials, such as soil and rock, and also of concrete and various grouts. The CAP model derives its name from a movable cap or secondary yield curve, as shown in Figure 25. The abscissa and ordinate are the invariants representing pressure and shear stresses.

Figure 25 shows ranges of shear and normal stress permitted to occur in the model. Points interior to both Mohr-Coulomb (shear yielding) line and the cap (compaction) line represent elastic behavior. Points on these lines represent yielding. The cap tends to expand by a work-hardening process as yielding occurs on the cap curve.

98
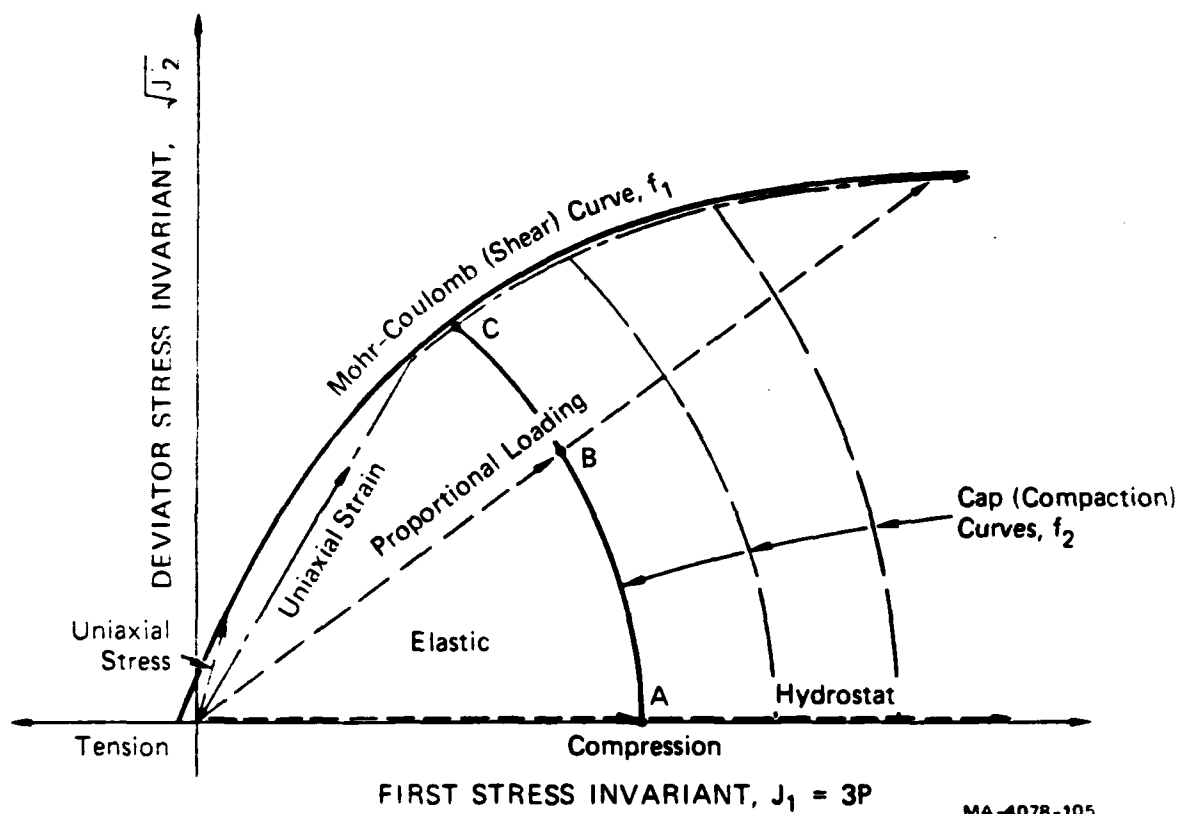
FIGURE 25   MOHR-COULOMB AND CAP YIELD CURVES WITH FOUR LOADING
PATHS THAT INTERSECT THE YIELD CURVES

The CAP model fits into the framework of plasticity established by Prandtl, Reuss, Hill, and others (see Reference 44 for background on plasticity). The model treats the material as isotropic and homogeneous, with work-hardening and an associated flow rule. The first yield curve (Mohr-Coulomb) shown in Figure 25 is the one common to other plasticity models. It accounts for shear yielding and for dilatation. The second or cap yield curve accounts for compaction of the material; the curvature provides for the shear-enhanced compaction seen in porous geologic materials.

The small tensile strength of concrete is represented by the small portion of the Mohr-Coulomb curve that extends to the left of the vertical axis. In the tensile range, the curve may be considered a threshold stress level for initiation and opening of cracks. The curve shows a decreasing tensile strength with increasing J_1 (mean tensile stress); that is, a hydrostatic tensile state leads to lower shear strengths than a uniaxial tensile state. This relation between strengths agrees with tensile data on brittle materials such as concrete.

The CAP models may require special treatment in wave propagation calculations because of the interaction of pressure and deviatoric components. Thus, they do not fit the pattern of the preceding porous models in which pressure could be computed by one model, and deviator stress by a different model.

5. Use of CAP1 Model in C-HEMP. CAP1 represents a porous material using nonlinear elastic moduli, a cap curve, a Mohr-Coulomb curve, and an isotropic tensile damage process. Table 2 contains the expressions for these functions and sample values determined for a concrete with a compressive strength of 24 MPa (3500 psi). The elastic moduli are derived from loading and unloading data. The Mohr-Coulomb curve is determined in two steps from compaction and tensile data. First the A_1, A_2 and A_3 are derived by fitting the yield curve from uniaxial strain experiments. Then the curve is modified in the tensile range by specifying J_{10} (intercept on J_1) and the parameter n which determines the distance in the compression range to be affected by the modifica-

100

tion. The W factor for the cap should be determined from a family of proportional loading tests. The concrete parameters in the table were determined from sets of quasistatic experiments and from plate impact tests.

6. Composite Models. Composite models may represent a mixture of two or more materials. Some composite models are for a mixture of gases or particulate solids and the geometrical configuration of the components is not important. For other composites, the geometry of the components is very important: an example is a fiber reinforced epoxy. Here we describe a model which was developed to represent reinforced concrete with a single mat of reinforcing steel. The steel is simulated as a steel sheet at the midplane of a cell of the reinforced concrete. Hence, specific bars are not treated, but the effect of the bars in stiffening and strengthening the concrete in the plane of the steel is represented.

Table 2 CAP1 PARAMETERS FOR A CONCRETE

Parameter			Static Value	Dynamic Value
Elastic Moduli[a,b]				
Bulk	$K = K_o + K_2 J_1$			
Shear	$G = G_o + G_2 \sqrt{J_2'}$			
	K_o	Zero pressure bulk modulus	6.3 GPa	7.0 GPa
	K_2	Coefficient of linear term	−60	−55
	G_o	Zero stress shear modulus	4.7 GPa	5.25 GPa
	G_2	Coefficient of linear term	180	125
Mohr-Coulomb Curve[c]				
	$\sqrt{J_2'} = A_1 + A_2 \exp(J_1/A_3) + A_4 \exp\left(J_1/A_5\right)$			
	A_1	Asymptote of curve	90.0 MPa	104.0 MPa
	A_2	Shear yielding parameters	−83.0 MPa	−83.0 MPa
	A_3	Shear yielding parameters	270.2 MPa	270.2 MPa
	J_{10}	Intercept of Mohr-Coulomb curve on J_1 axis	3.0 MPa	61.0 MPa
	n	Parameter controlling extent of tensile effect on shear curve (used to compute A_4 and A_5).	1.0	1.0
Cap Curve[d]				
	$P^2 + J_2'/W^2 = P_H^2$			
	$P_H(0)$	Pressure for initiation of compaction	−16.0 MPa	−35.0 MPa
	W^2	W is the ratio of semiaxes of the cap ellipse	1.25	1.25

Table 2 (Concluded)

Tensile Damage

S_{cr}	Minimum tensile stress required in calculations	2.0 MPa	2.0 MPa
D	Tensile plastic strain required for separation	0.001	0.001

---

[a] J_1 and J_2' are first invariant of the stress tensor and second invariant of the deviator stress tensor.

[b] Stresses are positive in tension.

[c] The last two Mohr–Coulomb parameters are computed as follows from the input above:

$$A_4 = -[A_1 + A_2 \exp(J_{10}/A_3)] \exp(-n)$$

$$A_5 = J_{10}/n$$

[d] $P_H(0)$ is only the first pressure point on a hydrostatic compaction curve like that given above for POREQST.

The composite model in C-HEMP, called REBAR, provides a series of features that are important in treating reinforcing. The cell behavior is markedly anisotropic; that is, strength and moduli of the cell differ greatly along the plane of the reinforcing (initially the y-z plane) and normal to the plane. The reinforcing plane is permitted to rotate in the x-y plane during the calculation to account for the expected response of the reinforcing mat to a projectile penetration. The concrete may fracture on the reinforcing plane with about the same strength as unreinforced concrete; hence, debonding behavior is approximated by the model.

The method for determining the stresses on a layered composite are outlined briefly, together with the iteration process required to solve the problem for nonlinear stress-strain relations in the components. In the model, external stresses and strains are first transformed to directions parallel and normal to the plane of the reinforcing. Then all stress calculations are made in the geometry that matches the reinforcing directions. The stress state is derived from the strain increments shown on a cell in Fig. 26. The kinematic requirements we applied are that the strains in the steel and concrete parallel to the plane of reinforcing match the imposed strains, and that the sum of the normal displacements, $\Delta\varepsilon_{1S}h_S + \Delta\varepsilon_{1C}h_C$, equals the imposed displacement, $\Delta\varepsilon_1 h$, where h quantities are thicknesses defined in Fig. 26.

The force equilibrium requirements are that the stresses normal to the reinforcing plane be equal, and that a weighted average of the transverse stresses on the concrete and steel portions provide the lateral stress for the computational element.

The stress-strain relations are solved for the current state of stress at each time increment by an iterative technique in the REBAR subroutine. The REBAR routine is provided with the strain increment tensor for the time step. REBAR transforms the stress and strain increment tensors to the reinforcing plane, and estimates the normal strains in each component. Then REBAR calls appropriate stress-strain subroutines for the steel and concrete to determine the stress state in

104
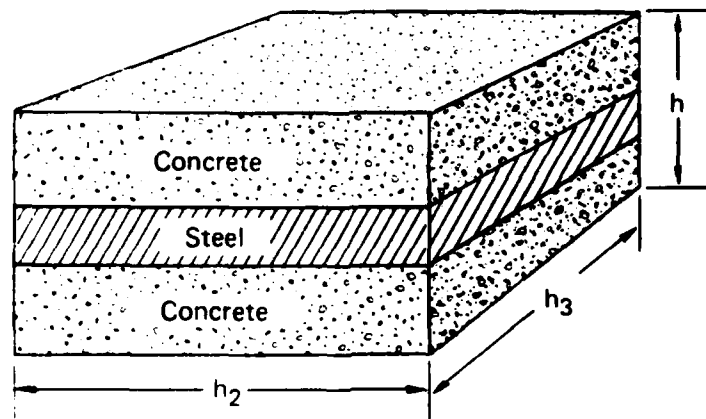
(a) Original Cell Configuration
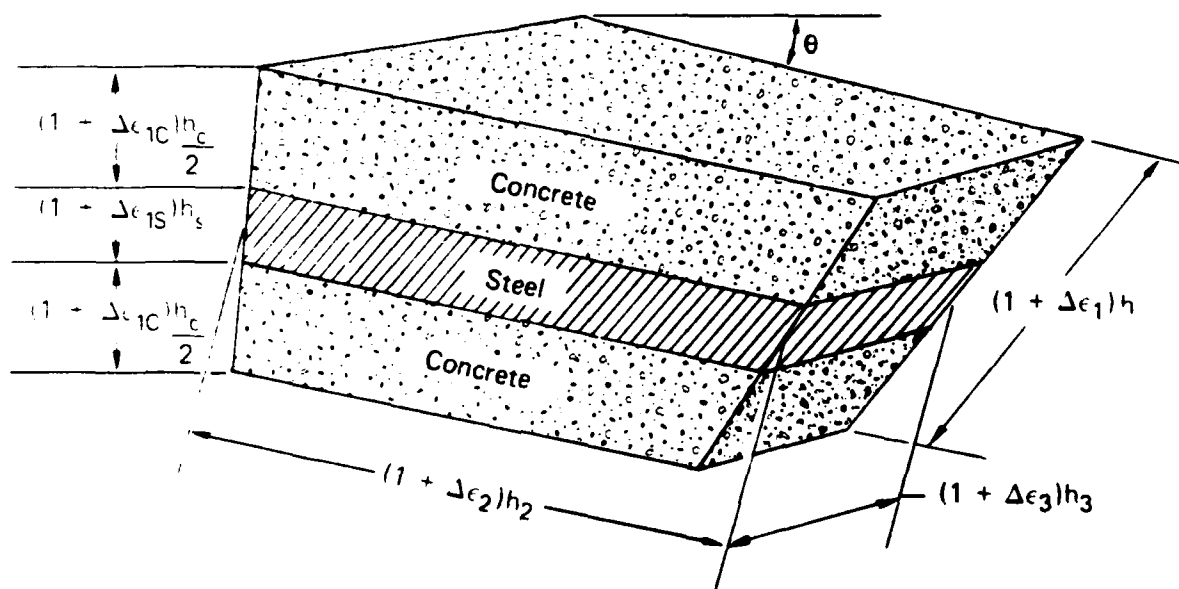
(b) Rotated and Deformed Cell Configuration

MA-4078-114

FIGURE 26   COMPOSITE CELL TREATED BY THE REBAR SUBROUTINE

105

each. The normal stresses from the two components are compared, the normal strains are modified, and the calls repeated until the normal stresses are approximately equal.

The REBAR model for a composite material imposes special demands on a wave propagation code. In our simulations of reinforced concrete walls under impact, we used a CAP model for unreinforced portions of the wall, and a steel model for the projectile. Then in the area of the reinforcing, we used the REBAR model. We used the same steel and concrete models for direct calls by the code and for the calls through REBAR. Hence, it was necessary to construct the call statements such that CAP could determine the stresses in the main arrays for a pure concrete cell, and only provide an estimate of one component of the stress tensor when the call came through REBAR. The necessary flexibility was achieved by allowing all information to pass through the call statements.

E. Models for Fracture

Fracture under tensile or shear stresses is often a dominant process in determining material response. Therefore, it is essential to have a fracture model which is able to represent the fracture phenomena observed or expected. Here we describe three types of fracture model. All can be added to compressive models to give a more complete response for a material. These three types span the range of complexities of available models, from a simple spall model to a nucleation-and-growth micromechanical model.

But first let us examine the physical nature of fracture and then consider the models with which it may be represented. Our observations have indicated the following characteristics:

- Damage in the form of voids, cracks and shear bands, grows as a function of time and the applied stress. Hence a single stress or strain at any time cannot be expected to characterize the dynamic fracture process. At the least some time-integral quantity (such as impulse) must be used to represent the dynamic strength.

106

- As the damage occurs, the stiffness of the material decreases; hence, the wave propagation character changes. If the developing damage is not permitted to alter the wave processes in a computational procedure, then subsequent stress histories and damage must be invalid.

- Even incipient damage levels are important, because, while the voids, cracks, or bands are difficult to observe, they may seriously weaken a structure.

While the foregoing features represent experimental observations well enough, it may be possible to simplify or eliminate some of these features for computational purposes.

In the remainder of the chapter several computational models are introduced. An effort is made to indicate under what circumstances each might correctly characterize fracture. First, the very simplest models are given and later more complex ones that more nearly represent the experimental observations.

1. Static Criteria

Under static conditions it is often assumed that fracture occurs when a peak stress is reached. For multidimensional problems, the peak stress may be replaced by an effective shear stress based on a Mises, Tresca, or Coulomb criterion. Alternatively, a critical tensile strain or some "effective" strain criteria may be used also under wave propagation conditions.

Bertholf[33] used the critical tensile stress criterion in the two-dimensional wave-propagation codes TOODY and CSQ to determine the occurrence of spall in a target impacted by a hypervelocity pellet. The critical stress value was derived from plate impact experiments that had evidenced full spall. The resulting simulations by Bertholf modeled the experimentally observed spall quite well. Cherry[34] implemented a similar criterion in the two-dimensional code TENSOR to study the collapse of the overburden above an explosion at some depth in the earth. In Cherry's case, tensile failure in one direction did not alter strength in the orthogonal directions. Thus, an anisotropy of damage was permitted.

107

Under what conditions can such a simple peak stress criterion be used with some justification? Probably the following conditions should be met:

- The experimental data on which the criterion is based (the plate impacts in Bertholf's case) should exhibit the same stress levels, durations, and wave shapes as those in the problem to be simulated.

- Damage should occur abruptly – within the rise time of a wave, for example.

- Subsequent stress histories and damage are not of interest.

The second and third conditions both deal with the waves that emanate from the region where damage is occurring. Because such waves are not treated correctly in the computations, effects from these waves cannot be interpreted from the computer results.

Addition of a peak stress (or static) damage criterion to a wave propagation code is usually a small task. Such criteria are often present already in the codes. If an isotropic fracture criterion is used, then one new constant is required for each material and one indicator for each cell of the material. Following the stress computation at each cycle for each cell, the three principal stresses are compared with the criterion. If fracture occurs, the stresses are zeroed and the added indicator is set. Thereafter, the stresses are computed as usual but they are zeroed unless they are compressive. For an anisotropic criterion such as Cherry's, a tensile strain (or tensile opening) should be stored for each principal direction for each cell. This strain quantity can be used both as an indicator and also to determine when recompression occurs.

2. Dynamic-Passive Criteria

Dynamic fracture criteria account explicitly for the gradual (time-dependent) growth of damage. Passive criteria monitor the development of damage but do not modify the wave propagation calculations to account for this damage.

108

An example of this dynamic type of criterion is the one introduced by Tuler and Butcher.[35] They represented the damage K by a time integral of the tensile stress σ above some threshold stress σ_o.

$$K = \int_0^{t_1} \left(\sigma - \sigma_o\right)^\lambda \, dt \qquad (166)$$

where integration is only over times when $\sigma - \sigma_o$ is tensile. Here λ is an exponent, usually about 1 or 2.

The critical damage level is presumed to be a material constant K_{cr}. This critical level may refer to full separation, incipient damage, or any other defined level (if an appropriately quantitative definition of damage level can be constructed). This model requires three constants; K_{cr}, λ, and σ_o. With the parameter λ set to 1, Equation 166 is an impulse criterion; at 2, it is an energy criterion. When Equation 166 is used to fit experimental data, λ generally has a non-integral value, and K_{cr} has very odd units.

Dynamic experiments must be performed to obtain the three material constants for the Tuler-Butcher model. The experiments should span the stresses and durations expected in the calculations. A typical set of experiments might produce the results in Figure 27. In this figure, the well-chosen data points just span the amount of damage K_{cr} that is of interest. Usually there will be more experimental points just below the damage threshold: these aid in determining σ_o. With such a set of data, we can determine the three constants by trial. Note that both duration and stress level must be varied in the experiments to provide a basis for the determination.

The Tuler-Butcher criterion may be readily inserted into finite difference wave propagation codes of the Lagrangian type. (The code should have Lagrangian features so that the computed damage quantity K follows a particular material particle.) For each cell the quantity K is stored, in addition to the three constants for each material. The criterion was designed for one-dimensional impact problems: if a three-dimensional problem such as Cherry's were considered, the criterion

109
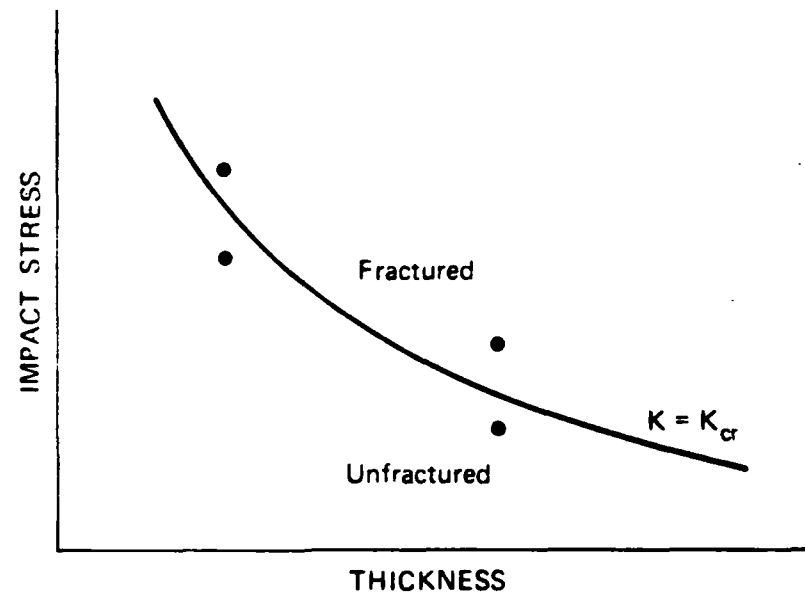
MA-314522-50

FIGURE 27 FRACTURE DATA FROM A SERIES OF FLAT PLATE IMPACTS
TO OBTAIN THE DAMAGE CRITERION FOR THE TULER-
BUTCHER MODEL

110

could be extended to three K values of each cell, one for the direction where the stress threshold was first exceeded, and two for the orthogonal directions. Thereafter, the orientation of the damage plane must be tracked in the calculations. The criterion is inserted immediately following the stress calculations.

The Tuler-Butcher criterion has several advantages over the simpler peak stress criteria. The integral represents more realistically the time-dependent growth of observed damage. Because the criterion is not so critically dependent on a peak stress, larger finite difference cells may be used and still accurately determine the criterion. Such a time-integral criterion is appropriate for extending fracture data obtained with a nearly square pulse shape to more general pulse shapes such as sinusoidal or multiple.

This criterion has the disadvantage of requiring several well-designed experiments plus computer simulations of the experiments. Because there is no physical model from which λ and K_{cr} can be obtained, "reasonable" values cannot be selected intuitively without such experimental data. Another disadvantage is the developing damage does not have an effect on the wave propagation processes; hence, subsequent stress histories and computed damage must be invalid.

3. Dynamic-active Criteria

The dynamic-active criteria follow the gradual development of damage during the wave-propagation process and permit the damage to alter that process. Arbitrary levels of damage may be treated by these methods: an initial designation of a damage level such as full spall is not necessary.

Two approaches have been attempted: The first is a macroscopic approach developed by Norris[36] and his coworkers. The second, in which microscopic flaws are treated, was developed at SRI and is discussed under Nucleation and Growth models.

111

In the macroscopic approach of Wilkins the usual stress-strain relations are used for each cell until a critical plastic strain is reached. Then a single crack is permitted to grow across the cell. This growth occurs at a prescribed velocity and in a direction governed by the orientation of the applied tensile stresses. As the cracks grow, the cell weakens, reaching zero strength as the crack severs the cell. As a cell breaks, nearby cells must take up the load. They may also begin to crack and so the crack appears to extend. Because the direction of crack growth can be arbitrary in the model, both within a cell and from cell to cell, fairly complex and realistic cracking patterns may be treated. The two principal material constants—critical plastic strain for crack initiation and the growth velocity—are derived from experiments with notched specimens. These tests are simulated with a two-dimensional wave propagation code with trial material constants until the experimental results are satisfactorily represented by the computed results.

The main advantage of this macrocrack approach is that the large, observed cracks are treated directly. In addition these cracks may wander across the computational grid; neither their presence nor trajectory needs to be known in advance. The stress-strain relations for a damaged cell are anisotropic, thus tending to direct the growth of the crack. Another advantage of the model is that material constants have a clear physical meaning.

This model has several significant drawbacks. The coding is much more complex than for the earlier models considered. Variables must be stored to define the orientation and length of the crack in each cell, plus the accumulated plastic strain. The anisotropic stress-strain relation must be developed and used. In addition, the material constants are derived from a combination of notch test experiments and multiple simulation calculations; these two-dimensional calculations tend to be lengthy and expensive.

4. Nucleation and Growth Models

The nucleation-and-growth (NAG) models developed at SRI[37] and studied by Kreer[38] and by Stevens, Davison, and Warren[39] deal with the nucleation of microscopic flaws, their growth and coalescence, and the formation of fragments. Three models have been constructed for treating ductile fracture, brittle fracture, and shear banding. Nucleation may occur physically by widening of inherent flaws in the material, cracking of hard inclusions, separating along grain boundaries, or by other mechanisms. In the models, however, nucleation means the appearance of the void, crack or shear band at an observable and easily identifiable size on photomicrographs at a scale of about 100X. This nucleation occurs in the model as a function of stress, stress duration, or strain and strain rate. Following nucleation, the voids or cracks or shear bands grow at a rate that is dependent on the stress level or plastic strain, duration of loading, and the current size of the flaw. The models also account for the stress reduction that accompanies the development of damage. When the number and size of flaws meet a coalescence criterion in the brittle fracture and shear banding models, the flaws begin to join and form isolated fragments. With continued loading, all the material forms fragments and complete separation may occur.

The computational models of ductile and brittle fracture and of shear banding are implemented in subroutines that may readily be inserted into one- and two-dimensional Lagrangian wave propagation computer codes. While the material is undergoing fracture, these subroutines are called instead of the usual equation-of-state subroutines.

Basic to the development of the NAG models is the quantitative determination of the damage observed on cross sections of impacted samples. In ductile fracture, the damage occurs as nearly spherical voids; in brittle fracture, the flaws are cracks; in shear banding, the flaws appear as shear cracks.

113

The ductile and brittle fracture parameters are usually derived from experiments like that shown in Figure 28 in which a thin flyer plate is propelled against a thicker target plate. Then the target is sectioned as shown in the inset in Figure 29, and the length, orientation, and distance from the impact plane of all voids or cracks are measured. These surface distributions are then transformed statistically to volumetric distributions by a method analogous to Scheil's.[45] These volumetric crack size distributions are all approximated by the equation

$$N_g(R) = N_o \exp(-R/R_1) \qquad (167)$$

where N_g is the cumulative number/cm^3 of cracks or voids with radii larger than R, N_o is the total number/cm^3 and R_1 is a distribution shape parameter.

Nucleation in the model occurs as the addition of new cracks to the existing set. These new cracks or voids are presumed to occur in a range of sizes with a size distribution like Equation 167. At nucleation, the parameter R_1 equals R_n, the nucleation size parameter (a material constant). The number of cracks or voids nucleated is governed by a nucleation rate function:

$$\dot{N} = \dot{N}_o \exp \left[\left(\frac{\sigma_{\phi\psi} - \sigma_{no}}{\sigma_1} \right) - 1 \right] \qquad (168)$$

where $\dot{N}_o$, σ_{no}, and σ_1 are fracture parameters and $\sigma_{\phi\psi}$ is stress normal to the plane of the cracks. (For ductile fracture, $\sigma_{\phi\psi}$ is replaced by the pressure.)

The growth law, derived from experimental data on both ductile and brittle fracture, is:[37,40]

$$\frac{dR}{dt} = T_1 \left(\sigma_{\phi\psi} - \sigma_{go} \right) R \qquad (169)$$

114

0.236 cm   0.635 cm

154.2 m/s

Sectioning Plane
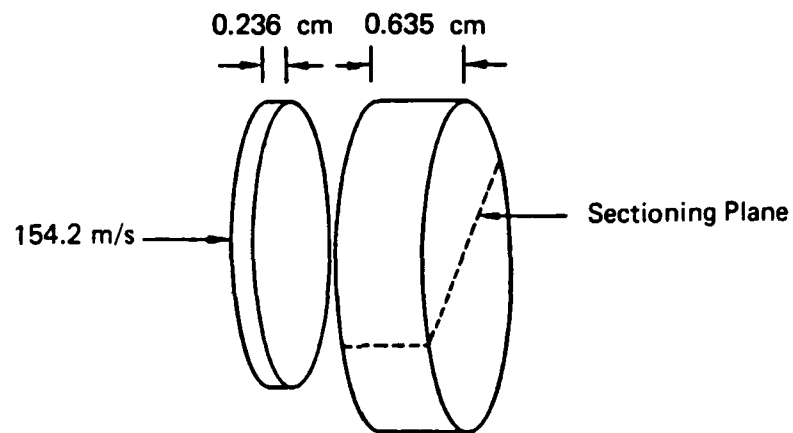
(a) Impact Configuration for 1145 Aluminum
Specimen No. 872

200 μf
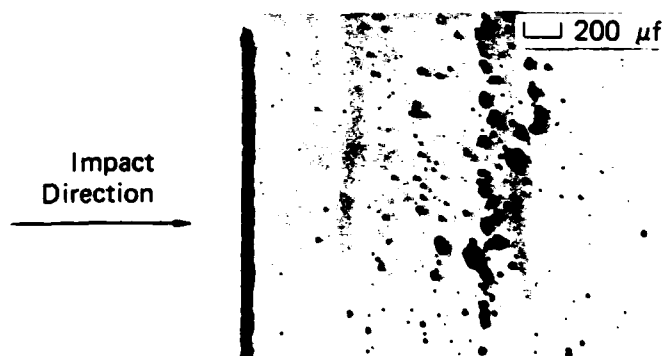
Impact
Direction

(b) Section Through Target Showing Ductile
Fracture Damage

MP-314522-48

FIGURE 28   CONFIGURATION FOR A FLAT PLATE IMPACT EXPERIMENT
IN 1145 ALUMINUM AND OBSERVED DAMAGE ON A CROSS
SECTION

115
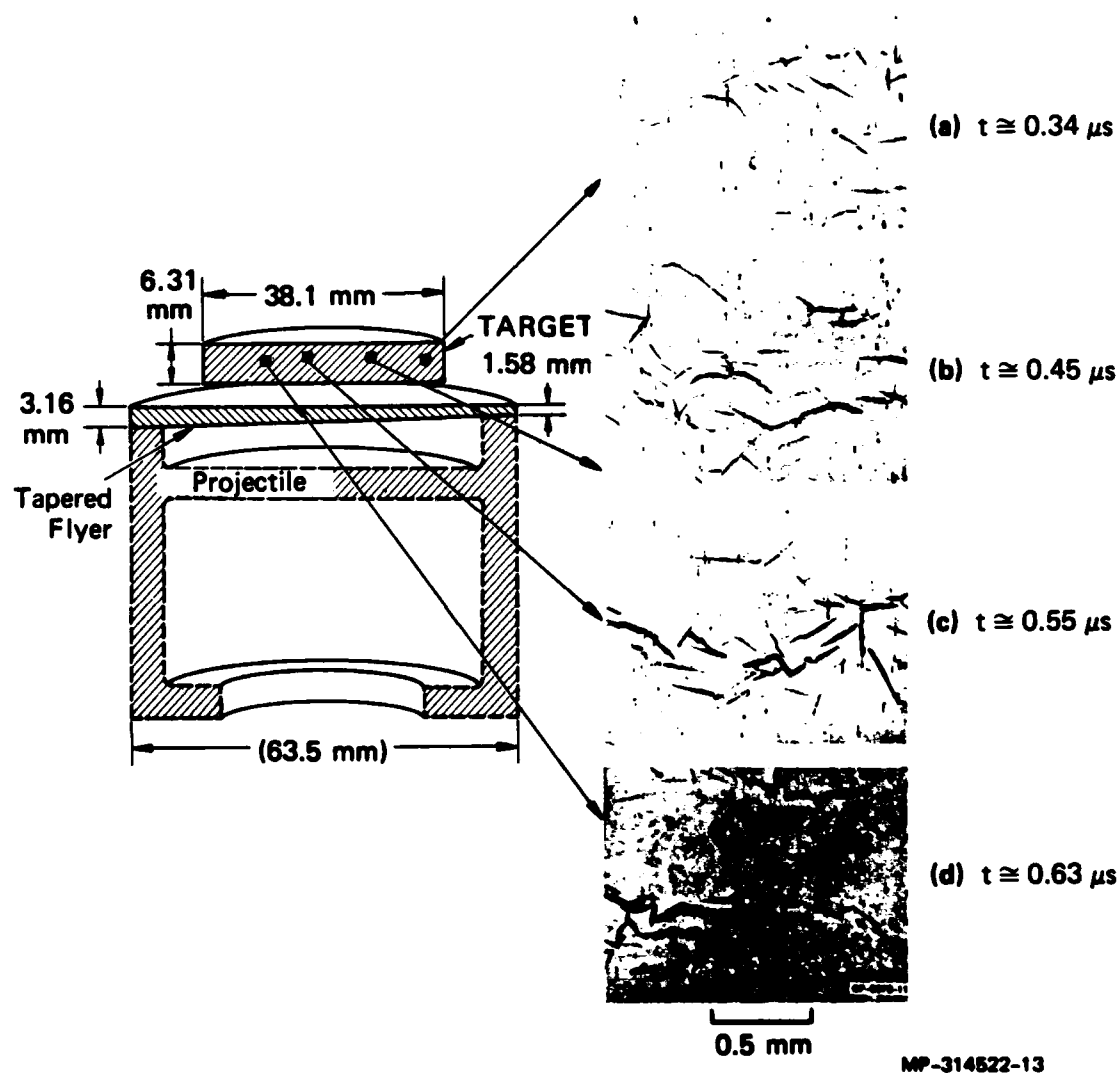
FIGURE 29   CONFIGURATION OF A TAPERED FLYER IMPACT EXPERIMENT
IN ARMCO IRON (SHOT S1) AND OBSERVED DAMAGE ON A
CROSS SECTION OF THE TARGET

116

where T_1 is a growth coefficient and σ_{go} is the growth threshold stress. Here σ_{go} is usually treated as a constant material parameter.

A relationship between the fragment sizes and the numbers and sizes of the preceding cracks is required to model the fragmentation process. From our observations in both rocks and metals it appears that the fragments are typically chunky objects with an average of six to eight sides, each side probably being produced by one crack. Thus, for large fragments, the crack radius may approximate the fragment radius and the number of fragments may be one-third to one-fourth the number of cracks.

All the stresses are computed from the strains in the solid material, not the gross strains. This gross strain is presumed to be composed of a solid strain and a change in crack volume associated with growth and nucleation:

$$\Delta \epsilon = \Delta \epsilon_s + \Delta \epsilon_g + \Delta \epsilon_n \tag{170}$$

For the model calculations, only $\Delta \epsilon$ is known. $\Delta \epsilon_s$ is related to the applied stresses through the usual elastic-plastic relations. $\Delta \epsilon_g$ represents the increase in strain associated with opening of the existing growing cracks. $\Delta \epsilon_n$ represents the increase in strain associated with opening of new cracks. Appropriate stresses are found by requiring that Equation 170 be satisfied. Each term on the right is a nonlinear function of stress; therefore the solution is conducted by an iteration procedure.

The shear band model treats a statistical distribution of bands at each point in the material. The bands are envisioned in the model as small, circular, planar regions that have lost their cohesive strength. In our experiments with fragmenting cylinders, projectile penetrations, and Taylor tests (blunt cylinder impacts on unyielding targets), the shear bands occur in a range of sizes. As an example, Figure 30 shows the size distributions of bands seen on the inside of a cylinder expanded by explosives detonated along the cylinder axis. The counted bands are also shown schematically in the figure. They have been transformed

117

(a) Cross Section of Cylinder
    With Damage

(b) Surface Data

(c) Volume Data

$N_o e^{-R/R_1}$
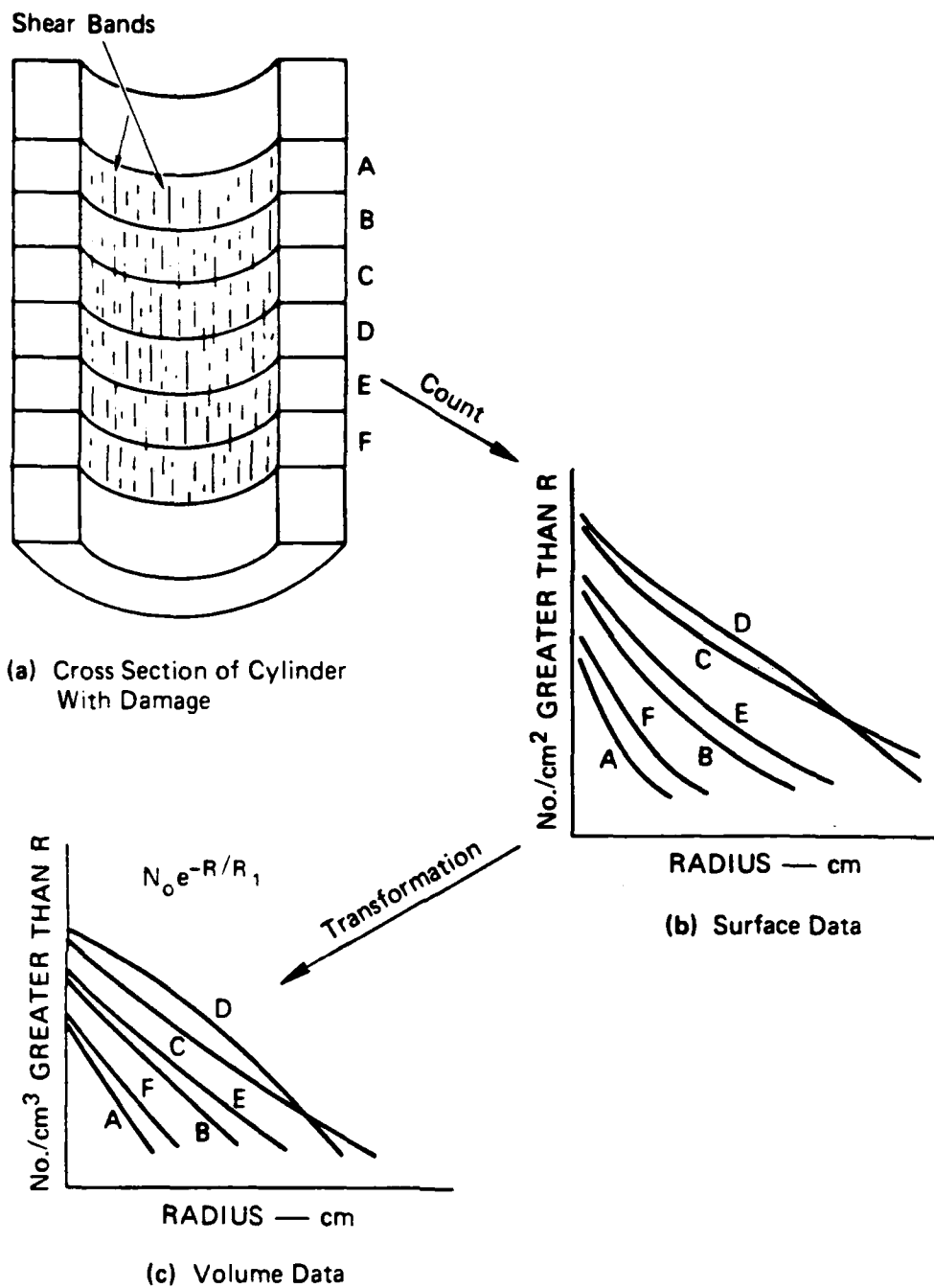
MA-7893-98

FIGURE 30   STEPS IN OBTAINING CUMULATIVE SHEAR BAND DISTRIBUTIONS
            FROM CONTAINED FRAGMENTING CYLINDER DATA

118

to a volumetric distribution with Scheil's method. At nucleation the distribution is assumed to be exponential, with the form of Eq. 167. After growth and further nucleation the size distribution retains an exponential form.

In our experiments the bands usually occur in discrete orientations, on the planes of maximum shear strain. In the model, we chose to represent the damage in nine orientations, as shown in Figure 31. Each orientation can be considered to consist of bands on that specific plane or to represent bands with orientations that range over a solid angle of $4\pi/9$. A size distribution, such as that in Figure 32, is assigned to each orientation. For three-dimensional motions, the nine band orientations represent all possible bands, and all quadrants are equally well represented. In two-dimensional motions, some reduction in orientations can be made by using only planes that have unique normal and shear stresses. Also, normal and shear strains on the plane must represent permitted strains on the material, that is, no ϵ_{xz} and ϵ_{yz}. The SHEAR models have been used only for one- and two-dimensional geometries although they account for three-dimensional stresses and damage orientations.

For SHEAR4 we combined orientations 5 and 8 and orientations 6 and 9, so only seven orientations are required. In two dimensions these pairs of orientations have identical stresses. Strains on these pairs of planes combine to provide zero values for the ϵ_{xz} and ϵ_{yz} strains. As deformation occurs, the bands rotate with respect to each other, so they do not retain the angular relationship shown.

In SHEAR3 all the orientations rotate together with the average rotation of the material. Without independent rotations, orientations 1 and 3 and orientations 2 and 4 are equivalent. Hence, we used only four orientations in SHEAR 3: 1, 2, 5, and 6 (7 is inactive because it receives no shear strain).

Bands begin to appear in the model when the plastic shear strain on any plane exceeds a critical value. After the threshold strain is reached, bands are nucleated according to a rate function containing

119
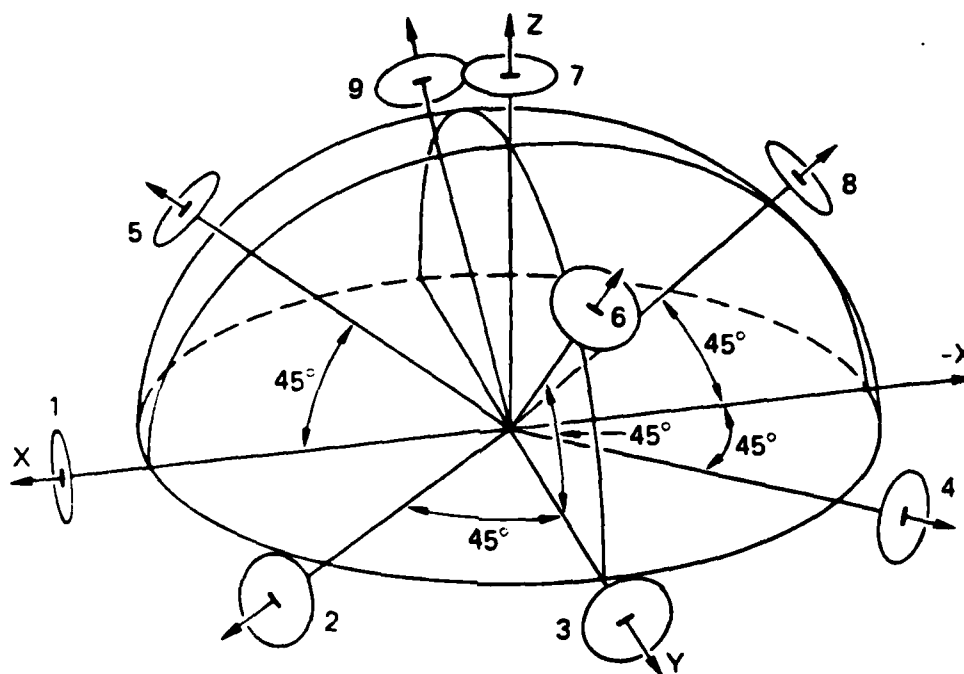
MA-7893-3A

FIGURE 31   RELATIVE LOCATIONS OF THE COORDINATE
DIRECTIONS AND INITIAL ORIENTATION
OF THE SHEARING PLANES

120
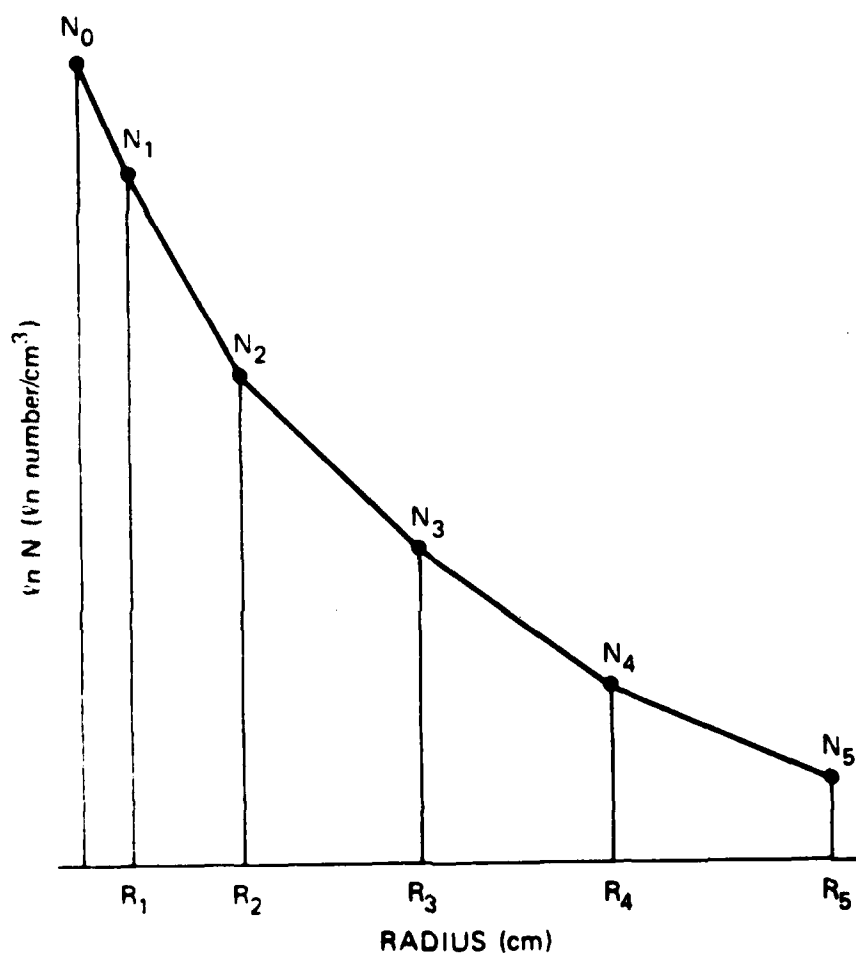
FIGURE 32   SHEAR BAND SIZE DISTRIBUTION
REPRESENTED BY A SERIES OF
POINTS AND EXPONENTIAL LINE
SEGMENTS

121

plastic strain, strain rate, the critical strain, and a critical strain rate. The critical strain rate is that required to maintain approximately adiabatic conditions. The nucleation rate is

$$\dot{N} = \alpha \, N_0 \, H\!\left(\epsilon_m^P - \epsilon_0\right) \, \dot{\epsilon}_m^P \, \exp\!\left(-\dot{\epsilon}_0 / \dot{\epsilon}_m^P\right) \tag{171}$$

where $\alpha = \sigma_y/(\rho E_m)$, σ_y, p and E_m are yield strength, density, and melt energy, and N_0 is the number of potential nucleation sites per unit volume. H is a Heaviside function, ϵ_m^P and $\dot{\epsilon}_m^P$ are continuum in-plane plastic strain and strain rate, ϵ_0 is the plastic strain at the maximum shear stress (about 20% in 4340 steel), and $\dot{\epsilon}_0$ is the strain rate required to attain adiabaticity at the nucleation sites.

The bands grow under the imposed strain rates according to the following relation, subject to some restrictions:

$$dR/dt = T_1 \, \dot{\epsilon}_m^P \, R \tag{172}$$

where R is the band radius in plan and T_1 is the growth coefficient. The restrictions are that dR/dt cannot exceed the shear wave speed, V_s, and that the total strain taken by the band cannot exceed the total imposed strain. The strain taken by the band is

$$\Delta\epsilon = \pi \, b \, \sum_i N_i\!\left(R_{2i}^3 - R_{1i}^3\right) \tag{173}$$

where $b = B/R$, B is the average slip over the plane of the band, and R_1 and R_2 are the band sizes before and after growth, respectively. The summation is over all the band sizes in the orientation. If $\Delta\epsilon$ from equation (173) exceeds the imposed strain, then the final band radius is reduced to force $\Delta\epsilon$ to agree with the imposed strain.

The bands are assumed to be initially isolated, and their nucleation and growth can be treated as if they were each a single band in an infinite medium. However, at some time the bands begin to interact strongly, coalesce, and finally form fragments. The condition

122

for full fragmentation is written by considering the fragmented state.
Each fragment has some small number of faces, each formed by bands. The
sizes of the fragment faces are related to the band sizes. With these
considerations, we have derived a criterion for fragmentation:

$$\tau_\ell = c \int_0^{R_{max}} R^3 dN \tag{174}$$

The factor c allows for the spacing of bands normal to their plane. The
parameter τ_ℓ describes the degree of fragmentation on the ℓth plane.
When τ_ℓ reaches one, full fragmentation has occurred on that plane.

To solve for the stress state resulting from an imposed strain
increment, it is necessary to determine the plastic strains and
developing shear band damage. For our model, these strains and damage
are computed on each band orientation plane. In SHEAR3 the yield occurs
by a rate-independent process.

For the SHEAR4 model, yielding on each plane is allowed to develop
gradually, following the stress-relaxation process:

$$d\sigma_\ell'/dt = 2G \, d\varepsilon_\ell'/dt - \left(\sigma_\ell' - Y_{\ell s}\right)/T \tag{175}$$

where σ_ℓ' is the shear stress on the plane ℓ, G is the shear modulus, ε_ℓ'
is the tensor shear strain acting on the plane, T is the time constant
(either a material constant or a constant chosen for computational
convenience), and $Y_{\ell s}$ is the shear strength on the plane ℓ. Equation
(175) is integrated numerically over four to ten subcycles within each
imposed time increment. During these subcycles, the overstress, σ_ℓ' −
$Y_{\ell s}$, will gradually decrease and plastic strain will increase on the
yielding planes. Each time increment begins with a cell-centered
elastic calculation of the stresses, based on the strain increments.
From these stresses the shear strains ε_ℓ' on each plane are determined.
On yielding planes, plastic strain is developed and used to modify the
imposed strain for the next cell-centered calculation. During the
subcycles, the overstress, $\sigma_\ell' - Y_{\ell s}$, gradually decreases and plastic

123

strains increase on the yielding planes. The stress-relaxation process therefore provides a means for spreading the plastic strains over several orientation planes.

The SHEAR models are able to represent the local growth of micro shear band damage within a cell, but they also can depict the large-scale propagation of shear bands from one cell to another. Such large-scale bands are those that separate the plug from a target or sharpen a projectile. This formation of large bands is not required by the model formulation, but occurs by the natural interaction of cells with damage.

The ductile and brittle fracture and shear banding models have been inserted into one- and two-dimensional wave propagation computer programs. The subroutines containing these models (DFRACT, BFRACT, SHEAR3, and SHEAR4) act as equation-of-state routines. Such routines are provided the strain and must compute the stresses. These models compute stress but also compute the current damage. At any time in the calculation a complete listing of the fracture damage present in a cell may be obtained.

The main advantage of the NAG approach is that damage is obtained in such detail that precise comparisons with observed damage can be made. Residual strength properties can be assessed from the computed damage. The stress-strain relations are modified to account for developing damage so that subsequent waves are handled with some accuracy. The NAG computations are independent of stress pulse shape and source: thus the same parameters describe fracture under plate impact, explosive loading, or sudden radiant heating. The NAG approach also has the advantage that there is more material information involved in it and hence it is more likely to represent reality. Some of the parameters are estimable from static fracture data, some from shock front thickness, others from microscopic observation; hence, the parameters appear to have physical significance.

The increased memory required for the fracture quantities and the increased computer time are the main drawbacks of the NAG models. The fracture parameters must be derived from several plate impact or

124

contained fragmenting cylinder experiments plus a series of simulation calculations.

Samples of the input for SHEAR3 are given in the first and third problems of Section VI. A BFRACT sample is in the fourth problem. Input for these models are also outlined further in the next section.

IV   INPUT FOR C-HEMP

This section describes the input required for C-HEMP. Most of the input is in a free-field format, but the title and data for some material models are in fixed formats.

First, a sample input for simulating a fragmenting round is exhibited: Figure 33. The first line is a title, read in alphanumeric format. Subsequent lines are in groups headed by labels that begin on the first line. For example, "GENERAL" is a heading for some general control parameters. Under this heading are three lines of values in this sample. In these lines there are parameter names followed by values. The next two lines begin with "COM": these are comment lines. Comment lines are read and printed but not interpreted. "MATERIAL" begins a set of 9 lines describing RHA steel. In this group is "SHEAR3", the model which is called to represent the steel. The data following "SHEAR3" in this set is read and interpreted by SHEAR3. The second material is an explosive (PETN) and the EOSTAB subroutine is used for the isentrope. The next lines after "EOSTAB FIXED FORMAT" are ready by EOSTAB in fixed format. Farther down in the input are other major labels (keywords): BLOCK, GRID, BOUNDARY, SLIDE, and HISTORY. Under "BLOCK", the labels XA and YA are each followed by four values. More multiple values appear after "SLIDE". The interpretation of the "HISTORY" input is somewhat different: the two values following "XD" are the X and Y coordinates of the point where the XD (X-velocity) is requested.

The input procedures are described in the following subsections. The emphasis here is on the free-field input procedure which has a format that is novel to C-HEMP. Of course, fixed format lines need not conform to these rules. The title line has no required form, and the data for models, such as EOSTAB, in Figure 33, must conform to the formats in EOSTAB.

127

```
                HEMP 2-D SHEAR3 ROUTINE TEST W/ 4340 FRAGMENTING ROUND
GENERAL       IPRINT=100        NMAX=800          STOPT=1.0E-04
              CLIN=0.1          CQSQ=4.0
              NGEOM=2           NPLOT=200         PSCRIB=1.
COM    THE RHA IS BEING TREATED WITH AN INITIAL ESTIMATE OF THE SHEAR3
COM     PARAMETERS. THEY MAY CAUSE TOO MUCH DAMAGE.
MATERIAL      AMAT=RHA          RHO=7.85
              EQSTC=1.59E12     EQSTD=5.17E12     EQSTS=5.17E13
              EQSTE=7.36E10     EQSTG=1.69        EQSTH=0.25
              YC=.68E10         MU=8.19E+11       TSR=0.05 1.0
   SHEAR3     BFR = 14. 0.146 .01 .2 1.5 .07 .04 1. .577 2. 2. 0 8. 0.
              ES = 0. 0.02 0.07 0.12 0.17 0.27 0.47 1.3
              YS = 6.8E9 7.7E9 8.7E9 9.5E9 10.4E9 11.1E9 12.4E9 14.E9
              FNUC =-1. 1. 1. 1. 1. 1. 1.
              EN3
MATERIAL      AMAT=PETN         RHO=1.0              EQSTG=1.45 WVAR=7
   EXPLODE    QEXPL=3.013E10  DIST=0.5      XDET = 0.8
COM    THE TABULAR DATA FOR THE ISENTROPE IS READ WITH FIXED
COM     FORMAT IN EOSTAB.
   EOSTAB    FIXED FORMAT
   IMAX =            13 DENSITY    LOG
   RHO,P =   1.043E+00 4.557E+10 8.166E-01 2.523E+10 6.394E-01 1.437E+10
             5.007E-01 8.417E+09 3.920E-01 5.063E+09 3.070E-01 3.127E+09
             2.404E-01 1.981E+09 1.882E-01 1.286E+09 1.474E-01 8.529E+08
             1.154E-01 5.772E+08 9.037E-02 3.978E+08 7.076E-02 2.785E+08
             2.660E-02 7.506E+07
MATERIAL      AMAT=PMMA         RHO=1.18
              EQSTC=8.94E10     EQSTD=4.57E10     EQSTE=1.0E10
              EQSTG=1.0         EQSTH=0.25        EQSTS=4.36E11
              YC=1.03E8         MU=8.19E11
MATERIAL      AMAT=S4140        RHO=7.85
              EQSTC=1.59E12     EQSTD=5.17E12     EQSTE=7.36E10
              EQSTG=1.69        EQSTH=0.25        EQSTS=5.17E13
              YC=6.0E09         MU=8.19E11
MATERIAL      AMAT=LEAD         RHO=1.14E01
              EQSTC=5.01E11     EQSTD=4.99E11     EQSTE=9.16E09
              EQSTG=2.20        EQSTH=0.25        EQSTS=2.02E12
BLOCK         XA= 0.635        13.335       13.335         0.635
              YA= 0.           0.           2.28           2.28
              NC12=40          NC23=6                  AMAT=PETN
   EXPLODE
GRID          XA= 0.           15.24        15.24          0.
              YA= 2.28         2.28         3.42           3.42
              NC12=25          NC23=3                  AMAT=RHA
COM           SLIDE 1 TO 2
BLOCK         XA= 0.           15.24        15.24          0.
              YA= 3.42         3.42         4.37           4.37
              NC12=25          NC23=1                  AMAT=PMMA
```

JA-314522-117

FIGURE 33   INPUT FOR CONTAINED FRAGMENTING CYLINDER SIMULATION

128

```
BLOCK          XA= 0.          15.24         15.24        0.
               YA= 4.37         4.37         10.16       10.16
               NC12=25         NC23=10              AMAT=S4140
BLOCK          XA= 0.          15.24         15.24        0.
               YA=10.16        10.16         12.7        12.7
               NC12=25         NC23=2               AMAT=LEAD
BOUNDARY       NBCTYP=1        YAFECT=3.          YCONST=0.
COM    SLIDE LINE IS BETWEEN THE EXPLOSIVE AND RHA CYLINDER ONLY.
SLIDE          NSL 7,14,21,28,35,42,49,56,63,70,77,84,91,98,105,112,119
               NSL 126,133,140,147,154,161,168,175,182,189,196,203,210
               NSL 217,224,231,238,245,252,259,266,273,280,287
               VAL=0.0 NMS 288,292,296,300,304,308,312
               NMS 316,320,324,328,332,336,340,344,348,352,356,360,364
               NMS 368,372,376,380,384,388
               IDIR=1
HISTORY        XD 0.79375 0.19,  P 6.985 1.14,  YD 0.3048 2.35125
               SYY 6.985 2.35125,  YD 6.985 2.35125,  SYY 0. 2.8
               2.0 2.8, 4.0 2.8, 6.0 2.8, 8.0 2.8 10.0 2.8 12.0 2.8
```

JA-314522-118

FIGURE 33   INPUT FOR CONTAINED FRAGMENTING CYLINDER SIMULATION
(Concluded)

129

We begin the discussion of input with the free field syntax, and then summarize the input data groups, and then describe each data group in detail.

A. Free-Field Input Format

The free-field data read from FORTRAN unit 5 conforms to the following format:

KEYWORD LABEL = VALUE VALUE VALUE   LABEL = VALUE VALUE VALUE VALUE...
KEYWORD LABEL = VALUE...
SUBKEYWORD LABEL = VALUE VALUE...
  [end-of-file]

The identifiers represented by KEYWORD, SUBKEYWORD, and LABEL are alphanumeric and may have any length so long as the enti e word is on one line. Only the first 8 characters of the word are used in the program as an identifier. Abbreviations to the words (such as MAT for MATERIAL) may be used if they are unique. Longer versions (such as BLOCKTARGETOF4340STEEL) can be used for ease of reading, but do not affect the treatment by the code. Words must start with an alpha character. The data values can be numerical or alphanumerical. Numerical data values may be represented in any appropriate FORTRAN format. All physical quantities should be in cgs units unless otherwise indicated. The material names are data values which must be in alpha form. Therefore, the code initially interprets them as LABELS. To force the code to interpret any characters as words, use quotes around them: "4340 STEEL". Note that the quoted form also allows for an intervening separator, the blank.

The labels and data values must be separated by one or more of the separation symbols: blank, comma, equal sign, and semicolon.

The data are divided logically into data groups, each associated with a specific task carried out by the code in setting up the problem. Each free-field data group consists of a keyword, such as

130

"GENERAL", subkeywords ("SHEAR3"), labels ("IPRINT"), and data values associated with the labels. Subkeywords and data values are optional components of the data group. The tasks are identified by keywords, such as "GENERAL" and "MATERIAL". The keyword is usually the name of the subroutine that performs the associated task. Each keyword must begin in column 1; the associated data group may then be continued onto subsequent card images, which must have a blank or dollar sign in column 1.

Subkeywords are the names of subroutines which are called to read portions of the data. Most of these are special material models. The labels are usually the names of variables or arrays into which the data values are to be read. Each label may be followed by one or more data values.

Four special indicators are also provided: COM, FIX, END, and END DATA. Card images beginning with COM are treated as comment lines and are not processed as input (except the title line, which is always read as is). The FIX indicator causes an interruption of the free-field input; its main purpose is to permit the use of special material models that do not handle the free-field logic and therefore require fixed-format input. Normally, free-field input resumes after the last fixed-format card image is read. The END label terminates processing of the current line. When any of these indicators are encountered, the rest of the line is echoed even if it is not processed. Thus, COMMENT is equivalent to COM, and FIXED FORMAT is equivalent to FIX. When the composite label END DATA is encountered, all input processing stops. Hence, unused data can be stored in the deck after the END DATA words without affecting a calculation.

The C-HEMP convention is that all special material models control the reading of their own data. The MATERIAL data group permits the inclusion of a subkeyword (such as, "EOSTAB") to identify special data; when subroutine MATERIAL processes the subkeyword, it calls the subroutine containing the special material model. The subkeyword must not start in column 1: the subkeyword and its associated data subgroup belong to the MATERIAL data group.

131

The HISTORY group accepts a special format that allows several data values to be associated with more than one label.

The C-HEMP input system has two additional capabilities. An array element may be specified as part of a label: BFR(6) = 3.2. A repeat count may be used to enter multiple data values; 3*1.0 is equivalent to 1.0 1.0 1.0.

Because the code lays out the finite difference mesh and initializes the material arrays during the input process, the order in which data groups appear is important.

B. Summary of Data Groups

Here is a checklist of data groups, with ordering rules.

- GENERAL -- General options for the run; may appear anywhere in the input data stream. Required.

- MATERIAL -- One group of material properties for each material. All MATERIAL groups must precede all layout groups (BLOCK, GRID, BOUNDARY, and SLIDE). At least one MATERIAL group is required. Optionally, one or more data subgroups for special material models (EP, SHEAR3, SHEAR4, EXPLODE, BFRACT, EOSTAB) may appear at the end of a MATERIAL group; the special data must be repeated for each material the model is to apply to.

- BLOCK -- Sets up a block of cells for a single material. At least one BLOCK or GRID required.

- GRID -- Like BLOCK, but starts a mesh for an independent object.

- BOUNDARY -- Sets up boundary conditions. Must follow the last of the BLOCK and GRID groups. The default boundary condition is a free surface. If other conditions are desired, they are entered through BOUNDARY.

- REZON -- Parameters for the automatic rezoner. Must follow the last of the layout groups. Optional.

- SLIDE -- Identify special boundary conditions. Must follow the last of the BLOCK and GRID groups. Optional.

132

- HISTORY -- Tags locations in storage for output after every computational cycle. Must be the last group. Optional.

- RESTART -- After the last computational cycle, a restart dump file is written on file 10. If that file has been saved, then the problem may be restarted at this cycle. When restarting, the line first after the title must begin with RESTART (left justified). This line must be followed by the input blocks GENERAL and MATERIAL and optionally HISTORY. Set the restart file to File 9. In the GENERAL block only changes from data formerly specified need to be given. NMAX or STOPT has to be changed. These are both counted from the start of the original run. If the first run stopped at NMAX=200, specifying NMAX=300 will make the code run 100 more cycles. For the MATERIAL block a complete set of data, changed or unchanged, must be given. Input to BLOCK, REZONE, GRID, BOUNDARY, SLIDE or WALL may give unpredictable results.

In addition, the WALL keyword is recognized but ignored. Use BOUNDARY for wall boundary conditions.

C. Detailed Description of Input Data Groups

The special parameters and rules required for each input data group are given in this section. Required quantities are marked. Default values are zero unless otherwise noted. Unless otherwise indicated, all physical quantities must be expressed in cgs units. Some variables (e.g., AMAT) may appear in more than one group with different functions.

GENERAL

This data group is used for parameters that will affect wave propagation or input/output for the entire run.

- CLIN -- Linear artificial viscosity coefficient. (See Section II.E) Default: 0.05

- CQSQ -- Quadratic artificial viscosity coefficient. (See Section II.E) Default: 4.0

- IPRINT -- Cell and node edits are printed every IPRINT cycles. Default: 10

- ISOBAR — This indicator constitutes a request that isobar contour data be dumped to File 19 during the computation.

- NPLOT — Plot data are dumped to File 16 every NPLOT cycle by PLOTT on calls from CYCLE. The default, 0, suppresses plot output.

- PSCRIB — Set to any nonzero value to produce a separate history plot file on File 17 (see the HISTORY data group). Default: 0

- STOPT (Required) — Computation is terminated if the time exceeds STOPT seconds.

- NMAX (Required) — Computation is terminated if the cycle number exceeds NMAX.

- NGEOM — 1 for plane strain, 2 for cylindrical coordinates (with Y in the radial direction). Default: 1

- NSLIDE — Number of slide lines. Computed in GENR from the input.

- JP — No longer in use.

- TPLOT — Plot data are dumped to File 17 every TPLOT seconds. The default, 0, inhibits plot output. If both TPLOT and NPLOT are positive, plot data will be written every NPLOT cycles and every TPLOT seconds.

- DTMIN — If the time step for a cell goes below this value, the stresses in the cell and the natural time step for the cell are no longer computed. The sound velocity of the cell is set negative to flag the condition. The default, 0, inhibits use of this feature.

MATERIAL

This group specifies the material properties for a single material; there must be a separate MATERIAL group for each material used in the mesh layout. The default material model is the Mie-Gruneisen equation of state for pressure, and deviator stress calculated from an elastic-plastic model with linear work hardening and Coulomb friction. These default models are in subroutine CYCLE. Parameters for special material

134

models are specified by inserting, at the end of the MATERIAL group, one
or more special material model subgroups (see below).

When multiple values are entered for a single variable, each
successive entry overwrites the previous one. Thus, the sequence RHO =
3.5 1.0 2.2 3.3 sets the density to 3.3. With arrays, however, succes-
sive entries occupy successive positions in storage, with no check
against array dimensions.

The ESC label is available for convenience in inputting a large
number of material parameters. Positions in the ESC array are equiva-
lenced to parameter values in the order shown in Table 1, Section
II.J. For example, $ESC(L) = RHO(L)$; $ESC(L+4) = MU(L)$, and $ESC(L+15) =$
$EMELT(L)$ where $L = LE(m)$, the starting location for data pertaining to
the mth material. The variable EMELT can be initialized only through
the ESC array. $ESC(L+10)$ is not currently equivalenced to any
variable. The variables in the ESC array are defined as follows:

- AMAT (Required) -- The material name, entered as a
  contiguous string of up to 8 characters, e.g., AMAT =
  STEELS1. Use single quotes to input a name containing
  blanks: AMAT = 'STEEL S1.'

- BFR -- Special material model array initialized during
  CALLs to the model subroutine. BFRACT3 uses this
  array. Some material models, such as SHEAR3 and SHEAR4,
  are provided with local BFR arrays that do not share
  storage with the COMMON arrays.

- (EMELT) -- Melt energy. Name this quantity "ESC(16)"
  for input.

- EQSTA, EQSTV -- Parameters for the PEST model. (Not
  implemented.)

- EQSTC (Required), EQSTD, EQSTS -- The first, second, and
  third series-expansion coefficients for the bulk
  modulus.

- EQSTE -- Sublimation energy. (Not implemented.)

- EQSTG (Required) -- Gruneisen ratio.

- EQSTH -- Gas Gruneisen ratio. (Not implemented.)

135

- EQSTN — (Not implemented.)

- G2 — 2* shear modulus. (Computed by MATERIAL).

- MU — Shear modulus. The default, zero, provides a fluid behavior with no shear stress.

- PMIN — Minimum pressure permitted, a spall strength. Use a negative value. The default, zero, is interpreted as no limit on pressure.

- RHO (Required) — Density. If RHO and RHOS are not both entered, the missing value is taken from the one supplied.

- RHOS (Required) — Starting density of the solid portion of a porous material. See RHO for default.

- TSR — Special material model array. Five spaces are allocated for each material, but only the first one is currently in use. This one is a coefficient for an antihourglassing viscosity. Recommended values are between 0.02 and 0.10.

- YAD — Work-hardening modulus. The default, zero, provides for perfect plasticity.

- YC — Yield strength. For zero yield strength (the default), the material acts as a fluid.

A number of indicators are provided in the input to designate the type of material model and the amount of storage for the properties.

- WFR, WPOR, WDS, WCMP, WPR — Indicators for special material models. These indicators tell the code to call the special model subroutines to do stress-strain calculations. Some models (EPP, SHEAR3, SHEAR4, EXPLODE, BFRACT3, POREQST, REBAR, CAP1), initialize their own indicators. For undefined values, the default action is taken (i.e., no model called, except for WPR). The following values are recognized:

        WFR   (FRacture Models)
          1   DEFRACT
          2   BFRACT (subroutine BFRACT3)
          3   SHEAR3
          4   SHEAR4
          5   (no fracture)
          6   DFRACTS

136

```
WPOR      (PORous equations of state)
    1     POREQST
    2     POREQST
    3     POREQST
    4     CAP1

WCMP      (COMPosite models)
If not 0, REBAR

WDS       (Deviator Stress models)
    7     EP (subroutine EPP)

WPR       PRessure models)
    0     Mie-Gruneisen
    1     EXPLODE
    2     PW = EQSTC(M) (used for constant pressure
          boundaries)
```

- WEQS — Space allotted in the ESC array for each material's properties. The current default, 50 variables, suffices for all standard models.

- WVAR — Space allotted in the COM1 array for each cell's special material parameters. The general default is zero. Special models EPP, SHEAR3, and SHEAR4 determine WVAR automatically.

- WBFR, WTRI, WTSR, WYAM — Indicators not used, but retained for compatibility with earlier versions.

The input for particular models is described in detail elsewhere, and only general rules are presented here. The model data group must be associated with one of the subkeywords listed below. A model may require special storage for material quantities and/or cell quantities (such as damage parameters); see WEQS and WVAR above under MATERIAL. The following models are available:

BFRACT -- Brittle fracture; subroutine BFRACT3.

CAP1 -- Cap yield model for porous materials

DFRACT -- Dynamic ductile fracture

DFRACTS -- Quasistatic ductile fracture

EOSTAB -- Tabular equation of state: pressure model.

137

EPP — Von Mises plasticity with work-hardening

EXPLODE — Detonation. See EXPLODE under the BLOCK data group for further initialization requirements.

POREQST — Porous equation of state

REBAR — Composites

SHEAR3, SHEAR4 (or SHEAR) — Shear-banding.

In addition, the subkeyword EXTRA is provided but not implemented.

BLOCK or GRID

Each BLOCK or GRID data group specifies the mesh layout for a single quadrilateral block of material. The user can construct the layout for a complicated structure by entering several BLOCK groups; the code automatically constructs a single object with connected cells from a series of BLOCK groups. The GRID keyword is used like the BLOCK keyword, but has the additional meaning that subsequent blocks are to be part of an independent mesh, as when beginning the layout for a new object. A slide line must then be provided between the group of blocks. A typical layout using GRID would be:

```
GRID (or BLOCK) labels ...
BLOCK labels ...
GRID labels ...
BLOCK labels ...
BLOCK labels ...
```

This sequence of input lines sets up two independent submeshes, one consisting of two blocks and the other of three. One submesh could represent a penetrator, for example, and the other a target.

The labels available in the BLOCK data group are:

- AMAT (Required) — Material name, a character string of 1 to 8 characters, including blanks. Must match one of the names specified under a MATERIAL data group, e.g., AMAT = 'STEEL S1'

138

- XA (Required), YA (Required) — Arrays of four X and Y values specifying the coordinates of the corners of a quadrilateral block in counterclockwise order. Example:

| XA = | 1. | 4.0 | 3.2 | -0.6 |
| YA = | 1.1 | 1.1 | 2.6 | 2.1 |

  The order given here for these corner nodes is used in the interpretation of Rij (cell size ratio), NCij (number of cells) and SLIDE i to j.

- XDNOT, YDNOT — Arrays of four values specifying the X and Y velocity components of the corners of the block. Listed counterclockwise in the same order as for XA, YA values. If only one XDNOT or YDNOT is specified, all four nodes are presumed to have the same velocities.

- CASE — Determines the layout geometry.

  CASE = 1:   (Default.) Cells all the same size. Defaults: R (cell ratio) = 1, NC12 = NC43, NC23 = NC14. Specify NC12, NC23. See examples 1 through 4 in Section VI.

  CASE = 2:   Varying cell sizes. Same as CASE = 1, but cell ratios are individually set. Defaults: R = 1, R12 = R43, R23 = R14. Specify two NCs, two Rs. See an example in problem 3 of Section VI.

  CASE = 3:   Varying cell numbers and sizes. Rs as in CASE = 2, but required that NC12 = NC14 and NC23 = NC43. Specify two NCs and two Rs. This layout procedure works best for square blocks. (See example 5 in Section VI.)

  CASE = 4:   Layout of circles and ring sectors. This case can be obtained by specifying CASE = 4, or by inserting the word CIRCLE. The X and Y values have different meanings here than for the preceding BLOCK case. The orientation of the nodes is fixed as shown in Fig. 34. XA(1), YA(1) is the center of the circle. XA(2), YA(2) is point 2 at the outer radius. XA(3) is the extent of the ring sector or circle in degrees (counterclockwise). XA(4), YA(4) is the point on the inner radius of the ring sector. NC12 is required: it is the number of cells along the radius from the inner radius to the outer. NC43 = NC12. NC23 and NC14 can

139
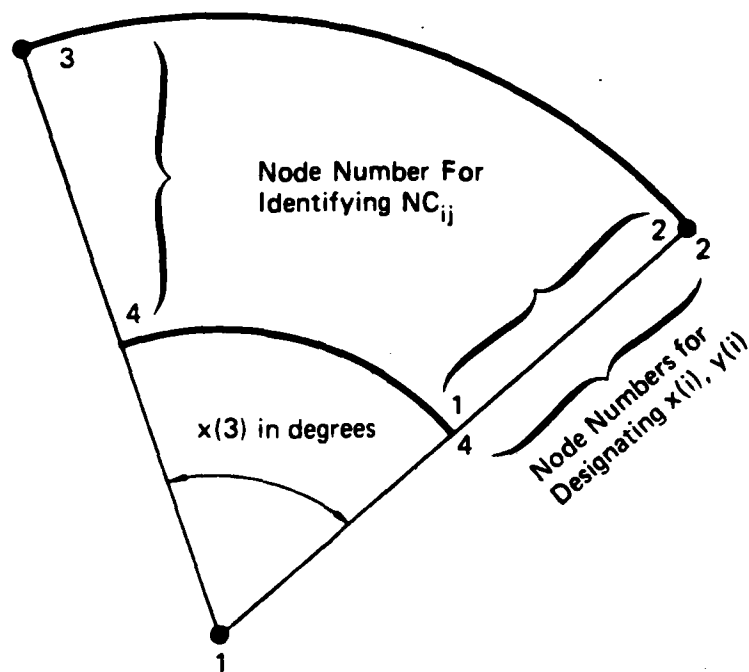
JA-314522-119

FIGURE 34 DESIGNATION OF THE NODAL INPUT PARAMETERS FOR DEFINING AN ARC OR A CIRCLE FOR LAYOUT BLCIRC

140

be specified. If either or both are left undefined, they are computed to provide nearly square cells. A sample layout of this type is shown in Fig. 17.

CASE = 5: The layout of ellipses has not been implemented yet. It is expected that satisfactory treatments could be obtained in most cases using circles, sectors, rings, and ring sectors with CASE 4.

- NC12, NC23, NC43, NC143 — NCij is the number of cells along the block edges from corner node i to node j. See CASE for defaults.

- R12, R23, R43, R14 — Rij is the ratio of successive cell dimensions along edges of the block from corner node i to node j. See CASE for defaults.

- EXPLODE — Must be specified if the EXPLODE material model is specified for the material in this block. The resulting call to EXPLODE causes the times (TBURN) of initiation of detonation in the cells to be initialized. (See example 5 in Section VI.)

- SLIDE i TO j — Provides for a partial separation of the current block from previous blocks. The boundary nodes between the corner nodes i and j (proceeding counterclockwise around the quadrilateral) are not connected to previous blocks, but the corner nodes are connected. The SLIDE provision provides the needed nodes for a slide line; see SLIDE for further instructions on specifying slide lines. For example, an edge-cracked or center-cracked panel could be constructed. For full separations between blocks, it is simpler to use the "GRID" indicator. Examples: SLIDE 1 TO 3 and SLIDE 4 TO 1.

BOUNDARY

The purpose of the BOUNDARY specifications are to provide a range of motion boundary conditions to keep nodes along an axis of symmetry, to represent an impenetrable wall, impose velocity boundaries, and the like. The boundary specifications have been separated into groups according to the complexity of the conditions. These groups are labelled by the NBCTYP indicator, an input quantity.

141

<u>NBCTYP 1</u>: For this case the user can specify x and y controls on lines in the x or y direction, or on individual points. The operation can be visualized as the specification of a moving wall which will affect the motion of some nodes. This method is appropriate for a limited range of controls because it is dependent on the orientation of the objects and the directions required of the controls. However, this case meets a lot of needs in practical problems. For this method, the user must specify the nodes affected, the X or Y values of the wall that will control the motion, and the type of control. The selected nodes are indicated by the variables XCONST and YCONST. If both XCONST and YCONST are specified, a single point is designated; if only one is given, then a line of nodes with constant X or Y is selected. Here the user must provide the XCONST or YCONST values, even though they are zero, because there are no defaults for these two. Next the user specifies the X and Y values and velocities of the controlling line or point (the wall). These values are listed as XBC, XDBC, YBC, and YDBC. If one position value is given, a wall line is provided; if two position values, a wall point. The wall line or point positions at any time are given by

$$X_w = XBC + t*XDBC, \text{ and}$$

$$Y_w = YBC + t*YDBC, \text{ where t is the time.}$$

Last, the user designates the type of control desired. For example, the X value of the selected nodes may be required to remain greater than or equal to the current X value of the wall, less than or equal to the current X value, or equal to the current X value of the wall. These control types are given by values of 1, 2, or 3 for XAFECT and YAFECT.

<u>NBCTYP 2</u>: This boundary condition requires that the velocities of the designated nodes remain unchanged. Only the selected boundary nodes and the control type must be specified for this boundary condition. That is, specify the nodes by lines with a common X or Y value or points with a pair of X and Y values (XCONST and YCONST). Then give the effect using XAFECT and YAFECT (only values of 3, for control, and 0 for no control are allowed). This boundary condition is used for simple wall

142

conditions and to permit an initial velocity to remain fixed along a boundary. The wall line or point positions at any time are given by

$$X_w = X_{oi} + t*\dot{X}_{oi}, \text{ and}$$

$$Y_w = Y_{oi} + t*\dot{Y}_{oi}, \text{ where}$$

X_{oi} and $\dot{X}_{oi}$ are the initial X-position and X-velocity of the ith node.

NBCTYPs 3 through 6: These four boundary types allow the user to specify a wall of general shape (as a series of points) and to indicate what kind of contact will occur on the boundary. The wall points may be moving with fixed velocities so that motion of a rigid projectile, for example, could be represented. The input consists of the series of points describing the wall and designators for the boundary nodes which are affected. The wall is specified by the number of points in the series (NBCPT), the series of XBC and YBC values, wall velocities given by XDBC and YDBC values, and the direction indicator (IDIR). To allow the WALL subroutine to determine the relationship between the wall and the nodes of the material, it is necessary to indicate the initial orientation in some way. We adopted the convention that if we travelled along the wall in the order in which the points are given, the material should be on the right. For this case, IDIR is +1; otherwise IDIR is -1. The boundary nodes which are affected are given by the user with the XCONST and YCONST values as for the other NBCTYPs. The nature of the contact between the wall and the material nodes is given by the indicator NBCTYP. This indicator determines whether nodes can slide along the wall or are struck at first contact, and whether they can separate again or must remain in contact. These designations are given in the following listing of the input quantities.

The input quantities used with the BOUNDARY group are given below. Some of these are dimensioned so that they all pertain to the nth boundary condition, but some are not dimensioned because their information is immediately stored with the nodal information in the BC or BCV arrays.

143

- NBCTYP(n) -- Indicator for the boundary condition type. Required for each condition (n is provided by the code). The types are:

    1 -- Simple control on the X and/or Y values. Type of control is given by XAFECT and YAFECT.

    2 -- Retain initialized X and/or Y velocities. Type of control is given by XAFECT and YAFECT.

- XAFECT, YAFECT -- Type of boundary condition control used with NBCTYPs 1 and 2. These indicators determine separately the controls on the X and Y directions. The the XAFECT and YAFECT have the following meanings:

    0 or 4 -- Free condition, no control.

    1 -- X or Y is maintained greater than or equal to X_w or Y_w.

    2 -- X or Y is maintained less than or equal to X_w or Y_w.

    3 -- X or Y is kept equal to X_w or Y_w.

- XBC(j,n) and YBC(j,n) -- jth point in the series for designating the nth wall. Neither j or n indices are provided by the user. For NBCTYP 1 only one value of XBC and/or YBC is used. For NBCTYPs 3 through 6 XBC, YBC are arrays of coordinate pairs designating the wall.

- IDIR -- Indicator for the relative location of the boundary wall and the material. If we travel along the wall in the order in which the points are given, the material should be on the right for IDIR = +1. For material on the left, IDIR is -1.

- XCONST and YCONST -- X and Y values used to designate nodes that are affected by the boundary conditions. There is no default for these values; each must be set, although they may be zero. If only XCONST (or YCONST) is specified, then all nodes with X = XCONST (or Y = YCONST) are given the boundary condition. If both XCONST and YCONST are specified, the condition applies to the one point specified. Subsequent input overwrites earlier assignments. Hence, if adjacent sides of a block are specified by boundary conditions, the node at the corner between the sides will carry only the second set of conditions. In such cases it is usually necessary to separately designate boundary conditions for this node. A set of parameters XCONST, YCONST, XAFECT and YAFECT constitute a Boundary Line Set. For each Set, XCONST and

YCONST designate the nodes affected, and XAFECT and YAFECT indicate the nature of the boundary control. Each Boundary Line Set must appear on a separate line of the input.

- XDBC(j,n) and YDBC(j,n) -- Velocities of the wall points. Neither j nor n indices are provided by the user. Only the first members of the arrays (j = 1) are used for NBCTYP = 1. The complete arrays are used for NBCTYPs 3 through 6.

Some samples of the boundary groups are presented to illustrate the use of the conditions.

Sample 1, Compression test on a short cylinder with a 1 cm radius and 1 cm length. The compressing piston is treated as a rigid wall with an X velocity of 1 m/s.

```
BOUNDARY NBCTYP = 1  XCONST = 1.  XAFECT = 2
YCONST = 1.  XAFECT = 2.
XBC = 1.,  XDBC = -100.


BOUNDARY NBCTYP = 1
XCONST = 1.  YCONST = 0.  XAFECT = 2  YAFECT = 3
XBC = 1.,  XDBC = -100.
```

Here we have entered two groups of conditions. The first causes the X-values of nodes along the front and sides of the short cylinder to remain less than or equal to the wall position, but the Y-values are free. The second condition requires that the node at the axis along the front remain along the axis, as well as less than or equal to the X-position of the wall. Note that the second condition overwrites the first condition for the point at (1., 0.).

Sample 2, Impact of a blunt projectile into a hemispherical cup. The projectile lies along the axis of symmetry from X = -4.93774 to 13.06226 cm and has a radius of 4 cm. It is just touching the inside of a hemispherical cup of radius 9 cm and with its center at X = 5 cm. First the input designates boundary type 4. Then the nodes along the front of the projectile at 13.06226 are indicated as boundary nodes

145

which will interact with the wall, and then the nodes along the circumference at Y = 4 cm. These two Boundary Line Sets XCONST and YCONST appear on separate lines so that they are treated separately. Next the series of points defining the hemispherical cup are entered. These are in the positive direction, so IDIR is +1.

```
BOUNDARY NBCTYP = 4   XCONST = 13.06226
YCONST = 4.
XBC = 5.000, 6.563, 8.078, 9.500, 10.785, 11.894, 12.794,
YBC = 9.000, 8.863, 8.457, 7.794, 6.894, 5.785, 4.500,
XBC = 13.457, 13.863, 14.000
YBC = 3.078, 1.563, 0.000   IDIR = 1
```

REZON

This group specifies the parameters controlling the automatic rezoner. A sample of the input follows:

```
REZONE    NFREQ = 10      REZMIN = 0.05    REZWT = 1.0
          XCONST = 1.0    YAFECT = 2
          XCONST = 1.0    YCONST = 0.5    XAFECT = 1
```

The input quantities provide three types of control over rezoning. NFREQ controls the frequency with which the nodes of the mesh are examined and rezoned if necessary. REZMIN and REZWT govern the amount of motion that a node can undergo in rezoning. The remaining parameters allow the user to indicate which nodes are not to be rezoned.

Often the user will want to restrict rezoning of nodes on external boundaries, internal boundaries, and slide lines. The rezoner can treat motion along boundaries and slide lines, but it may also move corner points and otherwise alter the grid in unphysical and unnecessary ways. When more than one restriction is desired, the second and subsequent ones must be entered in separate REZON data groups.

146

NCONST, Number of a node for which the rezoning is restricted in
(TO)   both X and Y directions. With the "TO" label, a range of
         nodes can be specified. Samples of this input are

         NCONST = 13

         NCONST = 13 TO 43

The first of these input lines requests that node 13 be
skipped for rezoning in both X and Y directions. The
second line specifies a range of nodes, starting at node
13 and continuing through 43. With this specification, it
is convenient to protect a large block of nodes from
rezoning. A trial layout is usually needed to determine
what the node numbers are.

NFREQ   The cycle counter controlling frequency of rezoning. For
         any cycle N where N = NFREQ + 2 (n is any positive
         integer), all odd-numbered nodes are scanned for possible
         relocation. On the next cycle, even-numbered nodes are
         scanned. For the third and fourth cycles, odd- and even-
         numbered nodes are scanned starting with the last node and
         proceeding towards the first. NFREQ = 5 is a reasonable
         request. Therefore, if NFREQ = 5, no rezoning occurs at
         cycles 1, 6, 11, etc., while at any other cycle either
         odd- or even-numbered nodes are scanned for possible
         rezoning. The default of zero indicates that no rezoning
         is desired.

NXCONST, Number of a node for which rezoning is restricted in the X
NYCONST, (or Y) direction. With the "TO" label, a range of nodes
(TO)   can be specified. Samples of this input are

         NXCONST = 15

         NYCONST = 18 TO 21

The first of these lines restricts rezoning in the X
direction for node 15. The second restricts rezoning in
the Y direction for nodes 18 through 21.

REZMIN   The minimum relative distance that a node has to be offset
         from the ideal position before it is relocated. The
         distance is relative to a typical dimension of the polygon
         that the neighbors of the node form. 0.1 may be a
         reasonable number, but we have often had to specify a
         number as small as 0.01 in difficult runs. The default is
         0.1.

147

REZWT   Fraction of the distance the node is moved from its old position (X_{old}) to the centroidal position (X_{cent}).

$$X_{new} = X_{cent} \cdot REZWT + X_{old} \cdot (1 - REZWT)$$

For REZWT use the default value of 1. If smaller values are used, more diffusion is introduced because more frequent rezoning is required.

XCONST,   X and Y values of nodes which the user does not wish to
YCONST   rezone. They are used in conjunction with XAFECT and YAFECT below. All nodes that lie on the line X = XCONST will not be rezoned in the X and/or Y direction if XAFECT and/or YAFECT is set. The second line of the sample input above specifies that all nodes for which X = 1.0 shall not be rezoned in the Y direction. The third line restricts rezoning in the X direction for the node at X = 1.0, Y = 0.5. There are no defaults for XCONST and YCONST, they must be specified to be used.

XAFECT=1   Indicator (set to 1) for inhibiting rezoning in the X direction for the nodes that are specified by XCONST and/or YCONST.

YAFECT=2   Similar to XAFECT. Set to 2 to inhibit rezoning in the Y direction.

A set of the parameters XCONST, YCONST, XAFECT, and YAFECT constitute an Inhibitor Group. For each group XCONST and YCONST designate the nodes affected, and XAFECT and YAFECT indicate the inhibited direction of rezoning. Each Inhibitor Group must occur on a separate line of the input. Note that the second Inhibitor Group in the sample above affects a point that was also specified by the first Inhibitor Group. The second instruction overwrites the first so that now the point (1.0, 0.5) is free to be rezoned in the Y direction. The Inhibitor Groups are used to specify appropriate conditions along lines of symmetry or to disallow rezoning in a quiescent region.

SLIDE (Read by GENR)

This group is used to initialize the slide-line logic. The current implementation requires the specification of individual node numbers. To determine these, set up the rest of the input and run the code with NMAX = 0 (zero computational cycles). Then examine the INITIAL LAYOUT

part of the output to determine the node numbers along desired slide boundaries.

NSL An array of nodes that are on the slave side of the slide line. Slave and master do not have any special meaning in the present slide line implementation except that they specify in which direction the slide line runs and serve to assemble the nodes into two groups. The node numbers should refer to consecutive nodes as one goes along the slide line boundary. For IDIR=1 (see IDIR command below) the material should be on the right side when one goes through the node numbers in the order they are entered. For IDIR=-1 the material should be on the left side. (NSL is required for a slide line.)

NMS An array containing the master side node numbers of the slide line. Similar to NSL. For IDIR=1 the material should be on the left side when one goes through the node numbers (NMS is required for a slide line.)

IDIR Used in conjunction with NSL and NMS above. +1 for master material on the left as we proceed along the slide line. -1 for a slide line specified in the opposite sense. Default is +1.

CINT The cohesion C_o in the friction mode, dyn/cm^2.

TANP The coefficient of friction Tan (ϕ), used to compute a shear stress τ: $\tau = C_o + \sigma_n Tan(\phi)$ where σ_n is the normal stress.

ETA The coefficient of viscosity A_v used to compute a shear stress on the slide line: $\tau = A_v U$, where U is the relative velocity.

HISTORY

This group is used to tag locations in storage for output after every computational cycle. The available designators are listed in Table 3. They include the node and cell array variables, plus some quantities (such as $\bar{\sigma}$ and σ_1) which are derived from array values. For array quantities that are not specifically listed, use the labels COMC and COMN. A unique format is required for the HISTORY group: one or more series of labels followed by (X, Y) coordinate pairs; for example:

HISTORY, Z,AM,COMC24,1.0,1.5 BC,COMN3,3.5,2.0

149

This coding requests that the variables Z, AM, and the 24th cell variable be printed for material initially located near X = 1.0, Y = 1.5, and that the variable BC and the third nodal variable be printed for material initially near X = 3.5, Y = 2.0. Commas and spaces can be used as separators as desired.

When requesting nodal variables near a slide line or material boundary, care should be taken to correctly position the x,y points. HISTORY first determines the cell containing this requested point. Then it selects the nearest of the four nodes of this cell. With this method the user can request a history of a node on either side of a slide line, although the nodes may initially coincide.

Table 3. Variable Names Used in Historical Listing Requests

- A -- Cell area.

- AM -- Mass assigned to a nodal point (g or g/cm).

- BC, BCN -- Boundary condition indicators.

- COMC -- Use this label for cell variables not listed by name; i.e., for extra variables. Locations in the COMC array can be determined from Tables E.1 and E.2, from the COMMON listing in HCOM1.FOR, and from the CALL statements in CYCLE. For example, the 6th extra variable would be requested by: COMC24 (24 = 18 standard variables + 6th extra variable). The number must immediately follow the letters COMC. The cell density, for example, could be requested by COMC4.

- COMN -- Like COMC, but for nodal variables.

- D -- Density.

- DEXX, DEYY, DEZZ, DEXY -- Strain increment components.

- E -- specific internal energy.

- EPS -- Equivalent plastic strain.

- EXX, EYY, EZZ, EXY -- Cumulative strain components, not corrected for rotation.

- FX, FY -- X and Y components of force assigned to a nodal point (dyn or dyn/cm).

- SXX, SYY, SZZ -- Thermodynamic stress components, positive in tension.

150

- TH — Gross cell rotation, radians, positive counterclockwise.

- TXX, TYY, TZZ, TXY — total (mechanical) stress components, positive in tension.

- WH — Cell condition indicator (initialized at 2 and updated by material models).

- WMAT — Material number (assigned to materials in order of appearance in input).

- P — Thermodynamic pressure, positive in compression.

- SBAR — Equivalent stress.

- SPRIN1, SPRIN2, SPRIN3 — Principal stress components, positive in tension.

- SP2 — Sound speed squared.

- X, Y — Nodal positions.

- YO, XO — Initial nodal positions.

- XD, YD — Nodal velocities.

- YY — Yield stress.

- Z — Mass, in g or g/cm.

To produce a historical plot file, use PSCRIB (described under the GENERAL data group).

EPP, Elastic-Plastic Model

The following input quantities are used for EPP:

- TYPE — 1 (Default value) for work hardening by power law form, $Y = A \epsilon^n$.

  2 for work hardening by a linear function of strain, $\Delta Y = A \Delta \epsilon$.

  3 for work hardening by a polynomial fraction developed by Norris.

- YS — Yield values, or constants for the third type of yield function.

- ES — Equivalent plastic strain values.

Samples of this input for type 1 appear in Problems 1 and 2 of Section VI.

151

SHEAR3

Shear banding routine (described in Reference 4).

- BFR -- The constants in the shear banding model, 14 values total, values 8-14 are given defaults in the code.

- FNUC -- Indicator for active planes. Six values can be given for compatibility with SHEAR4, but only the first four planes are computed by SHEAR3. One (1.0) indicates active; zero (0.0) makes the code bypass the plane. We have the following planes in order.

    Bands are normal to X or Y axes.

    Normal to a line at 45° between X and Z (mode 2).

    Normal to a line at 45° between X and Z (mode 1).

    Normal to a line at 45° between X and Z (mode 3).

- YS -- Yield values for the work hardening curve, treated as for TYPE 1 under EPP.

- EST -- Equivalent plastic strain values for the work hardening curve.

- EN3 -- Signals the end of SHEAR3 input; must be supplied (need not have a value).

Samples of this input are in Problems 1 and 3 of Section VI.

SHEAR4

Shear banding routine (similar to SHEAR3, but providing a more complete treatment of anisotropy).

- BFR -- The constants in the shear banding model, 14 values total, values 8-14 are given defaults in the code.

- FNUC -- Indicator for active planes. One (1.0) indicates active; zero (0.0) makes the code bypass the plane, six values total. We have the following planes in order.

    Normal to X axis.

    Normal to a line at 45° between X and Y (mode 2).

    Normal to Y axis.

    Normal to a line at 45° between -X and Y (mode 2).

152

Normal to a line at 45° between X and Z (mode 3).

Normal to a line at 45° between Y and Z (mode 1).

- YS -- Yield values for the work hardening curve, treated as for TYPE 1 under EPP.

- EST -- Equivalent plastic strain values for the work hardening curve.

- PRINT -- Specifies the print-out from SHEAR4.

  0   no printing

  1   deformation information only

  2   deformation plus volume damage (if any)

  3   deformation plus volume damage (if any) plus surface damage (if any)

- END -- Signals end of SHEAR4 input; must be supplied (need not have a value).

The following input variables are used in the EXPLODE calculations.

DIST   Number of cells over which the detonation front is spread. This parameter is also the indicator that a running detonation is required.

DET   Detonation velocity, may be inserted or computed by EXPLODE, cm/s.

EOSTAB Indicator for the use of a tabular isentrope.

EQSTG $\gamma - 1$, the Grueneisen ratio

QEXPL   Chemical energy released by the detonation, erg/g.

TBURN   Delay time for the beginning of detonation, s.

XDET,   Coordinates of the point or region of the initiation of
YDET   detonation, cm. If only XDET (or YDET) is input, this region is a line of constant X (or Y). With both XDET and YDET, the detonation begins at a point. If two values of each are entered, initiation begins along a line through the points.

BFRACT

The subroutine BFRACT3 [Ref. 41] provides a stress-strain relation for solid material undergoing brittle fracture during wave

153

propagation. The model incorporated here is micromechanical in that it treats in detail the nucleation and growth of arrays of microcracks. The output of the subroutine includes the usual stress tensor, and also a detailed listing of the damage. The damage information consists of

- The orientation of the plane of damage: PHI and THETA in degrees.

- The level of damage: TAU, ranging from zero (no damage) to 1.

- A cumulative crack size distribution given by a series of number-radius values.

The numbers of cracks are given as number per cubic centimeter and the radii are in centimeters.

Several forms are available for both the nucleation and the growth processes. Nucleation can occur by either a stress-based or a strain-based formula. Probably the stress-based form is more appropriate for high rate loadings (microsecond times) and the strain-based nucleation is applicable to longer duration loads. Crack growth can occur by a process like that for ductile voids, or at a constant fraction of the longitudinal or Rayleigh velocity.

At each listing of the damage, a surface crack size distribution can also be given. This surface distribution (number per unit area versus radius) is computed as the cracks that would be observed on a surface sliced through the material. Finally, a listing is given of the fragment size distribution. The radius given here is the radius of an equivalent sphere of the same mass as the fragment.

The fracture data are read into BFRACT in three groups in fixed formats: a sample of the data is given in Section VI (Figure 46). These follow the indicator "BFRACT" in the listing. The first line contains seven values in the BFR array. The next line contains SIZE, SRTIME, BETT, GAMM, VOLCRIT, TFRAG, and PBORE: these seven were BFR(8) to BFR(14) in earlier versions. The third line contains three indicators INITNUC, INITGRO, and INITPRI. All these variables are defined below.

154

BFR(1) controls the crack growth velocity. A positive value is interpreted as the coefficient B_1 in the equation for crack growth velocity:

$$V = B_1 L \qquad (176)$$

where L is the longitudinal velocity for elastic wave propagation. A negative value of BFR(1) indicates a ductile growth relation of the form

$$V = B_1 (\sigma - B2) \qquad (177)$$

where σ is the normal stress on the fracture plane, and $B_2 = $ BFR(2).

BFR(2) controls the initiation of crack growth. A positive value means that a fracture toughness criterion is used, and B_2 is the fracture toughnes, K_{1C}, with units of $dyn/cm^{3/2}$. In this case only cracks above the critical size are allowed to grow. A negative value of B_2 means a threshold stress as in Eq. (177).

BFR(3) is the size parameter of the nucleated size distribution. This initial distribution is

$$N_g = N_o \exp(-R/B_3) \qquad (178)$$

where N_g is the number per unit volume with radii greater than R, and N_o is the total number of cracks nucleated per unit volume.

BFR(4) is the nucleation rate coefficient, $number/cm^3/s$, in the nucleation expressions

$$\Delta N = B_4 \left[(\sigma - B_5)/B_6 \right] \Delta t \qquad (179a)$$
$$\text{for stress-based nucleation}$$
$$\Delta N = B_4 \left(L/B_3 \right) \Delta t \qquad (179b)$$

$$\Delta N = B_r \left(\bar{\epsilon}^p - B_5 \right) \Delta t \qquad \text{for strain-based nucleation} \qquad (180)$$

where σ is the normal stress on the plane of fracture, L is the elastic longitudinal wave velocity, $\bar{\epsilon}^p$ is the plastic strain, and Δt is the time increment.

BFR(5) controls the nucleation process. Positive values mean that a strain nucleation process is being used, and B_5 is the threshold strain for nucleation: Eq. (180). For negative values, B_5 is the threshold stress for the stress-based nucleation formula, Eq. (179a).

BFR(6) participates in both of the stress-based nucleation process. For positive values, B_6 is the total possible number of cracks per unit volume developed in Eq. (179b). A negative value of B_6 is the denominator in the nucleation formula, Eq. (179a).

BFR(7) is the maximum crack size for the nucleated distribution, cm. Thus, in Eq. (178), R runs from zero only up to B_7.

NSIZ is the number of size intervals for the crack size distribution. The dimensions of the arrays require that NSIZ not exceed ten.

SRTIME is the coefficient used in computing the stress relaxation time constant. This time constant is

$$T_c = SRTIME*R/L \tag{181}$$

where R is the radius of the cracks being considered. With a positive value of SRTIME, the crack volume does not instantaneously increase to the elastic value of V_c, but is given by

$$V = V_c - (V_c - V_o)exp(-\Delta T/T_c) \tag{182}$$

where V_o is the crack volume at the previous time, and ΔT is the time interval.

BETT is the ratio of the number of fragments to the number of cracks.

156

$$N_f = BETT*N_c \tag{183}$$

GAMMA is the ratio of the fragment radius to the crack radius.

$$R_f = GAMMA*R_c \tag{184}$$

VOLCRIT is the value of the crack volume (dimensionless) that defines the threshold of coalescence.

TFRAG is the coefficient of fragment volume, V_f,

$$V_f = TFRAG*\Sigma N_f R_f^3 \tag{185}$$

PBORE is a switch that allows the borehole gas pressure to act on cells that are fracturing.

INITNUC is an indicator for determining the nucleation process. For a value of 1 and a fracture mechanics growth process, the full range of cracks are nucleated, although some may be below the critical size.

INITGRO is an indicator for determining the growth process. For a value of 1 and the constant growth velocity process, the Rayleigh wave velocity instead of the longitudinal velocity is used.

INITPRI controls some of the printing processes. For a value of 1, the nucleation and growth functions that have been requested are listed with the input. For INITPRI = 2, the surface damage is also listed at each time the volume damage is given. For INITPRI = 3, the preceding listings are given, the surface damage information is fitted to an exponential form, and the coefficients are listed.

EOSTAB

The EOSTAB subroutine provides a tabular isentrope appropriate to the representation of gases, including explosive gases. The isentrope is read into the subroutine as a series of pressure-volume points. During calculations the subroutine interpolates between successive points to determine the pressure corresponding to the current density.

157

The input points to define the isentrope can be provided as either volume-pressure pairs or density-pressure pairs. The sample in Section IV (Figure 33) shows density-pressure points as indicated by the label "DENSITY". The pairs can be inserted in the order of either ascending or descending pressure.

During initialization, if a pressure is provided, the routine computes a density corresponding to that pressure on the isentrope. This provision is useful for initializing the material with a preload pressure. The computed density is then used to define the initial density for the material.

In the wave propagation calculations the subroutine is provided with the density. EOSTAB computes the pressure by interpolating along the isentrope defined by the series of points. If "LOG" is specified in the input as shown in Figure 33 of Section IV, the pressure is computed by linear interpolation between logarithms of pressure and density.

$$P = P_1(D/D_1)^x \tag{186}$$

where

D is the current density,

P_2 and P_1 are the pressures at each end of the interpolation interval,

D_2 and D_1 are the densities at each end of the interval, and

$x = \log(P_2/P_1)/\log(D_2/D_1)$.

If "LOG" is not specified, the interpolation is linear between pressure and density. For either type of interpolation, values of pressure outside the range are obtained by extrapolation from the end point data.

The input includes three variables, plus the density-pressure array. The three variables are:

IMAX, the number of data points to be inserted. No default.

A3, a label with a value of "DENSITY" or "VOLUME", to show whether density or volume values are to be inserted. The default is "DENSITY".

158

TYPE, a lable with a value of "LOG" or "LINEAR", to request either logarithmic or nonlogarithmic interpolation. The default is "LINEAR".

These variables are presented in fixed formats, as shown in Figure 33. The variables for the first line are a label, IMAX, A3, and TYPE given in the format (A10, I10, A10, A10).

The density-pressure array is read in as a series of points: ρ_1, P_1; ρ_2, P_2; etc. The format is A10 (for a label), 6E10.3. The points can be inserted in either ascending or descending order of pressure.

V OUTPUT

This section describes the printed and plotted output from C-HEMP. The printed output includes the standard listing of the input and computed results, plus any error messages. Some guidance is given for making changes in the listed output. Plots of the histories, the mesh, and of contours of variables over the mesh are available. The variables provided in these listings and plots are defined in the Glossary, Appendix C. The files used in the input and output operations are listed in Appendix A. For information about the output from special material models, see the documentation in Section III on the models.

A. Output Listings

Given below is a list of the sections that appear in the printed output, in the order in which they appear.

- Run Title

    The first line of output specifies the code version number and the run date.

- Input Listing

    The run data are listed exactly as they appear in the input file. The listing may be interrupted by messages from material models being initialized (e.g., EXPLODE).

- Historical Listing Requests

    The code automatically chooses the nodes and the cells closest to the requested X-Y positions (using centroids for cells). Each variable-position combination results in a history request. For each request the variable name is printed, along with the computed node or cell number in

161

parentheses. The X and Y location values given with each request are the requested values, not the computed values. JEDA and JEDT are used by the code to select the requested variables.

● Initial Cell Layout

The cells are listed by number, along with initial cell quantities and information about position in the mesh. The WNOD values specify the node numbers at the cell corners. The listed x and y values are those of the centroid of the cell. The spatial location of a cell can also be determined by looking up X and Y for its corner nodes in the node layout (see below). Cell quantities (and nodal quantities as well) are stored in an array called COM1; for a given cell, LC is the offset in COM1 to the beginning of storage for that cell. LC can be thought of as an alternate, unique cell identifier. AMASS is the cell mass. Its definition depends on the problem symmetry as specified by NGEOM.

● Initial Node Layout

The nodes are listed by number, along with initial nodal quantities and information about position in the mesh. The cells around each node are identified under WCELL by their LC identifier. The corresponding cell numbers can be found by locating the LC values in the cell layout. A node's LN number is the offset in the COM1 array to the beginning of storage for that node. Adjacent nodes are listed under WNDND by node number. Nodes along boundaries may have nonzero values in the BC indicator column.

● Edits

Every IPRINTth time step (see GENERAL in Section III Detailed Description of Input Data Groups), the code outputs a printed record ("edit") of the condition of the model at that

162

time step. One complete edit is also printed at the very end
of the run. The cell edit is printed first, then the node
edit. Since data values are output after the computation for
each cell or node, messages from special material models, the
rezoner, and the slide routines may interrupt edit listings.

The X and Y values printed in the cell edit are those of
the cell's centroid. The stress is listed in terms of the
thermodynamic stresses S-XX, S-YY, S-ZZ, and TXYW, the
pressure PW, and the artificial viscous stress QW. The
density, energy, and sound-speed-squared are also listed. H
is an indicator whose interpretation is determined by the
material model used.

The node edit prints out the position (X, Y) and velocity
(XDNH, YDNH) of each node. The mass assigned to nodes is
computed by partitioning the mass of surrounding cells in a
way that depends on problem geometry (NGEOM = 1 or 2) and
boundary status. For BC and BCN, see the Glossary of Output
Labels section below.

- Summary

    After each edit a summary of the system energies and
momenta are printed out. For this summary, the node positions
are at time t^{n+1} = TIME in the listing. Velocities are at
time $t^{n+1/2}$ = TIME-DT/2. Stress and internal energy are at
time t^{n} = TIME-DT.

- Stop Message

    After each time step, the code checks several stop
criteria and terminates if one or more is met. The stop
message indicates the current values of both the criteria and
the appropriate indicators. (The criteria are set in the
GENERAL input data group.) This message is followed by an
edit of the final state of all cells and nodes.

163

- Scribes

　　　The data requested in the HISTORY input group are saved
after each time step and printed out in "scribes" at the end
of the run. In addition to the requested quantities, the
problem time, the time step size DT, and the incremental
calculation time DELTIM are printed. The cell controlling
each time step is identified by its number LT, the minimum
dimension DX, and the crossing time DTW. The X-Y locations
that appear in the variable headings are those requested, not
those calculated by the code. Listed variable names may
differ from corresponding internal names. If the total number
of variables is more than will fit on a page, the historical
output is divided into strips; NSCRIB= 1 identifies the first
strip, NSCRIBE= 2 the second, and so on.

Two types of augmentation of the histories may be desirable:
addition of histories of global quantities and addition of
specially constructed, non-array quantities for cells. Global
quantities can be added (permanently, not under INPUT control)
by simple changes in HISTORY and CYCLE. For example, suppose
that we wish to add the total internal and kinetic energy
quantities TIE and TKE. These are computed just before the
nodal historical values are stored in the SJ array in CYCLE;
hence, they are available. Therefore, we add statements such
as the following at the end of HISTORY to increase the size of
NJED and to prepare titles for the new histories:

```
NJED = NJED + 2
JEDN(NJED) = 8H TIE
JEDN(NJED-1) = 8H TKE
```

Next we insert statements into CYCLE at CYCL_ 853 such as

164

SJ(NJED) = TIE

SJ(NJED-1) = TKE

If many histories are being requested, we may also check that NJED is still within the dimensioned size for the history arrays.

Many special variables have already been added to the historical listing requests, so one of these can be followed to insert additional requests. First a name for the new quantity should be added to the DATA statement for CARD in HISTORY at line HIST_ 16. The first 48 are reserved for cell quantities and the next 32 for nodal quantities. Then the computation and storage of the new quantity is added to CYCLE in the vicinity of CYCL_ 596. The GO TO statement at CYCL_546 should be revised to reflect the increase in the list.

- Notice of Termination of Execution

    For normal runs, the penultimate message is a notice of the total computation time (CPU) in seconds. The run may actually use additional time for file closing and other overhead. The last message gives the cycle number at which the restart dump was written.

B. Error Messages

Many error messages are provided by C-HEMP to aid the user in correcting the input or in understanding other problems which the code has encountered. The input errors can generally be overcome by re-examining the input rules and the input stream being used. The messages show which labels were not interpretable. Other messages may indicate more basic problems such as poorly shaped cells, or possibly a shortcoming in the code.

165

HEMP

One message is given by HEMP to indicate the end of the job. If NERROR is nonzero, then an error of some kind has occurred. Earlier messages from other routines should indicate the type of error.

```
STOP CRITERIA - NMAX = 1000    STOPT = ... NERROR > 0 ...
        CURRENT VALUES - N = ...                NERROR = 0
```

BFRACT3

BFRACT3 is equipped to perform iterations and subcycling to obtain a solution for the stress and damage. A counter IFRAG is incrmented in case BFRACT3 must reset to a smaller subcycle size or is having trouble with convergence. As IFRAG is increased, more print commands are triggered. These print statements have the form:

"BFRACT3 103 L, N = ..."

where the number following "BFRACT3" is a nearby statement number. If convergence does not occur after 10 resets, the run is halted with the message:

"BFRACT3 540 L,N,NMULT,IH = ..."

Generally this error occurs when BFRACT3 has been given unrealistic sets of strains by the main program, or the storage of the special data arrays is incorrectly matched between the program and BFRACT3.

If a simple error occurs in BFRACT3, the message is:

****** ERROR IN BFRACT3 ******

which is followed by a listing of the cell and cycle number, density and time step. Negative density or time step will cause this error. This error message probably indicates that bad information has been provided by the calling program.

BLCAS3

An error message can occur from BLCAS3 if the NC values are not in the correct relationship. The message has the form:

166

"NC12 MUST EXCEED NC23 FOR CASE 3 LAYOUT

NC12,NC23,NC14,NC43 = 12 14 15 10 STOP IN BLCAS3 AT 540"

An immediate stop occurs following this message.

BLOCK

Two error messages are written in BLOCK; both pertain to incorrect input. The first indicates that BLOCK does not recognize a LABEL in the input:

'GARBAGE IS NOT A VALID SUBVALUE TYPE FOR THE CARD BLOCK
SUBR. BLOCK"

where 'GARBAGE' is the unknown LABEL. The second message occurs if BLOCK cannot match the material name to those provided:

"ERROR, NO MATCH FOUND FOR MATERIAL GARBAGE IN DATA FOR BLOCK"

where 'GARBAGE' is the unknown name found in the BLOCK data. These errors are actually detected in FIND, but reported in BLOCK.

BLWARP

The subroutine BLWARP reports problems it may have in fitting a hyperbolic paraboloid to the input velocity data. The message is

"ERROR IN VELOCITY INTERPOLATION AT 53 IN BLWARP"

Included with the message is a list of the X and Y coordinates of the block being examined. The computation stops with the message

"STOP BLWARP 53"

listed with the system messages. Similar messages occur at locations 58 and 66 in BLWARP. To correct these problems, the input should be examined first. If the input contains no errors, then the parameters with the message (DISCRIMINANT, A, B, C of the parabolic fit) should be studied to determine the problem.

167

BOUNDARY

The messages from BOUNDARY indicate errors in the input. The first message states that the given label cannot be found in the BOUNDARY list.

"GARBAGE IS NOT A VALID SUBVALUE TYPE FOR THE CARD BOUNDARY"

where 'GARBAGE' is the unidentified label. The second error message indicates that more than one XCONST or YCONST value was provided for a single boundary condition.

"TOO MANY XCONST OR YCONST VALUES, XON, YON = 2.00 1.00"

The BOUNDARY input data must be inserted after the BLOCK data so that BOUNDARY can operate directly on the X, Y values. If the BOUNDARY data is given first, the following message is provided, and the computation halts:

"BOUNDARY DATA CANNOT PRECEDE BLOCK DATA, LNODE = 0"

CAP

The CAP subroutine performs subcycling and iterations to attempt to obtain a solution for the current stress state. If necessary, it resets to a smaller set of strain increments, counting these resets with an index NCAP. When resetting occurs, printing is triggered at several places. The messages have the form:

"CAP 390 ..."

where 390 is a nearby statement number. If the permitted number of subcycles is exceeded, the following message is printed:

"STOP CALLED FOR NMAX = NINC = 30"

Then the program halts, with the message to the system: "STOP 3121."

CYCLE

Three error messages are written in CYCLE. The first signals a negative area in a quadrilateral:

168

"CYCLE LOC 210:   L = ..."

where 210 is a nearby statement number. The coordinates of the cell are listed with the message. This is a fatal error, so NMAX (the maximum number of cycles permitted) is reset to $N - 1$ so that the calculation will halt in HEMP at the end of the current cycle.

The second message indicates that an error has occurred in the storage of the historical variables. This text may indicate an error in the historical name in the input, or that the values are out of order.

"CYCLE 820:   ERROR IN HISTORY, JEDT = TER"

where 'TER' is the unidentified label. This error causes an immediate halt, with the message on the system: "STOP 666".

During the energy checking in CYCLE, a message may be printed to indicate that some unexpected change in energy has occurred:

"CYCLE 2420:   ENERGY CHANGE, L, LCEL, LCAD = ..."

This message is simply informative, and does not cause a halt.

EPP

The subroutine EPP can print two messages associated with the input of data. The first indicates that the labels in the input do not correspond to those in its list:

"GARBAGE IS NOT A VALID SUBVALUE TYPE FOR THE CARD NTYPE
READ IN EPP, LM3 = 6"

Here "GARBAGE" is the unidentified input label, NTYPE is the first label in the list for EPP, and LM3 indicates that the unidentified label is the 6th in the input for EPP.

The second message complains that an inappropriate value for NTYPE has been read:

"NTYPE TOO LARGE   NTYPE = 5"

Only three types are provided for.

169

EXPLODE

Two messages are provided from EXPLODE in case of errors in the input. If the number of explosives exceeds 6, the calculation halts with the message to the system "STOP EXP MATLS > 6". If EXPLODE cannot identify one of the input labels, the message given is:

"GARBAGE IS NOT A VALID SUBVALUE TYPE FOR THE CARD NTYPE
READ IN EXPLODE, LM3 = 10"

With this second message, the calculation halts at the conclusion of the input.

GENERAL

If GENERAL cannot identify a label provided to it in the input, it gives the message:

"GARBAGE IS NOT A VALID SUBVALUE TYPE FOR THE CARD CLIN
READ IN GENERAL"

where 'GARBAGE' is the unidentified label. The program halts at the end of the input.

GENR

GENR provides the usual message if it cannot identify a label presented to it in the input:

"GARBAGE IS NOT A VALID CARD TYPE-SUBR. GENR-"

where 'GARBAGE' is the unidentified label. In addition, GENR checks the total number of input errors, and writes:

"*****
3 INPUT ERRORS FOUND BY GENR, PROGRAM HALTS
*****"

Then a STOP is called and this message is put on the system output:

"STOP I/O ERR IN GENR."

HISTORY

If HISTORY cannot identify one of the labels in the input stream, it provides the message:

"GARBAGE DOES NOT MATCH ANY HISTORICAL DESCRIPTOR"

where "GARBAGE" is the unidentified label. The input labels should be examined to verify that they are those intended, that they match those in the DATA statement for CARD in HISTORY, and that they are unique.

MATERIAL

If MATERIAL cannot identify one of the labels in the input, it gives the message:

"GARBAGE IS NOT A VALID SUBVALUE TYPE FOR THE CARD MATERIAL"

where "GARBAGE" is the name of the unrecognized label.

POREQST

If the input to POREQST is unrecognized, it writes the following message:

"GARBAGE IS NOT A VALID SUBVALUE TYPE FOR THE CARD PORQST"

where 'GARBAGE' is the name of the unidentified label. A second message can occur if the number of porous regions used exceeds 6:

"ERROR IN INPUT TO POREQST FOR MATERIAL 3, NREG = 8, ONLY 6 REGIONS ARE PERMITTED"

If this error occurs, the pressure-volume curve for POREQST must be segmented in a different manner so that no more than 6 regions are used. For this error, the program halts with the message "STOP POREQST 152".

A third message can occur if the initial bulk modulus AK is too small, so that the pressure will not follow the P-V curve:

"INPUT ERROR IN POROUS REGION 3, MODULUS IS NOT LARGE ENOUGH TO REACH YIELD SURFACE."

171

In this case the calculation halts with the system message "STOP POREQST 185".

REZON

The subroutine REZON provides messages if the input does not meet its requirements:

"GARBAGE IS NOT A VALID SUBVALUE TYPE FOR THE CARD REZON"

where 'GARBAGE' is the unidentified label. If more than one XCONST or YCONST value occurs in a rezoning group, the message is:

"TOO MANY XCONST OR YCONST VALUES ON A LINE,
XON = 2.00 YON = 1.00 -REZON-"

If the REZON data precedes the BLOCK data, the following message is written:

"REZONE DATA CANNOT PRECEDE BLOCK DATA, LNODE = 0"

These errors can be corrected by following the input rules in Section IV.

REZONH

Several errors may be detected in the REZONH routine and these will halt the calculation with the system message "STOP 666". Along with that message will be one of the following on the standard printed output:

"REZONH ERROR NODE 63 HAS BAD CONNECTION"

"REZONH ERROR TOO LITTLE CELL MASS..."

"REZONH ERROR NEW DENSITY < OLD DENSITY MIN IN ..."

"REZONH ERROR NEW DENSITY > OLD DENSITY MAX IN ..."

"REZONH CONSERVATION ERROR..."

If one of these error messages occurs, the printout should be examined to ascertain the nature of the difficulty. The problem may be circumvented by modifying the input to the REZON routine.

172

SPALST

The calculations of the stress state in SPALST often require several iterations. If the number of iterations exceed 10, the following message is printed:

"SPALST--ITER = 11, BT, FT = ..."

If the number of iterations exceeds 12, the subroutine ceases to calculate, and simply returns, giving the message:

"--STOP IN SPALST, ITER = ..."

However, the subroutine does not actually stop the calculation.

WALL

Several error or cautionary messages are present in WALL but have been commented out in the current version. They are labeled "WALL @ 2420" so that they can be located by statement number.

VI EXAMPLES

This section presents five examples of C-HEMP input. The emphasis is on input format and layout logic; the input for material models is not discussed in detail.

Example 1: Rod Penetrating A Plate, With Shear Banding

The input for this problem appears in Figure 35. The purpose of the computation was to explore the role of shear banding during penetration of a 4340 steel rod fired normally into a plate of rolled-homogeneous armor (RHA) at 800 m/s. This is a cylindrically symmetric problem in two dimensions. The mesh is shown in Figures 36 and 37. We suggest that the user start by making an initial run using the EP material model for both penetrator and target.

The first line of input is a title.

The free-field input begins with the GENERAL data group, although it need not appear first. NGEOM=2 specifies cylindrical symmetry. The run is to terminate after 600 calculational cycles or a problem time of 10^{-4} seconds, whichever occurs first. As IPRINT is 600, one singel edit of the node and cell variables will be printed at the end. NPLOT=100 means that data for plotting the mesh will be generated every 100 cycles. In addition, PSCRIB=1 will cause certain variables (selected under the HISTORY data group) to be written to a file.

The first material specified is that of the penetrator. The abbreviation S4340 is used; it could be enclosed in single quotes ('S4340'), but need not, since it contains no embedded blanks. The anti-hourglassing viscosity entered with the TSR label is required because of the large nonuniform distortion expected in the penetrator. The code's default equation of state will be used to calculate the thermodynamic pressure, and the EPP model will be used to calculate the

```
            HEMP 2-D SHEAR3 TEST A20   (4340-->RHA  PENETRATION)
GENERAL     IPRINT=600          NMAX=600         STOPT=1.0E-04
            CLIN=0.1            CQSQ=4.0         TRIQ=0.02
            NGEOM=2             NPLOT=100        PSCRIB=1.
MATERIAL    AMAT=S4340          WEQS=50          RHO=7.85
            EQSTC=1.59E12       EQSTD=5.17E12    EQSTS=5.17E13
            EQSTE=7.36E10       EQSTG=1.69       EQSTH=0.25
            YC=1.03E10          MU=8.19E11       WVAR=7
            TSR=0.10 1.0
   EP       ES=0. 3.E-2 1.
            YS=1.03E10 1.07E10 1.37E10
MATERIAL    AMAT=RHA            WEQS=50          RHO=7.85
            EQSTC=1.59E12       EQSTD=5.17E12    EQSTS=5.17E13
            EQSTE=7.36E10       EQSTG=1.69       EQSTH=0.25
            YC=.68E10           MU=8.19E11       WVAR=7
            TSR=0.05 1.0
            ESC(16)=1.05E10
   SHEAR3   BFR = 14. 0.146 .01 .2 1.5 .07 .04 1. .577 2. 2. 0 8. 0.
            ES = 0. 0.02 0.07 0.12 0.17 0.27 0.47 1.3
            YS = 6.8E9 7.7E9 8.7E9 9.5E9 10.4E9 11.1E9 12.4E9 14.E9
            FNUC = 1. 1. 1. 1. 1. 1. 1.
            EN3=0
BLOCK       XA=        -1.27          0.0          0.0         -1.27
            YA=         0.0           0.0        0.3175       0.3175
            NC12=10    NC23=10    XDNOT=800.E2       AMAT=S4340
GRID        XA=         0.0          0.635        0.635          0.0
            YA=         0.0           0.0          1.2           1.2
            NC12=10                NC23=20           AMAT=RHA
BLOCK       XA=         0.0          0.635        0.635          0.0
            YA=         1.2           1.2          3.81          3.81
            NC12=10                NC23=26           AMAT=RHA
BOUNDARY    NBCTYP=1           YAFECT=3.        YCONST=0.
SLIDE       VAL=0.0   NSL 122,123,124,125,126,127,128,129,130
            FITNSL=0.0
            NMS 111,112,113,114,115,116,117,118,119,120,121
            IDIR=1             FHALL=0.         FITNMS=0.0
REZONE      NFREQ=5            REZMIN=0.1       REZWT=1.0
            YCONST=0.0         YAFECT=2.
REZONE      XCONST=0.0         XAFECT=1.        YAFECT=2.
REZONE      XCONST=-1.27       XAFECT=1.        YAFECT=2.
REZONE      XCONST=0.635       XAFECT=1.        YAFECT=2.
REZONE      YCONST=3.81        YAFECT=2.
REZONE      YCONST=1.2         YAFECT=2.
HISTORY     COMC20  0.09 .15, 0.09 .21, 0.09 .27,  0.09 .33,
                    .09 .39,  0.09 .45, 0.09 .51
```

JA-314522-120

FIGURE 35 INPUT FOR ROD PENETRATION EXAMPLE

176
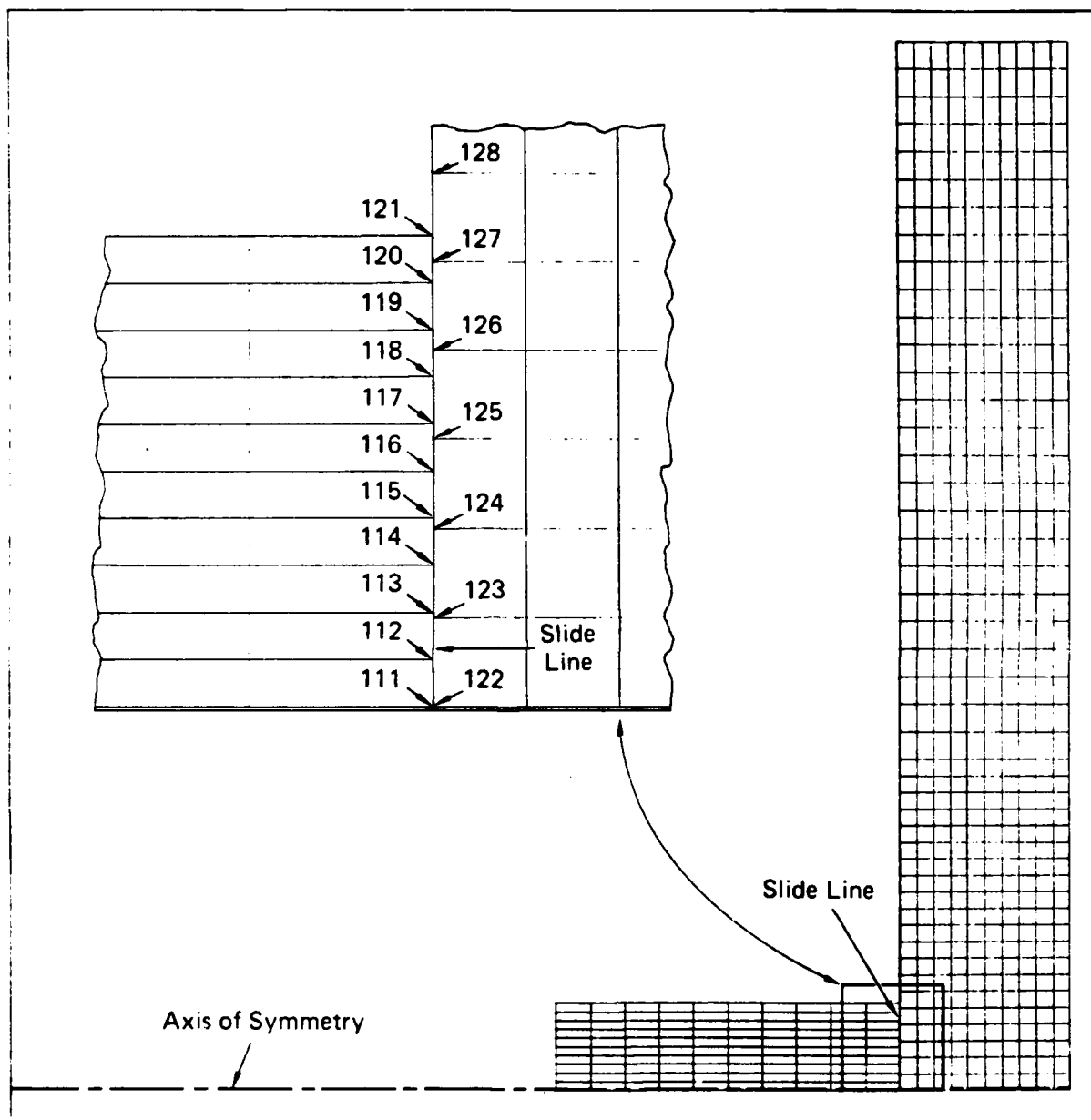
FIGURE 36 INITIAL CELL LAYOUT FOR ROD PENETRATION EXAMPLE

177

NODE EDIT AT N= 300 TIME= 8.126E-06 DATE=15-MAY-84

16-MAY-84

PREPARED BY SR

JA-6423-10

FIGURE 37 CELL CONFIGURATION AFTER 8 μs FOR ROD PENETRATION
EXAMPLE

stress deviators. EPP combines elasticity, Mises plasticity, and a workhardening curve. The input for the curve is a series of yield and plastic strain coordinates. The first segment of the curve is linear; subsequent segments are linear in log-log space. Note that the EPP subkeyword does not start in column 1.

The second material specified, RHA, is that of the target. The shear banding model SHEAR3 will be used to compute all stresses as well as to calculate shear band damage. Most of the model parameters are included in the model's BFR array. The yield-plastic strain curve entered under ES and YS can be used with the EPP model in making a no-damage initial run. SHEAR3 uses all the regular material properties: RHO, EQSTC, EQSTD, EQSTS, EQSTG, EMELT, and MU. EMELT is input as ESC(16).

The first BLOCK data group specifies the layout for the penetrator. The impact plane will be placed at X = 0. The XA and YA pairs specify the X and Y positions of the block corners, starting from the lower left and proceeding counterclockwise. Since CASE is omitted, the code assumes the default, rectangular cells of uniform size. The mesh is to have ten cells in the X-direction (NC12=10) and ten in the Y=direction (NC23=10). Only one XDNOT is specified, so all the nodes have the same initial X-velocity, the impact velocity. Omission of YDNOT makes the initial Y-velocity identically zero. The AMAT material name S4340 matches the AMAT name in the first MATERIAL group exactly, as required.

The target mesh is specified in two data groups. The first is introduced by the keyword GRID because a separate object is being described, and a slide line will be used between the penetrator and the target. The mesh will consist of a small high-resolution block under the penetrator where intense deformation is expected, and a larger low-resolution block for representing the target away from the impact region. Rectangular cells are specified in both blocks.

Next comes the BOUNDARY data group for specifying the boundary condition at the axis of symmetry. Simple control on Y along the axis is desired, so NBCTYP=1 is used. The type of control, "equal to YBC," is specified with YAFECT=3. Being unspecified, YBC takes its default

179

value, zero. Thus, the points on the boundary are required to stay on the line Y = 0, with no constraint on X. The points to be affected by this boundary condition are now specified. We can select the nodes along Y = 0 by entering YCONST=0. finally, we note that YCONST and YBC have the same value (0.), as required.

Now we specify the slide line between the penetrator and the target. At the present time it is necessary to enter the slide nodes explicitly. (For determining the node numbers, see the section on SLIDE in Section IV.) In the present case, the master nodes (NMS=. . .) are in the penetrator, and the slave nodes (NSL=. . .) are in the target. Both sets of nodes are specified from the symmetry axis outward. Since, in the ordering direction, the master nodes are on the left, IDIR must be set equal to +1.

Use of the rezoner is quite helpful in this problem because of the enormous distortions experienced by cells near the edge of the penetration zone. The rezone rate, set by NFREQ=5, requires rezoning at cycles 6, 7, 8, 9, 11, 12, 13, 14, etc., with about one-quarter of the nodes being rezoned on each cycle. REZMIN=0.1 is the threshold for node movement. To prevent conflict with boundary conditions, one specifies several constraints on the rezoner in a series of REZON data groups. The first group, for example, preserves the axis of symmetry by preventing the rezoner from moving nodes on the X-axis (YCONST=0.) in the Y-direction (YAFECT). The REZON groups that follow protect the slide line nodes, the back of the projectile, the back of the target, the edge of the target, and the boundary between the target blocks. These REZON groups are probably more than needed. The main requirement is to eliminate rezoning at corners and at points along boundaries where the cell sizes change.

The HISTORY data group specifies that the 20th cell variable in COMMON is to be printed at every time step for cells centered near the X-Y points specified. The variable requested is the first one in SHEAR3's array CN; it happens to be the equivalent plastic strain. (The location of variables in special arrays is dependent on which material

180

model is being used.) Comparison of the X-Y pairs with the BLOCK speci-
fications shows that the cells being monitored are at the front of the
target.

Example 2:   Cold-On-Hot Symmetric Taylor Test

This problem arose while we were checking whether a certain experi-
mental configuration would be useful in determining the constitutive
relations of hot 4340 steel. (It turned out to be insufficiently
definitive for our purposes.) A cold rod of 4340 steel was to be
impacted at 457 m/s against a stationary rod identical to the first,
except that it was heated to several hundred degrees C. It was assumed
that the temperature difference would mainly reduce the yield stress and
rate of work-hardening. The calculation is performed in the center-of-
mass reference frame. The input is listed in Figure 38, and the layout
is shown in Figure 39. Figure 40 shows the mesh at 1200 cycles.

Again, there is a one-line title, followed by the GENERAL data
group. The linear artificial viscosity coefficient is now specified to
provide a nondefault value. The two materials are identical except for
nondefault yield behavior. The TSR values give the hourglassing
viscosity coefficients. Although only the first eight characters of the
material names will be processed, extra characters have been appended
for legibility. Each rod will be represented by two submeshes, with
higher resolution near the impact plane where most of the deformation
will occur. The rods are to be separated by a slide line. The HISTORY
requests are given in paired groups that specify equivalent points in
the two rods. The variables requested (Y, X, XD, etc.) are repeated for
clarity, though they need not have been.

Example 3:   Contained Fragmenting Cylinder Test

In this example an explosive is detonated inside a cylinder of RHA
steel to investigate its material properties at high strain rate. Shear
banding is expected to be important in the RHA, so the shear-banding
model SHEAR3 is used. The test material is encased in a sleeve of 4140

181

```
              TAYLOR: COLD 4340ST => HOT, W/SLIDE, 457M/S
GENERAL       IPRINT=100          NMAX=1200           STOPT=5.0E-05
              CLIN=0.1            CQSQ=4.0
              NGEOM=2             NPLOT=300           PSCRIB=1.
MATERIAL      AMAT=COLD4340ST     RHO=7.85
              EQSTC=1.59E12       EQSTD=5.17E12       EQSTS=5.17E13
              EQSTE=7.36E10       EQSTG=1.69          EQSTH=0.25
              YC=1.29E10          MU=8.19E11
              TSR=0.10 1.0
 EP           ES=0. 3.E-2 1.
              YS=1.29E10 1.30E10 1.31E10
MATERIAL      AMAT=HOT4340ST      RHO=7.85
              EQSTC=1.59E12       EQSTD=5.17E12       EQSTS=5.17E13
              EQSTE=7.36E10       EQSTG=1.69          EQSTH=0.25
              YC=6.45E09          MU=8.19E11
              TSR=0.10 1.0
 EP           ES=0. 3.E-2 1.
              YS=6.45E09 6.50E09 6.55E09
BLOCK         XA=    -4.445    -0.9525    -0.9525      -4.445
              YA=      0.0       0.0     0.47625       0.47625
              NC12=15    NC23=5      R12=.90909         R23=1.0
              AMAT=COLD4340ST    XDNOT=22850.
BLOCK         XA=   -0.9525      0.0       0.0        -0.9525
              YA=      0.0       0.0     0.47625       0.47625
              NC12=10    NC23=5
              AMAT=COLD4340ST    XDNOT=22850.
GRID          XA=      0.0     0.9525     0.9525        0.0
              YA=      0.0       0.0     0.47625       0.47625
              NC12=10            NC23=5
              AMAT=HOT4340ST     XDNOT=-22850.
BLOCK         XA=     0.9525     4.445     4.445        0.9525
              YA=      0.0       0.0     0.47625       0.47625
              NC12=15    NC23=5      R12=1.1            R23=1.0
              AMAT=HOT4340ST     XDNOT=-22850.
BOUNDARY      NBCTYP=1            YAFECT=3.           YCONST=0.
SLIDE         NSL 157,158,159,160,161,162
              NMS 151,152,153,154,155,156
              IDIR=1
HISTORY       Y 0.001 .47625, .47625 .47625, .95 .47625
              Y -0.001 .47625, -.47625 .47625, -.95 .47625
              X XD 4.445 0.
              X XD -4.445 0.
              COMC20 0.001 0.01, 0.001 .476
              COMC20 -0.001 0.001, -0.001 .476
```

FIGURE 38   INPUT FOR TAYLOR TEST EXAMPLE

182

Axis of Symmetry   Slide Line

Cold 4340   Hot 4340

156   162
155   161
154
160
153
159
152
Slide   158
Line
151   157
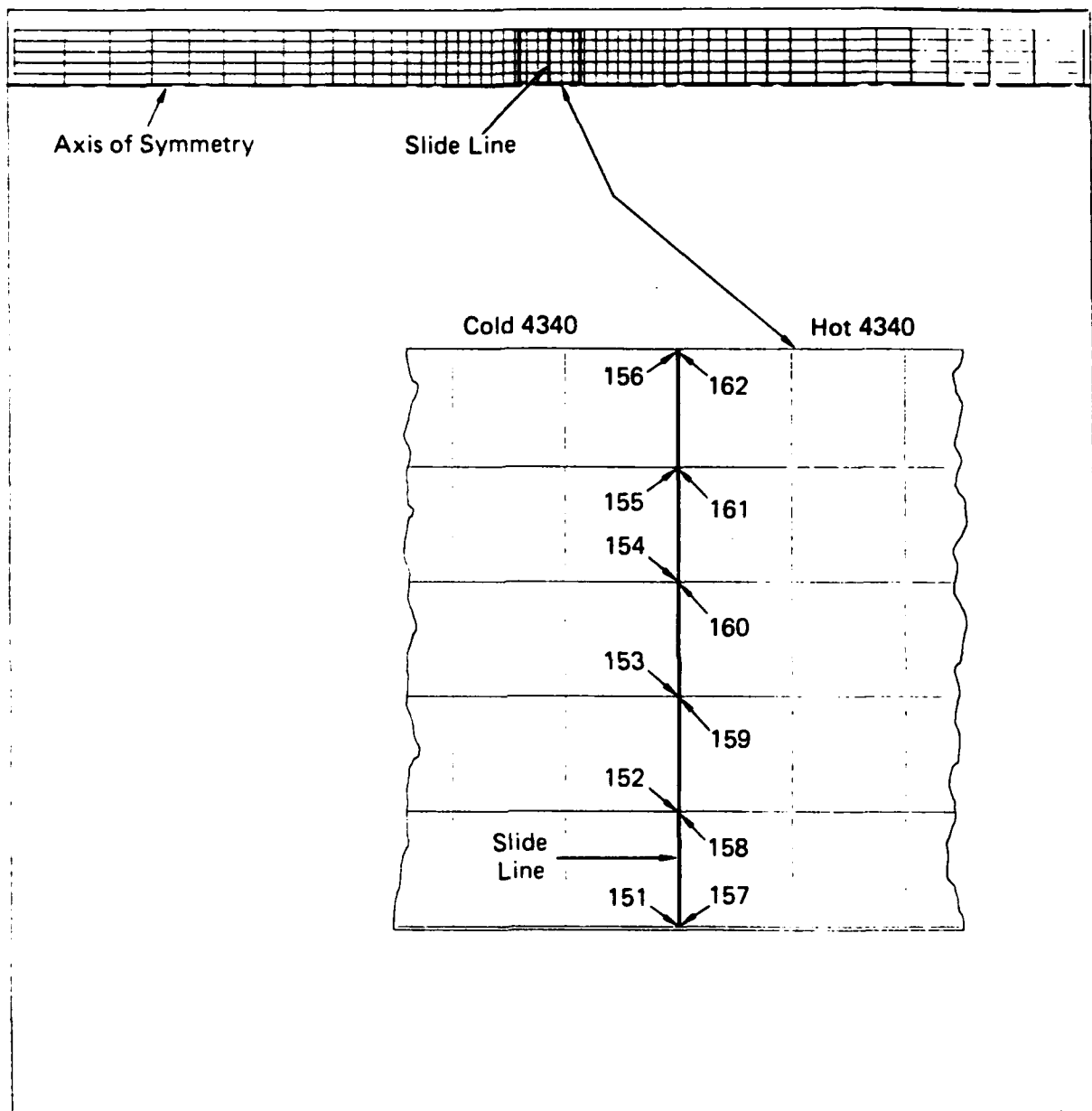
JA-314532-152

FIGURE 39   INITIAL CELL LAYOUT FOR TAYLOR TEST EXAMPLE

183

TAYLOR: COLD 4340ST => HOT, W/SLIDE, 457M/S

SRI HEMP CELL LAYOUT
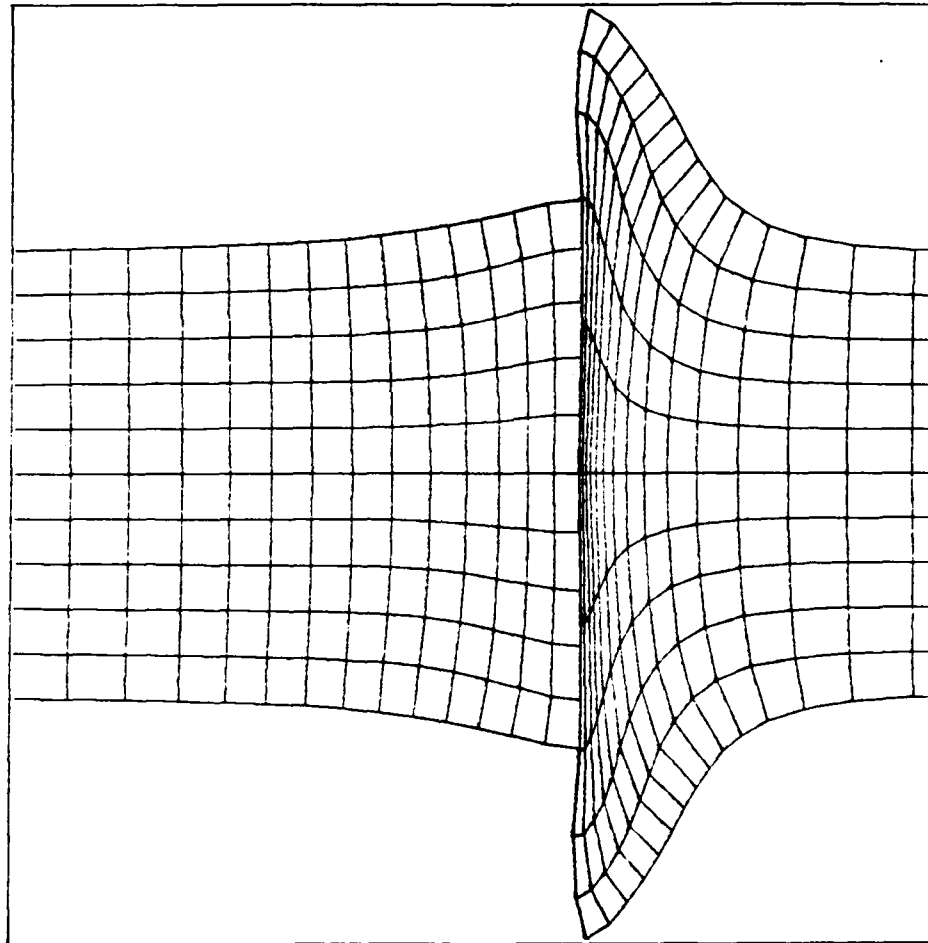
NODE EDIT AT N= 1200 TIME= 2.503E-05 DATE=22-JUN-84

22-JUN-84

PREPARED BY SR'

JA-6423-12

FIGURE 40   CELL CONFIGURATION AFTER 25 μs FOR TAYLOR TEST
EXAMPLE

184

steel to limit the amount of radial strain, but with a layer of PMMA in between to allow some radial expansion. A lead outer shell acts as a momentum trap. The explosive, PETN, is detonated from one end. The amount of deformation suffered by the RHA depends on its axial position, mainly because of the pressure gradient in the explosive gaseous products. Therefore, the simulation requires accurate modeling of the pressure in the gas. It has been found that a slide line must be provided between the explosive and the test material to maintain reasonable cell shapes and to represent the average motion in the gas; the presence of a boundary layer in the gas is ignored.

The input for this problem is found in Figure 41, and the mesh is shown in Figures 42 and 43. The data stream demonstrates some special features of C-HEMP's free-field input scheme: the inclusion of comment lines, and provision for fixed-format input. The SHEAR3 shearbanding model is to be used for the RHA. The melt energy is passed through ESC(16). A tabular equation of state is used for the explosive gases; the label beginning with the characters "FIX" indicates that the following lines (up to the next keyword) are to be read (and echoed) by the EOSTAB subroutine, which has not been fitted with C-HEMP's free-field input. Comment statements have been added. (They begin with the characters "COM".)

Figure 44 shows pressure versus time for a cell that was initially at X = 6.985 cm and Y = 1.14 cm. We note that the pressure goes higher than the peak value in the EOSTAB specification. This is possible since the EOSTAB routine extrapolates for points outside the interval.

Example 4: Steel-Propellant Impact

In this example a sphere of propellant is impacted from the side by a cylindrical steel flyer. This is a simulation of an experiment in which the object was to determine the conditions under which the propellant might detonate. Because detonation is thought to be sensitive to both fracturing and temperature, a fracture model was used. The mesh shown in Figure 45 was chosen so that cells would be reasonably shaped

185

```
              HEMP 2-D SHEAR3 ROUTINE TEST W/ 4340 FRAGMENTING ROUND
GENERAL        IPRINT=100        NMAX=800          STOPT=1.0E-04
               CLIN=0.1          CQSQ=4.0
               NGEOM=2           NPLOT=200         PSCRIB=1.
COM    THE RHA IS BEING TREATED WITH AN INITIAL ESTIMATE OF THE SHEAR3
COM      PARAMETERS.  THEY MAY CAUSE TOO MUCH DAMAGE.
MATERIAL       AMAT=RHA          RHO=7.85
               EQSTC=1.59E12     EQSTD=5.17E12     EQSTS=5.17E13
               EQSTE=7.36E10     EQSTG=1.69        EQSTH=0.25
               YC=.68E10         MU=8.19E+11       TSR=0.05 1.0
   SHEAR3      BFR = 14. 0.146 .01 .2 1.5 .07 .04 1. .577 2. 2. 0 8. 0.
               ES = 0. 0.02 0.07 0.12 0.17 0.27 0.47 1.3
               YS = 6.8E9 7.7E9 8.7E9 9.5E9 10.4E9 11.1E9 12.4E9 14.E9
               FNUC = 1. 1. 1. 1. 1. 1. 1.
               EN3
MATERIAL       AMAT=PETN         RHO=1.0           EQSTG=1.45 WVAR=7
   EXPLODE     QEXPL=3.013E10 DIST=0.5   XDET = 0.8
COM    THE TABULAR DATA FOR THE ISENTROPE IS READ WITH FIXED
COM      FORMAT IN EOSTAB.
   EOSTAB      FIXED FORMAT
   IMAX =              13 DENSITY    LOG
   RHO,P =   1.043E+00 4.557E+10 8.166E-01 2.523E+10 6.394E-01 1.437E+10
             5.007E-01 8.417E+09 3.920E-01 5.063E+09 3.070E-01 3.127E+09
             2.404E-01 1.981E+09 1.882E-01 1.286E+09 1.474E-01 8.529E+08
             1.154E-01 5.772E+08 9.037E-02 3.978E+08 7.076E-02 2.785E+08
             2.660E-02 7.506E+07
MATERIAL       AMAT=PMMA         RHO=1.18
               EQSTC=8.94E10     EQSTD=4.57E10     EQSTE=1.0E10
               EQSTG=1.0         EQSTH=0.25        EQSTS=4.36E11
               YC=1.03E8         MU=8.19E11
MATERIAL       AMAT=S4140        RHO=7.85
               EQSTC=1.59E12     EQSTD=5.17E12     EQSTE=7.36E10
               EQSTG=1.69        EQSTH=0.25        EQSTS=5.17E13
               YC=6.0E09         MU=8.19E11
MATERIAL       AMAT=LEAD         RHO=1.14E01
               EQSTC=5.01E11     EQSTD=4.99E11     EQSTE=9.16E09
               EQSTG=2.20        EQSTH=0.25        EQSTS=2.02E12
BLOCK          XA= 0.635    13.335     13.335      0.635
               YA= 0.       0.         2.28        2.28
               NC12=40      NC23=6               AMAT=PETN
   EXPLODE
GRID           XA= 0.       15.24      15.24       0.
               YA= 2.28     2.28       3.42        3.42
               NC12=25      NC23=3               AMAT=RHA
COM            SLIDE 1 TO 2
BLOCK          XA= 0.       15.24      15.24       0.
               YA= 3.42     3.42       4.37        4.37
               NC12=25      NC23=1               AMAT=PMMA
                                                           JA-314522-122
```

FIGURE 41   INPUT FOR PROBLEM 3: CONTAINED FRAGMENTING CYLINDER
             TEST EXAMPLE

186

```
BLOCK         XA= 0.          15.24        15.24        0.
              YA= 4.37         4.37        10.16       10.16
              NC12=25         NC23=10         AMAT=S4140
BLOCK         XA= 0.          15.24        15.24        0.
              YA=10.16        10.16        12.7        12.7
              NC12=25         NC23=2          AMAT=LEAD
BOUNDARY      NBCTYP=1      YAFECT=3.       YCONST=0.
COM   SLIDE LINE IS BETWEEN THE EXPLOSIVE AND RHA CYLINDER ONLY.
SLIDE         NSL 7,14,21,28,35,42,49,56,63,70,77,84,91,98,105,112,119
              NSL 126,133,140,147,154,161,168,175,182,189,196,203,210
              NSL 217,224,231,238,245,252,259,266,273,280,287
              VAL=0.0 NMS 288,292,296,300,304,308,312
              NMS 316,320,324,328,332,336,340,344,348,352,356,360,364
              NMS 368,372,376,380,384,388
              IDIR=1
HISTORY       XD 0.79375 0.19,  P 6.985 1.14,  YD 0.3048 2.35125
              SYY 6.985 2.35125,  YD 6.985 2.35125,  SYY 0. 2.8
              2.0 2.8, 4.0 2.8, 6.0 2.8, 8.0 2.8 10.0 2.8 12.0 2.8
```

JA-314522-123

FIGURE 41   INPUT FOR PROBLEM 3: CONTAINED FRAGMENTING CYLINDER
TEST EXAMPLE (Concluded)
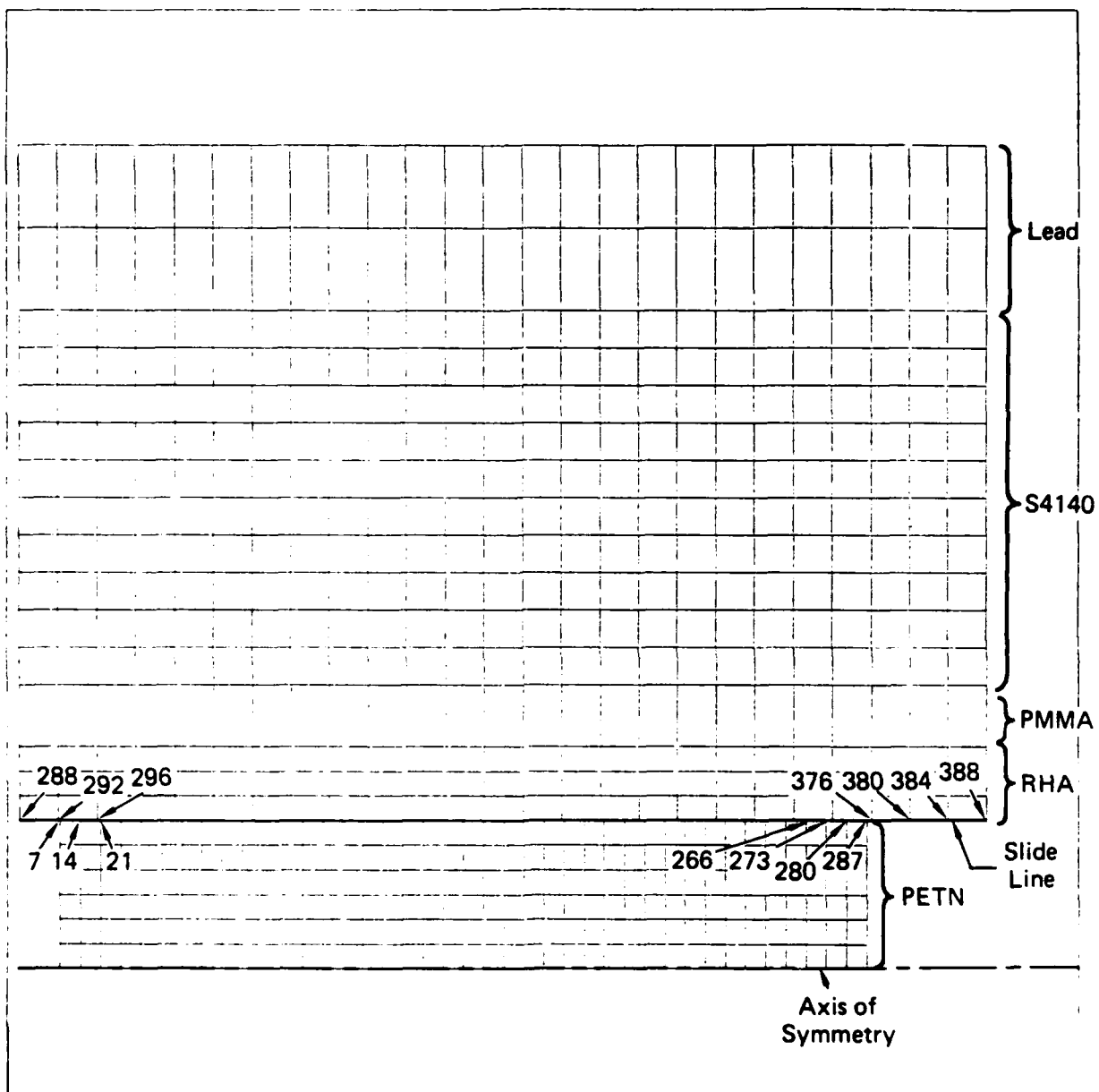
FIGURE 42   INITIAL CELL LAYOUT FOR CONTAINED FRAGMENTING CYLINDER
EXAMPLE
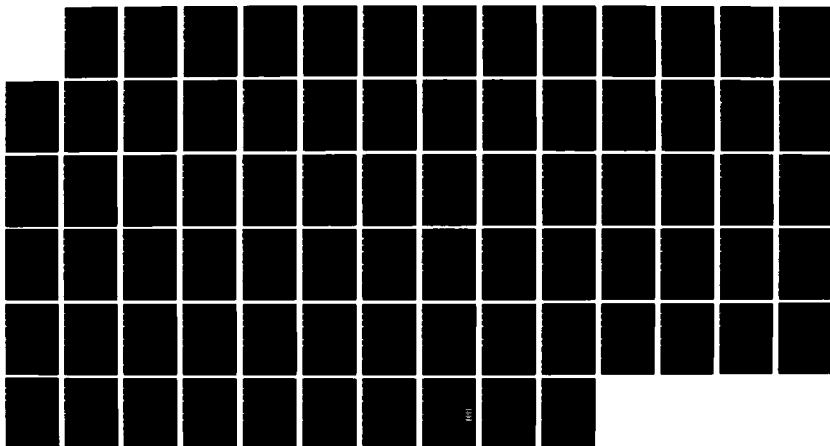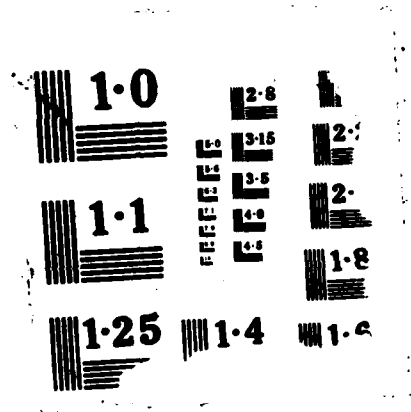
HEMP 2-D SHEAR3 ROUTINE TEST W/ 4340 FRAGMENTING R
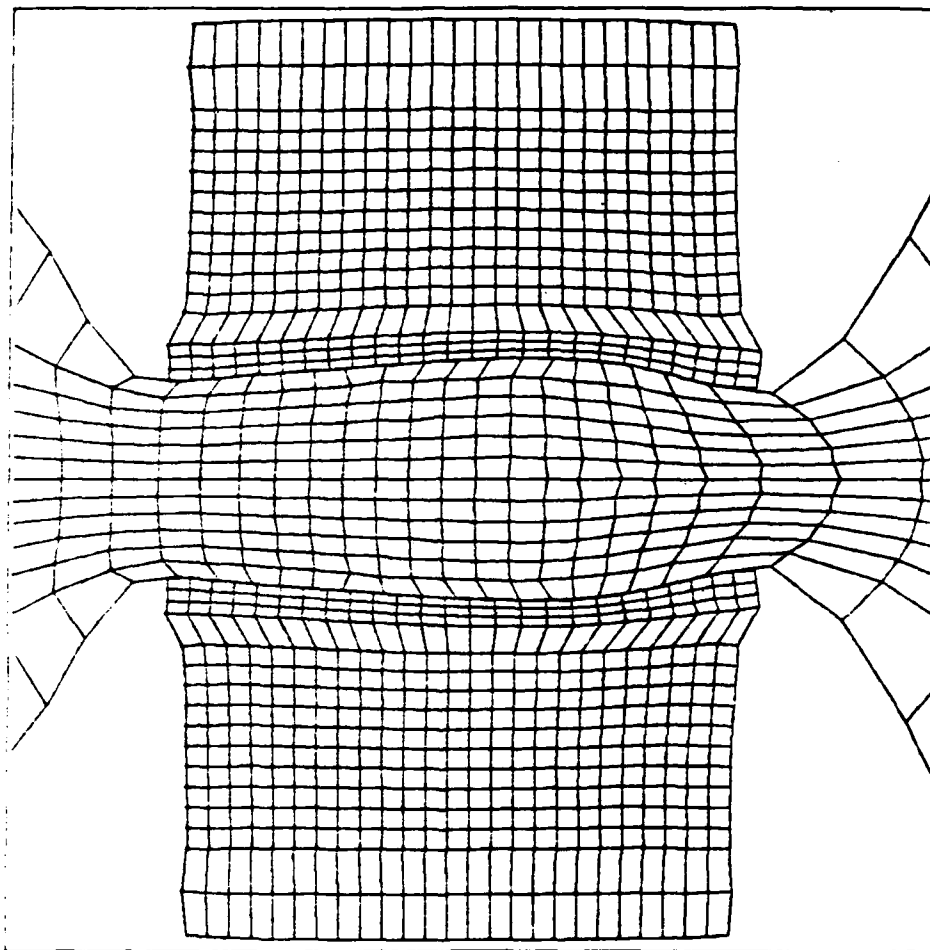
NODE EDIT AT N= 342 TIME= 1.002E-04 DATE=17-JUN-84

-84   PREPARED BY SR.

JA-6423-14

FIGURE 43   CELL CONFIGURATION AFTER 100 μs FOR CYLINDER TEST
             EXAMPLE

189
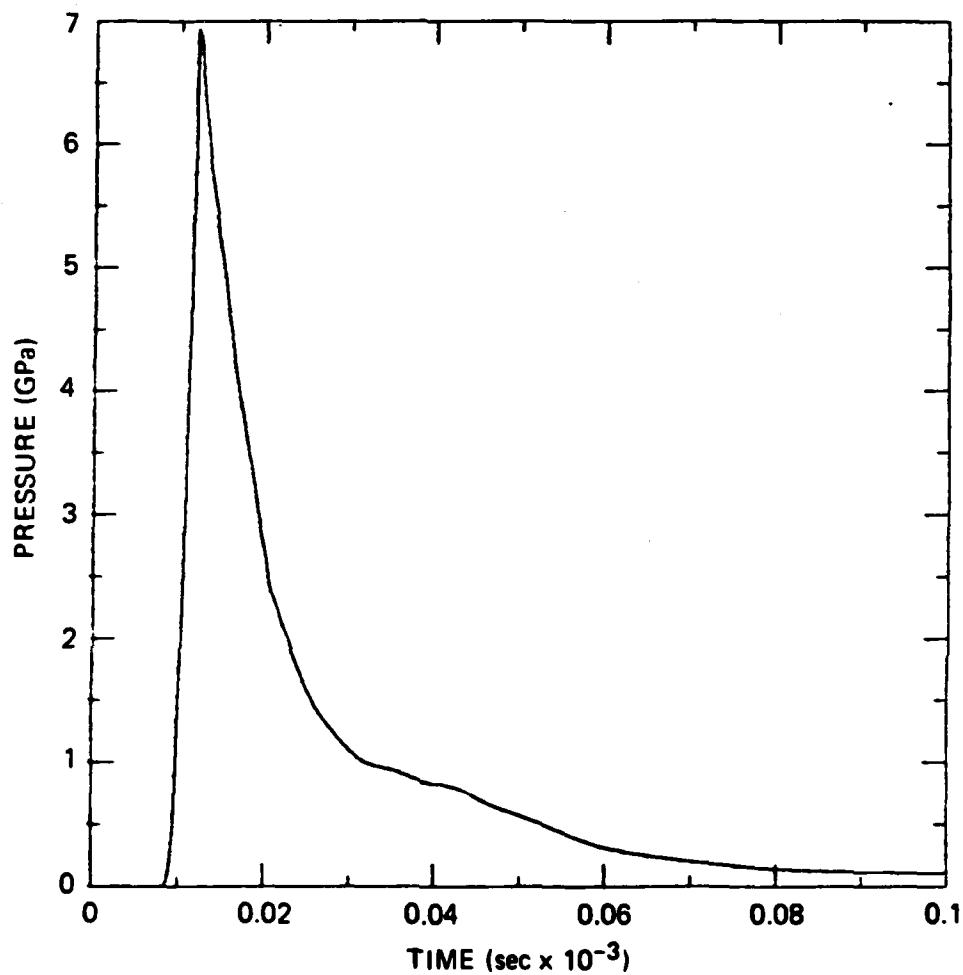
HEMP 2-D SHEAR3 ROUTINE TEST W/ 4340 FRAGM

JA-6423-15

FIGURE 44   PRESSURE HISTORY FOR EXPLOSIVE INITIALLY AT x = 6.985 cm.
y = 2.35 IN CYLINDER TEST EXAMPLE

190

PROPELLANT IMPACTED BY STEEL
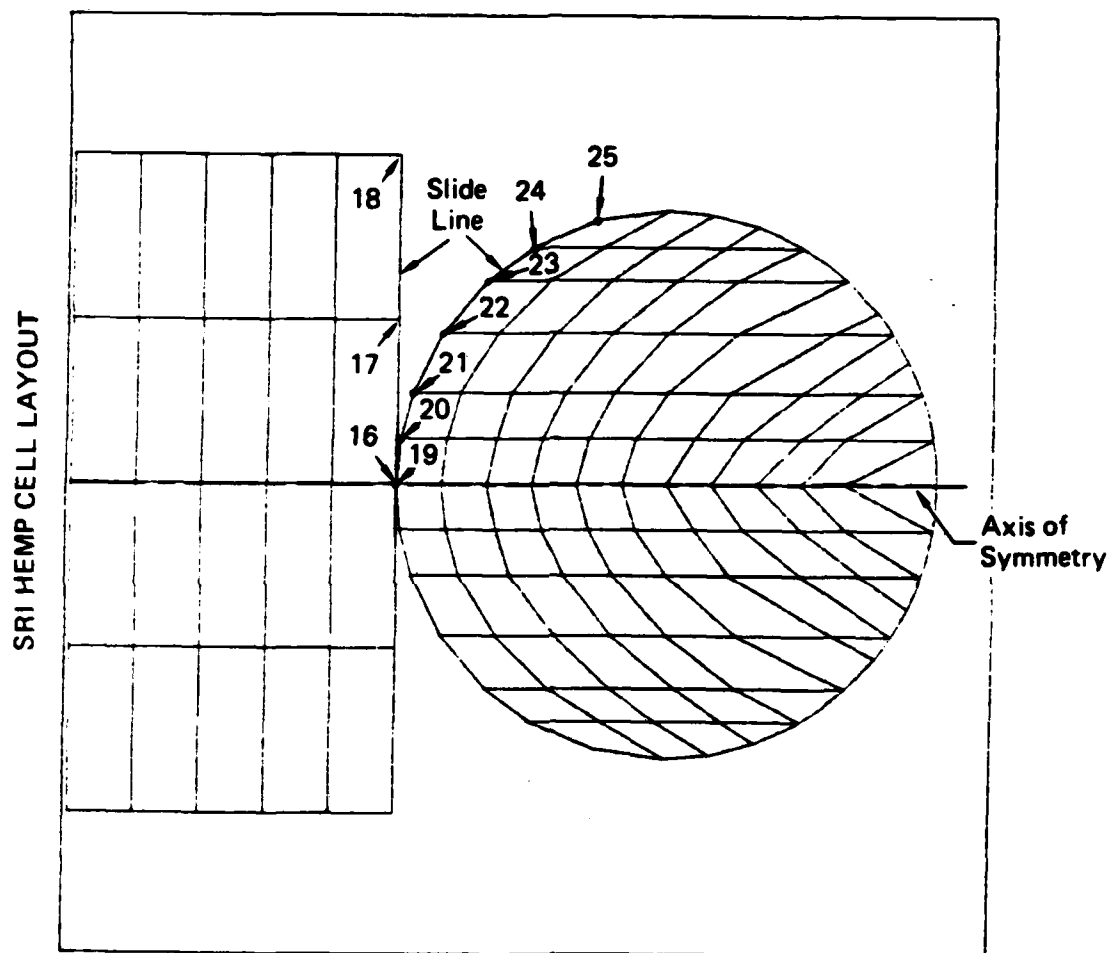
JA-6423-16A

FIGURE 45   INITIAL CELL LAYOUT FOR PROPELLANT IMPACT TEST EXAMPLE

191

after impact. Because of the unusual layout, it was necessary to specify the X-Y positions of every node in the propellant sub-block.

See Figure 46 for the input. For the steel impactor, the default Mie-Grüneisen equation of state and constant yield stress are used. Anti-hourglassing viscosity is introduced through the TSR array. The propellant uses the BFRACT model (the subroutine name is BFRACT3). Although only the first eight characters of material names are processed, a long propellant name has been used for clarity.

The BLOCK keywords have also been augmented with extra characters for clarity. This points up a peculiarity of the input logic: only the first eight characters are processed, the rest of the characters are ignored. The layout for the impactor is elementary, but the circular target must be specified one cell at a time. Note that the first target cell is identified by the keyword GRID, because a new object is being described. The axis of symmetry is specified in the BOUNDARY data group. A slide line is provided between the impactor and the target. Figure 47 shows the mesh at 502 cycles. The run stopped here because of a cell size that became too small.

Example 5: Explosive Sheet Detonated Over A Surface

This example is a preliminary calculation for an experimental designed to study the propagation of shock waves thorugh a porous soil. The soil is overlaid by a square sheet of explosive that is detonated from one edge (see Figure 48). The problem is three-dimensional, but only a two-dimensional (plane strain) section is simulated. This example features a running detonation, a slide line, and blocks with variable cell dimensions.

Figure 49 gives the input. The running detonation is specified under the input for EXPLODE. The soil requires a porous model, and the indicator WPOR must be set to unity so that the POREQST model will be used in performing stress-strain calculations for the soil. In addition, space for 15 extra variables is provided. A special Coulomb friction parameter is provided by ESC(10), which has no general variable

```
                   PROPELLANT IMPACTED BY STEEL
GENERAL       IPRINT=100        NMAX=1000         STOPT=3.0E-04
              CLIN=0.1          CQSQ=4.0
              NGEOM=2           NPLOT=100         PSCRIB=1.
MATERIAL      AMAT=IMPACTOR     RHO=7.85
              EQSTC=1.5889E12   EQSTD=5.17E12     EQSTS=5.17E13
              EQSTE=7.36E10     EQSTG=1.69        EQSTH=0.25
              YC=1.03E10        MU=8.188E11
              TSR=0.10
MATERIAL      AMAT=PROPELLANT   RHO=1.85
              EQSTC=5.666E10    EQSTD=3.913E11    EQSTS=1.817E12
              EQSTE=1.00E10     EQSTG=1.0         EQSTH=0.25
              YC=5.0E08         MU=1.244E10
  BFRACT      FIXED FORMAT
  BFR 1     -1.500E-02 1.280E+08 5.200E-03 6.000E+07-5.000E+08-
1.000E+08            2.000E-02   (continuation of line above in A10,
7E10.3 format)
  BFR 2      1.000E+01 6.000E+00 3.300E-01 1.000E+00 2.000E-01 4.000E+00
  INDS =             1          1          3
BLOCKSTEEL XA =  0.    7.62    7.62    0.        AMAT=IMPACTOR
           YA =  0.    0.      7.62    7.62      NC12=5  NC23=2
           XDNOT=2.0E4
GRID       XA =  7.62   8.67833   8.80333   7.70883   AMAT=PROPELLANT
           YA =  0.     0.        1.05833   1.05833   NC12=1  NC23=1
BLOCK-01 NC12=1 NC23=1   XA= 8.67833   9.73667   9.97000   8.80333
                         YA= 0.00000   0.00000   1.05833   1.05833
BLOCK-02 NC12=1 NC23=1   XA= 9.73667 10.79500 11.05333   9.97000
                         YA= 0.00000   0.00000   1.05833   1.05833
BLOCK-03 NC12=1 NC23=1   XA=10.79500 11.85333 12.13667 11.05333
                         YA= 0.00000   0.00000   1.05833   1.05833
BLOCK-04 NC12=1 NC23=1   XA=11.85333 12.91167 13.25333 12.13667
                         YA= 0.00000   0.00000   1.05833   1.05833
BLOCK-05 NC12=1 NC23=1   XA=12.91167 13.97000 14.63667 13.25333
                         YA= 0.00000   0.00000   1.05833   1.05833
BLOCK-06 NC12=1 NC23=1   XA=13.97000 15.02833 15.80333 14.63667
                         YA= 0.00000   0.00000   1.05833   1.05833
BLOCK-07 NC12=1 NC23=1   XA=15.02833 16.08667 17.14500 15.80333
                         YA= 0.00000   0.00000   1.05833   1.05833
BLOCK-08 NC12=1 NC23=1   XA=16.08667 17.14500 18.20333 17.14500
                         YA= 0.00000   0.00000   1.05833   1.05833
BLOCK-09 NC12=1 NC23=1   XA=17.14500 18.20333 20.23167 18.20333
                         YA= 0.00000   0.00000   1.05833   1.05833
BLOCK-10 NC12=1 NC23=1   XA=18.20333 20.32000 20.29000 20.23167
                         YA= 0.00000   0.00000   0.61667   1.05833
BLOCK-11 NC12=1 NC23=1   XA= 7.70883   8.80333   9.10333   7.98317
                         YA= 1.05833   1.05833   2.11667   2.11667
BLOCK-12 NC12=1 NC23=1   XA= 8.80333   9.97000 10.30333   9.10333
                         YA= 1.05833   1.05833   2.11667   2.11667
```

FIGURE 46   INPUT FOR PROPELLANT IMPACT TEST EXAMPLE

```
BLOCK-13 NC12=1 NC23=1   XA= 9.97000 11.05333 11.57000 10.30333
                         YA= 1.05833  1.05833  2.11667  2.11667
BLOCK-14 NC12=1 NC23=1   XA=11.05333 12.13667 12.72000 11.57000
                         YA= 1.05833  1.05833  2.11667  2.11667
BLOCK-15 NC12=1 NC23=1   XA=12.13667 13.25333 13.97000 12.72000
                         YA= 1.05833  1.05833  2.11667  2.11667
BLOCK-16 NC12=1 NC23=1   XA=13.25333 14.63667 15.47000 13.97000
                         YA= 1.05833  1.05833  2.11667  2.11667
BLOCK-17 NC12=1 NC23=1   XA=14.63667 15.80333 17.14500 15.47000
                         YA= 1.05833  1.05833  2.11667  2.11667
BLOCK-18 NC12=1 NC23=1   XA=15.80333 17.14500 18.55334 17.14500
                         YA= 1.05833  1.05833  2.11667  2.11667
BLOCK-19 NC12=1 NC23=1   XA=17.14500 18.20333 19.95667 18.55334
                         YA= 1.05833  1.05833  2.11667  2.11667
BLOCK-20 NC12=1 NC23=1   XA= 7.98317  9.10333  9.97000  8.67833
                         YA= 2.11667  2.11667  3.51000  3.51000
BLOCK-21 NC12=1 NC23=1   XA= 9.10333 10.30333 11.35333  9.97000
                         YA= 2.11667  2.11667  3.51000  3.51000
BLOCK-22 NC12=1 NC23=1   XA=10.30333 11.57000 12.67000 11.35333
                         YA= 2.11667  2.11667  3.51000  3.51000
BLOCK-23 NC12=1 NC23=1   XA=11.57000 12.72000 13.97000 12.67000
                         YA= 2.11667  2.11667  3.51000  3.51000
BLOCK-24 NC12=1 NC23=1   XA=12.72000 13.97000 15.63667 13.97000
                         YA= 2.11667  2.11667  3.51000  3.51000
BLOCK-25 NC12=1 NC23=1   XA=13.97000 15.47000 17.90333 15.63667
                         YA= 2.11667  2.11667  3.51000  3.51000
BLOCK-26 NC12=1 NC23=1   XA=15.47000 17.14500 19.26167 17.90333
                         YA= 2.11667  2.11667  3.51000  3.51000
BLOCK-27 NC12=1 NC23=1   XA=17.14500 18.55334 19.63667 19.26167
                         YA= 2.11667  2.11667  2.86500  3.51000
BLOCK-28 NC12=1 NC23=1   XA=18.55334 19.95667 19.80667 19.63667
                         YA= 2.11667  2.11667  2.50000  2.86500
BLOCK-29 NC12=1 NC23=1   XA= 8.67833  9.97000 11.22000  9.73667
                         YA= 3.51000  3.51000  4.73300  4.73300
BLOCK-30 NC12=1 NC23=1   XA= 9.97000 11.35333 12.65333 11.22000
                         YA= 3.51000  3.51000  4.73300  4.73300
BLOCK-31 NC12=1 NC23=1   XA=11.35333 12.67000 14.18677 12.65333
                         YA= 3.51000  3.51000  4.73300  4.73300
BLOCK-32 NC12=1 NC23=1   XA=12.67000 13.97000 15.63667 14.18667
                         YA= 3.51000  3.51000  4.73300  4.73300
BLOCK-33 NC12=1 NC23=1   XA=13.97000 15.63667 18.20333 15.63667
                         YA= 3.51000  3.51000  4.73300  4.73300
BLOCK-34 NC12=1 NC23=1   XA=15.63667 17.90333 18.90167 18.20333
                         YA= 3.51000  3.51000  4.00000  4.73300
BLOCK-35 NC12=1 NC23=1   XA=17.90333 19.26167 19.09500 18.90167
                         YA= 3.51000  3.51000  3.75000  4.00000
```

FIGURE 46   INPUT FOR PROPELLANT IMPACT TEST EXAMPLE
(Continued)

```
BLOCK-36 NC12=1 NC23=1  XA= 9.73667 11.22000 12.45333 10.79500
                        YA= 4.73300  4.73300  5.49917  5.49917
BLOCK-37 NC12=1 NC23=1  XA=11.22000 12.65333 13.72000 12.45333
                        YA= 4.73300  4.73300  5.49917  5.49917
BLOCK-38 NC12=1 NC23=1  XA=12.65333 14.18667 15.30333 13.72000
                        YA= 4.73300  4.73300  5.49917  5.49917
BLOCK-39 NC12=1 NC23=1  XA=14.18667 15.63667 17.14500 15.30333
                        YA= 4.73300  4.73300  5.49917  5.49917
BLOCK-40 NC12=1 NC23=1  XA=15.63667 18.20333 17.63667 17.14500
                        YA= 4.73300  4.73300  5.18433  5.49917
BLOCK-41 NC12=1 NC23=1  XA=10.79500 12.45333 13.97000 12.30333
                        YA= 5.49917  5.49917  6.35000  6.12667
BLOCK-42 NC12=1 NC23=1  XA=12.45333 13.72000 15.02833 13.97000
                        YA= 5.49917  5.49917  6.26167  6.35000
BLOCK-43 NC12=1 NC23=1  XA=13.72000 15.30333 16.08667 15.02833
                        YA= 5.49917  5.49917  5.98667  6.26167
BLOCK-44 NC12=1 NC23=1  XA=15.30333 17.14500 16.63667 16.08667
                        YA= 5.49917  5.49917  5.76333  5.98667
BLOCK-45 NC12=1 NC23=1  XA=18.20333 20.23167 20.09667 19.95667
                        YA= 1.05833  1.05833  1.66667  2.11667
BOUNDARY       NBCTYP=1            YAFECT=3.           YCONST=0.
SLIDL          NSL 19,20,43,53,63,71,77
               NMS 16,17,18
               IDIR=1
HISTORY        P XD 7.67 0., 11.47 0.5292, 16.137 0.5292, 20.32 0.
                    8.72 2.8, 12.97 2.8, 18.80 2.5, 10.97 5.0
                    13.97 5.0, 17.137 5.0, 13.987 6.32
               SXX SYY SZZ  14.8596 0.5292, 16.137 0.5292, 15.764 1.587
               YD   10.47 5.0, 12.97 2.8, 13.987 6.32
```

JA-314522-126

FIGURE 46   INPUT FOR PROPELLANT IMPACT TEST EXAMPLE
(Concluded)

195

PROPELLANT IMPACTED BY STEEL

SRI HEMP CELL LAYOUT
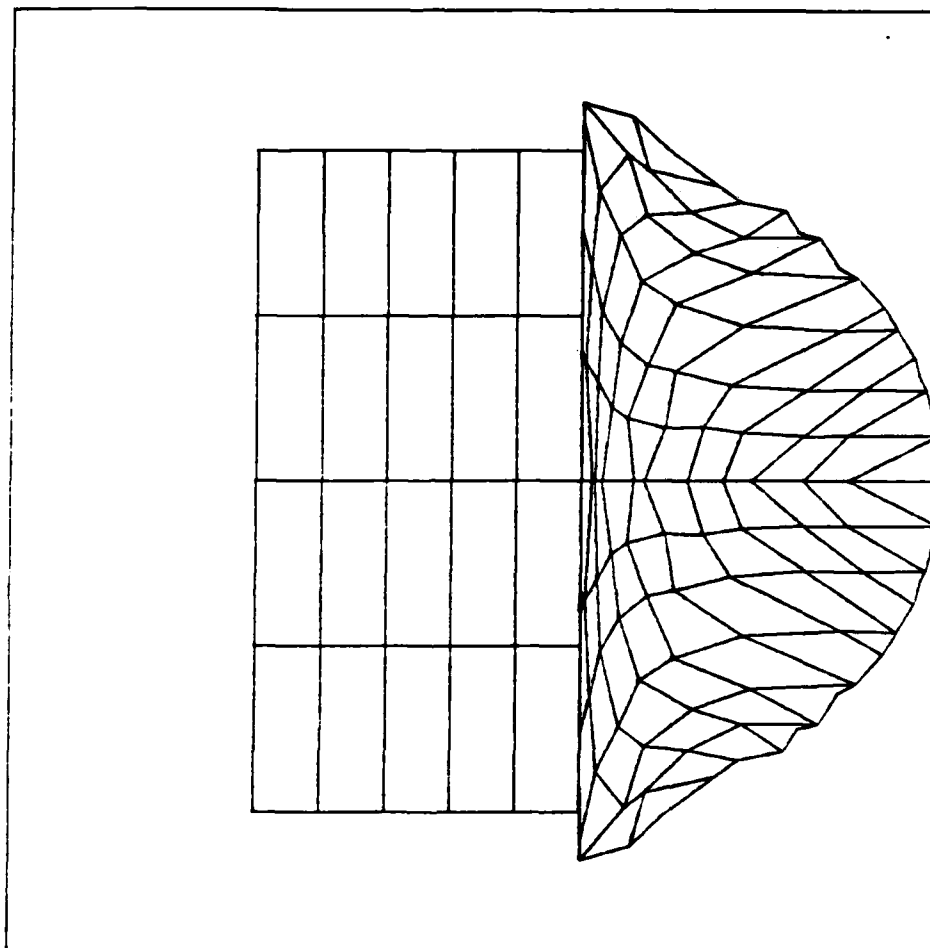
NODE EDIT AT N= 502 TIME= 3.001E-04 DATE=16-MAY-84

11-JUN-84

PREPARED BY SR
JA-6423-17

FIGURE 47   CELL CONFIGURATION AFTER 300 μs FOR PROPELLANT
IMPACT TEST EXAMPLE

EXPLOSIVE SHEET OVER SOIL TESTBED

NODE EDIT AT N=   1 TIME= 1.000E-12 DATE=15-MAY-84

11-JUN-84   PREPARED BY SR

JA-6423-18

FIGURE 48   INITIAL CELL LAYOUT FOR EXPLOSIVE SHEET EXAMPLE

197

```
        EXPLOSIVE SHEET OVER SOIL TESTBED
GENERAL     IPRINT=100        NMAX=500          STOPT=2.E-3
            CLIN=0.1          EQSQ=4.0
            NGEOM=1           NPLOT=100         PSCRIBE=1.
MATERIAL    AMAT=EXPLOSIVE    RHO=1.13          EQSTG=1.305
  EXPLODE   QEXPL=5.0E10      DIST=.5           XDET= 0.
MATERIAL    AMAT=YUMATESTBED  RHOS=2.60         WPOR=1
            EQSTC=4.00E11     EQSTD=0.          EQSTE=8.80E10
            EQSTG=1.17        EQSTH=0.25
            ESC(10)=1.2       MU=2.E11          PMIN=-1.E6
            RHO=1.825         YC=1.0E6
            TSR=0.05,0.3
  POREQST   RHOP=1.825   2.1978   2.35    2.53    3.305
            COSQ=10.    20.    10.    10.    10.
            C1= .3    .5    .3    .3    .3
            P1=1.E7          NREG=4     AK=1.E11     MUP=2.E10
            YZERO=1.E6
            P2=6.0E8    1.49E9    8.75E9    9.E10
            DELP= -8.E7    -1.4E8    -1.E8    0.
BLOCK       XA=  0.         0.         731.        731.
            YA= 10.        0.         0.          10.
            NC12=4        NC23=150     AMAT=EXPLOSIVE
  EXPLODE
GRID        XA=   0.      -250.      -250.         0.
            YA=   0.       0.        -250.       -250.
            R12=1.05      R23=1.05   R43=1.05    R14=1.05
            NC12=13       NC23=8     NC43=8      NC14=13
            CASE=3        AMAT=YUMATESTBED
BLOCK       XA=   0.       0.        731.        731.
            YA=   0.      -250.      -250.         0.
            R12= 1.05     R23= 1.    CASE=2
            NC12=13       NC23=73    AMAT=YUMATESTBED
BLOCK       XA= 731.      731.       981.        981.
            YA=   0.      -250.      -250.         0.
            R12= 1.05     R23=1.05   R43=1.05    R14=1.05
            NC12=13       NC23=8     NC43=8      NC14=13
            CASE=3        AMAT=YUMATESTBED
SLIDE  NMS 605,606,607,608,609,610,611,612,613,614,615,616,617,618
       NMS 619,620,621,622,623,624,625,626,627,628,629,630,631,632
       NMS 633,634,635,636,637,638,639,640,641,642,643,644,645,646
       NMS 647,648,649,650,651,652,653,654,655,656,657,658,659,660
       NMS 661,662,663,664,665,666,667,668,669,670,671,672,673,674
       NMS 675,676,677,678,679,680,681,682,683,684,685,686,687,688
       NMS 689,690,691,692,693,694,695,696,697,698,699,700,701,702
       NMS 703,704,705,706,707,708,709,710,711,712,713,714,715,716
       NMS 717,718,719,720,721,722,723,724,725,726,727,728,729,730
```
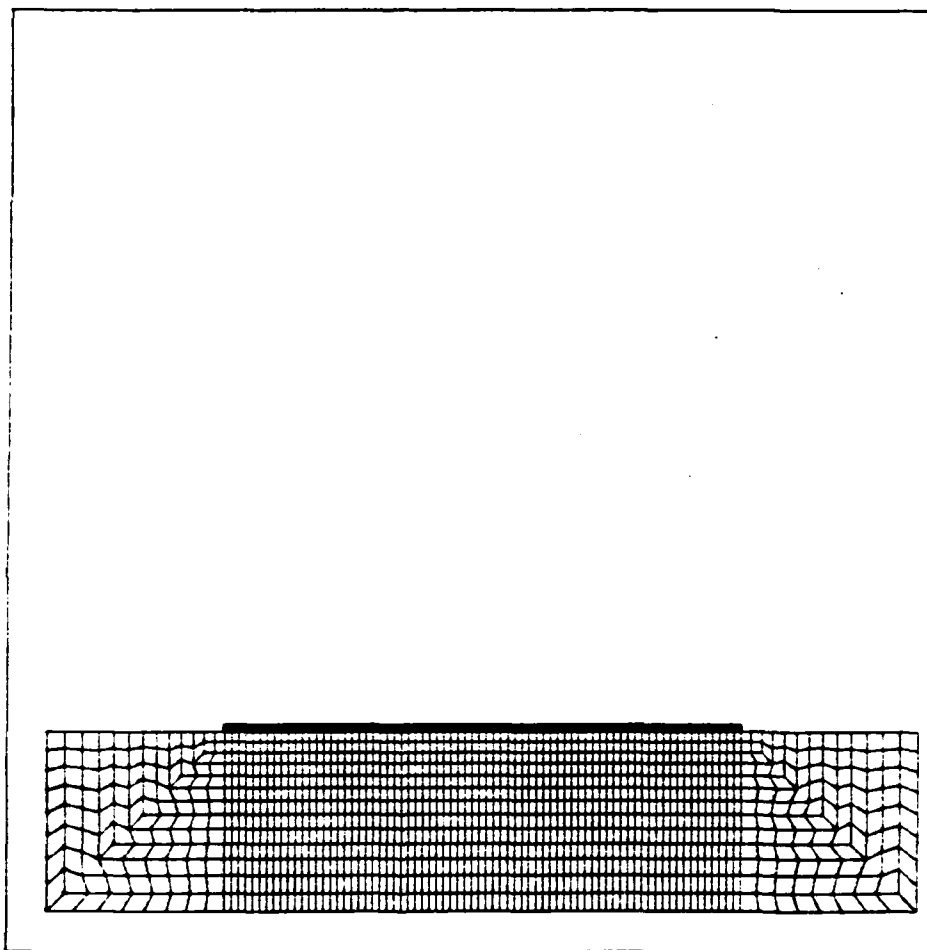
FIGURE 49   INPUT FOR EXPLOSIVE SHEET EXAMPLE

```
NMS 731,732,733,734,735,736,737,738,739,740,741,742,743,744
NMS 745,746,747,748,749,750,751,752,753,754,755
NSL 873,856,841,828,815,804,793,784,777,770,765,760,756,890
NSL 891,892,893,894,895,896,897,898,899,900,901,902,903,904
NSL 905,906,907,908,909,910,911,912,913,914,915,916,917,918
NSL 919,920,921,922,923,924,925,926,927,928,929,930,931,932
NSL 933,934,935,936,937,938,939,940,941,942,943,944,945,946
NSL 947,948,949,950,951,952,953,954,955,956,957,958,959,960
NSL 961,962,1913,1917,1921,1927,1933,1941,1951,1961,1973,1985
NSL 1999,2015,2031
IDIR=1
HISTORY  P 241.2,1.25   363.1,1.25   484.9,1.25   245.3,-7.057
           365.5,-7.057   485.7,-7.057   245.3,-36.71   365.5,-36.71
           485.7,-36.71   245.3,-69.41   365.5,-69.41   485.7,-69.41
           245.3,-105.5   365.5,-105.5   485.7,-105.5
       XD,YD 245.3,-36.71   245.3,-69.41
```

FIGURE 49   INPUT FOR EXPLOSIVE SHEET EXAMPLE (Concluded)

assignment. A small anti-hourglassing viscosity is specified with the
TSR values. The EXPLODE label in the BLOCK specification for the explo-
sive causes the burn times to be initialized in the explosive cells.
The soil mesh consists of three blocks. In the second (middle) one, the
cell dimension decreases with Y. In the first and third blocks (on the
ends), the cell dimensions vary along two edges of the block but not on
the other two; this causes the code to automatically set up larger cells
away from the high strain-rate region. Figure 50 shows the mesh at 500
cycles.

EXPLOSIVE SHEET OVER SOIL TESTBED
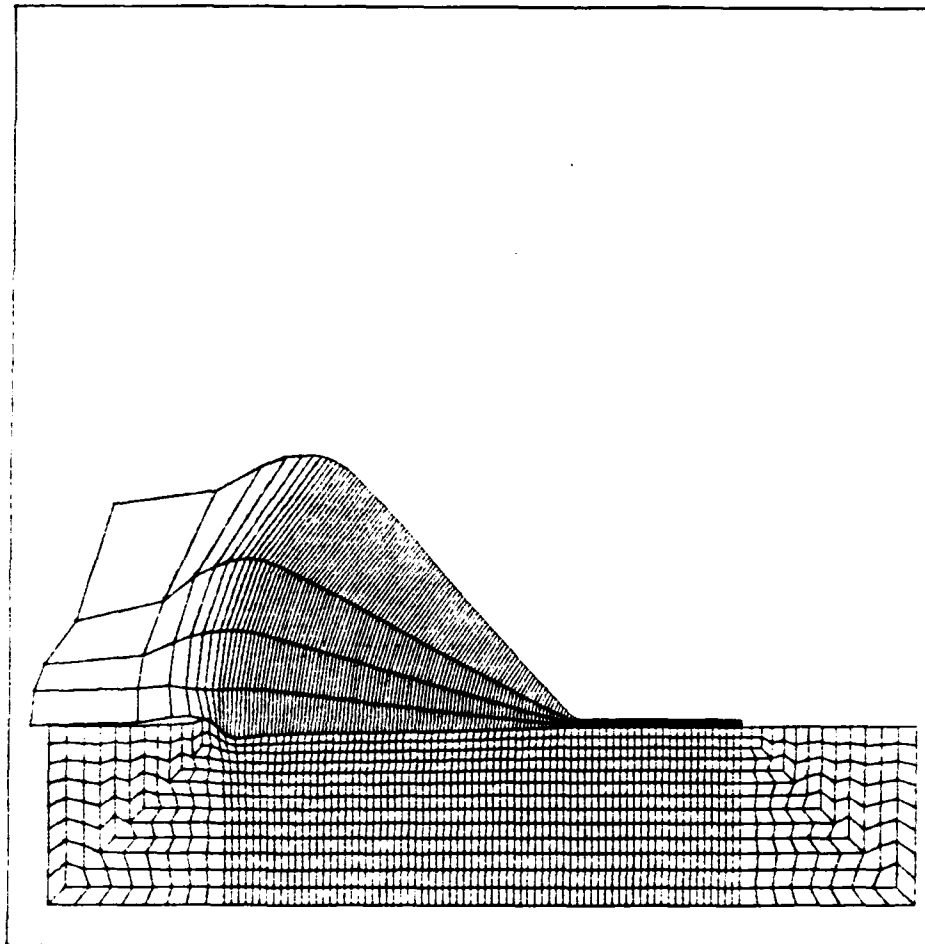
NODE EDIT AT N= 500 TIME= 7.616E-04 DATE=16-MAY-84

11-JUN-84

PREPARED BY SR·

JA-6423-19

FIGURE 50   CELL CONFIGURATION AFTER 762 μs FOR EXPLOSIVE
SHEET EXAMPLE

201

REFERENCES

1. D. R. Curran, R. Burback, R. D. Caligiuri, M. Cowperthwaite, D. C. Erlich, L. Seaman, and D. A. Shockey, "Computational Model for Armor Penetration," SRI International First Annual Report on Contract DAAK11-78-C-0115 for U.S. Army Ballistic Research Laboratory, Aberdeen, MD, and Army Materials and Mechanics Research Center, Watertown, MA (November 1979).

2. D. C. Erlich, L. Seaman, R. D. Caligiuri, and D. R. Curran, "Computational Model for Armor Penetration," SRI International Second Annual Report on Contract DAAK11-78-C-0115 for U.S. Army Ballistic Research Laboratory, Aberdeen, MD, and Army Materials and Mechanics Research Center, Watertown, MA (November 1980).

3. D. C. Erlich, L. Seaman, T. Cooper, R. D. Caligiuri, and D. R. Curran, "Computational Model for Armor Penetration," SRI International Third Annual Report (Vol. 1) on Contract DAAK11-78-C-0115 for U.S. Army Ballistic Research Laboratory, Aberdeen, MD (April 1983).

4. L. Seaman, "Development of a Model for Shear Banding: SHEAR3, "SRI International Third Annual Report (Vol. 2) on Contract DAAK11-78-C-0115 for U.S. Army Ballistic Research Laboratory, Aberdeen, MD (April 1983).

5. J. Dein and L. Seaman, "User's Guide to C-HEMP, a Two-Dimensional Wave Propagation Code," SRI International Third Annual Report (Vol. 3) on Contract DAAK11-78-C-0115 for U.S. Army Ballistic Research Laboratory, Aberdeen, MD (April 1983).

6. M. L. Wilkins, "Calculations of Elastic-Plastic Flow," in Methods of Computational Physics, Vol. 3: Fundamental Methods of Hydrodynamics, B. Adler, ed., Academic Press, New York (1964).

7. W. Herrmann, "A Lagrangian Finite Difference Method for Two-Dimensional Wave Propagation," Air Force Weapons Laboratory, Albuquerque, NM, Technical Report No. WL-TR-64-107 (November 1964).

8. L. D. Bertholf and S. E. Benzley, "TOODY II, A Computer Program for Two-Dimensional Wave Propagation," Sandia Corporation, Albuquerque, NM, Report SC-RR-41 (November 1968).

9. R. Hoffman, "STEALTH, a Lagrange Explicit Finite-Difference Code for Solids, Structural, and Thermodynamic Analysis," Science Applications, Inc. Report EPRI NP-260 for Electric Power Research Institute, Palo Alto, CA (August 1976).

10. L. Seaman, "TROTT Computer Program for Two-Dimensional Stress Wave Propagation," SRI International Final Report (Vol. 3) on Contract DAAK11-77-C-0083 for U.S. Army Ballistics Research Laboratory, Aberdeen, MD (August 1978).

11. T. Cooper, "A Computer Code for Numerical Simulation of Shock Waves in Fluids and Solids," Swedish Detonic Research Foundation, Stockholm, Sweden Report DS 1980:16 (1980).

12. Hageman, L. J., and Walsh, J. M., "HELP, A Multi-material Eulerian Program for Compressible Fluid and Elastic-Plastic Flows in Two Space Dimensions and Time," Vol. I, Systems, Science and Software, La Jolla, California, August 14, 1970.

13. Matuska, D. A. and Durrett, R. E., The HULL Code, A Finite Difference Solution to the Equations of Continuum Mechanics, AFATL-TR-78-125, November 1978.

14. Johnson, G. R., Vavrick, D. J., and Colby, D. D., Further Development of the EPIC3 Computer Program for Three-Dimensional Analysis of Intense Impulsive Loading, AFATL-TR-78-81, July 1978.

15. Mark H. Wagner and Christopher C. Fulton, "Numerical Analyses of Penetration Dynamics in Support of Investigations of Scaling Relations for Earth Penetrators," Final Report by California Research and Technology, Inc., for U.S. Army Engineer Waterways Experiment Station, Vicksburg, Mississippi (November 1977).

16. K. H. Warren, HEMPDS User's Manual, Report by Lawrence Livermore National Laboratory, UCID-18075, August 1982.

17. John O. Hallquist, User's Manual for DYNA2D — An Explicit Two-Dimensional Hydrodynamic Finite Element Code with Interactive Rezoning, Lawrence Livermore Laboratory Report UCID-18756, February 1982.

18. John O. Hallquist, User's Manuals for DYNA3D and DYNAP (Nonlinear Dynamics Analysis of Solids in Three Dimensions) Lawrence Livermore Laboratory Report UCID-19156, July 1981.

19. J. von Neumann and R. D. Richtmyer, "A Method for the Numerical Calculation of Hydrodynamic Shocks," J. Appl. Phys., 21, p. 232 (1950).

20. Steven L. Hancock, Finite Difference Equations for PISCES 2DELK, A Coupled Euler Lagrange Continuum Mechanics Computer Program, Technical Memo TCAM 76-2 by Physics International Company, April 1976.

21. R. D. Richtmyer and K. W. Morton, <u>Difference Methods for Initial-Value Problems</u>, 2nd Ed., Interscience Publishers, New York (1967).

22. W. Herrmann, P. Holzhauser, and R. J. Thompson, "WONDY, A Computer Program for Calculating Problems of Motion in One Dimension," Sandia Corporation, Albuquerque, NM, Report SC-RR-66-601 (February 1967).

23. M. H. Rice, R. G. McQueen, and J. M. Walsh, "Compression of Solids by Strong Shock Waves," Solid State Physics. Vol. 6, F. Seitz and D. Turnbull, Eds. (Academic Press, New York, 1958).

24. D. R. Stull et al., <u>JANAF Thermochemical Tables</u>, Dow Chemical Company, Contract No. AF 04(611)-7554, sponsored by Project Principia of the Advanced Research Projects Agency (August 1965), with Addenda published in August 1966 and August 1967.

25. D. Norris, Lawrence Livermore National Laboratory, private communication (August 1978).

26. W. Herrmann, "Constitutive Equation for the Dynamic Compaction of Ductile Porous Materials," Journal Applied Physics, Vol. 40, No. 6, p. 2490, May 1969.

27. R. J. Lawrence and D. S. Mason, "WONDY IV--A Computer Program for One-Dimensional Wave Propagation with Rezoning," Sandia Laboratories Report SC-RR-810284, Albuquerque, New Mexico, August 1971.

28. L. Seaman and R. K. Linde, "Distended Material Model Development, Vol. I: Experiments and Theory for the Model," AFWL-TR-68-143, Stanford Research Institute, Menlo Park, California, May 1969.

29. L. Seaman, R. E. Tokheim and D. R. Curran, Computational Representation of Constitutive Relations for Porous Material, Final Report by SRI for Defense Nuclear Agency, DNA 3412F, May 1974.

30. M. M. Carroll and A. C. Holt, "Static and Dynamic Pore-Collapse Relations for Ductile Porous Materials," J. Appl. Phys., Vol. 43, No. 4 pp. 1626-1636, April 1972.

31. M. M. Carroll and A. C. Holt, "Steady Waves in Ductile Porous Solids," Journal Applied Physics, Vol. 44, No. 10, p. 4388, October 1973.

32. B. M. Butcher, "Numerical Techniques for One-Dimensional Rate-Dependent Porous Material Compaction Calculations," SC-RR-710112, Sandia Laboratories, Albuquerque, New Mexico, April 1971.

33. L. D. Bertholf, L. D. Buxton, B. J. Thorne, R. K. Byers, A. L. Stevens, and S. L. Thompson "Damage in Steel Plates from Hypervelocity Impact: Part II. Numerical Results and Spall Measurement," J. Appl. Phys. (August 1975).

205

34. J. T. Cherry, J. Sweet, and E. J. Halda, "The Relation Between Fracture-Induced Porosity, Site Geology and the Containment of an Underground Nuclear Explosion," Report SSS-IR-74-2142, to Defense Nuclear Agency, under Contract No. DNA 001-74-C-0070 by Systems, Science and Software (June 1974).

35. F. R. Tuler and B. M. Butcher, "A Criterion for the Time Dependence of Dynamic Fracture," Int. J. Frac. Mech. 4 (4), 431-437 (December 1968).

36. D. M. Norris, Jr., J. E. Reaugh, B. Moran, and D. F. Quinones, "Computer Model for Ductile Fracture: Applications to the Charpy V-Notch Test," Lawrence Livermore Laboratory Report NP-961, Research Project 603, prepared for Electric Power Research Institute (Jan. 1979).

37. T. W. Barbee, Jr., L. Seaman, R. Crewdson, and D. Curran "Dynamic Fracture Criteria for Ductile and Brittle Metals," J. Materials 7 (3), 393-401 (1972).

38. J. R. Kreer, "Dynamic Fracture in 6061-T6 Aluminum," Technical Report No. AFWL-TR-70-180, Air Force Weapons Laboratory, Albuquerque, NM (January 1971).

39. A. L. Stevens, L. Davison, and W. E. Warren, "Void Growth During Spall Fracture of Aluminum Monocrystals," in Dynamic Crack Propagation, G. C. Sih, Ed. (Noordhoff International Publishing, The Netherlands, 1973), p. 37.

40. L. Seaman, D. A. Shockey, and D. R. Curran, "The Growth Law for Crack Propagation Under Shock Conditions," in Dynamic Crack Propagation, G. C. Sih, Ed. (Noordhoff International Publishing, The Netherlands, 1973), p. 629.

41. L. Seaman, D. R. Curran and W. J. Murri, "A Continuum Model for Dynamic Tensile Microfracture and Fragmentation," to appear in Jour. of Appl. Mech. ASME, Vol. 52, No. 3, Sept. 1985, p. 593-600.

42. K. Terzaghi, Theoretical Soil Mechanics (John Wiley and Sons, Inc., New York, 1943).

43. D. C. Drucker and W. Prager, "Soil Mechanics and Plastic Analysis or Limit Design," Quarterly of Applied Mathematics, Vol. 10, p. 157 (1952).

44. R. Hill, The Mathematical Theory of Plasticity (Claredon Press, Oxford, 1950).

45. E. Scheil, "Die Berechnung der Anzahl und Grossenverteilung kugelformiger Kristalle in undurchsichtigen Korpern mit Hilfe durch einen ebenen schnitterhaltenen Schnittkreise," Z. Anorg. Allgem. Chem. 201, 259 (1931).

APPENDIX A

PROGRAM FLOW AND DESCRIPTION OF THE ROUTINES

A brief description of the flow of program control in C-HEMP is given here with a description of the routines. There are three stages of execution in the code: initialization of the materials and the finite-difference grid, calculation of the wave propagation process, and printing of the histories of variables at requested locations. The flow-chart in Figure 51 suggests this three-part structure.

Here is a brief explanation of what is accomplished during the three execution stages:

- Initialization. Subroutine GENR supervises reading the input and laying out the grid, and sets up the map of array storage. GENR may call any of the routines listed below it for reading the input data and preparing the grid. For reading the material data, GENR calls MATERIAL, and MATERIAL may in turn call the constitutive models (EXPLODE to BFRACT3) to read their own input data. BLOCK defines the grid and assigns material to the cells. For explosives, BLOCK calls EXPLODE to initialize the detonation time in each cell.

- Calculation. Subroutine CYCLE manages the calculations for each time step and calls the appropriate material models. The basic wave propagation calculations of position, velocity, energy and strain are handled within CYCLE. The constitutive models are called to determine stress quantities. The other subroutines are called by CYCLE to rezone the grid, treat boundary conditions, and store data for plotting.

- Printing. Historical information stored during the computation is printed or written to external files after the last computational cycle.

The following is a list of all routines and COMMON blocks referenced in C-HEMP. Reference names are listed by function under the following headings:

(1) Main running routines and service routines

(2) Layout and input routines

(3) Wave propagation routines

(4) Material routines

(5) COMMON blocks.

More information about each routine is given in the listings in Volume II.

Main Running Routines and Service Routines

DATE — Not part of C-HEMP; system routine that returns run date

EDIT -- Prints historical information stored during computation

GENR — Coordinates initialization

HEMP -- The main program

RESTART — Handles restart of a run

SECOND -- Not part of C-HEMP; system routine that returns elapsed CPU time in seconds

SUMMARY -- Prints out sums of energies and momenta.

Layout and Input Routines

BLCAS2 — Part of BLOCK, lays out a block with varying-size cells

BLCAS3 -- Part of BLOCK, lays out a block with varying-size cells

BLCIRC — Part of BLOCK, lays out a circle

BLELLIP -- Part of BLOCK, lays out an ellipse (planned)

BLOCK — Lays out a block of cells

BLWARP -- Part of BLOCK, lays out velocities when there is a variation of velocity over a block

BOUNDARY — Initializes boundary conditions

EXTRA -- Input extra variables to special material routines (not implemented)

FIND -- Locates a name in a list

GENERAL -- Input general running data

HISTORY -- Input historical listing requests

MATERIAL -- Input material properties data

ORDER -- Numbers nodes, eliminates redundant nodes, initializes contiguity arrays (WCELL, WNOD, WNDND)

POP -- Reads card images, identifies label and data fields

REZON -- Input data for the rezoner.

Wave Propagation Routines

CFORCE -- Computes forces on nodes

CYCLE -- Handles all the switching and logic for propagation over a single time step and stores historical data

DTQUAD -- Calculates time step

INSEC -- Part of REZONH

OPENANG -- Auxiliary to RSQUAD

PLOTT -- Produces file of edit data for plotting

REZONH -- Performs rezone calculations

RSQUAD -- Reduces a quadrilateral to a triangle when the element configuration is approaching inversion

RSQUAD2 -- Auxiliary to RSQUAD

RSQUAD3 -- Auxiliary to RSQUAD

SLIDE -- Computations for slide lines

TSTEP -- Calculates time step; auxiliary to the rezone routine

TRAPEZ -- Part of REZONH

VQUAD -- Calculates volume of a quadrilateral

WALL -- Computations for wall boundary conditions.

211

Material Routines

BFRACT3 — Brittle fracture

CAP1 -- Cap model for porous material

CAPPR -- Part of CAP1, calculates pressure in solid mateial

DFRACT -- Dynamic ductile fracture model

DFRACTS — Static ductile fracture model

EOSTAB -- Tabular equation of state (used with EXPLODE)

EPP — Model of elastic and Mises plastic behavior with work hardening

EQST — Part of POREQST, computes pressure of solid

EXPLODE -- Detonation model

FMELT -- Thermal softening model (not implemented)

POREQST -- Porous equation of state

REBAR -- Model for composite material (not implemented)

RESOLV -- Part of SHEAR4, resolves stresses on damage planes

SHEAR3 — Shear band model

SHEAR4 -- Shear band model

SPALST — Part of BFRACT3, computes stresses during yielding in the presence of a free surface

SURF -- Converts volume damage distribution to surface damage distribution for SHEAR4 and BFRACT3.

COMMON Blocks

Many of the COMMON blocks are located in separate COMMON decks. These decks are listed in parentheses.

A001 (HCOM1) -- Cell and node pointers

A002 (HCOM1) -- Cell and node variables

A003 (HGEN) -- General running parameters

A004 (HCOM2) -- Material pointers and material properties

A005 (HBOUND) — Boundary condition arrays

BOUNDI (HBOUND) -- Boundary condition arrays

BOUNDR (HBOUND) — Boundary condition arrays

CAPOR -- Communication between CAP1 and CAPPR

CONNEC -- Local array in REZONH

FRAGM -- Used for calculation of fragment distribution in SHEAR3 and CYCLE

ISO -- Isobar storage indicator RISBAR (communicates between GENERAL and CYCLE)

NSCRB (HSCRB) -- History and title arrays

POR -- Local common in POREQST

PSYCHL -- Local common in CYCLE for organizing stress quantities

REST -- Used in the restart routine

RSL -- Passes quantities between SHEAR4 and RESOLV (listed iwth SHEAR4)

SHR3 -- Local common SHEAR3

SHRIN -- Local common in SHEAR4

TPL -- TPLOT.

Files Used in C-HEMP

Besides the usual input and output files, several other files are used in C-HEMP. These files and their uses are given in Table A.1.

Table A.1. FILES USED IN C-HEMP

File Number	Name	Use
4		Storage for historical variables to be printed and plotted at the end of the calculation.
5	INPUT	Normal input file, also used for screen input to HEMPGRID.
6	IOUT	Normal output file.
7		File used for stopping C-HEMP. To stop the calculation manually during a run, write 'STOP HMP' on file 7.
9		Restart file read in RESTART to continue a calculation.
10		Restart file written during a calculation.
13		File used in POP, FIND and HISTORY for decoding the input stream.
17		Input file for HEMPGRID.
19		File containing node positions and pressure at nodes for grid plots and contour plots.
20		File containing fragmentation data generated in SHEAR4 and listed in CYCLE
66		File used in HEMPGRID for output.

214

APPENDIX B

INSERTION PROCEDURE FOR MATERIAL CONSTITUTIVE RELATIONS

As subroutines are developed for describing the constitutive relations of materials, they can be added to C-HEMP for performing wave propagation calculations. This appendix describes the procedure for inserting material model subroutines and provides a sample case.

A wave propagation code normally has four main categories of operations: reading the input data, initializing a finite difference grid, performing calculations for each time increment at each grid point, and printing the computed information. A material model subroutine may be involved in all or some of these operations. Call statements must be provided in C-HEMP at appropriate locations to accomplish these tasks. Also the new subroutine should be provided with separate sections for each operation and an indicator to show which operation to perform. For example, in SHEAR4 the formal parameter NCALL indicates the operation required, as follows:

NCALL = 0 Initialize the routine and read data for one material

1 Read data for one material

2 Calculate stresses and damage

3 Calculate stresses and damage, and print results

4 Print results only.

The calls for NCALL = 0 and 1 are in MATERIAL, the initializing routine for material models. For NCALL = 2 and 3, the call statement is in CYCLE. Other calling strategies are also possible. For example, DFRACT (a model for high-rate ductile fracture) is initialized on the first call from CYCLE; there are no other calls. EXPLODE (a subroutine to represent detonation of explosives) is called from MATERIAL to read data and then called from BLOCK for each cell during the layout to initialize array variables. During propagation calculations, EXPLODE is called by CYCLE.

217

At the point of insertion of each call statement, four elements are provided.

(1) The appropriate branching statements are needed to switch to the new model when it is required. For SHEAR4, it was decided to treat the model as a fracture routine and designate it by WFR(M) = 4. Then the available branching statements in MATERIAL and CYCLE were amplified to include one more branch.

(2) Variables in C-HEMP must be initialized, calibrated, or given sign changes to match the dimensions and signs appropriate to the new subroutine.

(3) The call statement is provided.

(4) Some variables may need to be reset following the calculations in the routine. Then a jump is provided to the appropriate section of CYCLE or MATERIAL to continue the calculation.

Items (2) and (4) are discussed further below following introduction of a call statement.

A sample call statement for SHEAR4 is listed here as it appears in CYCLE (the same call can be used in MATERIAL):

CALL SHEAR4, (NCALL, IN, MAT, L, N, STRESS, DEFTOT, TAU, DW, D(LM),

DT, EW, E(LM), EP, ESC(M), COM1(LM+19), ENVAR, LABEL, RLABEL,

JPOSN, JMULT, NUM, IERR, LM3)

Because SHEAR4 represents a fairly complex case, this call statement will be discussed in detail.

The initialization of NCALL for use in MATERIAL was described above. For CYCLE, NCALL (LS is the name used in CYCLE) is initialized just before the call statement. NCALL is set to 2 normally, but it is set to 3 on cycles when an edit listing will occur. The parameter IN is the file containing input data. Normally IN is 5. MAT is the material number. The coordinate number L indicates the cell being treated; it is used for printout only. N is the cycle number. STRESS is an array containing five stress quantities: σ'_{xx}, σ'_{yy}, σ'_{zz}, σ'_{xy} and P. DEFTOT is the deformation increment array: ϵ_{xx}, ϵ_{yy}, ϵ_{zz}, $\epsilon_{xy} - \alpha$, $\epsilon_{xy} + \alpha$, where

218

α is material rotation, positive counterclockwise. SHEAR4 expects the stresses and strains to be positive in tension and pressure to be positive in compression, so no sign changes are required to prepare the stress and strain quantities. If necessary, sign and magnitude changes can be made in the stresses just preceding the call statement. The current and previous density and energy values are DW, D(LM), EW, and E(LM). The standard material properties are provided in the ESC array; these quantities are defined in the section of input for the MATERIAL routine. ESC is a one-dimensional array, with the index M being the starting location for properties of material number MAT. Unless otherwise specified, for MAT = 1, M = 1; for MAT = 2, M = 51; for MAT = 3, M = 101; etc. All the cell quantities are stored in a single large array called COM1. The particular locations assigned to cell L being at LM = LVAR(L). For example, D(LM), E(LM), and the STRESS array are all contained in the COM1 array but are identified separately for clarity. SHEAR4 requires a large number of additional variables for each cell. These extra variables are provided in the COM1 array, starting at COM1(LM+19).

Following insertion of a new material model, it is a good plan to run a simple problem with frequent edits to determine whether the routine is performing satisfactorily.

APPENDIX C

GLOSSARY OF TERMS IN C-HEMP

All physical quantities for the terms listed below are in cgs units.

A   Cell area, cm^2. Input label to obtain the HISTORY of an area.

AM   Mass assigned to a nodal point, g or g/cm.

AMASS   Total cell mass. For NGEOM = 1 (plane-strain, two-dimensional), a cell has unit thickness. For NGEOM = 2 (axisymmetric), the mass is that of the entire toroidal volume represented by the cell. Units are g or g/cm.

AMAT   The name of a material (input), alphanumeric.

AREA   Label for area of the cell in the plane of the layout, cm^2

BC   A packed boundary condition indicator. Boundary conditions are sequenced as they are encountered in the input; BC equals the sequence number + 0.1*XAFECT + 0.01*YAFECT, where XAFECT and YAFECT are the constraints on X and Y.

      The sequence number for a simple boundary condition or a wall is a counter N representing the order of the input. Hence, the first boundary condition request might lead to a BC value of 1.02, and a second condition might lead to BC = 2.11. For nodes on a slide line, the sequence number provides two bits of information: whether the node is a master or slave, and to which slide line it belongs. For master nodes, the sequence number is 20N − 10; and for slaves, it is 20N; where N is the order in which the slide line is listed in the input. Therefore, for slide lines the BC numbers are 10.00, 30.00, etc. for master nodes; and 20.00, 40.00 etc. for slaves.

BCN   An index used in slide-line calculations to designate which slave node is adjacent to a master node, and vice versa. BCN is the index I of the nearest-neighbor node

223

	in the NSL(I,N) or NMS(I,N) array (for slave or master nodes, respectively). Used in SLIDE.
BETT	Ratio of the number of fragments to the number of cracks, used in BFRACT3 (input).
BFR	An array of parameters for the brittle fracture routine BFRACT3 (input), various units.
BFRACT3	Subroutine containing a nucleation-and-growth material model describing high-rate brittle fracture.
BLCAS2	Subroutine (associated with BLOCK) for laying out the cells in a block with varying cell sizes.
BLCAS3	Subroutine (associated with BLOCK) for laying out the cells in a block in which numbers and sizes of cells vary.
BLCIRC	Subroutine (associated with BLOCK) for laying out circles, arcs, and sectors.
BLOCK	Subroutine and Keyword for heading the description of the cell layout for each block of cells (input).
BLWARP	Subroutine (associated with BLOCK) for initializing a velocity which varies over a block.
BOUNDARY	Subroutine and Keyword for heading the description of the boundary conditions (input).
CALTIM	Total elapsed CPU time for the calculation.
CAP1	Subroutine containing a cap plasticity model for describing a porous material.
CAPPR	Subroutine for computing the solid pressure for CAP1.
CASE	Designator for the layout procedure requested during the input. CASE = 1 makes all the cells in the block the same. 2 gives varying cell sizes. 3 provides varying cell sizes and numbers. 4 makes circles or arches.
CELL	Label for cell number.
CFORCE	Subroutine for computing the forces on the nodes.
CINT	The cohesion C_0 in the friction resistance to sliding of a slide line (input), dyn/cm^2

CIRCLE   Designator for CASE 4 for layout of a block of cells as a
            circle, arch, or sector.

CLIN   Linear artificial viscosity coefficient. (See Section
            II.E). An input parameter with the default value of
            0.05.

COMC   Label used to indicate cell variables not listed by name,
            but available in the COM1 array: input for HISTORYcal
            listings.

COMN   Label used to indicate node variables not listed by name,
            but available in the COM1 array: input for HISTORYcal
            listings.

CQSQ   Quadratic artificial viscosity coefficient. (see Section
            II.E). An input parameter with the default value of 4.

CYCLE   Subroutine for controlling all calculations for a time
            step. Specifically treats strain, time step, and
            boundary calculations, and calls stress-strain models,
            REZONE and SLIDE routines.

D   Density, g/cm^3. Input label to obtain the HISTORY of a
            density.

DATE   System routine that returns the date of the calculation.

DELTIM   Incremental computational time for each cycle.

DENSITY   Label for initial cell density, g/cm^3.

DET   Detonation velocity, may be read in or computed by
            EXPLODE, cm/sec.

DEXX,   Components of the strain increment tensor. Input label
DEYY,   to obtain the HISTORY of a strain increment.
DEZZ,
DEXY

DFRACT   Subroutine containing a nucleation-and-growth material
            model for high-rate ductile fracture.

DFRACTS   Subroutine containing a nucleation-and-growth material
            model for quasi-static ductile fracture.

DIST   Number of cells over which the detonation front is
            spread. A zero value indicates a constant-volume
            explosion (input).

DT   Current time increment, sec.

225

DMIN   An input parameter requesting a minimum time step for all
          cells. For a nonzero value, if the natural time step
          drops below DTMIN, the stresses and time step are no
          longer computed for the cell.

DTQUAD   A routine for computing the minimum crossing time for a
          quadrilateral.

DTSQM   Square of the time step of the cell with the smallest
          time step, sec^2. Used in CYCLE.

DTW   A preliminary time-step estimate for the next cycle, sec.

DW   Current cell density, g/cm^3. Used in CYCLE and in
          material models.

DX   Minimum cell dimension of the cell governing the time
          step, cm.

E   Specific internal energy, erg/g. Input label to obtain
          the HISTORY of an energy.

EDIT   Subroutine that prints historical information stored
          during the computation.

EMELT   Melt energy for a material (input), erg/g.

EN3,   Labels used with SHEAR3 and SHEAR4 to indicate the end of
END   the data for the model.

EOSTAB   Subroutine containing a tabular equation of state
          (pressure-volume relation). Also, a Keyword for use of a
          tabular equation of state.

EP, EPP   Subroutine containing an elastic-plastic model for the
          deviator stress.

EPS   Plastic strain. Input label for obtaining HISTORY of
          plastic strain in a cell.

EQST   Subroutine containing the Mie-Grueneisen equation of
          state for a material undergoing compression.

EQSTA   Parameter used in the PUFF expansion equation of state,
          not currently implemented in C-HEMP.

EQSTC   Bulk modulus for a material, (input), dyn/cm^2.

226

EQSTD, EQSTS	Coefficients of the quadratic and cubic terms in compressive strain for the series giving the pressure Hugoniot (input), dyn/cm^2.
EQSTE	Sublimation energy for a material (input), erg/g.
EQSTG	Grueneisen ratio for a material (input).
EQSTN	Parameter used in the PUFF expansion equation of state, not currently implemented in C-HEMP.
EQSTV	Parameter used in the PUFF expansion equation of state, not currently implemented in C-HEMP.
ES, EST	Array containing a series of strain values to define the work-hardening curve for the EPP, SHEAR3, and SHEAR4 models (input).
ETA	The coefficient of viscosity A_v used to compute a shear stress on the slide line (input), $dyn-sec/cm^3$.
EW	Current cell energy, erg/g. Used in CYCLE and in MATERIAL models.
EXPLODE	Subroutine containing constant-volume and running-detonation treatments for explosives.
EXX, EYY, EZZ, EXY	Cumulative strains. Input labels for obtaining the HISTORY of a strain.
FIND	Subroutine for locating a name in a list.
FMELT	Function containing a thermal softening model (not implemented).
FNUC	An array indicating whether each shear plane in the SHEAR3 and SHEAR4 models are to be treated as active (input).
FX, FY	X and Y components of force assigned to a nodal point, dyn or dyn/cm. Input labels to obtain the HISTROY of the nodal force.
GAMMA	Ratio of the fragment radius to the crack radius, used in BFRACT3 (input).
GENERAL	Subroutine, and Keyword for heading the overall control parameters for
GENR	Subroutine which coordinates the initialization process.

227

GRID   Keyword for heading the description of the cell layout
            for a block of cells which are separated from the
            previous cells (input).

G2   Twice the shear modulus, dyn/cm^2

H   Indicator whose meaning is determined by the material
            model used. For example, in CAP1, H = 5 means elastic
            response, 6 means yielding on the Mohr-Coulomb curve, 7
            is yielding on the cap curve, 8 is yielding on both
            curves, 9 is consolidated and 10 denotes separation.

HEMP   The main program

HISTORY   Subroutine, and Keyword heading the description of the
            requests for historical listings of variables from a
            calculation (input).

IDIR   Direction indicator associated with wall boundaries and
            slide lines (input).

INITGRO   Indicator for determining the growth process in BFRACT3
            (input).

INITNUC   Indicator for determining the nucleation process in
            BFRACT3 (input).

INITPRI   Indicator for controlling the special printing from the
            BFRACT3 routine (input).

INSEC   A routine used with REZONE.

INT-ENRG   Total internal energy, in SUMMARY.

IPRINT   Cell and node edits are printed every IPRINT cycles.
            This input parameter has the default value of 10.

ISOBAR   An input indicator requesting that cell parameters be
            written to File 19 during the calculation, in preparation
            for contour plots to be constructed by a post-processor
            (ISOPLOT).

JEDA   For historical requests, indicates that internal list
            where a particular variable may be found. List 1 is for
            stored array variables, lists 2 and 3 for unstored cell
            quantities, list 4 for stored nodal quantities and list 5
            for unstored nodal quantities. Unstored quantities are
            recalculated every time step. Written in HISTORY.

JEDL   For historical requests, the cell or node number assigned
           to the requested position. Written in HISTORY.

JEDN   For historical requests, the name of the requested
           quantity. Written in HISTORY.

JEDT   For historical requests, indicates position of a variable
           in its internal list (see JEDA). Written in HISTORY.

KIN-ENRG   Total kinetic energy, in SUMMARY.

LC   Starting location in COM1 array of storage space for a
           cell's variables.

LN   Starting location in COM1 array of storage space for a
           node's variables.

LT   The number of the cell controlling the time step. Used
           in CYCLE.

LV   A pointer to a node's storage of velocity information.

MASS   Label for a node mass, in EDIT.

MASS   Label for total mass, in SUMMARY.

MATERIAL   Subroutine, and Keyword for heading the material
           properties information (input), and material name in
           SUMMARY.

MATL   Array containing material names.

MU   Shear modulus for a material, (input), dyn/cm^2.

N   Computational cycle number, set in HEMP.

NBCTYP   Boundary condition type indicator (input). Type 1 gives
           simple conditions along X and Y directions; 2 maintains
           the initial velocities on the affected nodes; and 3
           through 6 provide for more complex sliding and sticking
           conditions on walls of general shape.

NCij   The number of cells between corner nodes i and j in the
           layout of a block of cells (input).

NCONST   Number of a node for which rezoning is to be restricted
           in both the X and Y directions (input).

NCONST   Range of nodes for which rezoning is to be restricted in
  i to j   both the X and Y directions (input).

229

NERROR   Error count.

NFREQ   The cycle counter controlling frequency of rezoning
            (input).

NGEOM   Geometry indicator for the calculation: 1 for plane
            strain, a nd 2 for axisymmetry. The default is 1 (input).

NMAX   Requested maximum number of cycles for the calculation
            (input).

NMS   Array of node numbers on the master side of a slide line
            (input).

NODE   Label for node number.

NPLOT   Plot data are written to File 16 every NPLOT cycles by
PLOTT   on calls from CYCLE (input).

NR OF   When the time step for a cell goes down severely because
QUAD   one of its nodes tends to invert the cell, then the
RESETS   position of that node is frozen relative to the other
            nodes. Each such operation (on each time step) is
            counted as a quad reset.

NR OF   Number of rezone operations. One operation is the
REZONES   relocation of one node to a new position.

NSCRIBE   For histories written in EDIT, the number of the printout
            sets.

NSIZ   Number of size intervals for the crack size distribution
            used in BFRACT3 (input).

NSL   Array of node numbers on the slave side of a slide line
            (input).

NSLIDE   Number of slide lines requested. Computed in GENR from
            the input data.

NXCONST   Number of node for which rezoning is to be restricted
NYCONST   in the X (or Y) direction (input).

OPENANG   A subroutine used with RSQUAD for determining the opening
            angle between two lines.

ORDER   Subroutine for organizing the contiguity arrays:
            WCELL, WNOD, and WNDND.

P   Pressure, dyn/cm^2. Input label for obtaining a HISTORY
            of the pressure in a cell.

PBORE   Switch that allows the borehole gas pressure to act on cells that are fracturing (input). Used in BFRACT3.

PHI   Angle from the Z direction toward the X-Y plane. Used to orient the shear planes in the SHEAR3 and SHEAR4 models, radians.

PLOTT   A subroutine that produces a file of data for plotting.

PMIN   A minimum (tensile) pressure which may be requested for a material (input), dyn/cm^2. A zero value means no limit will be used.

POP   Subroutine for reading lines of input, and identifying labels and data fields.

POREQST   Subroutine containing a material model for a porous material.

PRINT   Input parameter for SHEAR4 to specify the desired printout.

PSCRIB   An input parameter which is set to a nonzero value to request a plot file (File 17) of the HISTORY data.

PW   Current thermodynamic pressure, positive in compression, dyn/cm^2. Used in CYCLE and in MATERIAL models.

QEXPL   Chemical energy released by the detonation (input), erg/g.

QW   Current artificial viscous pressure, positive in compression, dyn/cm^2. Used in CYCLE.

Rij   Ratio of successive cell lengths along the edges of a block from corner node i to node j (input).

REBAR   Subroutine containing a composite model describing the anisotropic response of reinforced concrete. The CAP1 model is used for the concrete and a standard elastic-plastic model is used for the steel reinforcing.

RESOLV   Subroutine for resolving stresses on the shearing planes, used with SHEAR4.

RESTART   Subroutine, and Keyword indicating that the run is a restart of a previous calculation. This Keyword immediately follows the title line in the input.

REZ	Rezone indicator for limiting rezoning at a node: 0 - no control; 1 - control in X-direction; 2 - control in the y-direction; and 3 - control for both X and Y.
REZMIN	The minimum relative distance that a node has to be offset from the optimum position before it is rezoned (input).
REZWT	Fraction of the distance the node is moved from its old position toward the new optimum position.
REZON	Subroutine, and Keyword for heading the description of the control parameters for the automatic rezoner, REZONE (input).
REZONE	Subroutine used to automatically rezone or reposition the nodes during a calculation.
RHO	Initial density for a material (input), g/cm^3.
RHOS	Reference solid density for the material, (input), g/cm^3.
RSQUAD	Routine which reduces a quadrilateral to a triangle to avoid inversion.
RSQUAD2	An auxiliary routine for RSQUAD.
RSQUAD3	An auxiliary routien for RSQUAD.
S-XX	Label for the normal thermodynamic stress in the X-direction, positive in tension, dyn/cm^2
S-YY	Label for the normal thermodynamic stress in the Y-direction, positive in tension, dyn/cm^2.
S-ZZ	Label for the normal thermodynamic stress in the Z-direction, positive in tension, dyn/cm^2
SBAR	Equivalent stress, dyn/cm^2. Input label for obtaining the HISTORY of the equivalent stress.
SECOND	System routine which provides the elapsed CPU time in seconds.
SHEAR3, SHEAR4	Subroutine containing a nucleation-and-growth material model describing shear banding, fracture, and fragmentation.
SLIDE	Subroutine, and Keyword for heading the description of the control parameters for the slide line (input).

232

SLIDE i to j	Input parameters providing for a partial separation of the current block of cells from the previous blocks. Boundary nodes between corner nodes i and j are not connected to previous blocks.
SP	Sound speed for a material, cm/sec.
SPALST	Subroutine for computing the stress state on a spalled plane, used with BFRACT3.
SPRIN1, SPRIN2 SPRIN3	Principal stress components, dyn/cm^2. Input labels for obtaining a HISTORY of these stress quantities.
SP2	Square of the sound speed. Input label for obtaining a HISTORY of this quantity.
SPSQ	Sound speed squared, cm^2/s^2. Used in CYCLE.
SPSQT	Sound velocity squared for the cell with the smallest time step, cm^2/s^2. Used in CYCLE.
SRTIME	Dimensionless coefficient used in computing the stress relaxation time constant used in BFRACT3 (input).
STOPT	Requested termination time for the calculation (input).
SUM-ENRG	Total kinetic plus internal energy, in SUMMARY.
SUMMARY	Subroutine which prints the sums of the energies and momenta for the entire object.
SURF	Subroutine for converting the volume damage distribution to a surface damage distribution, used with SHEAR4 and BFRACT3.
SXX, SYY, SZZ	Thermodynamic stress components, dyn/cm^2. Input labels for obtaining a HISTORY of the stresses.
TANP	The coefficient of friction, Tan (ϕ), used to determine the shear stress on a slide line (input).
TAU	Dimensionless damage level used in BFRACT3, SHEAR3, and SHEAR4.
TBURN	Delay time for the beginning of detonation (input), sec.
TEADD	Energy present in the problem at the start plus energy added during the run. TIE and TKE should add up to TEADD to within 10% or so.

TFRAG   Dimensionless coefficient of the fragment volume used in BFRACT3 (input).

TH   Gross cell rotation in radians, positive counter-clock-wise. Input label to obtain a HISTORY of the rotation.

THETA   Angular rotation in the X-Y plane of shear banding planes in the SHEAR3 and SHEAR4 models, radians.

TIE   Total internal energy in problem. Written in CYCLE.

TIME   Label for the total elapsed problem time, sec.

TKE   Total kinetic energy in problem. Written in CYCLE.

TMCELL   Total cell mass in problem, g.

TMNODE   Total node mass in problem; should be equal to TMCELL, g.

TPLOT   Requested plot frequency. Plot data are written to File 17 every TPLOT seconds (input).

TSR   An anti-hourglassing viscosity coefficient (input).

TSTEP   A routine for computing the time step for a cell; auxiliary to REZONE.

TRAPEZ   A routine which is auxiliary to REZONE.

TXX, TYY Total mechanical stress components, dyn/cm^2. Input
 TZZ,   labels for obtaining a HISTORY of the stresses.
 TXY

TYME   The internal name for the total elapsed problem time (see TIME), sec.

TYPE   Work hardening process indicated for the EPP material model: 1 means power law hardening; 2 means linear; and 3 means a polynomial form (input).

VOLCRIT   Dimensionless crack volume that defines the threshold of coalescence (input). Used in BFRACT3.

VQUAD   A routine for calculating the volume of a quadrilateral.

WALL   Subroutine for imposing wall boundary conditions.

WCELL   Array of cell-variable storage locations (LC values) for cells around a node. The cells are listed in counter-clockwise order around the node. Five locations are provided; unused locations are left at zero. Written in BLOCK and rearranged in ORDER.

234

WCMP   Indicator for composite models (input).

WDS   Indicator for special deviator stress models (input).

WEQS   An indicator for the number of locations allotted in the ESC array for each material's properties (input).

WFR   Indicator for fracture models (input).

WH   Cell condition indicator. Input label for obtaining the HISTORY of the cell condition.

WMAT   Material number.

WNDND   Array of node numbers for nodes adjacent to a given node. WCELL and WNDND are associated so that $WCELL_i$ is CCW from $WNDND_i$. For interior nodes, the first WNDND value is the smallest node number. On the boundary, the first WNDND is to the right of the central node when facing the material. Five locations are provided; unused locations are left at zero. Written in ORDER.

WNOD   Array of node numbers around a cell. The nodes are numbered counterclockwise beginning with the node nearest the first node specified in the input XA, YA arrays. Written in BLOCK.

WPOR   Indicator for porous models (input).

WPR   Indicator for pressure models (input).

WVAR   Space allotted in the COM1 array for each cell's special material parameters. May be given by the user, but several models compute the space needed.

X   X (axial) position of a node. Input label for obtaining a HISTORY of the nodal position, cm.

X-MOMNTM   Total momentum in X-direction, in SUMMARY.

XO   Initial X position of a node, cm.

XA   X coordinate value for a node used in the layout (input), cm

XAFECT   Indicator for the type of boundary control. 0 or 4 means no control; 1 means X is maintained greater than or equal to the X value of the wall; 2 means X is maintained less than or equal to the X value on the wall; and 3 means that X is maintained at the X value of the wall (input).

235

XBC   Array defining the X values of points along a boundary wall (input), cm.

XCONST An X value used to designate a node or nodes that are affected by a boundary or rezoning condition (input).

XD   X-velocity, cm/sec. Input label for requesting the HISTORY of velocity at a node.

XDBC   An array containing the X-velocities of wall boundary lines (input), cm/sec.

XDET   Coordinate of the point or line for initiation of detonation of an explosive (input), cm.

XDNH   Current nodal velocity in the X-direction, cm/s. Used in CYCLE.

XDNOT Velocity in the X direction for a node or for an entire block of cells (input), cm/sec.

Y   Y (radial) position of a node. Input label for obtaining a HISTORY of the nodal position, cm.

Y-MOMNTM Total momentum in Y-direction, in SUMMARY.

YO   Initial Y position of a node, cm.

YA   Y coordinate value for a node used in the layout (input), cm.

YAD   Work-hardening modulus for a material, (input), dyn/cm^2.

YAFECT Indicator for the type of boundary control. 0 or 4 means no control; 1 means Y is maintained greater than or equal to the Y value of the wall; 2 means Y is maintained less than or equal to the Y value on the wall; and 3 means that Y is maintained at the Y value of the wall (input).

YBC   Array defining the Y values of points along a boundary wall (input), cm.

YC   Yield strength of a material (input), dyn/cm^2.

YCONST A Y value used to designate a node or nodes that are affected by a boundary or rezoning condition (input).

YD   Y-velocity, cm/sec. Input label for requesting the HISTORY of velocity at a node.

YDBC   An array containing the Y-velocities of wall boundary
            lines (input), cm/sec.

YDET   Coordinate of the point or line for initiation of
            detonation of an explosive (input), cm.

YDNH   Current nodal velocity in the Y-direction, cm/s. Used in
            CYCLE.

YDNOT   Velocity in the Y direction for a node or for an entire
            block of cells (input), cm/sec.

YIELD   Label for the initial yield strength, dyn/cm^2.

YS   Array containing a series of yield values defining the
            work-hardening curve for the EPP, SHEAR3, and SHEAR4
            models (input), dyn/cm^2.

YY   Yield strength, dyn/cm^2. Input label for obtaining a
            HISTORY of the yield strength.

Z   Cell mass, g or g/cm. Input label for obtaining a
            HISTORY of the cell mass.

Poulter Laboratory Technical Report 001-86 February 1986

This appendix is the final report on an internally sponsored research study of the rotation problem in two-dimensional calculations. It is included in this final report because of its relevance to the topic of this manual.

ROTATION TRANSFORMATIONS FOR TWO–DIMENSIONAL CALCULATIONS

By: Lynn Seaman

SRI INTERNATIONAL

Menlo Park, California 94025 USA

1. INTRODUCTION

Rotation adjustments that are made at each time increment in two-dimensional wave propagation and structural calculations should account for three effects. First, the stress tensor is transformed to account for the material rotation. Second, micro features, such as cracks, are rotated with the material. And third, to aid in understanding the results of calculations, the average rotation of the cell material is computed. Treatments for these rotation topics are reviewed in the present study. Because the conditions that cause large rotations also require a rezoning treatment in the calculations, we examine how to combine a precise rotation procedure with rotation. Then we examine when rotation adjustments are needed (that is, for which types of material models and which kinds of problems).

In the last two decades it has been generally recognized that material rotation must be accounted for in our stress-strain calculations, or the computed stress tensor will depend on its coordinate system. At present, rotations are commonly accounted for by using the Jaumann rotation rate computed from the coordinate motions of the computational cell:

$$\Delta\alpha = (du/dy - dv/dx)\Delta t/2 \tag{1}$$

where $\Delta\alpha$ is the increment of rotation in radians, and u and v are coordinate velocities in the x and y directions. This rotation correction has recently been found to be appropriate only for small shear strains (See, for example, Dienes[1]).

To indicate the nature of the approximation involved in Eq. (1), let us consider a block subjected to simple shear, as shown in Figure 1. The block is sheared by moving points 2 and 3 by $u\Delta t$. From Eq. (1), the rotation is

$$\Delta\alpha = \frac{u\Delta t}{2\Delta y} \tag{2}$$

The diagonals of the square rotate by this amount. Yet the line 03 rotates by $(u\Delta t)/(\Delta y)$ and the line 01 does not rotate. Hence, the combination of shear with rotation appears to produce a complex state in which different elements rotate differently. Thus $\Delta\alpha$ from Eq. (2) is only an "average" rotation for the material. In the following sections the average rotation is examined further.
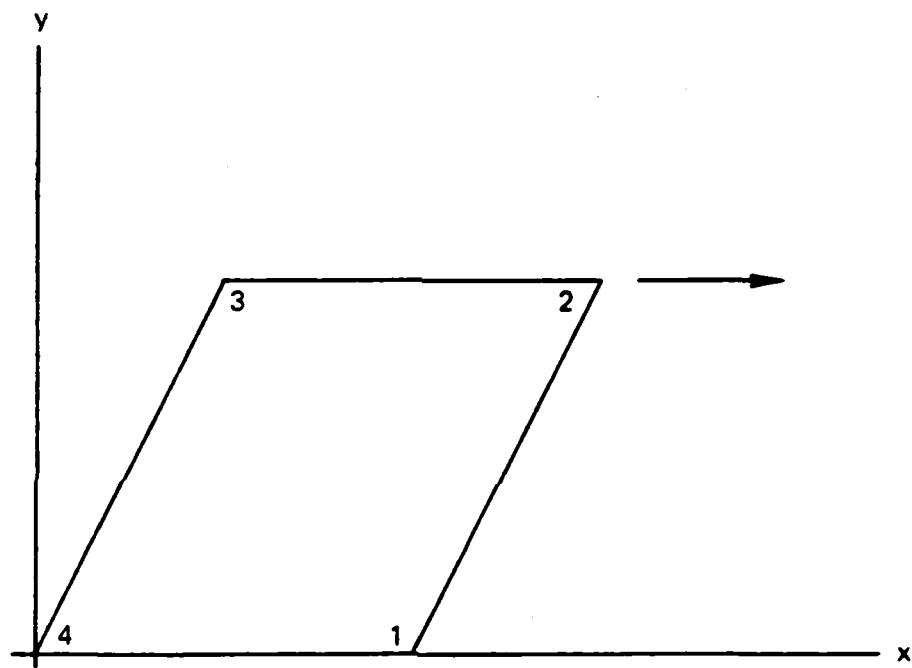
JA-6423-20

FIGURE D-1   DISTORTION OF A BLOCK IN SIMPLE SHEAR

242

For an example of the difficulty with large rotation problems, let us consider the case where the incremental motion in Figure 1 gives an angular change of $\Delta\alpha = 1°$. Then continue the motion for 180 increments. Eqs. (1) and (2) would give a total angular change of $180°$. Yet from the figure, it is clear that no rotation greater than $90°$ occurred, so the average rotation must be less than $45°$. (The actual rotation is about $38°$.)

In the foregoing discussion we presume that we can follow the crystallographic planes on which the stress acts. Hence, we are assuming that the stress tensor follows these planes. Therefore, the stress rotation calculations are made to follow the motion of the planes. However, as pointed out by Drucker[2], when plastic slip occurs in the material, the crystallographic planes do not follow the macroscopic motion of the material. Yet we cannot readily determine the actual motion of these planes without a detailed theory of plastic flow that includes the development of anisotropy. In the following development of the rotation problem, we assume that the material remains homogeneous and isotropic throughout the flow, and we disregard Drucker's important physical question.

This paper first presents a review of three recent analyses of the rotation problem. Then we derive separately the procedure for the rotation of lines and of the stress tensor. We recommend steps for conducting the analysis and discuss methods for rezoning the quantities needed in the rotation procedure. Finally, through use of the procedure, we determine the conditions under which the procedure is important.

2. BACKGROUND

Recent work has been done by Dienes[1], Marsden and Hughes[3], and Hallquist[4] in determining the appropriate transformations to undertake to handle the rotation of material undergoing large shear deformations.

John Dienes[1] has developed a three-dimensional analysis for material rotation, considering the corrections required to transform the stress tensor and determine the correct angle. The analysis was applied to elastic material initially; however, he has noted that the concept is appropriate for any rotation, elastic or plastic. His corrections to the stress tensor take the same form as the Jaumann equations:

$$\hat{\sigma} = \dot{\sigma} - \Omega\sigma + \sigma\Omega \tag{3}$$

where $\hat{\sigma}$ is the stress rate tensor corrected for rotation, $\dot{\sigma}$ is the stress rate directly from the constitutive equation, and Ω is the tensor representing the angular velocity of the material

$$\Omega = \dot{R}R^T \tag{4}$$

and R is the rotation tensor (defined later). Figure 2 (from Dienes' text) shows that σ_{12} grows monotonically with shear strain when the Dienes' correction is used, whereas with the traditional Jaumann method the stress oscillates for very large strains.

Now we consider in some detail the method outlined by Dienes[1] for determining the rotation of the material of a cell from the locations and velocities of the material. He begins with the deformation and velocity gradient tensors. He solves the problem for the general three-dimensional case, but we restrict attention to a two-dimensional problem. First we present a description of his solution, then a method based on the development, and finally the numerical procedure he recommends.

Dienes' method begins with the deformation tensor F with components

$$F_{ij} = \frac{\partial X_i}{\partial \xi_j} \tag{5}$$

where X_i is the current coordinate and ξ_j is the Lagrangian position. Next Dienes derives the material rotation Ω from the vorticity W, left stretch tensor V, and the deformation rate tensor D. The vorticity and deformation rate tensors are both obtained from the velocity gradient G.

$$G_{ij} = \frac{\partial u_i}{\partial X_j} \tag{6}$$

where u_i is the velocity in the ith direction. As Dienes also shows, G is related to the deformation gradient as follows.

$$G = \dot{F}F^T \tag{7}$$

The deformation rate tensor D is

$$D_{ij} = 1/2(G_{ij} + G_{ji}) \tag{8}$$

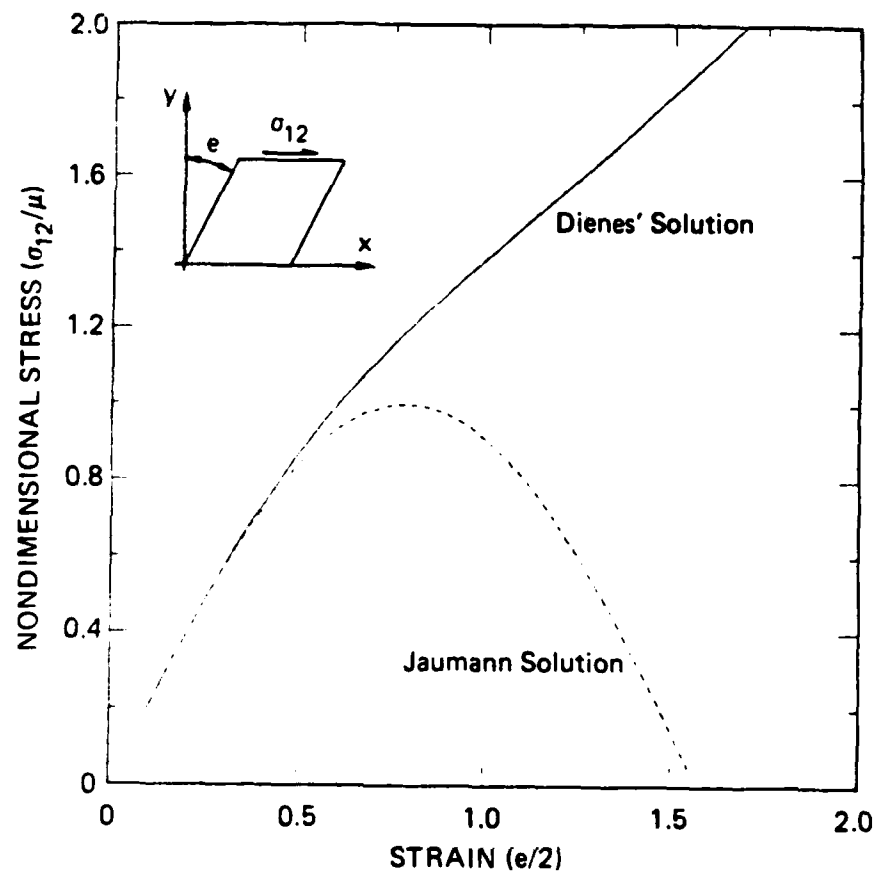and the vorticity W is

$$W_{ij} = 1/2(G_{ij} - G_{ji}) \tag{9}$$

The vorticity is the rotation quantity customarily used with the Jaumann rotation computation.

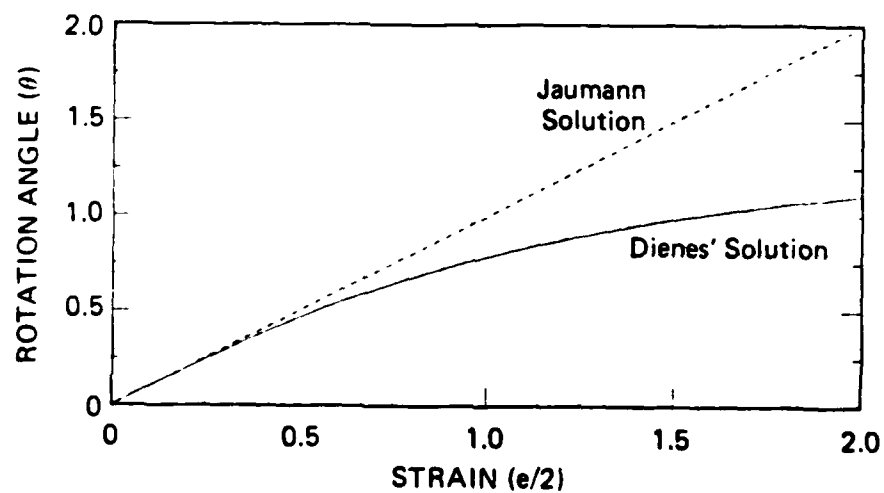The left stretch tensor V is named for its position in the defining relation:

$$F = VR \tag{10}$$

where R is the rotation tensor. To compute V, he forms the product B

$$B = FF^T \tag{11}$$

(a) Comparison of Shear Stresses for Simple Shear

(b) Comparison of Rotation Angles

JA-6423-21

FIGURE D-2   COMPARISON OF SHEAR STRESS AND ANGLE OF ROTATION
COMPUTED BY THE METHODS OF DIENES AND JAUMAN
IN SIMPLE SHEAR

245

from which he derives $\mathbf{V}$ by the method of Bellman[5]:

$$\mathbf{V} = \mathbf{B}^{1.2} \tag{12}$$

The rotation tensor $\mathbf{R}$ is obtained by inverting Eq. (10):

$$\mathbf{R} = \mathbf{V}^{-1}\mathbf{F} = \begin{bmatrix} \cos\theta & -\sin\theta \\ \sin\theta & \cos\theta \end{bmatrix} \tag{13}$$

With this definition of the rotation tensor, the rotation is positive counterclockwise. From the $\mathbf{D}$ and $\mathbf{V}$ tensors, he defines two more tensors:

$$\mathbf{Z} = \mathbf{DV} - \mathbf{VD} \tag{14}$$

and

$$\mathbf{S} = \left[\mathbf{I}\mathrm{tr}(\mathbf{V}) - \mathbf{V}\right]^{-1} \tag{15}$$

With $\mathbf{Z}$ he defines a vector $\mathbf{z}$ such the $Z_{ij} = \epsilon_{ijk}z_j$ and ϵ is the permutation tensor. His angular velocity of the material axes, ω ($\Omega_{ij} = \epsilon_{ijk}\omega_j$) is then given by

$$\omega_i = w_i + S_{ij}z_j \tag{16}$$

where $W_{ik} = \epsilon_{ijk}w_j$. Thus the Sz term acts as a correction to the rotation W, which is customarily used in the Jaumann rate equations.

In his paper Dienes gave the following steps for computing the rotation in a computer code, but did not recommend this procedure.

(1) Compute the current $\mathbf{F}^n$ and $\mathbf{G}^{n+1/2}$ from the nodal positions and velocities. Evaluate $\mathbf{D}^{n+1/2}$ and $\mathbf{W}^{n+1/2}$ from $\mathbf{G}^{n+1/2}$. Here n refers to the beginning of the time step, so quantities labeled n+1/2 are defined at the middle of the time step.

(2) Compute $\mathbf{V}^n$ from the square root of $\mathbf{FF}^T$.

(3) Compute $\mathbf{R}^n$ from Eq. (13)

(4) Compute $\mathbf{S}^{n+1/2}$ and $\mathbf{Z}^{n+1/2}$ from $\mathbf{V}^n$ and $\mathbf{D}^{n+1/2}$.

(5) Compute $\omega^{n+1/2}$ from Eq. (16)

This procedure requires computation of the $\mathbf{F}$ tensor (hence, storage of the Lagrangian coordinate ξ). The time consuming steps are the computation of the square root of $\mathbf{FF}^T$ and the matrix inversion for determining $\mathbf{S}$. The procedure is very accurate.

Dienes recommended a second procedure with the following steps:

(1) Compute $\mathbf{G}^{n+1/2}$ and then $\mathbf{W}^{n+1/2}$ from $\mathbf{G}^{n+1/2}$.

(2) Compute $\mathbf{Z}^{n+1/4}$ from $\mathbf{V}^n$ and $\mathbf{D}^{n+1/2}$.

(3) Calculate $\mathbf{S}^n$ from $\mathbf{V}^n$ (Eq. 15).

(4) Obtain $\dot{\mathbf{V}}^{n+1/2}$ from $\mathbf{G}^{n+1/2}\mathbf{V}^n - \mathbf{V}^n(\mathbf{W}^{n+1/2} + \mathbf{S}^n\mathbf{Z}^{n+1/4})$, where the SZ product is computed in the sense of Eq. (16).

(5) Update $\mathbf{V}^{n+1}$ from $\mathbf{V}^n$ and $\dot{\mathbf{V}}^{n+1/2}$.

(6) Compute the angular velocity ω from Eq. (16).

This method requires storage of $\mathbf{V}$, but not of the Lagrangian coordinates. The lengthy calculation is the matrix inversion in step 3. Note that in both of these approaches Dienes obtains the rotation quantity $\omega = \dot{\theta}$ explicitly, and in the first method, $\mathbf{R}$ is also obtained. This method is also very accurate.

Marsden and Hughes[3] have suggested a simplified way to obtain the stretch tensor from the $\mathbf{B}$ tensor. Instead. of computing $\mathbf{V}$, they obtain the right stretch tensor $\mathbf{U}$. This tensor is defined by

$$\mathbf{F} = \mathbf{R}\mathbf{U} \tag{17}$$

They begin the computation by forming the product tensor $\mathbf{C}$:

$$\mathbf{C} = \mathbf{F}^T\mathbf{F} \tag{18}$$

Then $\mathbf{U}$ is given by

$$\mathbf{U} = \frac{\mathbf{C} + \sqrt{\mathrm{Det}\,\mathbf{C}}\ \mathbf{I}}{\sqrt{\mathrm{tr}\,\mathbf{C} + 2\sqrt{\mathrm{Det}\,\mathbf{C}}}} \tag{19}$$

Thus. their method has the following steps:

(1) Compute $\dot{\mathbf{F}}^n$ from $\mathbf{G}^{n+1/2}\mathbf{F}^n$, and evaluate $\mathbf{F}^{n+1} = \mathbf{F}^n + \dot{\mathbf{F}}^n\,\Delta t$.

(2) Compute $\mathbf{U}^{n+1}$ from $\mathbf{F}^{n+1}$ as in Eq. (19).

(3) Compute $\mathbf{R}^{n+1} = \mathbf{F}^{n+1}(\mathbf{U}^{n+1})^{-1}$.

They do not explicitly compute θ or ω because neither is needed for the rotation of the stress tensor. The $\mathbf{F}$ tensor must be stored between cycles. $\mathbf{U}$ is obtained from Eq. (19), requiring two square roots. and a matrix inversion is required to obtain $\mathbf{R}^{n+1}$ in step 3.

Hallquist[4] uses the method of Marsden and Hughes[3] with some modifications in his NIKE2D code. In this finite element code he computes the $\mathbf{R}^n$, $\mathbf{R}^{n+1/2}$, and $\mathbf{R}^{n+1}$ rotation tensors. With $\mathbf{R}^n$ he rotates the initial stress tensor σ^n from the external coordinate system to the material orientation. The strain increment $\Delta\epsilon^{n+1/2}$ is rotated to the material orientation with $\mathbf{R}^{n+1/2}$. Then σ^{n+1} is computed by the material model, and the stress tensor is transformed back to the external coordinate system. $\mathbf{R}$ is not stored between cycles, so the 3-step procedure above is performed three times at each cell and each cycle.

From the foregoing it appears that there are procedures available to transform the stress tensor and to follow the rotation of the cell material. However, it is not clear how

these methods can be used under conditions in which rezoning is also being used. The rotation procedures and rezoning are examined in the following study.

3. DEVELOPMENT OF THE ANALYSIS FOR ROTATION OF LINES

The rotation analysis is developed first for the motion of a line in a linear deformation field. This result may be applied to the rotation of line-like features such as microcracks (which appear as lines on some cross sections), rolling planes, or the principal directions of an anisotropic material. Then the line analysis is applied to determine the average rotation of a block undergoing large shear deformation.

A line segment L in a linear deformation field will be stretched (or shortened) and rotated. Let us consider here only the rotation aspect. The rotation $\Delta\omega$ is given by the cross product

$$\Delta\omega = -\frac{\Delta\vec{\delta} \times \vec{L}}{|L|^2} \tag{20}$$

where $\Delta\vec{\delta}$ is the motion of one end of the line with respect to the other, and L is the line length. Then $\Delta\delta$ can be written in terms of x and y coordinates:

$$\frac{\Delta\vec{\delta}}{|L|} = \vec{i}\frac{(\partial u/\partial x)\Delta x + (\partial u/\partial y)\Delta y}{|L|} + \vec{j}\frac{(\partial v/\partial x)\Delta x + (\partial v/\partial y)\Delta y}{|L|}$$

$$= \vec{i}\left(\frac{\partial u}{\partial x}\cos\phi + \frac{\partial u}{\partial y}\sin\phi\right) + \vec{j}\left(\frac{\partial v}{\partial x}\cos\phi + \frac{\partial v}{\partial y}\sin\phi\right) \tag{21}$$

The angle ϕ is the angle of the line with respect to the x coordinate, measured positively counterclockwise. Similarly, the vector $\vec{L}$ is

$$\frac{\vec{L}}{|L|} = \vec{i}\frac{\Delta x}{|L|} + \vec{j}\frac{\Delta y}{|L|} = \vec{i}\cos\phi + \vec{j}\sin\phi \tag{22}$$

When we place the expressions for $\Delta\vec{\delta}$ and $\vec{L}$ in Eq. (20), we obtain the increment of rotation:

$$\Delta\omega = -\frac{\partial u}{\partial x}\sin\phi\cos\phi - \frac{\partial u}{\partial y}\sin^2\phi + \frac{\partial v}{\partial x}\cos^2\phi + \frac{\partial v}{\partial y}\sin\phi\cos\phi \tag{23}$$

Equation (23) is used to obtain the rotation for lines or other line-like features in two-dimensional calculations.

Now let us consider the rotation of several lines in a block of material as a means of obtaining the average rotation of the material. We assume that our block has a large number of lines drawn on it. Then we shear the block and follow the motion of the lines. If we apply a simple shear $d\omega/dt = \partial u/\partial y$, then the rotation $d\theta$ of a line at an angle θ from the X-axis is

$$\frac{d\theta}{dt} = -\frac{d\omega}{dt}\sin^2\theta \tag{24}$$

For a constant $d\omega/dt$, this equation can be integrated over time to obtain

$$\cot\theta = \cot\theta_0 + \Delta\omega \tag{25}$$

where θ_0 is the initial value of θ. An alternate form is

$$\Delta\theta = \theta - \theta_0 = \text{arccot}(\cot\theta_0 + \Delta\omega) - \theta_0 \tag{26}$$

where $\Delta\theta$ is the change in the orientation θ.

Now we can find the average rotation for a cell by finding the average $\Delta\theta$ for a large number of planes. A set of 18 planes uniformly distributed from $\theta_0 = 0°$ to $170°$ was studied. Simple shear strain like that in Figure 1 was imposed in $1°$ increments for 180 steps. As shown in Figure 3, the rotations of the planes varied from $0°$ to $115°$. Next we analyzed the planes in orthogonal pairs. The average rotations of pairs that were initially orthogonal ranged from $36°$ to $80°$, compared with the exact value of $57.52°$ $= \arctan \pi/2$. The accuracy of the average rotation gradually improved as we considered sets of 4 lines and 8 lines. The average rotation for all 18 planes was $57.64°$. Hence, the correct rotation of the material can be found by following the rotation of planes, but this procedure would not be practical if only an average rotation were desired, because of the excessive number of planes needed to provide a satisfactory accuracy.

4. AVERAGE CELL ROTATION

In this section we wish to develop a practical means for performing the rotation calculation. The following requirements will be considered for judging the system to be practical:

* Only the current nodal positions and velocities are required, but not a history of these quantities.

* The system should minimize the computational time and the additional storage.

* The system must permit standard rezoning procedures to occur, that is, rezoning should not disturb the rotation calculation, and the new variables required (if any) must be rezonable.

* Only the incremental rotation angle is needed at any time, in addition to the standard quantities. This requirement is given in more detail in the Application section.

The method we propose using begins with the computation of the tensors $\mathbf{G}^{n+1/2}$, $\dot{\mathbf{F}}^{n+1/4}$, and $\mathbf{F}^{n+1}$. Then θ is computed from the polar decomposition theorem. From θ
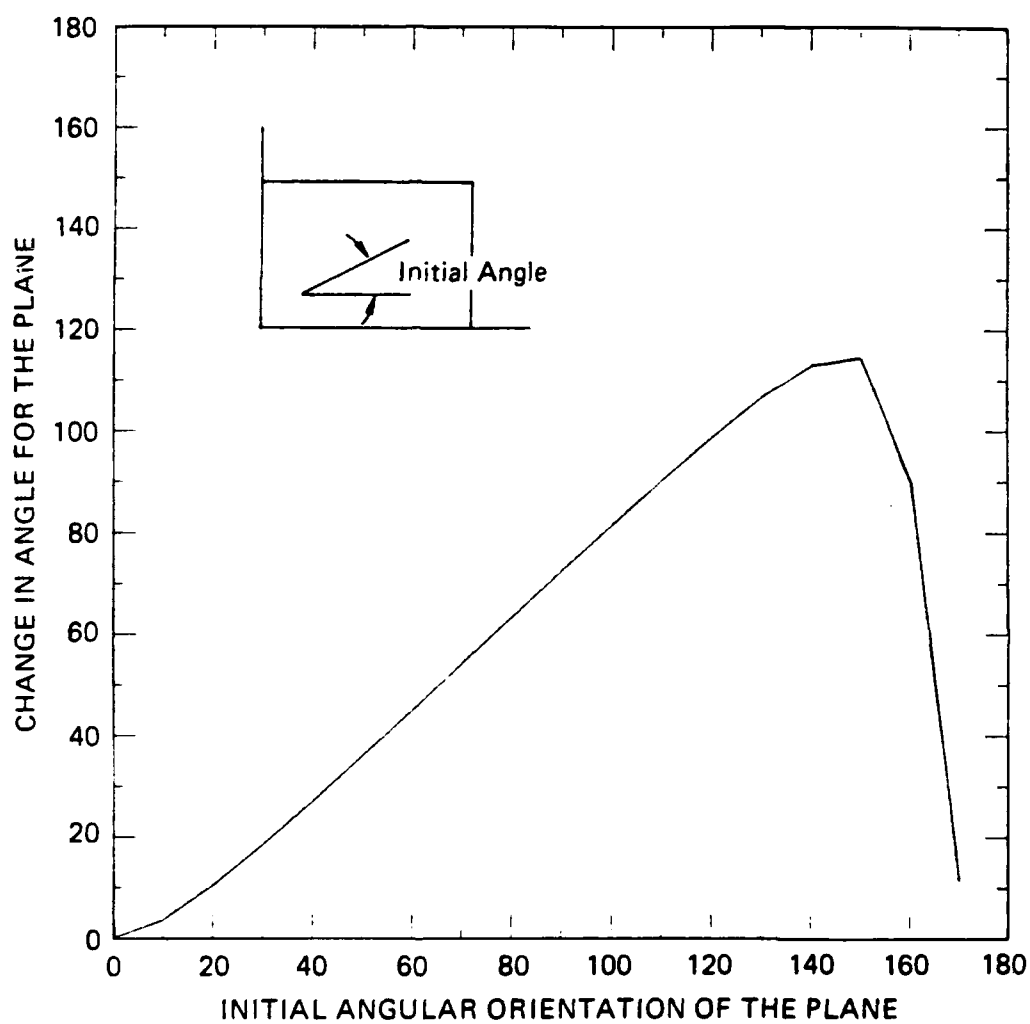
FIGURE D-3   ANGULAR CHANGES FOR PLANES

JA-6423-22

and the stored value of θ_0, the increment $\Delta\theta$ is computed. The rezoning aspect of this calculation is treated in the next section. Here we examine the definition of the deformation tensor $\mathbf{F}$, the computation of θ, and tests of the procedure.

Deformation Tensor Calculation

The deformation tensor must be determined in a way that is natural for our finite-difference codes. To begin, we write the current coordinates X_i as functions of the initial coordinates ($\xi = \xi_1$, $\eta = \xi_2$) and time

$$X_i = f_i(\xi_j, t) \tag{27}$$

and plan to compute this function by fitting it to the nodes around a cell at some time. We want to have a single function $\mathbf{F}$ that represents the cell material, yet we must fit the function to the K nodes around the cell. For this fitting purpose we could define the function X_{ik}, the X_i value at the kth node, by the series

$$X_{ik} = A_{10} + A_{11}\xi + A_{12}\eta + A_{13}\xi\eta + A_{14}\xi^2 + A_{15}\eta^2 + \ldots \tag{28}$$

where the A_{im} are constants obtained by the fitting process. By differentiating Eq. (28) for X_i with respect to ξ_j, we obtain the deformation gradient F_{ij}, according to Eq. (5). For a four-node cell, these components of $\mathbf{F}$ are

$$F_{11} = \frac{\partial x}{\partial \xi} = \frac{x_{13}\eta_{24} - x_{24}\eta_{13}}{A_0 + A_1}$$

$$F_{12} = \frac{\partial x}{\partial \eta} = \frac{x_{24}\xi_{13} - x_{13}\xi_{24}}{A_0 + A_1} \tag{29}$$

$$F_{21} = \frac{\partial y}{\partial \xi} = \frac{y_{13}\eta_{24} - y_{24}\eta_{13}}{A_0 + A_1}$$

$$F_{22} = \frac{\partial y}{\partial \eta} = \frac{y_{24}\xi_{13} - y_{13}\xi_{24}}{A_0 + A_1}$$

where $x_{mn} = x_m - x_n$, $\xi_{mn} = \xi_m - \xi_n$, and m and n refer to node numbers. Clearly, in this method the original coordinates ξ_m and η_m must be retained for all cells. Yet these original coordinates are not rezonable quantities, so this method of computing $\mathbf{F}$ cannot be used with rezoning.

An alternate method for determining $\mathbf{F}$ is to start with an initial value, and update it at each time step in the calculation using $\dot{\mathbf{F}}$ computed from Eq. (7).

$$\dot{\mathbf{F}}^{n+1/4} = \mathbf{G}^{n+1/2}(\mathbf{F}^{-1})^n \tag{30}$$

where n indicates that these tensors are from the nth time step. Then the $\mathbf{F}$ at the next time step is calculated using $\dot{\mathbf{F}}$:

$$\mathbf{F}^{n+1} = \mathbf{F}^n + \dot{\mathbf{F}}^{n+1/4}\,\Delta t \tag{31}$$

251

This second method, using $\dot{\mathbf{F}}$, seems the most direct, but requires storage of $\mathbf{F}$ from the previous cycle. (The $\dot{\mathbf{F}}^{n+1/4}$ is also not at the correct time $t^{n+1/2}$ to make a central calculation in Eq. 31.) We choose this method of computing $\mathbf{F}$ for our procedure.

Computation of the Rotation Angle θ

For computing the rotation angle θ we consider the left and right stretch tensors $\mathbf{V}$ and $\mathbf{U}$, and the rotation tensor $\mathbf{R}$. Because of the symmetry of $\mathbf{V}$ and $\mathbf{U}$, and because $\mathbf{R}$ represents a counterclockwise rotation of θ, we recognize that we can write these tensors in the following way:

$$\mathbf{V} = \begin{bmatrix} V_{11} & V_{12} \\ V_{12} & V_{22} \end{bmatrix} , \quad \mathbf{U} = \begin{bmatrix} U_{11} & U_{12} \\ U_{12} & U_{22} \end{bmatrix} \quad \text{and} \quad \mathbf{R} = \begin{bmatrix} \cos\theta & -\sin\theta \\ \sin\theta & \cos\theta \end{bmatrix} \quad (32)$$

We can write out Eq. (5) term by term and solve for the unknown components of $\mathbf{V}$, $\mathbf{U}$, and $\mathbf{R}$.

$$F_{11} = V_{11} \cos\theta + V_{12} \sin\theta = U_{11} \cos\theta - U_{12} \sin\theta$$

$$F_{12} = -V_{11} \sin\theta + V_{12} \cos\theta = U_{12} \cos\theta - U_{22} \sin\theta \quad (33)$$

$$F_{21} = V_{12} \cos\theta + V_{22} \sin\theta = U_{11} \sin\theta + U_{12} \cos\theta$$

$$F_{22} = -V_{12} \sin\theta + V_{22} \cos\theta = U_{12} \sin\theta + U_{22} \cos\theta$$

The solution of either set of four simultaneous equations leads to

$$\tan\theta = \frac{F_{21} - F_{12}}{F_{11} + F_{22}} \quad (34)$$

The angle θ can be obtained with the arctangent function or, for small angles, with a series expansion in $t = \tan\theta$. The following truncated series are accurate to 10^{-5}.

$$\theta \approx t - \frac{t^3}{3} + 0.1839\, t^5 \quad \text{for } t < 0.37 \quad (35a)$$

$$\theta \approx t - \frac{t^3}{3} + \frac{t^5}{5} - \frac{t^7}{7} + 0.0875\, t^9 \quad \text{for } t < 0.59 \quad (35b)$$

The results of the arctangent function are ambiguous so that θ is only obtained within some multiple of π. To remove the ambiguity, we examine $\theta - \theta_0 = \Delta\theta$, where θ_0 is the angle at the previous time step. Generally, in wave propagation calculation, $\Delta\theta$ is $< 1°$. Therefore, $\Delta\theta$ is approximately a multiple of π. Then θ must have passed over a discontinuity in the arctangent definition. The discontinuity is removed by subtracting the multiple of π from θ.

To find the rotation rate ω, we first compute the current orientation θ of the material from $\tan\theta$ (Eq. 34). Then

$$\omega = \frac{\theta - \theta_0}{\Delta t} \quad (36)$$

where θ_0 is the orientation at the previous cycle. At this point we have available ω, θ and the deformation tensor $\mathbf{F}$.

Computation of $\mathbf{V}$, $\mathbf{U}$, and $\mathbf{R}$

For the rezoning procedures considered later it maybe necessary to obtain the $\mathbf{V}$, $\mathbf{U}$, and $\mathbf{R}$ tensors. If these are of interest, we can proceed as follows. The sine and cosine factors in $\mathbf{R}$ can be computed from components of the deformation tensor:

$$\sin\theta = \frac{F_{21} - F_{12}}{\sqrt{\left(F_{21} - F_{12}\right)^2 + \left(F_{11} + F_{22}\right)^2}} \tag{37a}$$

$$\cos\theta = \frac{F_{11} + F_{22}}{\sqrt{\left(F_{21} - F_{12}\right)^2 + \left(F_{11} + F_{22}\right)^2}} \tag{37b}$$

With the sine and cosine available, we can simply solve for the $\mathbf{V}$ components from Eqs. (33).

$$V_{11} = F_{11} \cos\theta - F_{12}\sin\theta$$

$$V_{12} = F_{11} \sin\theta + F_{12} \cos\theta \tag{38}$$

$$= F_{21} \cos\theta - F_{22} \sin\theta$$

$$V_{22} = F_{21} \sin\theta + F_{22} \cos\theta$$

and the $\mathbf{U}$ components are

$$U_{11} = F_{11}\cos\theta + F_{21}\sin\theta$$

$$U_{12} = -F_{11}\sin\theta + F_{21}\cos\theta \tag{39}$$

$$= F_{12}\cos\theta + F_{22}\sin\theta$$

$$U_{22} = -F_{12}\sin\theta + F_{22}\cos\theta$$

An alternate procedure to the above would involve using Hughes' method of finding $\mathbf{U}$ from taking the square root of $\mathbf{F}^T\mathbf{F}$; the results are identical.

Summary of the Method

In summary, the strategy we are suggesting for two-dimensional problems differs slightly from those of Dienes and Hughes. We are interested mainly in obtaining the rotation angle θ and the increment $\Delta\theta$. In this method it is necessary to store the full $\mathbf{F}$ tensor and the rotation θ. During each time step we make the following computations:

(1) Compute $\mathbf{G}$ (Eq. 6), and evaluate $\mathbf{D}$ (Eq. 8) and $\mathbf{W}$ (Eq. 9) from it.

(2) Using $\mathbf{G}$ and the stored $\mathbf{F}$, compute $\dot{\mathbf{F}}$ (Eq. 30), and evaluate the current $\mathbf{F}$ tensor (Eq. 31).

(3) Compute $\tan\theta$ (34) and evaluate θ. Adjust θ as needed to account for the ambiguity of the arctangent.

(4) Compute the increment of rotation from $\Delta\theta = \theta - \theta_0$.

(5) Perform the stress rotation calculations using $\Delta\theta$ in the same way that we have generally used W_{12}.

The stress rotation calculations have the form

$$\sigma_{xx} = \sigma_{xxo} - 2\,\sigma_{xyo}\,\Delta\theta$$

$$\sigma_{yy} = \sigma_{yyo} + 2\,\sigma_{xyo}\,\Delta\theta \qquad (40)$$

$$\sigma_{zz} = \sigma_{zzo}$$

$$\sigma_{xy} = \sigma_{xyo} + (\sigma_{xxo} - \sigma_{yyo})\,\Delta\theta$$

This new procedure requires four extra storage locations in addition to the orientation θ. The computation time for the procedure is mainly taken by the additional square root and the arc tangent.

Tests of the Rotation Procedure

A number of tests were made on the foregoing rotation procedure to evaluate its accuracy and speed, and especially to determine whether it works correctly for very large angles. The following problems were run:

(1) Apply a uniform tension to a body and then gradually rotate the body, computing the current stress tensor at each step. This is a rigid body rotation so the angle and stress tensor should be obtainable even using the Jaumann method with $\omega = W_{21}$.

(2) Extend a block gradually while rotating it. This is again a rotation without shear, yet a more complex test. The results should match those of test 1 at the end point.

(3) Distort a block in simple shear and follow the computed orientation θ and the stress tensor.

(4) Shear a block during rotation and follow the orientation and stress tensor.

In each case 400 steps were used and the stresses and orientation θ were examined at several intermediate steps as well as at the end. The rotation was through an angle of $360°$. In all cases the final computed value of θ was accurate within 0.1%. The error was found to be directly related to the imposed angular increment. The stress computation obtained in simple shear is shown in Figure 4 and compared with the exact solution of Dienes.

254
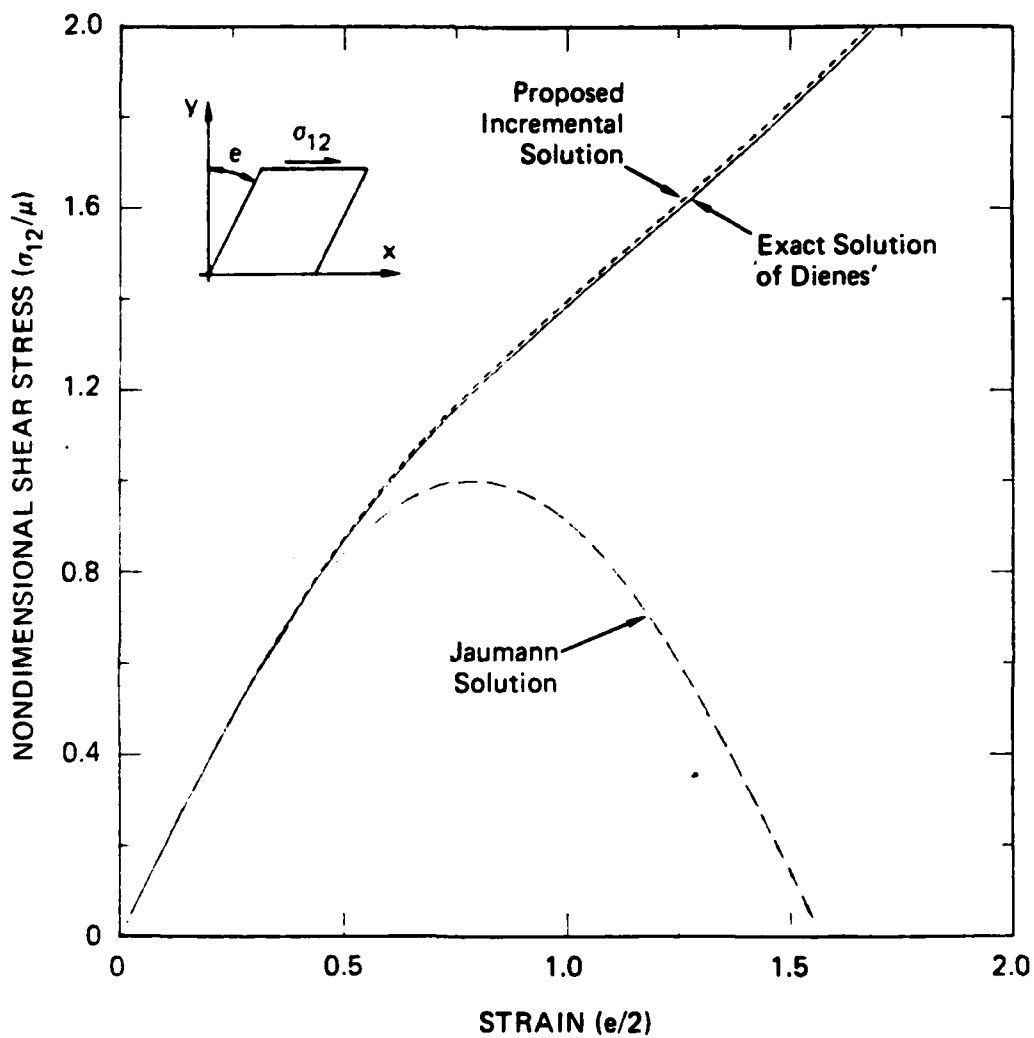
FIGURE D-4   COMPARISON OF SHEAR STRESS COMPUTED INCREMENTALLY
BY THE PROPOSED METHOD WITH THE EXACT SOLUTION

255

5. REZONING OF THE ROTATION QUANTITIES

During a large distortion computation it is usually necessary to rezone the cells -- that is, to construct a new mesh with less distortion in the individual cells. After the new mesh is constructed, the properties in the old cells are assigned to the new cells. Generally, each new cell will contain some material from two or more of the old cells. The properties (for example, energy, pressure, stress tensor, yield strength, plastic strain) of the mixed materials in the new cell are computed by weighting each property according to the mass contributed by the old cell. For example, property P is computed from

$$P_{new} = \frac{\sum\limits_{k=1}^{K} m_k P_k}{\sum\limits_{k=1}^{K} m_k} \tag{41}$$

where m_k is the mass contributed by the kth old cell to the new cell. This mass-weighting method is essentially an averaging technique, and thus results in some smearing of the properties during rezoning.

To fit into the rezoning procedure, it is essential that the variables used in the rotation calculation be rezonable in a manner like that in Eq. (41). We have selected the tensors F and V (or U), and the scalar θ as candidates for rezoning. The angle θ is scalar and represents a physical quantity that can be appropriately averaged in combining properties from two groups; hence the angle is rezonable.

The stretch tensors each represent the state of distortion in the cell material. Following Dienes[1], they can be diagonalized as follows:

$$V = T \Lambda T^{-1} \tag{42}$$

where Λ is diagonal, and T represents an orthogonal transformation. Hence the fundamental information contained in V or U is Λ_{11}, Λ_{22}, and the transformation angle α associated with T, where

$$T = \begin{bmatrix} \cos\alpha & -\sin\alpha \\ \sin\alpha & \cos\alpha \end{bmatrix} \tag{43}$$

These three quantities (Λ_{11}, Λ_{22}, and α) meet our criteria for averageable quantities, and therefore are rezonable. An alternate set of independent quantities are the trace and determinant of U, and the angle α. Here the determinant of U has the physical meaning of the exponential of the areal strain, and hence, it is a quantity that we may especially want to preserve during rezoning. The five quantities are all readily computed from the U tensor:

$$\text{trace } U = \text{tr}U = U_{11} + U_{22} \tag{44}$$

$$\text{determinant } \mathbf{U} = \det \mathbf{U} = U_{11} U_{22} - U_{12}^2 \qquad (45)$$

$$\Lambda_{11}, \Lambda_{22} = \frac{\text{tr} \mathbf{U}}{2} \pm \sqrt{\frac{1}{4}(\text{tr} \mathbf{U})^2 - \det \mathbf{U}} \qquad (46)$$

$$\alpha = \frac{1}{2} \arctan \frac{2U_{12}}{U_{11} - U_{22}} \qquad (47)$$

The same rezoning results are obtained by using the set Λ_{11}, Λ_{22}, and α or the set tr $\mathbf{U}$, det $\mathbf{U}$, and α. Following the rezoning of these invariants, the new $\mathbf{U}$ tensor is constructed by computing $\mathbf{U} = \mathbf{T} \Lambda \mathbf{T}^{-1}$ using the new Λ and $\mathbf{T}$ tensors.

The foregoing is clearly a lengthy procedure, and thus it is worthwhile to form an approximate method. For a first approximation, we may choose to rezone the U_{ij} components, yet preserve the areal strain (det $\mathbf{U}$). To start the calculation, we compute $\mathbf{U}$ from $\mathbf{F}$ using either Eq. (19) or (39). Then we compute the area strain factor $A = \det \mathbf{U}$ and generate a $\mathbf{u}$ tensor with reduced components

$$u_{ij} = U_{ij}/\sqrt{A} \qquad (48)$$

These reduced $\mathbf{u}$ tensors are then used in the rezoning process to form a reduced tensor for the new cell.

$$u_{ijs} = \frac{\sum m_k U_{ijk}/\sqrt{A_k}}{\sum m_k} \qquad (49)$$

Next the determinant $A_s = \det u_{ijs}$ is computed and the areal strain factor from the old cells is rezoned.

$$\overline{A} = \frac{\sum m_k A_k}{\sum m_k} \qquad (50)$$

Finally the $\mathbf{U}$ tensor for the new cell is formed.

$$U_{ij} = u_{ijs}\sqrt{\overline{A}/A_s} \qquad (51)$$

In this way the new $\mathbf{U}$ has a mass-weighted areal strain. This rezoning method was tested for cases in which there were large rotations combined with either extension or shear. For 180° differences between rotations of the old cells, the $\mathbf{U}$ tensor components for the new cell were all within 1% of the exact value for the extension case and within 10% of the exact value for the shearing case. For the usual strain and rotation levels, this procedure should be satisfactory.

A simpler and faster rezoning approximation can be made by rezoning the $\mathbf{F}$ components directly. The determinant of $\mathbf{F}$ also equals the exponential of the areal strain, so we can preserve the areal strain using a procedure like the one applied above to the $\mathbf{U}$

tensor. As with the U tensor, we start by calculating the reduced components of F for the new cell:

$$F_{ijs} = \frac{\sum m_k F_{ijk}/\sqrt{A_k}}{\sum m_k} \qquad (52)$$

Then we compute the areal strain factor for the reduced F tensor: $A_s = \det F_{ijs}$. Then we compute the components of the F tensor for the new cell.

$$\overline{F}_{ij} = F_{ijs}\sqrt{\overline{A}/A_s} \qquad (53)$$

Rezoning tests with the F components gave meaningless results when old cells with rotations that differed by 180° were used. Errors of approximately 10% in the F components were obtained when the rotations of the old cells were within 45°, for either extension or shearing. Hence, the use of F in rezoning could only be considered satisfactory for fairly small angular differences between old cells.

Based on these initial observations, we developed a two-branch plan for rezoning, depending on the range in the rotation angles in the old cells contributing to the new cell:

(1) Cells with angular differences less than 20°: Mass-weight the components of the F tensor.

(2) Cells with large angular differences: Derive the U tensor and θ for each contributing cell. Mass weight U and θ. Then recover F for the new cell.

6. APPLICATIONS TO CONSTITUTIVE RELATIONS

The foregoing rotation calculations are intended for use with constitutive relations so that the stresses computed are objective (that is, independent of the motion of the coordinate system). The type of the constitutive relation determines the information required from the rotation procedure. Here we identify three types of relations:

(1) Isotropic elastic material. For isotropic material, calculation can be conducted either by rotating the stresses to the material coordinates using the R tensor, or the stresses can be incremented using $\Delta\theta$ as in Eq. (40). The results in Figure 2 show the small inaccuracies involved in computing the stresses and the rotation angle by the approximate, incremental rotation procedure.

(2) Isotropic plastic material. For material that may yield, the same rotation procedures can be used as for the elastic material. However, the continued straining tends to eliminate the errors in the stress transformation, so the stresses obtained from the approximate procedure are sufficiently accurate. The results of an ideal plastic calculation of simple shear with a yield strength of 20% of the shear modulus gave the results shown in Figure 5. The error

258
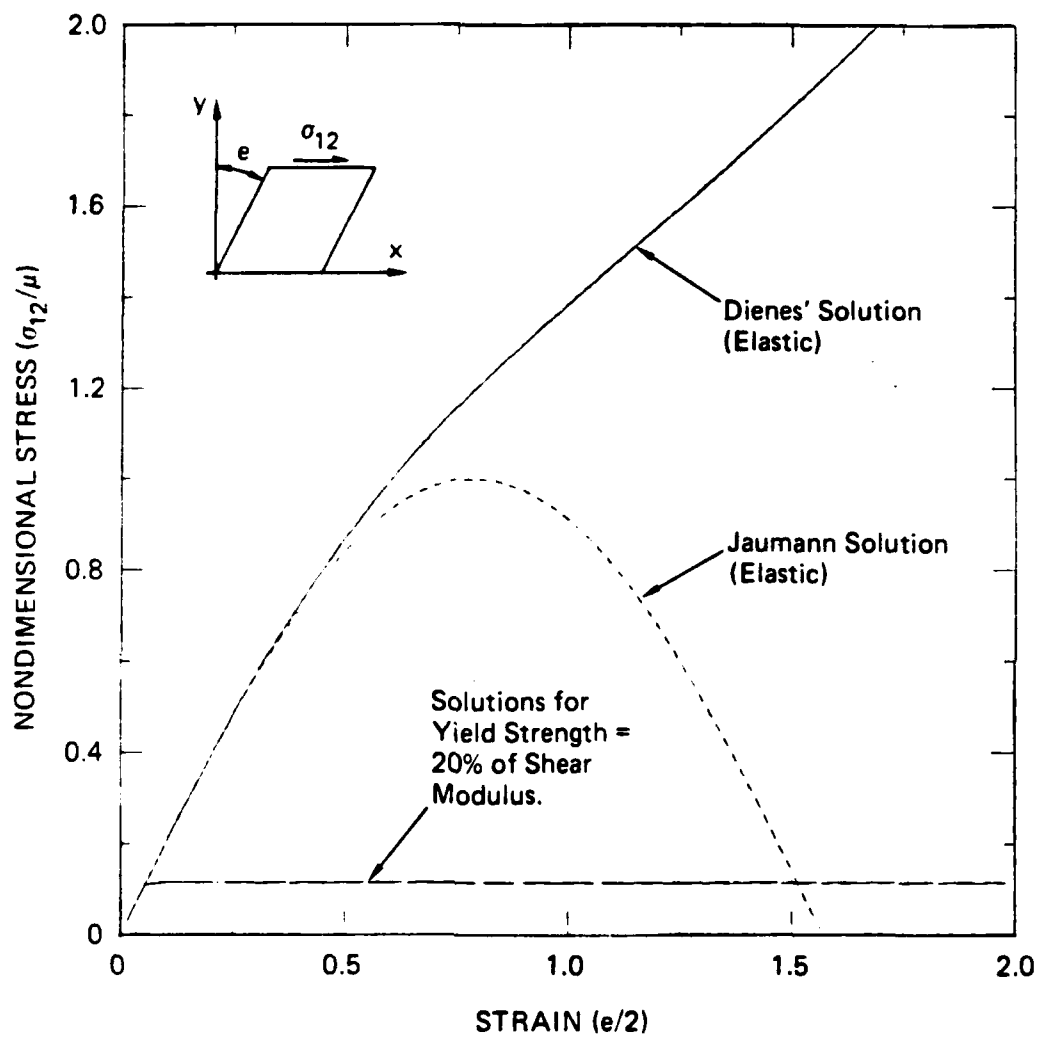
FIGURE D-5   COMPARISON OF SHEAR STRESSES FROM DIENES'
AND JAUMANN'S SOLUTIONS FOR ELASTIC AND
PLASTIC CASES

JA-6423-24

259

increases with yield strength. This excessively large yield strength was used to show that the errors are actually very small. The exact and Jaumann solutions for yielding are essentially indistinguishable. However, the angle calculation for the yielded case still has the inaccuracy illustrated in Figure 2b. Hence, if the rotation angle is not needed, the Jaumann solution is very satisfactory for yielding in isotropic material.

(3) Anisotropic material. For calculations with anisotropic material it is necessary to know the orientation of the material coordinates. In such a material it is assumed that the material planes all rotate together, maintaining their fixed angular relationship (Under conditions of large distortion, this fixity of angles is certainly not achieved according to the results in Figure 2b). The rotation tensor R or the angles θ and $\Delta\theta$ are required for the calculation.

Multiple-plane models such as the Peirce-Asaro-Needleman model[6], our BFRACT model[7], and our SHEAR model[8] contain a series of internal planes that follow the material motion. The rotations of these planes are computed correctly from the velocity gradient tensor G according to the equations in section 3. These models account for the relative motion of several planes and the gradual development of anisotropy. Hence, these constitutive relations do not require the foregoing rotation treatment.

7. SUMMARY

The rotation problem in two-dimensional calculations has been treated to determine methods appropriate to finite-difference wave propagation calculations involving rezoning. First, the nature of the rotation problem and the inaccuracies inherent in the standard Jaumann method for cases of large shear strain were outlined. An exact method was developed for the rotation of lines or planes in the material. A direct method for obtaining the rotation θ of the cell material was outlined based on the works of Dienes[1] and Marsden and Hughes[3]. The deformation tensor F is stored for each cell. The current angle θ is obtained from

$$\tan\theta = \frac{F_{21} - F_{12}}{F_{11} + F_{22}} \tag{34}$$

Three methods were explored for rezoning the quantities used in the calculation. We also outlined (1) a theoretically exact rezoning method based on the invariants of the U tensor, and (2) approximations based on the U and F components.

The rotation techniques are necessary under conditions of large shear strain for isotropic and simple anisotropic elastic materials in which all the material is assumed to

rotate together. For materials in which yielding occurs the stresses are correctly provided by the standard Jaumann method, although the rotation angle is not correct for large distortions. For multiple-plane material models in which specific planes in the material are followed, this rotation treatment is not necessary.

REFERENCES

1. J. K. Dienes, "On the Analysis of Rotation and Stress Rate in Deforming Bodies," Acta Mechanica, Vol. 32, p. 217-232 (1979).

2. D. C. Drucker, "Appropriate Simple Idealizations for Finite Plasticity," *Plasticity Today* Sawczuk, A., and Bianchi, G., eds., Elsevier Applied Science, U.K., 1985, from the International Symposium on Current Trends and Results in Plasticity, CISM, Udine, Italy, June 1983.

3. J. E. Marsden and T. J. R. Hughes, *Mathematical Foundations of Elasticity*, Prentice-Hall, 1983.

4. J. O. Hallquist, "NIKE2D - A Vectorized, Implicit, Finite Deformation, Finite Element Code for Analyzing the Static and Dynamic Response of 2-D Solids," Report UCID-19677 of Lawrence Livermore Laboratory, February 1983.

5. R. Bellman, *Introduction to Matrix Analysis*, McGraw-Hill, 1960.

6. D. Peirce, R. J. Asaro, and A. Needleman, "Material Rate Dependence and Localized Deformation in Crystalline Solids," Acta Metall., Vol. 31, No. 12, p. 1951-1976 (1983).

7. L. Seaman, D. R. Curran, and W. J. Murri, "A Continuum Model for Dynamic Tensile Microfracture and Fragmentation," Jour. of Appl. Mech., Vol. 52, p. 593-600, Sept. 1985.

8. Lynn Seaman and James L. Dein, "Representing Shear Band Damage at High Strain Rates," IUTAM Symposium on Nonlinear Deformation Waves, eds. U. Nigul and J. Engelbrecht, held in Tallinn, August 1982, publ. by Springer, Berlin (1983).

APPENDIX E

STORAGE LOCATIONS FOR COORDINATE AND CELL VARIABLES

All the cell and coordinate (node) variables are stored in a single large one-dimensional array called COM1. The array locations that pertain to each cell or node are identified by two auxiliary arrays, LC and LN. Extra array locations may be provided for a cell through the use of the indicator NVAR. Operations with these arrays are described below.

The standard 18 variables associated with cells and 24 variables for nodes are listed in Table E.1 and E.2. These variables are equivalenced to the COM1 array for convenience in identifying them. For example, consider cell i and node j. The information begins at I = LC(i) and J = LN(j). Some of the variables associated with this cell and this node are

$$Z(I) = COM1(I + 1) \qquad\qquad X(J) = COM1(J)$$
$$P(I) = COM1(I + 8) \qquad\qquad Y(J) = COM1(J + 1)$$
$$TXX(I) = COM1(I + 4) \qquad\qquad XD(J) = COM1(J + 4)$$

Thus all the variables associated with a particular cell or node are stored one after the other in the COM1 array. The starting locations, I or J, are given by the LC and LN arrays.

Table E.1 VARIABLES IN COM1 ARRAY FOR EACH NODE

Number	Location	Name	Description in COM1
1	COM1(L)	X(L)	Eulerian position in the x direction, cm.
2	COM1(L+1)	Y(L)	Eulerian position in the y direction, cm.
3	COM1(L+2)	XO(L)	Initial value of X(L), cm
4	COM1(L+3)	YO(L)	Initial value of Y(L), cm
5	COM1(L+4)	XD(L)	Particle velocity in the x direction, cm/s
6	COM1(L+5)	YD(L)	Particle velocity in the y direction, cm/s
7	COM1(L+6)	BC(L)	Boundary condition indicator
8	COM1(L+7)	BCN(L)	Number of mating node across a boundary
9	COM1(L+8)	AM(L)	Mass associated with the node, g or g/cm
10	COM1(L+9)	FX(L)	Force on the node in the x direction, dyn or dyn/cm
11	COM1(L+10)	FY(L)	Force on the node in the y direction, dyn or dyn/cm
12	COM1(L+11)	WREZ(L)	Indicator for rezoning
13 to 17	COM1(L+12) COM1(L+16)	WCELL(L)	Array of 5 values containing the LC numbers of the surrounding cells
18	COM1(L+17)	SCELL(L)	Negative of the number of cells around the node
19 to 24	COM1(L+18) COM1(L+23)	WNDND(L)	Array of 5 values containing the numbers of the nodes which are neighbors to the node at L.

Notes: When two dimensions are listed, the first is for axisymmetric problems and the second for planar problems.

L = LN(n), the starting location for data for the n-th node.

Table E.2. VARIABLES IN COM1 ARRAY FOR EACH CELL

Number	Location	Name	Description
1	COM1(L)	A(L)	Area in the x, y plane, cm^2
2	COM1(L+1)	Z(L)	Mass of the cell, g or g/cm
3	COM1(L+2)	WMAT(L)	Number of the material in the cell
4	COM1(L+3)	D(L)	Density, g/cm^3
5	COM1(L+4)	TXX(L)	Total stress in the x direction, dyn/cm^2
6	COM1(L+5)	TYY(L)	Total stress in the y direction, dyn/cm^2
7	COM1(L+6)	TZZ(L)	Total stress in the z direction, dyn/cm^2
8	COM1(L+7)	TXY(L)	Shear stress in the xy plane, dyn/cm^2
9	COM1(L+8)	P(L)	Pressure, dyn/cm^2
10	COM1(L+9)	E(L)	Specific internal energy, erg/g
11	COM1(L+10)	SP2(L)	Square of the sound speed, cm^2/s^2
12	COM1(L+11)	YY(L)	Yield strength, dyn/cm^2
13	COM1(L+12)	WH(L)	Indicator for material state
14	COM1(L+13)	TH(L)	Rotation, positive counter-clockwise, radians
15 to 18	COM1(L+14) COM1(L+17)	WNOD(L)	Array of 4 values containing the numbers of the nodes around the cell

Notes: When two dimensions are listed, the first is for axisymmetric problems and the second for planar problems.

L = LC(n), the starting location for data for the n-th cell.

The LC and LN arrays are computed such that the COM1 array is just filled, with no gaps remaining between variable sets for each cell and node. Generally node and cell information are interleaved according to the order in which the cells and nodes are initialized in BLOCK.

Some of the material models available with C-HEMP require extra variables above the basic set of stresses and energy provided. For such models, extra storage is requested for each cell containing the mth material by setting NVAR(m) - the number of extra variables requested - with the other material data. Then the number of variables provided for each of those cells is 18 + NVAR(m). The numbers of extra variables needed for some of the models are given in Table E.3.

Table E.3. EXTRA VARIABLES REQUIRED FOR SPECIAL MODELS

Material Model	NVAR
BFRACT3(a)	$3 * SIZE + 9$
CAP1	3
DFRACT	3
DFRACTS	3
EPP	2
EXPLODE	5
REBAR	10
SHEAR3	$4 + \sum_{i=1}^{4} FNUC_i [2 * BFR(13) + 1] + 3$
SHEAR4(b)	$41 + \sum_{i=1}^{7} FNUC_i [2 * BFR(13) + 1] + 5$

Notes: (a) "SIZE" is input, the number of intervals requested for the size distribution (not greater than 10)

(b) Computed and provided by the code.

268

To obtain historical listings of the extra variables, a request is made for a COMC or COMN variable, as described in Section IV C under HISTORY. An example of the necessary steps is given below for the plastic strain in one orientation of the SHEAR4 model.

Assume that we want a history of the plastic strain in the -xy orientation (the normal to this plane was originally in the -xy direction, or 135° from the x axis). According to the comment at line SHR4_64 in the SHEAR4 listing, this strain is the fourth in the array. From the comment in SHR4_28, the plastic strains begin with CN(2), so we are requesting CN(5). Next, we compare the formal parameters in SHEAR4 (SHR4_1) with the CALL statement in CYCLE at CYCL_344, and find that CN(1) is the equivalent of COM1(LM+19). Because we want CN(5), we will request COM1(LM+23). According to the instructions with the description of COMC under HISTORY in Subsection II C, the 24th element in the COM1 array is requested with "COMC24".

DISTRIBUTION LIST

No. of Copies	Organization	No. of Copies	Organization
12	Administrator Defense Technical Info Center ATTN: DTIC-DDA Cameron Station Alexandria, VA 22304-6145	1	Director US Army Air Mobility Research and Development Laboratory Ames Research Center Moffett Field, CA 94035
1	HQDA (DAMA-ART-M) Washington, DC 20310	1	Commander US Army Communications – Electronics Command
1	Commander US Army Materiel Command ATTN: AMCDRA-ST 5001 Eisenhower Avenue Alexandria, VA 22333-0001	1	ATTN: AMSEL-ED Fort Monmouth, NJ 07703 Commander ERADCOM Technical Library ATTN: DELSD-L (Reports Section) Fort Monmouth, NJ 07703-5301
1	Commander Armament R&D Center US Army AMCCOM ATTN: SMCAR-TSS Dover, NJ 07801	1	Commander US Army Missile Command Research, Development and Engineering Center ATTN: AMSMI-RD
1	Commander Armament R&D Center US Army AMCCOM ATTN: SMCAR-TDC Dover, NJ 07801	1	Redstone Arsenal, AL 35898 Director US Army Missile & Space Intelligence Center
1	Commander US Army Material Technology Laboratory ATTN: John Mescall Watertown, MA 02172		ATTN: AIAMS-YDL Redstone Arsenal, AL 35898-5500
1	Director Benet Weapons Laboratory Armament R&D Center US Army AMCCOM ATTN: SMCAR-LCB-TL Watervliet, NY 12189	1	Commander US Army Tank-Automotive Command ATTN: AMSTA-TSL Warren, MI 48397-5000
1	Commander US Army Armament, Munitions and Chemical Command ATTN: SMCAR-ESP-L Rock Island, IL 61299	3	Director US Army TRADOC Systems Analysis Activity ATTN: ATAA-SL White Sands Missile Range, NM 8002
1	Commander US Army Aviation Research and Development Command ATTN: AMSAV-E 4300 Goodfellow Blvd St. Louis, MO 63120	1	Commandant US Army Infantry School ATTN: ATSH-CD-CSO-OR Fort Benning, GA 31905

DISTRIBUTION LIST

No. of Copies	Organization	No. of Copies	Organization
1	Commander US Army Development & and Employment Agency ATTN: MODE-TED-SAB Fort Lewis, WA 98433	10	Central Intelligence Agency Office of Central Reference Dissemination Branch Room GE-47 HQS Washington, DC 20502
1	AFWL/SUL Kirtland AFB, FL 87117		**Aberdeen Proving Ground**

1	AFATL/DLODL
	Eglin AFB, FL 32542-5000
			Dir, USAMSAA
			  ATTN: AMXSY-D
			      AMXSY-MP (H. Cohen)

1	AFATL (Joe Foster) Eglin AFB, FL 32452-5000		Cdr, USATECOM ATTN: AMSTE-TO-F

2	US Army Research Office
	ATTN: George Mayer
	    Robert Singleton
	P. O. Box 12211
	Reseach Triangle Park,
	  NC 27709
			Cdr, CRDC, AMCCOM
			  ATTN: SMCCR-RSP-A
			      SMCCR-MU
			      SMCCR-SPS-IL

2	Naval Surface Weapons Center ATTN: William H. Holt Willis Mock, Jr. Dahlgren, VA 22448		
1	Naval Research Laboratory ATTN: Rick Mako Washington, DC 20375		

USER EVALUATION SHEET/CHANGE OF ADDRESS

This Laboratory undertakes a continuing effort to improve the quality of the reports it publishes. Your comments/answers to the items/questions below will aid us in our efforts.

1. BRL Report Number_____Date of Report_____

2. Date Report Received_____

3. Does this report satisfy a need? (Comment on purpose, related project, or other area of interest for which the report will be used.)_____

_____

_____

4. How specifically, is the report being used? (Information source, design data, procedure, source of ideas, etc.)_____

_____

_____

5. Has the information in this report led to any quantitative savings as far as man-hours or dollars saved, operating costs avoided or efficiencies achieved, etc? If so, please elaborate._____

_____

_____

6. General Comments. What do you think should be changed to improve future reports? (Indicate changes to organization, technical content, format, etc.)

_____

_____

_____

	_____
	Name
CURRENT	_____
ADDRESS	Organization
	_____
	Address
	_____
	City, State, Zip

7. If indicating a Change of Address or Address Correction, please provide the New or Correct Address in Block 6 above and the Old or Incorrect address below.

	_____
	Name
OLD	_____
ADDRESS	Organization
	_____
	Address
	_____
	City, State, Zip

(Remove this sheet, fold as indicated, staple or tape closed, and mail.)

Director
US Army Ballistic Research Laboratory
ATTN: DRXBR-OD-ST
Aberdeen Proving Ground, MD   21005-5066
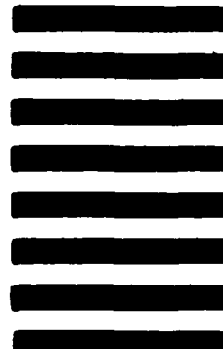
||| |||

NO POSTAGE
NECESSARY
IF MAILED
IN THE
UNITED STATES

OFFICIAL BUSINESS
PENALTY FOR PRIVATE USE. $300

BUSINESS REPLY MAIL
FIRST CLASS   PERMIT NO 12062   WASHINGTON, DC

POSTAGE WILL BE PAID BY DEPARTMENT OF THE ARMY

Director
US Army Ballistic Research Laboratory
ATTN: DRXBR-OD-ST
Aberdeen Proving Ground, MD 21005-9989

END

DATE

FILMED

DTIC

7-88

END

DATE

FILMED

DTIC

7-88